New approaches for cofactor recycling; application to chemical synthesis and electrochemical devices

A thesis submitted to the Board of the Faculty of Physical Sciences,

for the degree of Doctor of Philosophy, University of Oxford

Holly A. Reeve

Jesus College, Michaelmas Term, 2014

New approaches for cofactor recycling; application to chemical synthesis and electrochemical devices

A Thesis Submitted for the degree of DPhil, Michaelmas Term, 2014

Holly A. Reeve, Jesus College

The work in this Thesis addresses the challenges associated with using redox enzymes for chemical synthesis. The use of enzymes as catalysts in the synthesis of fine chemicals is becoming more wide spread, in part due their ability to catalyse reactions with incredible selectivity under relatively mild conditions. In particular, enzymes are useful for selective reduction of ketones to enantiomerically pure alcohols or amines, and partial oxidations of alkanes to alcohols. However, a key limitation to exploiting redox enzymes in these reaction pathways is the requirement for a specialised electron source, usually the expensive nicotinamide cofactors NADH or NADPH.

Existing cofactor regeneration methods use a second enzyme with a sacrificial substrate which is oxidised to generate a stoichiometric waste product; this complicates isolation of the desired product and prevents the environmental benefits of biocatalysis from being fully realised. In order to provide clean and efficient biocatalytic routes, improved recycling methods for these cofactors are crucial. This Thesis develops two novel methods for *in situ* cofactor recycling. The first is an electro-enzymatic system; an NAD^+-reductase enzyme is shown to use electrons directly from an electrode for supply of NADH to a co-immobilised cofactor-dependent enzyme. The second uses a hydrogenase, NAD^+-reductase and cofactor-dependent enzyme immobilised on conducting particles for H_2-driven NADH regeneration. This relies on the thermodynamically favourable reduction of NAD^+ by H_2 when the hydrogenase and NAD^+-reductase are in electronic contact, provided by the conducting particle.

The electro-enzymatic approach to NAD^+ reduction is then adapted for electrochemical devices; an enzyme catalysed fuel cell and a self-powered biosensor were considered.

Acknowledgements

First and foremost I would like to thank Prof Kylie Vincent for so much more than just her wonderful supervision. Kylie has been a constant source of inspiration and guidance to me over the last 4 years and I can not thank her enough. She has encouraged me to take on so many exciting challenges throughout my DPhil and I look forward to more in the future!

I am also hugely grateful to Dr Philip Ash who has also been an endless support throughout my DPhil. Thanks for talking ideas through with me, helping with IR experiments, reading my Thesis and so much more. Ian McPherson has also been a fantastic colleague and I thank him in particular for helping with equipment design – he has a solution to everything – and for proof reading. Jonathan Quinson is the carbon expert and I thank him for both his ideas and for following through with them, the 'tubes in tubes' will forever make me smile. I also want to thank Ricardo Hidalgo for his advice on Hyd-1 spectroscopy.

I would like to thank Dr Zulkifli Idris for his help, particularly in the early stages of my work and for teaching me everything I needed to about protein film electrochemistry. I am very appreciative for the hard work of all of the Part II students I have worked with including Tommy Lyle, Jenny Bradley, Ben Bluestone, Charles Stevens, Thomas Lonsdale and Chloe Tomlinson. More recently it has been great to watch this project expand and to work alongside Thomas Lonsdale, Kouji Urata and Tianze Zhu. I would like to thank everyone in the Vincent Group, past and present, as well as many others from the Armstrong and Wong Groups. Not only have you put up with me (even on my most over caffeinated days!) but you have all helped me no end and made every day so enjoyable. I could not have asked for a better group of people to work with. There are also many other people in the Chemistry Department that have made this possible – thank you.

There are lots people I have met or become better friends with over the last few years. Special thanks go to my lunch buddy Ness, to Ed for proof reading and to Emma for being awesome. Last but not least I thank Sean and my amazing family for all that they do for me.

Collaborations and assistance

Many of the enzymes used in this work were generously prepared and provided by collaborators or other research groups:

Enzyme	Collaborator
Ralstonia eutropha NAD^+-reductase	L. Lauterbach, O. Lenz Group (Technical University, Berlin, Germany)
Rhodococcus opacus soluble hydrogenase	K. Karstens, B. Friedrich Group (Humboldt University, Berlin, Germany)
E. coli hydrogenases (Hydrogenase-1 and Hydrogenase-2)	Armstrong / Vincent Group (University of Oxford)
D. vulgaris Miyazaki F. hydrogenase	W. Lubitz Group (Max-Plank-Institute, Mülheim, Germany)
Flavin monooxygenase	A. Bregman, A. Fishmann Group (Technion, Haifa, Israel)
*S*4-alcohol dehydrogenase	Johnson Matthey (X-Zyme)

I am grateful to the Lenz Group and in particular Dr Lars Lauterbach and Ms Katja Karstens for preparation of the NAD^+-reductase samples, hosting me in their lab in Berlin, teaching me how to prepare and purify enzyme samples and for sharing their expertise in handling the samples. I would also like to thank the Fishmann Group for providing samples of the FMO enzyme and for adopting me at the BioTrans conference in Manchester! I also enjoyed the time that Janina Preissler from the Lenz Group and Almog Bregman from the Fishmann Group spent with us in Oxford; I learnt a great deal working with both of them.

Some of the experiments in this Thesis were conducted by Part II (P2) students under my supervision. The relevant experiments are highlighted as such throughout. In each case, I developed the methodology and aided the students for this work. In some sections, data from

a previous DPhil student is discussed or reproduced, this is referenced as appropriate. A summary of the relevant sections is given below:

Section	Figure (F) or Table (T)	Person	Comments
3.2.3	F 3-5	Ms Chloe Tomlinson (P2)	
3.7.4	T 3-2	Mr Thomas Lonsdale (P2) Ms Janina Preissler (Masters Student, Humboldt University, Berlin)	Characterisation of NAD^+-reductase variants; the data is discussed but not shown
3.7.4, 4.2	T 3-2	Ms Jenny Bradley (P2)	Characterisation of *Rhodococcus opacus* HoxHYFU; the data is discussed but not shown
4.2.2	F 4-2(b)	Dr Zukifli Idris	Catalytic bias of *Ralstonia eutropha* data is shown for comparison to *Rhodococcus opacus* and discussed
5.6, 6.5		Mr Jonathan Quinson	Preparation of the carbon nanotube columns
5.8.	F 5-25	Ms Chloe Tomlinson (P2) Dr Philip Ash	Assistance in performing the experiment
6.3.3.	F 6-5	Dr Zulkifli Idris Dr Philip Ash	Assistance in performing the experiment
7	F 7-3, 5, 7, 8, 9	Ms Chloe Tomlinson (P2)	
8.2	F 8-3	Mr Thomas Lyle (P2)	
8.3	F 8-4	Ms Jenny Bradley (P2)	

Publications

1. Reeve, H.A. and Vincent, K.A in Catalysts for Alcohol-Fuelled Direct Oxidation Fuel Cells, eds. Z. X. Liang and T. S. Zhao, (RSC, Cambridge, 2012), pp. 206-226

2. Reeve, H.A., Lauterbach, L., Ash, P.A., Lenz, O., Vincent, K.A., 'A modular system for regeneration of NAD cofactors using graphite particles modified with hydrogenase and diaphorase moieties', *Chemical Communications*, 2012, **48** (10), 1589-1591

Previous publications:

3. Healy, A.J., Reeve, H.A., Parkin, A., Vincent, K.A., 'Electrically conducting particle networks in polymer electrolyte as three-dimensional electrodes for hydrogenase electrocatalysis', *Electrochimica Acta*, 2011, **56**, 10786-10790

4. Healy, A.J., Reeve, H.A., Vincent, K.A., 'Development of an infrared spectroscopic approach for studying metalloenzyme active site chemistry under direct electrochemical control', *Faraday Discussions*, 2011, **148**, 345 - 357

Abbreviations

ADH	alcohol dehydrogenase
BINAP	(2,2'-bis(diphenylphosphino)-1,1'-binaphthyl)
BP	black pearls / black pearls 2000
BSA	bovine serum albumin
CE	counter electrode
CNC	carbon nanotube column
CNT	carbon nanotube
CV	cyclic voltammogram
D. vulgaris	*Desulfovibrio vulgaris*
de	*diastereomeric excess*
DMSO	dimethyl sulfoxide
Dv MF	*Desulfovibrio vulgaris* hydrogenase 1
E	electrode potential
e	charge of an electron
E. coli	*Escherichia coli*
ee	*enantiomeric excess*
*E*onset	onset potential
*E*switch	switch potential
F	Faraday's constant = 96,485 C mol^{-1}
FAD	flavin adenine dineucliotide
FDH	formate dehydrogenase
FMN	flavin mononucleotide
FMO	flavin monooxygensae
FNR	ferrodoxin $NADP^+$-reductase
FTIR	Fourier transform infra-red
GDH	glucose dehydrogenase
GlyDH	glycerol dehydrogenase
HbpA	2-hydroxybiphenyl 3-monooxygenase
HoxFU	NAD^+-reducing subunits of the soluble hydrogenase
Hox~~HY~~FU	varient of the soluble hydrogenase with inactive hydrogenase dimer
HPLC	high performance liquid chromotography
Hyd-1	*Escherichia coli* Hydrogenase 1
Hyd-2	*Escherichia coli* Hydrogenase 2
IR	infra-red
k_I	inhibition constant
k_M	Michaelis constant
KPB	potassium phosphate buffer
LDH	lactate dehydrogenase
MBH	*Ralstonia eutropha* membrane bound hydrogenase
N_A	Avagadro constant
NAD^+	nicotinamide adenine dinucleotide (oxidised)

NADH	nicotinamide adenine dinucleotide hydride (reduced)
$NADP^+$	nicotinamide adenine dinucleotide phosphate (oxidised)
NADPH	nicotinamide adenine dinucleotide phosphate hydride (reduced)
P450	cytochrome P450
PFE	protein film electrochemistry
PG	pyrolytic graphite
PGE	pyrolytic graphite 'edge'
Q	charge
R	the gas constant = 8.314 J K^{-1} mol^{-1}
R. eutropha (*R. e*)	*Ralstonia eutropha* H16
RDE	rotating disk electrode
RE	reference electrode
RH	*Ralstonia eutropha* regulatory hydrogenase
Rh. opacus (*Rh. o*)	*Rhodococcus opacus*
r_t	retention time
SCE	saturated calomel electrode
SE	soluble extract
SH	soluble hydrogenase
SHE	standard hydrogen electrode
TOF	turnover frequency (number of product generated per second per enzyme)
TN	turnover number (moles product generated per mole cofactor used)
TTN	total turnover number (number of product generated per enzyme)
U mg^{-1}	units mg^{-1} = µmole min^{-1} mg^{-1}
UV-vis	ultraviolet-visible
WE	working electrode
WT	wild type
ε	extinction coefficient

Table of Contents

New approaches for cofactor recycling; application to chemical synthesis and electrochemical devices ..... **i**

Acknowledgements ..... **iii**

Collaborations and assistance ..... **v**

Publications ..... **vii**

Abbreviations ..... **ix**

Table of Contents ..... **xi**

Chapter 1 Introduction **1**

1.1 Traditional methods for ketone reduction 5

1.1.1 Using stoichiometric redox reagents 6

1.1.2 Using H_2 as a reducing equivalent 8

1.1.3 Electrochemical 10

1.1.4 Requirements for an ideal hydrogenation strategy 11

1.2 Enzymes for selective ketone reduction 11

1.2.1 Whole cells for chemical synthesis 14

1.2.2 Isolated enzymes for chemical synthesis 15

1.2.3 Use of immobilised enzymes 16

1.3 Enzyme catalysed O atom insertion reactions 17

1.4 Existing methods for cofactor regeneration 19

1.4.1 Enzyme catalysed cofactor regeneration 20

1.4.2 Electrochemical NAD^+ reduction 25

1.4.3 H_2-driven cofactor regeneration 30

1.4.4 Artificial cofactors 32

1.4.5 Is the 'cofactor challenge' still present? 33

1.5 The enzymes used in this work 34

1.5.1 Hydrogen cycling enzymes 34

1.5.2 Soluble NAD^+-reducing hydrogenase 36

1.6 Cofactor regeneration systems developed in this project 38

Chapter 2 Theory and Methods **41**

2.1 Electrochemistry 41

2.1.1 The Nernst equation 42

2.1.2 Protein Film Electrochemistry[192,193] 42

2.1.3 Electrochemical setup 44
2.1.4 Working electrodes – for analytical electrochemistry 45
2.1.5 Reference electrodes 46
2.1.6 Counter electrode 47
2.1.7 Electrochemical cells 48
2.1.8 Electrochemical techniques 49
2.1.9 Limitations and considerations 52
2.2 High surface area electrodes 53
2.2.1 Review of scale-up of hydrogenase electrodes 54
2.2.2 Materials used for high surface area electrodes 55
2.2.3 How much enzyme is immobilised and how active is it? 57
2.3 Enzyme kinetics and electrochemical analysis 58
2.3.1 Affinity constant (k_M) 58
2.3.2 Inhibition constant (k_I) 61
2.4 Ultraviolet-visible spectroscopy 62
2.4.1 Concentration determination using UV-vis spectroscopy 63
2.4.2 UV-vis spectrophotometers and experimental methods 64
2.5 High-performance liquid chromatography 65
2.6 Infrared spectroscopy 66
2.6.1 Theory of IR spectroscopy 67
2.6.2 *In situ* product detection 67
2.6.3 Monitoring immobilised enzymes using IR 69
2.7 Reagents 70
2.7.1 Buffers 70
2.7.2 Cofactors 71
2.7.3 Gases and preparation of gas mixtures 73
2.7.4 Other reagents 73
2.8 Enzyme samples 74
2.8.1 NAD^+-Reductase 74
2.8.2 Hydrogenases 75
2.8.3 Cofactor-dependent enzymes 76
2.9 Summary 77

Chapter 3 Electro-enzymatic NADH generation 79

3.1 Structure and electrochemistry of the NAD^+-reductase 79
3.1.1 The constructs used in this work 82
3.1.2 Overview of NAD^+-reductase electrochemistry 83
3.2 Development of high-surface area electrodes 84

3.2.1 Preparation of high surface area electrodes 84
3.2.2 Carbon paper electrodes 85
3.2.3 Carbon particle electrodes 88
3.2.4 Comparison of the catalytic activity per geometrical electrode area 90
3.3 Electro-enzymatic NADH generation 91
3.3.1 Investigating a suitable potential for NAD^+ reduction 92
3.3.2 Initial 'proof-of-concept' NADH generation 94
3.3.3 Confirming the electrochemically generated NADH is enzyme-active 97
3.3.4 Scale-up of the electro-enzymatic NADH generation system 98
3.4 Improving the stability of the electro-enzymatic system 100
3.4.1 Building robust, uniform electrodes from carbon paper 100
3.4.2 Using a Nafion polymer to increase the enzyme stability 102
3.4.3 Methoxy-poly(ethylene) glycol (mPEG) modification 104
3.5 Other NAD^+-reducing enzymes and constructs 104
3.5.1 A note on industrial scale enzyme preparation 105
3.5.2 Crude extract 106
3.5.3 *Rhodococcus opacus* soluble hydrogenase 108
3.5.4 Variants of the SH for electro-enzymatic NADPH generation 108
3.5.5 Can other types of NAD^+-reducing enzymes be used? 110
3.6 Summary and outlook 112

Chapter 4 Electrochemical characterisation of SH from *Rhodococcus opacus* 115
4.1 Introduction 116
4.1.1 The SH from *Rhodococcus opacus* 116
4.1.2 Isolation of the HoxHY and HoxFU moieties 117
4.2 Electrochemical analysis of the NAD^+-reducing subunits, HoxFU 117
4.2.1 HoxFU for NAD^+/NADH cycling 118
4.2.2 Catalytic bias 119
4.2.3 Determination of the affinity constants for NAD^+ and NADH 120
4.2.4 Product inhibition constants 123
4.3 Soluble hydrogenase HoxHY dimer 124
4.3.1 Determination of E_{switch} for *Rh. o* HoxHY 125
4.3.2 Stability of HoxHY from *Rh. o* 127
4.3.3 Electrochemical analysis of the O_2-tolerance of HoxHY from *Rh. o* 128
4.4 Summary 132

Chapter 5 H_2-driven NADH generation 133
5.1 Introduction 134

5.2 Electrochemistry of hydrogenases 138
5.2.1 *Desulfovibrio vulgaris* MF [NiFe] hydrogenase 139
5.2.2 *E. coli* hydrogenase 2 140
5.3 Methods and experimental design 141
5.3.1 Using electrochemistry to balance H_2 oxidation and NAD^+ reduction 141
5.3.2 Experimental set-up with *ex situ* UV-vis detection 143
5.3.3 Experimental set-up with *in situ* UV-vis detection 144
5.4 H_2-driven NADH generation 146
5.4.1 Towards *in situ* UV-vis detection 148
5.4.2 Enzyme-modified particles for H_2-driven NADH generation with *in situ* UV-vis detection 150
5.4.3 Factors affecting the kinetics of H_2-driven NADH generation 151
5.4.4 Analysis of the cofactor produced 152
5.4.5 Control experiments 154
5.4.6 Other carbon materials 155
5.5 Characterisation using carbon black particles 157
5.5.1 Changing the ratio of enzymes on the particles 158
5.5.2 Effect of pH on H_2-driven NADH generation 161
5.5.3 H_2-driven NADH generation at low H_2 partial pressure 164
5.5.4 Reusing the particles 166
5.6 Modularity of the system 167
5.6.1 Changing the hydrogenase 168
5.6.2 Changing the NAD^+-reductase 168
5.6.3 Operation in reverse for NAD^+ generation 169
5.6.4 H_2-driven NADH generation in a novel flow system 171
5.7 Infrared spectroscopy to probe the electron transfer 172
5.8 Summary 175

Chapter 6 Coupling NADH recycling to cofactor-dependent enzymes 179
6.1 Introduction 179
6.2 UV-vis assays of cofactor-dependent enzymes 181
6.3 Electrochemical NADH supply 184
6.3.1 Electrochemical cofactor cycling – LDH in solution 184
6.3.2 Characterisation of an immobilised ‘enzyme cascade’ 185
6.3.3 *In situ* detection of pyruvate generation 189
6.3.4 *Ex situ* detection of pyruvate generation 191
6.4 Carbon particles for H_2-driven cofactor supply 193
6.4.1 Cofactor-dependent enzyme in solution 193

6.4.2 Cofactor-dependent enzyme co-immobilised....194
6.5 Carbon nanotubes columns....202
6.6 Summary....204

Chapter 7 O_2-tolerant NADH recycling to supply oxygenase catalysis....205
7.1 O_2-tolerant hydrogenases....207
7.1.1 Thermodynamic considerations....207
7.1.2 Electrochemistry....209
7.1.3 Coupling H_2 oxidation and NAD^+ reduction....211
7.2 H_2-driven NADH supply in the presence of O_2....213
7.3 Use of biphenyl-2-ol 3 monooxygenase (HbpA)....214
7.3.1 Adsorption of substrate and product onto BP particles....216
7.3.2 Activity of HbpA in low O_2 mixtures....217
7.4 H_2-driven NADH supply to HbpA....218
7.5 Summary....220

Chapter 8 Electrochemical devices for cofactor-dependent oxidation reactions....221
8.1 Introduction....222
8.1.1 Electrochemical devices set-up....223
8.2 Towards a glycerol oxidation fuel cell....226
8.2.1 Limitations to using glycerol dehydrogenase....228
8.2.2 Electrochemical response from glycerol injections....228
8.2.3 Can glycerol dehydrogenase use crude biodiesel waste?....231
8.3 Development of a biosensor....232
8.4 Summary....233

Chapter 9 Conclusion....235

Bibliography....239

Appendices....i

Science Innovation Plus, Final Report 2013-2013....xiv

Chapter 1 Introduction

Individual isolated enzymes have drawn attention due to their ability to carry out highly specific biotransformations very efficiently under mild conditions. This activity can be exploited in a range of applications including chemical synthesis,[1–7] biosensors[8–10] and enzyme fuel cells.[11–15] This Thesis is primarily concerned with simplifying the use of redox enzyme systems for selective biotransformations in chemical synthesis however some of the techniques can also be applied to electrochemical devices.

The area of biotechnology for chemical synthesis requires input from chemists, microbiologists and chemical engineers to develop systems that can exploit the advantages that enzymes offer. Implementation of some biocatalytic systems has shown improvements in process emissions, waste production and energy consumption in comparison to traditional metal catalysis.[16–21] As such, biocatalysis was highlighted as *"key to creating a low-carbon economy"* in a 2009 report to the UK government by the Industrial Biotechnology Innovation and Growth Team.[22] Incredible advances in enzyme engineering have been made. It is now viable for chemical and pharmaceutical companies to design a biological catalyst for a particular reaction and set of reactor conditions.[23–25] A particularly well-analysed example of

this is the evolution of an enzyme for a biotransformation in the synthesis of Sitgaliptin where Merck and Codexis together developed an enzyme to carry out the selective reduction of a non-natural ketone to a single enantiomer of an amine, Figure 1-1.[26–28]

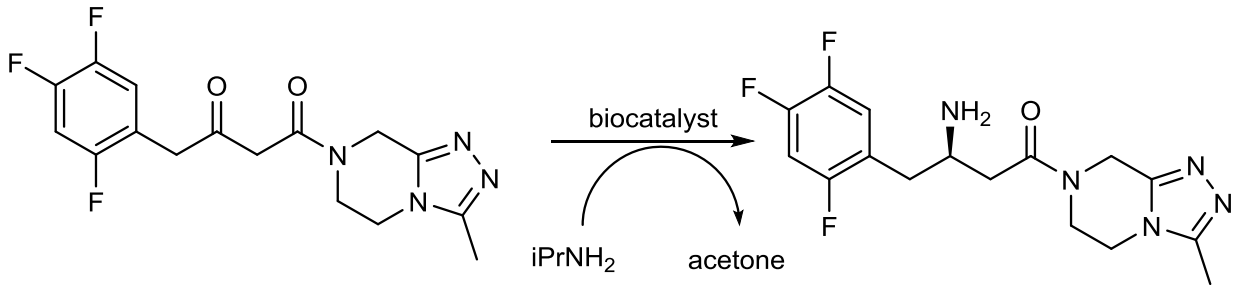

Figure 1-1: The biocatalytic step for selective reduction of a non-natural ketone to an amine in the synthesis of Sitagliptin.

This process gave a range of environmental and economic benefits and is one of few examples where a complete analysis of a traditionally catalysed synthesis can be directly and fairly compared to a biocatalytic process. Overall the biocatalytic process led to an increase in the yield (13 %) and productivity (g L^{-1} h^{-1}, 53 %) as well as a decrease in the total waste produced (19 %); the engineered enzyme tolerates 200 g L^{-1} substrate (higher than the metal catalyst) and operates in 50 % aqueous DMSO generating an optically pure product (>99.95 % *enantiometic excess* (*ee*)).[19] Significantly this avoided the requirement for a transition metal (Ru) catalysed hydrogenation step which requires specialist high-pressure equipment and expensive methods to ensure complete removal of the metal from the product. Furthermore the transition metal-catalysed hydrogenation was less selective than that of the enzyme leading to the need for further purification steps to isolate an optically pure product.

In particular enzymes can offer huge benefits for reduction reactions (as seen above), specifically for the reduction of prochiral molecules to enantiomerically pure products. Well-established examples include the reduction of a ketone to a chiral alcohol and enzyme cascades for reduction of a ketone to a chiral amine. Methods for selective reduction of a ketone to a chiral alcohol are essential, especially in the production of fine chemicals and

pharmaceuticals where enantioselectivity is crucial. It is expected that 95 % of pharmaceuticals will be chiral by 2020,[29] however, at present many chemical companies buy in building blocks with chiral centres due to the challenges associated with the traditional synthetic approaches. Furthermore, since oxidative chemical steps tend to have significant safety and toxicity concerns, companies tend to begin a synthesis with a more oxidised molecule and thus require a 'toolbox' of techniques for reductive steps.

Such biocatalytic systems require stoichiometric reductants and therefore co-substrates. Many of the co-substrates used as a 'hydride' and proton source are not very atom efficient (Section 1.4.1); consequently the environmental and economic benefits of these biocatalytic processes become much less clear as large quantities of carbon waste are generated. In this Thesis, the existing limitations of using redox enzymes for these kinds of transformations will be considered, and two novel approaches for using them developed. These approaches use either an electrode (electrons) or H_2 as clean reducing equivalents; both have been identified as 'green' alternatives to the existing methods[30] that could improve the environmental factor (*E* factor)[31] of enzyme catalysed reduction reactions. At present neither is used on an industrial scale due to a range of limitations (discussed in Section 1.4).

In this Introduction, first the traditional methods for reductive synthetic steps will be considered followed by the progress and limitations of enzyme catalysis in this area. In general, these discussions will be limited to the reduction of ketones to alcohols using isolated enzymes, as these are the test reactions chosen for a large part of this work, and further limited to reactions relevant to the pharmaceutical industry. Although similar methods may apply to other commodity chemicals, the process and product purity requirements are likely to be very different. The high-value low-volume pharmaceutical market tends to be better suited to isolated enzyme catalysis at present and in many cases the biocatalytic approaches surpass the traditional processes allowing them to become a 'first choice' synthetic method.[32–34] The systems developed will also be extended towards O atom insertion reactions. Although these

reactions lead to substrate oxidation, when using molecular oxygen as the O atom source electrons are required for its reductive activation. Finally the approaches developed in this work, focusing on two novel cofactor regeneration systems will be introduced along with an over view of the enzymes used. A brief schematic overview of the work carried out is shown in Scheme 1-1.

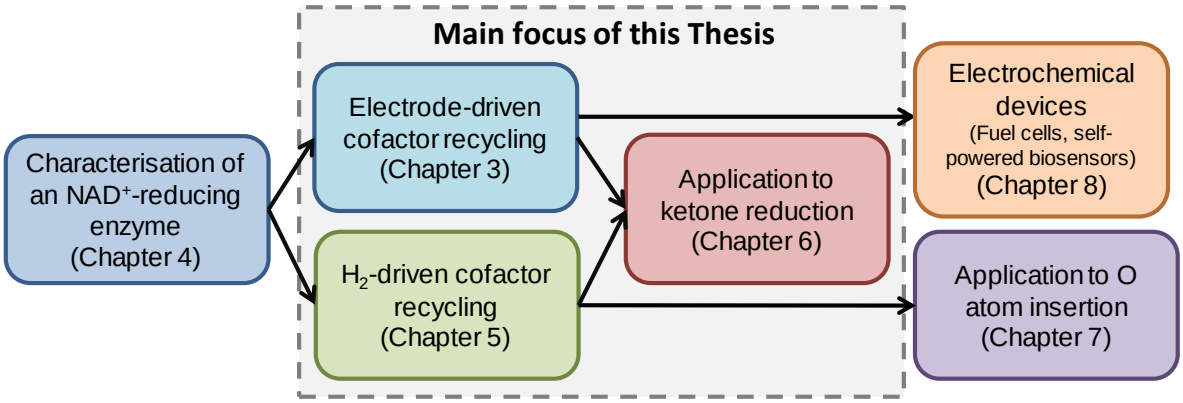

Scheme 1-1: This work develops two methods for using redox enzymes for chemical synthesis with a focus on the reduction of ketones. The systems are further extended towards oxidative synthetic steps and electrochemical devices.

In order to discuss the methods for selective ketone reduction the associated challenges and the nature of the ketone group should be revised. The carbon of a ketone group is sp^2 hybridised and has 3 σ bonds (2 to carbon and 1 to oxygen) and a π bond between the C and O atoms. The carbonyl group is planar with π-electron density above and below the plane. Due to the higher electronegativity of oxygen, the carbonyl group is polarised with a partial positive charge on carbon (Figure 1-2a); in a ketone, the charge on carbon can be stabilised if R_1 and/or R_2 are electron-releasing groups. For reduction of a ketone to an alcohol, H_2 must be added across the C=O double bond, this can be thought of as hydride addition to the electrophilic carbon and proton addition to the oxygen. This reaction leads to re-hybridisation of the carbon atom to sp^3, generating a chiral product if R_1 and R_2 are non-equivalent. Furthermore, if either R_1 or R_2 is chiral, multiple diastereoisomeric products are possible; the diastereoselectivity is controlled by stereoelectronic considerations (Felkin-Ahn model)[35] for an irreversible reaction and thermodynamic considerations in a reversible reaction.

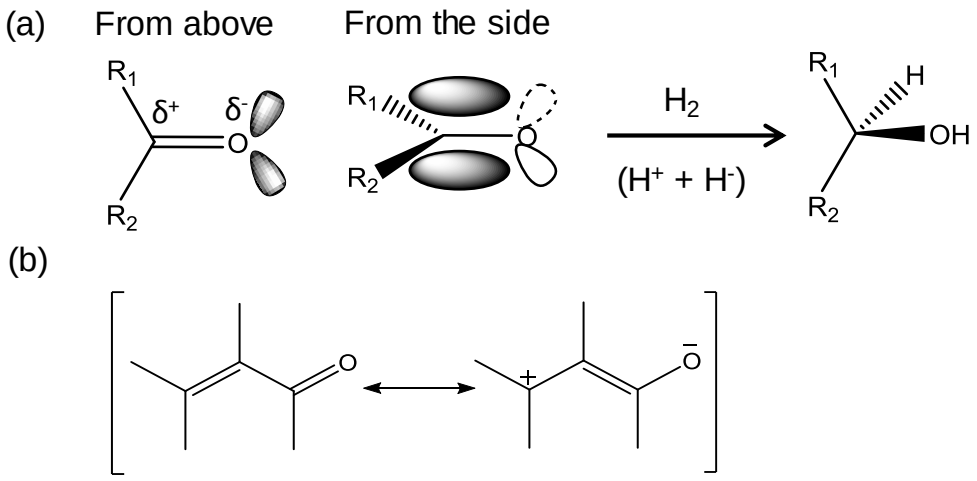

Figure 1-2: (a) The structure of a ketone and the hydrogenation product, an alcohol. (b) Unsaturated ketones are less active towards nucleophilic attack, either 1,2- or 1,4-reduction can occur leading to a mixture of products including the unsaturated alcohol.

The extent of ketone to alcohol conversion is determined by the equilibrium constant and is dependent on the stability of the ketone (increased if the R groups are electron donating) compared to the stability of the alcohol (decreased if the R groups are bulky). For these reasons, the equilibrium constant for ketone reduction tends to be much less favourable than for aldehyde reduction where R_1 is a hydrogen atom which does not stabilise the carbonyl and does not provide steric hindrance to the tetrahedral alcohol.

Unsaturated alcohols are key intermediates in the synthesis of flavours, fragrances and pharmaceuticals.[36,37] A considerable challenge for ketone hydrogenation is selective reduction of α,β-unsaturated ketones where the carbon of the carbonyl is less electrophilic than in the saturated analogue (Figure 1-2(b)). Depending on the method for reduction, a mixture of products including the unsaturated alcohol, saturated ketone and unsaturated alcohol are formed following 1,2 or 1,4 reduction.

1.1 Traditional methods for ketone reduction

The enantio- and/or chemo-selective reduction of a (prochiral) ketone to an alcohol is an important synthetic step. Here, traditional methods for carrying out ketone reduction reactions are reviewed to enable comparison to the analogous enzyme-catalysed reactions.

1.1.1 Using stoichiometric redox reagents

The most common reagents for ketone reduction are $LiAlH_4$ and $NaBH_4$. The metal-hydrogen bond in $LiAlH_4$ is highly polarised facilitating attack of the hydride onto the carbon-oxygen double bond to form an alkoxide. Co-ordination of the nucleophilic oxygen to the Lewis acidic metal ion further drives the reaction by increasing the polarisation across the C=O bond. The reaction is irreversible; work-up in the presence of a proton source generates an alcohol. Overall, this reaction equates to the addition of H_2 across the carbon-oxygen double bond.

Due to the very high reactivity of $LiAlH_4$, it has low chemoselectivity which prevents its use with highly functionalised starting materials. Carbonyl groups tend to be reduced in order of electrophilicity, aldehyde – ketone – ester – carboxylate however; many other functional groups can also be reduced (including epoxides, nitriles and nitro moieties). The reactivity of $LiAlH_4$ can be tuned by generation of alkoxyaluminium hydrides ($Li[AlH(OBu^t)_3]$) which attack aldehydes and ketones but not esters and nitriles. However, solid $LiAlH_4$ is highly flammable; careful control is required to prevent highly exothermic conditions.[38]

In general $NaBH_4$ is preferred since it is available in bulk, reliable and the more cost efficient hydride equivalent,[39] for this reason it is more commonly used for the reduction of ketones and aldehydes unless the substrate is too unreactive. Unlike $LiAlH_4$ which reacts violently with water and must be used in aprotic solvents, $NaBH_4$ can be used in solvents such as methanol and water. The $NaBH_4$ reducing agent can be modified to aid selectivity. The sodium can be replaced by other cations including Li and Ca to increase the reactivity towards esters. By adding bulky ligands to these reducing agents, substrate-controlled diastereoselective reductions can be achieved, this selectivity can be further improved using cryogenic temperatures however this adds expense. The use of chiral ligands can give enantioselectivity and therefore can be used for asymmetric ketone reduction.[40,41] The use of

cerium trichloride ($CeCl_3$) can further increase selectivity, particularly for selective 1,2-reduction of an unsaturated ketone to the alcohol (with no 1,4-reduction) and to selectively reduce a ketone in the presence of a (more reactive) aldehyde.

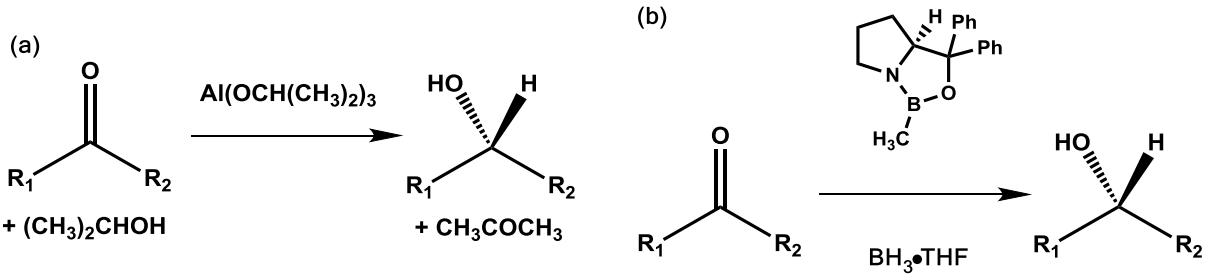

Figure 1-3: Methods for the reduction of ketone to secondary alcohols; (a) the Meerwein-Ponndorf-Werley reaction and (b) using Corey, Bakshi, and Shibata catalysts.

Another classical method for ketone reduction is the Meerwein-Ponndorf-Werley reaction which uses an aluminium alkoxide, commonly $Al(OPr^i)_3$, as a catalyst with an alcohol hydride source (often isopropanol) under thermodynamic conditions, Figure 1-3(a).[42,43] The reactions proceed under mild conditions and the equilibrium can be pushed to favour alcohol production by distillation of the acetone formed on hydride transfer. However, a large excess of the alcohol hydride source is required for high substrate to product conversion and side reactions can occur limiting the selectivity of the reactions. Furthermore, high catalyst loadings tend to be required.[42] Some enantioselectivity can be obtained by using a chiral hydride source[43] or catalyst.[44] However, aldehydes are reduced before ketones must therefore be protected if both functionalities are present in a starting material.

A final class of reductants considered here are boron hydride-based catalysts (Figure 1-3(b)),[45,46] where *ca* 1 equivalent of BH_3·THF is added with a Corey, Bakshi, and Shibata (CBS) type catalyst. Ketone reduction proceeds *via* a six-membered cyclic transition state yielding high enantioselecitity.[47] Example of CBS type catalysis include production of bioactive β-agonists[48] and carbinoxamine[49] with 99 % *ee*.

Sterically hindered Grignard reagents can be used for the reduction of a ketone to a tertiary alcohol;[50] however this discussion has been limited to the reduction of ketones to secondary

alcohols.

In each of these examples, the hydride source is required at super-stoichiometric quantities for substantial ketone reduction. This leads to generation of large quantities of metal waste which must be removed and thus complicates reaction workup and product isolation.[38] Although the reactivity can be tuned in each case, achiving high selecitivty in complex molecules remains a challenge.

1.1.2 Using H_2 as a reducing equivalent

Precious metal catalysts can be used for catalytic hydrogenation reactions using H_2 as the reducing equivalent thus eliminating the requirement of stoichiometric hydride reagents in solution and providing a highly atom efficient synthetic pathway. Such catalytic methods are considered to be more viable for the future as they save energy, are more economical and tend to be more environmentally friendly.[51] Metal-ligand complexes can be designed such that asymmetric reductions are also possible with tuning being made possible by using both steric and electronic considerations.[52] There is much continued research into design of metal catalysts for efficient, selective, hydrogenation reactions.

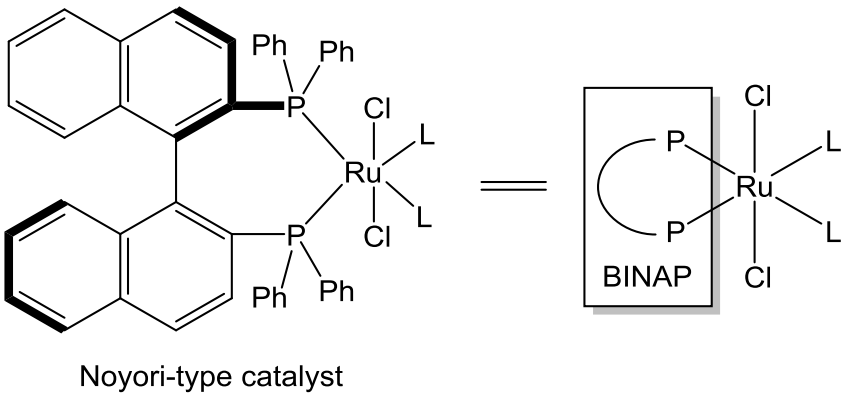

Figure 1-4: General structure of a Noyori-type pre-catalyst consisting of a metal (Rh or Ru) co-ordinated by BINAP (or a BINAP analogue), 2 chlorines and 2 other ligands (L). On addition of H_2, a metal hydride is formed and HCl is lost. Due to the chirality of the BINAP ligand, after binding the prochiral substrate, one diastereomeric transition state is energetically favoured.

Noyori shared the Nobel Prize in Chemistry in 2001[53,54] for his work in asymmetric hydrogenation of ketones and Noyori-type catalysts are widely reported and reviewed in the

literature.[55–60] Such catalysts tend to use BINAP ((2,2'-bis(diphenylphosphino)-1,1'-binaphthyl) or a BINAP analogue and other ligands (often from the solvent) to tune a metal for asymmetric hydrogenation catalysis, Figure 1-4.

As an example, in 2011 Goto *et al.* demonstrated the scale-up of an Ru catalyst system with a BINAP analogue (a novel bisphosphine, bidentate ligand) and another diamine ligand. This system operated at a substrate-to-catalyst ratio of 2000:1 and a H_2 pressure of 8.5 bar leading to full conversion with 94 % *ee*. A recrystallisation step provided an enantiopure product with 82 % yield. This was scaled-up to demonstrate generation of 34 kg product;[57] turnover frequencies were in the region of 65-85 h^{-1}.

Catalytic hydrogenation of α,β-unsaturated ketones using metals such as Pd, Rh, Ni and Pt often leads to 1,4-reduction; for this reason more selective catalysts are required.[61,62] Although progress is being made in this area most of the catalysts developed can achieve either high selectivity or high activity.[63–65] Tamura *et al.* report a highly active and selective catalyst (Ir-ReO_x/SiO_2) for generation of unsaturated alcohols using relatively mild conditions of water, 8-80 bar H_2, 303-343 K, with a total turnover number (TTN –defined in this work as mole product generated per mole catalyst used) of 5500 and an initial turnover frequency (TOF) of 126000 h^{-1} (= 35 s^{-1}).[66] However, this is still using a relatively high H_2 pressure, an expensive metal and by comparison with many enzymes gave a low TTN.

Similarly, Rh, Ru and Ir have been highlighted as catalysts for preparation of chiral intermediates by selective H_2 addition to alkenes, ketones, imines and heteroaromatic compounds. In particular they are attractive due to high activity and selectivity, broad substrate scope, optimal atom economy and for minimising by-product generation. At present, Fe, Cu and Co are being researched to replace these more expensive metals.

This area of research is growing; there are continual improvements to these catalytic hydrogenations for improved selectivity, higher activity, increased substrate to catalyst

loading and lower H_2 partial pressure requirements. However, at present many are limited by one or more of these factors. Furthermore, the requirement for specialist high pressure system and extensive purification (to remove and recover the toxic and expensive metals) adds significant costs to these synthetic approaches.

1.1.3 Electrochemical

An electrode can be considered as an 'ideal' electron source for a reduction reaction since no soluble reagent is required.[67] In general, the electrochemical step generates reactive intermediates *in situ* allowing reactions to occur without the use of harsh / toxic reagents. One of the first investigations into electrosynthesis was carried out in the early 1800's (Faraday, Kolbe)[68] and much research has been carried out since. However at present few industrial processes take advantage of these techniques, and electrochemical oxidations are much more widely reported than reductions.

Electrode materials for reductions tend to be C, Pt or Hg based and the systems operate in a N_2 atmosphere to prevent O_2 reduction at the electrode. In broad terms, electrosynthesis can be split into two classes; direct electrolysis, where the electrochemical step occurs at the electrode and indirect electrolysis, where a soluble mediator is used to transfer the electrons between the electrode and a substrate,[69] this is discussed further in Section 1.4.2. Carbonyl reductions tend to lead to non-selective reduction and particularly to dimerisation products (pinacol reaction) *via* one-electron one-proton additions; to improve the alcohol yield the rate of the second electron transfer must be faster than that of the dimerization, however, this requires very negative potentials equating to large energy requirements, electrode fouling and often undesired side reactions. The mechanism of phenyl ketone reduction at dropping mercury electrodes has been studied at a range of pH values.[70]

In 1976 Mairanovskii *et al.* demonstrated use of an Hg electrode for benzaldehyde reduction to the primary alcohol; they reported high conversion to the alcohol product at low

concentrations of benzaldehye however this was not possible at higher substrate loadings. The electrochemical reductions were carried out at *ca* -1.7 V *vs* SHE (a very negative potential).[71]

Related photoredox catalysis using metal (Ru or Ir) complexes and light are also growing areas of research.[72] Rono *et al.* demonstrated the first enantioselective Aza-pinacol cyclisation of a ketone *via* a proton coupled electron transfer with up to 95 % *ee*.[73] As previously metioned, at present there are very few examples of electrochemical processes applied to the synthesis of fine chemicals.

1.1.4 Requirements for an ideal hydrogenation strategy

This Section has highlighted the existing approaches to ketone reduction and associated limitations; there is a clear need for improved hydrogenation pathways. An ideal system would be catalytic and use either H_2 or an electrode as the reducing equivalent preventing carbon-based waste. The catalyst would:

- be non-toxic, inexpensive, renewable / biodegradable
- operate at low loading to enabling high turnover numbers (moles of product generated per mole of catalyst used)
- be active with respect to turnover frequency (moles of product per mole of catalytic site per second) and total turnover number (moles of product generated per mole of cofactor supplied)
- offer near perfect enantio-, regio- and chemo-selectivity
- be applicable in orgnic solvents

It is likely that the resulting process would simplify product isolation and be more environmentally and economically viable.

1.2 Enzymes for selective ketone reduction

Industrial use of cofactor-dependent enzymes is increasing and has been identified as an important method for introducing chiral alcohol and amine functionalities. Using enzymes to catalyse reactions with almost perfect selectivity, with no heavy metals or toxic reagents

could have a huge impact on the costs of downstream processing. In some cases the milder conditions generally required for enzyme catalysis can also decrease production costs and waste generation providing more efficient, cleaner synthetic pathways.[19,27] Furthermore the prices of some commonly used precious-metal catalysts (Pt and Rh in particular) are very high and often fluctuate; this is a significant challenge for chemical companies and can affect the prices of pharmaceuticals over time. In contrast, it is now possible to produce enzymes for as little as $10/kg (US $) in some cases, using cheap, renewable starting materials such as glucose. However, some enzymes that have undergone many rounds of engineering to catalyse a particular biotransformation, in a desired set of conditions (including > 100 g L^{-1}) starting material, high percentage of organic solvents, temperature and pH) can cost up to $1000/kg (US $). These two approaches can satisfy different applications depending on the productivity, purity and cost requirements for the desired product; in some cases the high costs can be justified if there is not an alternative route to a particular product. Overall, many enzymes can now be produced using commercially viable methods with industrially desired activities and prices.

Use of biocatalysts is not new; enzymes (or whole cells) have been used in a range of chemical industries (fermentation, paper, laundry detergents) for many years. However, the application of enzymes to synthetic chemistry, specifically targeted at generating enantiopure molecules for fine chemical industries including pharmaceutical, flavour and fragrance molecules is much newer due to a range of complications. A 2002 review of 134 industrial biotransformations (defined as producing >100 kg product per year) highlighted that 89 % generated chiral products that were used as fine chemicals.[74] Furthermore, 30 % used redox enzymes and these account for a large majority of asymmetric syntheses (i.e. generation of chiral molecules where kinetic resolution / de-racemisation is not required).

A significant challenge to using redox enzymes still lies in the requirement for cofactor

recycling (Figure 1-5, the 'cofactor challenge') and the negative effects that most existing approaches have on the environmental and economic factors for a biocatalysed transformation. For this reason, of the redox biotransformations used on an industrial scale, many use whole cells where the natural pathways for supplying reducing equivalents in the form of NADH, remain operational. When using isolated enzymes, substrate reduction requires a continuous source of the expensive cofactor NADH. A method to regenerate this cofactor *via* NAD^+ reduction is essential and usually uses a sacrificial reducing equivalent leading to formation of a waste, oxidised, by-product. These additional components have advantages (often aiding conversion of the desired reaction by shifting the equilibrium) and disadvantages, both economic (complicating final product isolation) and environmental (generation of carbon-based waste).

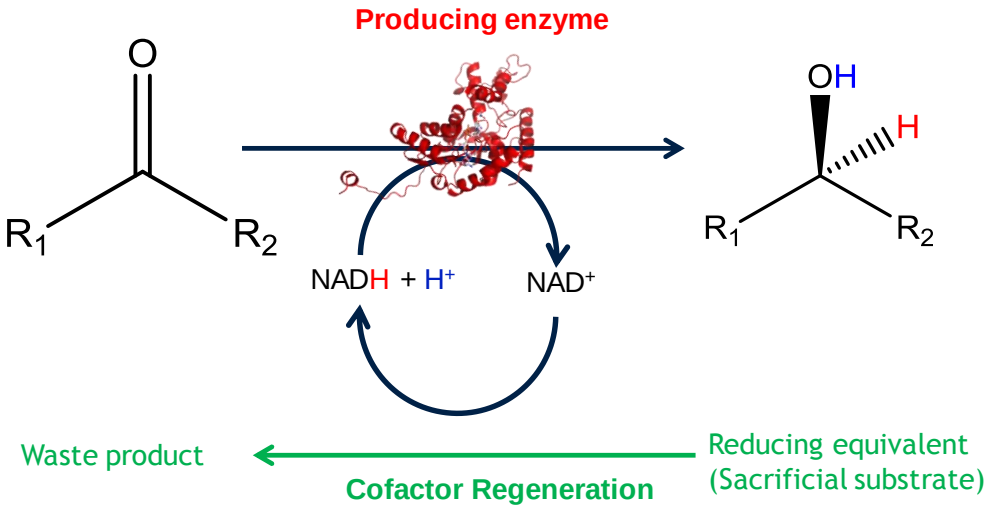

Figure 1-5: The 'cofactor challenge': enzyme catalysed reduction reactions require a stoichiometric, two electron reducing equivalent. This is supplied by a cofactor, often NADH. Each catalytic turnover uses NADH as a hydride source generating the oxidised cofactor NAD^+. This cofactor must be efficiently recycled for a process to be economically viable; this requires a stoichiometric reducing equivalent and generates a waste product.

The next sections review some industrial biocatalytic processes for hydrogenation reactions and discuss cofactor regeneration challenges and solutions. At this stage use of both NADH and the related (but more expensive) cofactor NADPH will be considered.

1.2.1 Whole cells for chemical synthesis

Many approaches to biocatalytic reduction reactions use metabolising cells – where entire catalytic pathways are operational including a range of redox enzymes – although it is also possible to use resting whole cells. Advantageously, this addresses the cofactor regeneration challenge since during metabolism energy is stored as reducing equivalents, some in the form of NADH often *via* the oxidation of glucose (a cheap energy source). The glucose is often oxidised to pyruvate and two NADH molecules, although there are examples of miniulating the metabolic pathway to increase the avaliablilty of reducing equivalents.[75] This means that the NAD^+/NADH ratio inside the cells is carefully maintained using the *in vivo* pathways. Enzymes also tend to be more stable within the cell environment than when isolated,[76] and there is no need for expensive enzyme purification steps. To ensure high purity products are made, it is essential to understand the metabolic pathways and the mechanisms for gene regulation[20] and to remove any enzymes that may act upon the desired product (or substrate) generating side-products. There are also problems associated with transport of substrate and product through the cell membrane which can prevent efficient mass transport and therefore maximum activity of the enzymes.[77] Goldberg *et al.* reviewed biocatalytic ketone reductions using whole cells in 2007.[76]

One example of a whole cell biotransformation is the reduction of ethyl 4-chloro-3-oxobutanoate to (*R*)-ethyl 4-chloro-3-hydroxyoxobutanoate, a valuable chiral building block.[78] An aldehyde reductase from *Sporobolomyces salmonicolor* and the glucose dehydrogenase from *Bacillus megaterium* were co-expressed in *Eschrichia coli* (*E. coli*) and used in a bi-phasic reaction mixture containing substrate, $NADP^+$ and glucose with *n*-butyl acetate as the co-solvent. The glucose dehydrogenase was over-expressed to increase the availability of NADH inside the cells. The product was obtained in 94 % yield, with 92 % *ee* and a turnover number (TN) of 13,500 (moles of product generated per mole of cofactor).

Eli Lilly researchers developed a combined organic chemistry and biocatalysis pathway for the production of LY300164 a type of orally active 2,3-denzodinazepine. *Zygosaccharomyces rouxii* was determined to be an excellent candidate for the reduction of a ketone functional group to generate the desired alcohol product with > 99.9 % *ee*.[79] Since high levels of substrate and product were toxic to the cells, the substrate was added adsorbed onto a resin at *ca* 80 g L^{-1} leading to a solution equilibrium of 2 g L^{-1} (a non-toxic level). The product also adsorbed providing *in situ* extraction and therefore a favourable driving force for the biotransformation.

However, there are considerable drawbacks to whole cell biotransformations. Conditions that enable both cell growth and efficient catalysis of the desired reaction are required; this tends to be achieved by compromising between the two and therefore preventing maximum productivity and the volumetric productivity of the catalyst is very low. Furthermore, the presence of additional enzymes often leads to undesired biotransformations and therefore generation of side-products. This lowers the efficiency of the system, increases the carbon-based waste and complicates product isolation due to the need for additional purification steps. For these reason, many biotransformations instead utilise isolated (purified) enzymes.

1.2.2 Isolated enzymes for chemical synthesis

Over the last 20 years, over-expressed or purified enzymes have become increasingly used in chemical synthesis;[5,32,80,81] this leads to higher purity products by preventing side products generated by other enzymes in the cells with proceeds with higher volumetric productivity than when whole cells are used. However, there are a range of disadvantages: cloning, over-expression and purification of isolated enzymes requires expensive equipment and is time-intensive; furthermore a cofactor recycling strategy is required.

Davis *et al.* at Codexis have demonstrated an alcohol dehydrogenase (ADH) for ketone reduction to an alcohol (used for the production of ethyl-(*S*)-4-chloro-3-hydroxybutyrate) with a glucose dehydrogenase cofactor regeneration system (see Section 1.4.1). After rounds of

directed evolution the biotransformations occurred with >99.5 % conversion to generate a product at > 99 % *ee*.[82] Schmidt *et al.* demonstrated the use of a lactate dehydrogenase from *Staphylococcus epidermidis* for the production of (*R*)-2-hydroxy-4-phenylbutyric acid from the relevant keto acid. This was achieved with > 99.8 % *ee* substantially decreasing the down-stream processing costs, with a TN of 900 (moles product generated per moles cofactor used). The enzyme showed high stability with a deactivation rate of 1.5 % day^{-1}.[83]

Recently, Dascier *et al.* directly compared the activity of using whole cells *vs* crude enzymes for a strain of *E. coli* over-expressing both an alcohol dehydrogenase and glucose dehydrogenase (for cofactor recycling, Section 1.4.1). The whole cells were *ca* 25 times slower, likely due to the requirement for diffusion of substrate across the cell membrane.[84]

In general isolated enzymes are used in batch reactors, and are disposed of after each cycle. However, two-phase systems are desirable since many ketone substrates have poor solubility in water. This led Liese *et al.* to develop an emulsion membrane reactor[85,86] which allows high substrate loadings, simple product extraction and prevents contact between the enzyme and the organic solution. Demonstrated for reduction of 2-octanone to (*S*)-2-octanol with > 99.5 % *ee*, high productivity and high turnover numbers (mole of product per mole of cofactor) were seen. Furthermore, since the product is extracted into the organic phase, downstream processing was simplified. Many types of reactor have been investigated and reviewed.[85]

Overall, the methods for engineering enzymes either to increase stability, activity or solvent tolerance and methods for utilising enzymes for chemical synthesis are improving and are in many cases industrially viable, particularly in the fine chemical sector where the targets tend to be high-value and required in low-volume.

1.2.3 Use of immobilised enzymes

More recently, there is a trend towards using immobilised enzymes in bioreactors for a range of applications including the synthesis of pharmaceutical intermediates and products.[87] This

simplifies recovery and reuse of the biocatalyst and thus extends their operational life-time and lowers the cost of catalyst-to-product. Immobilised biocatalysts also tend to show more resistance to thermal, chemical and shear forces in comparison to biocatalysts used in solution,[88,89] as such immobilisation is one of the most widely utilised approaches to improving enzyme stability.[90–92] Direct immobilisation (by adsorption) and covalent attachment to a carrier, as well as carrier free strategies have all been investigated.[93–96] The latter involves formation of cross-linked enzyme aggregates (CLEAs) which are gaining increasing attention. Such CLEAs can now be bought for research and commercial application. Bioreactors can be operated as batch, continuous or semi-continuous processes with fixed or stirred heterogeneous biocatalysts.

The simplest immobilisation strategy is direct adsorption onto a carrier. This is often possible due to van der Waals, hydrophobic/hydrophilic and hydrogen bond interactions. Since there is no chemical step, the activity of the enzyme tends to be unaffected; however the weak interactions can lead to significant enzyme leaching over time. Adsorption minimises the cost of the immobilisation process and can be achieved quickly after enzyme preparation for use while the enzyme samples are most active.

Simple and universal methods for enzyme immobilisation are not available and often the cost of the carrier precludes their use on a large scale. The most significant advances have been for lipase and protease enzymes although some commercial processes with NADH-dependent enzyme are now operational.[97]

1.3 Enzyme catalysed O atom insertion reactions

A second class of reactions was considered in this work: O atom insertion reactions. These involve the reduction of O_2 to generate an activated O species followed by inert C-H bond activation and O atom insertion. The biotransformation is an oxidation however, overall electrons are required to reduce the second O atom from O_2 to H_2O, Equation [1-1]. Once

again, these electrons are most commonly provided in the form of hydride from the NAD(P)H cofactors. Two particular classes of enzyme for these reactions are flavin monooxygenases and heme-containing cytochrome P450s.

$$R - H + O_2 + 2H^+ + 2e^- \rightarrow R - OH + H_2O \qquad [1\text{-}1]$$

The traditional non-biological methods for such O atom insertion reactions commonly use peroxyacids (HOOR) as a chemical oxidant for epoxidations and Baeyer-Villiger type reactions. However such reagents tend to be hazardous and expensive[98] and require a substrate with a degree of inherent nucleophilicity / electrophilicity and as such are not appropriate for non-activated C-C or C-H bonds. Hydrocarbons can undergo slow free radical autoxidation in air which can be improved using radical initiators and high temperature and pressure, however these reactions lack control and therefore selectivity.[99,100] There is also research into transition metal catalysis for O atom insertion reactions however these reactions tend to be limited by either selectivity or activity, requirement for extreme reaction conditions or expense of the catalyst.[101–103] For these reasons, many chemical companies prefer to buy in 'over oxidised' starting materials and carry out reduction steps as required.

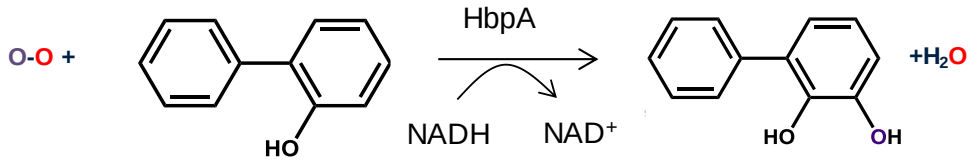

Figure 1-6: A flavin monooxygenase (biphenyl-2-ol 3-monooxygenase) is able to catalyse the selective oxidation of biphenyl-2-ol to 2,3-dihydroxybiphenyl using molecular oxygen and NADH as an oxygen and electron source, respectively.

In contrast, monooxygenase enzymes are able to perform O atom insertion reactions with high selectivity under ambient conditions that are difficult or impossible using the traditional methods.[104] A flavin monooxygenase (FMO) produced by Almog Bregman (Fishman Group, Haifa, Israel), biphenyl-2-ol 3-monooxygenase (HbpA), catalyses the oxidation of biphenyl-2-ol to 2,3-dihydroxybiphenyl (Chapter 7). Purification, characterisation and genetic

engineering of this enzyme[105–110] and other FMOs[104,111] has been previously carried out and is discussed in Chapter 7. Another class of monooxygenase enzymes are cytochrome P450s which contain a Fe-heme active-site. There are extensive reports of these enzymes in the literature and many successful techniques for generating variants with activity towards a desired substrate.[112–117]

These types of enzyme are able to carry out very selective O atom insertion reactions however the requirement for cofactor regeneration limits their use on an industrial scale.

1.4 Existing methods for cofactor regeneration

As previously discussed, a significant limitation to using enzymes as catalysts for reduction reactions, including O atom insertion reactions where electrons are required for reductive activation of O_2, is their requirement for electrons in the form of the expensive cofactors NADH or NADPH. A viable process therefore requires continuous cofactor regeneration; such a system should provide or improve the driving force for a desired reaction, not complicate final product isolation and allow each cofactor molecule to be cycled between 1000 and 10,000 times (in this work this is referred to as the turnover number, TN, moles of product generated per mole of cofactor used).[118,119]

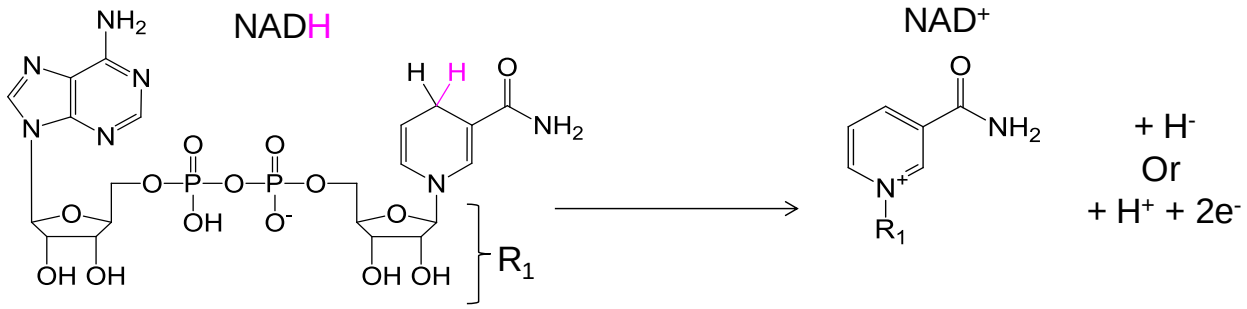

Figure 1-7: The structure of 1,4-NADH showing the hydride that is removed on oxidation (pink) and the structure of NAD^+.

At present all of the methods that are used on an industrial scale use a second enzyme for cofactor regeneration. This is due to complications of NAD^+ reduction since the electrons and

proton must be selectively added to form only 1,4-NADH (Figure 1-7); other forms of the cofactor are not enzyme-active and therefore become unsuitable for the biocatalytic systems.

This section reviews the industrially relevant and lab scale demonstrations of cofactor regeneration systems. These include enzymatic, electrochemical and H_2-driven systems.[118–121] Of these, the most established methods are enzymatic; the reasons for this are also considered.

1.4.1 Enzyme catalysed cofactor regeneration

There are two main approaches to enzyme-catalysed cofactor recycling, substrate-coupled or enzyme-coupled (Figure 1-8). Both strategies require a sacrificial substrate and produce a waste product affecting the purity of the final product and generating carbon based waste which is often burnt at the end. This limits the environmental benefits of a biotransformation.

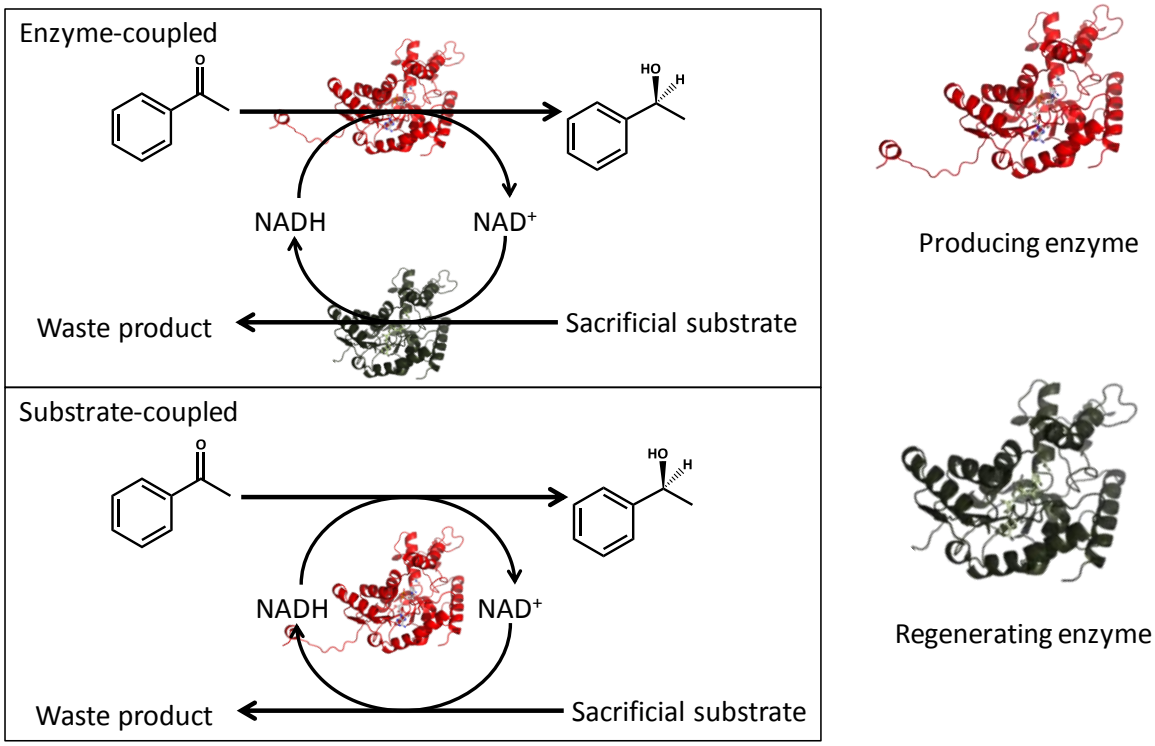

Figure 1-8: Schematic representations of the enzyme-coupled and substrate-coupled strategies to cofactor recycling. In each case a sacrificial substrate is required and a waste product produced.

Enzyme-coupled methods use a producing enzyme for a desired NADH-depenent reaction and a second, regenerating enzyme for catalytsis of an oxidation reaction using NAD^+ and

(re-)generating NADH. The system must be used under conditions in which both the producing enzyme and the regenerating enzyme can sustain catalysis. Commonly this requires a compromise in conditions and preventing maximum activity of the producing enzyme and therefore increasing the cost of enzyme-to-product. However, advantageously the second half reaction (catalysed by the regenerating enzyme) can be chosen such that it is able to drive high conversion of substrate to the desired product. For exmpale if the waste product is gaseous it is trivial to remove from solution and therefore acts to shift the equilibrium towards the desired product.

The second approach to enzyme-catalysed cofactor regeneration is substrate-coupled. Only one enzyme is used which decreases the enzyme-to-product cost. This enzyme catalyses both the desired reduction and the oxidation of a sacrificial substarte thus recycling the cofactor. This approach is most common for alcohol dehydrogenases (ADHs). Again, it is likely that a compromise in conditions is required for catalysis of both reactions to occur at a similar rate. Furthermore, a very large excess of sacrificial substrate is usually cruicial to drive high substrate to product conversion.

Overall, these limitations directly compromise some of the key advantages that enzymes can offer since they generate large quantities of (usually) carbon based waste which complicate product isolation and increase the cost of the biocatalytic process. Despite these limitations, enzymatic cofactor recycling is almost exlusively used for industrial applications. In some cases, elegant enzyme systems have been developed such that the second ‘regenerating’ enzyme carries out a useful oxidation biotransformation, on either a second substrate or even more efficient – the intermediate product. The most commonly used enzymes for regeneration of the NAD(P)H cofactor are listed and discussed below, along with the advantages and disadvantages for each.

Alcohol dehydrogenase

Box 1
Alcohol dehydrogenase (ADH)
Sacrificial Substrate: An alcohol (e.g. isopropanol)
Waste product: An aldehyde / ketone (e.g. acetone)
Advantages: Substrate-coupled cofactor regeneration means that only one enzyme is required.
Disadvantages: Unfavourable equilibrium constant, large quantities of carbon waste.

Employing alcohol dehydrogenases (ADHs) is the most common cofactor regeneration strategy (Box 1).[129] Of particular interest is the substrate-coupled approach (Figure 1-8) since only one enzyme is required. However, since both reactions (reduction of the substrate to the desired product and oxidation of the sacrificial substrate) are reversible, a large excess (> 20 fold) of sacrificial substrate is needed. In some cases this high concentration of an alcohol can be considered as a co-solvent[130] however this often leads to problems when using enzymes that are not solvent-tolerant. Advantageously, the cofactor does not need to leave the ADH active site in substrate coupled catalysis, often leading to high activities.[131] Methods for extraction of the waste product can also help shift the equilibrium in such systems. Overall, alcohol dehydrogenases are one of the most frequently used cofactor regeneration methods, particularly for biocatalytic ketone reductions however large amounts of carbon waste are generated which is not economically or environmentally desirable.[129]

Glucose dehydrogenase

Box 2
Glucose dehydrogenase (GDH) or **Glucose-6-phosphate dehydrogenase** (G6PDH)
Sacrificial Substrate: Glucose or glucose-6-phosphate
Waste product: Gluconic acid or 6-phosphoglucolactone
Advantages: The product undergoes irreversible hydrolysis to providing a driving force. The activity tends to be very high (>300 μmole min^{-1} per mg)
Disadvantages: A large excess of glucose is typically used generating a large amount of carbon based waste which has to be removed and burnt. Glucose is a food source and therefore there are ethical considerations towards using it in this way. The pH of the solution is changed on formation of gluconic acid.

Glucose is often used as a carbon source for cell growth and as such, glucose is the most

common sacrificial substrate for whole cell biotransformations using NADH-dependent enzymes. However glucose can also be used by glucose dehydrogenase as a reducing equivalent for cofactor regeneration for isolated enzyme catalysis; here the high activity[132] and irreversible hydrolysis of the oxidation product (Box 2) has promoted its use in industrial applications for example in the production of an intermediate of atorvastatin.[133] Again, this reaction leads to acidification of the solution - a problem on large scales – and generates large quantities of carbon-based waste. Use of GDH or G6PDH is the most common approach for reyclcing the NADPH cofactor.[129]

Recently Ning *et al.* demonstrated a GDH and ADH cross-linked enzyme aggregate (CLEA, Section 1.2.3) for efficient ketone reduction leading to an improvement in stability, pH and solvent tolerance and catalytic activity.[134]

Formate dehydrogenase

Box 3
Formate dehydrogenase (FDH)
Sacrificial Substrate: Formate (Formic acid)
Waste product: CO_2
Advantages: The product is easily removed by evaporation therefore providing a thermodynamic driving force. Formate is a cheap reducing equivalent.
Disadvantages: The production of CO_2 leads to acidification of solution which requires constant monitoring. Formate dehydrogenase enzymes tend to have low specific activity (in comparison to other cofactor regeneration methods)

Whitesides and Shaked first demonstrated formate dehydrogenase (FDH) from *Candida boidinii* for NADH regeneration[122] and since then it has become one of the most used systems for cofactor regeneration with many variants showing improved stability, NADP cycling or activity produced.[123,124] The most significiant advantage of using FDH for cofactor regeneration is the production of a gaseous waste product, CO_2 (Box 3). Simple removal provides a thermodynamic driving force for the overall reaction; however there are also clear environmental considerations to this approach. There are many examples of industrially used biocatalytic reduction reactions using FDH with substrate concentrations > 100 mM, some

with kg product yields for example in the production of (*R*)-2-hydroxy-4-phenylbutyric acid.[83] There are many papers and patents about cofactor regeneration by FDH; increasingly these demonstrate vairants that are more active,[125] more stable,[126] more easily produced[127] or that tolerate high quantities of organic solvents and that are therefore suitable for use in two phase systems.[128] Due to CO_2 release, the acidification of the reaction is a problem on large scales since buffers are no longer adequate for pH control. This must therefore be monitored and external base added. More recently formate dehydrogenases have been superseded due to their reletavely low activity.

Phosphite dehydrogenase

Box 4
Phosphite dehydrogenase
Sacrificial Substrate: Phosphites
Waste product: Phosphate
Advantages: Phosphites are cheap and provide a favourable equilibrium, the phosphate also acts as a buffer
Disadvantages: Low atom efficiency

The use of phosphites as reducing equivalents is one of the newest approaches to cofactor regeneration. The first examples were for NADPH generation although variants for NADH recycling are now available. Advantageously, the product, phosphate is a commonly used biological buffering system therefore this does not necessarily lead to additional complications in final product isolation. As yet, there are few applications of this enzymatic approach to cofactor recycling.

This brief review of enzymes for cofactor regeneration highlights that there is no ‘perfect’ solution to cofactor regeneration with a particular disadvantage being the low atom efficiency of each method. As discussed in the previous sections, use of either electrodes or H_2 as reducing equivalents could provide highly atom efficient approaches. Although none are successfully implemented on an industrial scale, there have been many attempts to develop these a research scale. In particular there are many reports of electrode systems for cofactor

recycling due, in part due to the possible applications in electrochemical devices (Chapter 8).

1.4.2 Electrochemical NAD^+ reduction

Electrochemical reduction of NAD^+ to NADH is often considered as an 'ideal' method for cofactor regeneration. In the literature it is often referred to as reagentless, as the electrons are provided by an electrode (Equation [1-2]) and thus it is suggested that when coupled to cofactor-dependent chemical steps, product isolation would be simplified.[135] However, in practice there are a number of problems with electrochemically driven biotransformations.

$$NAD^+ + H^+ + 2e^- \rightarrow NADH \qquad [1\text{-}2]$$

Although an electrode can provide reducing equivalents without adding a soluble component to the reaction mixture, a counter electrode is required. This completes the electric circuit but requires a second, oxidation reaction to occur. Often, a potential is applied across the two electrodes, this has costs associated – electricity – and compromises the environmental benefits (since at present, much of the electricity available is not renewable). Another common problem with electrode-driven chemical steps is that only the solution in close proximity to the electrode is productive, Figure 1-9(a). Specific problems for electrochemical NADH recycling are the production of enzyme-inactive forms of the cofactor and the need for potentials much more negative than the thermodynamic potential (equating to an energy loss). Limitations aside, electrodes should be considered for cofactor recycling along with innovative methods for coupling two desirable reactions (a reduction and an oxidation) to generate two useful products and novel reactor designs that allow high catalytic rates by maximising the electrode surface in contact with solution.

Direct electrochemical reduction

Direct electrochemical reduction of NAD^+ at non-modified metal or carbon electrodes does not occur with high current efficiencies. In many cases there is a high kinetic barrier (or

activation energy) associated with the process meaning that a significant 'overpotential' is required to drive the reaction at a useful rate, Figure 1-9(b).

This overpotential provides the extra energy required to overcome this barrier. However, a large overpotential for NAD^+ reduction equates to use of an often very negative potential which leads to electrode fouling and high energy inputs.[136] Furthermore, at the very negative potentials required it is likely that the reaction substrate and / or product will undergo direct, and non-selective, electron transfer with the electrode generating a range of side-products. This acts to lower the efficiency, decrease the product purity and increase product isolation costs. Furthermore enzyme inactive forms of the cofactor are generated due to one-electron steps and non-selective hydride transfers lowering the turnover number (moles of product generated per mole of cofactor used).[137,138] The generation of NAD radicals leads to dimerisation, even if two electrons are successfully added to the cofactor, the proton is able to add to the 2, 4 or 6 position - only 1,4-NADH is enzyme-active, Figure 1-7.

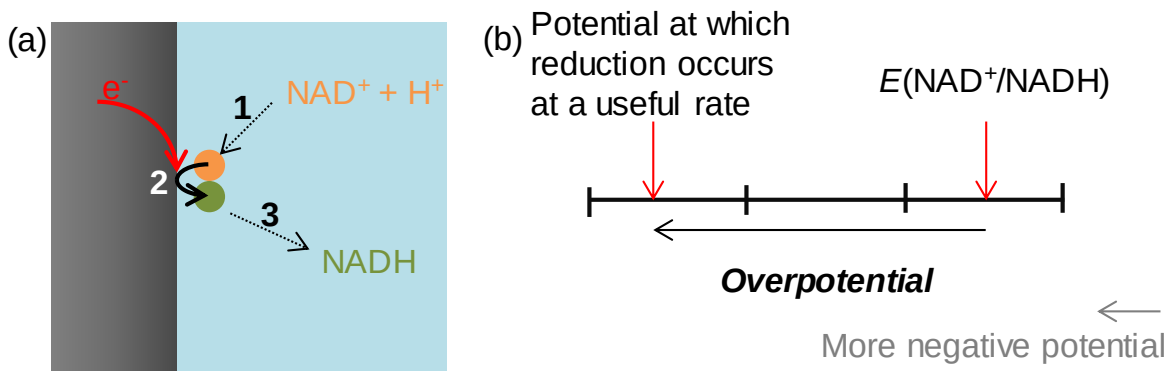

Figure 1-9: Electrons from an electrode can be used for the reduction of a substrate to form a product. (a) NAD^+ (orange) must (1) diffuse from the bulk solution to the electrode, (2) undergo electron transfer at the electrode to generate NADH (green) and (3) diffuse back into the bulk solution. If there is a kinetic barrier, a more negative potential is required (b). This overpotential is defined as the difference between the thermodynamic potential for the reaction and the potential at which reduction is seen electrochemically, at a useful rate; these potentials are indicated by red arrows on the arbitrary potential axis.

It is accepted that the formation of NAD_2 is due to the dimerisation process occurring more quickly than the addition of a second electron and a proton. Ali *et al.* therefore looked at the possibility of increasing the rate of this electron, proton addition to prevent formation of the

dimeric species. They used a glassy carbon electrode with electrochemically deposited Pt or Ni nano-particles, in the hope that the formation of Metal-H_{abs} species would increase the availability of protons at the electrode surface.[137] Their results showed the formation of 100 % biologically active NADH, at an optimum potential of *ca.* -1 V *vs* SHE. However, this overpotential requirement is still high and as such, side reactions of the desired substrate or product at the electrode would be likely thus decreasing the selectivity of a biotransformation. Ali *et al.* have also carried out a detailed comparison of direct NAD^+ reduction at bare Ti, Ni, Co and Cd electrodes and presented a relationship between M-H_{ads} bond strength and potential at which maximum generation of enzyme-active NADH is observed.[139] The most promising result was use of a Ti electrode which led to 96 % enzyme-active NADH at a moderate potential of -0.8 V *vs* SHE.

Mediated NAD^+ reduction

Since many of the problems of direct electrochemical NAD^+ reduction are derived from one electron transfers, there has been extensive research into two electron mediators. The electrode reduces a mediator, and the mediator can then transfer these electrons to the NAD^+ providing a middle ground between a heterogeneous electrochemical step and a homogeneous electron transfer, Figure 1-16. A mediator must be carefully selected such that it has a lower thermodynamic reduction potential than the substrate and is therefore able to reduce the starting material to the desired product and that the substrate is not directly reduced non-selectively at the electrode (Section 1.1.3) at the same potential; overall a catalytic quantity of mediator and cofactor can be used.

Figure 1-10(b) shows that less negative potentials can be used for mediated electrochemical reductions. This can prevent electrode fouling and undesired side reactions as well as improve the selectivity and / or efficiency of the system. Many soluble mediators have been trialled to both improve the selectivity and decrease the overpotential requirement for

NAD^+ reduction.[140–142] In particular mediators that can supply two electrons simultaneously (for example FMN) are desirable since this may prevent the formation of radicals and dimers. In effect these mediators are being used to lower the kinetic barrier to substrate reduction.

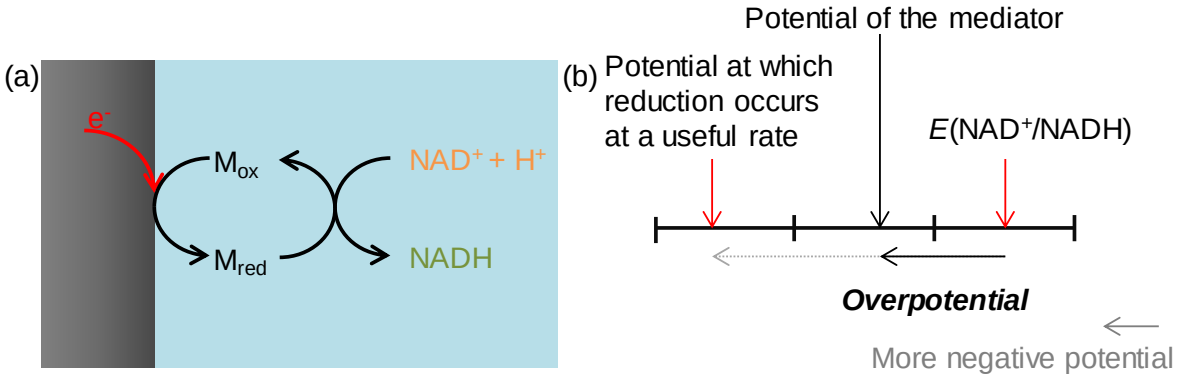

Figure 1-10: Mediators can be employed to transfer electrons from the electrode to NAD^+. (a) Electrons are used to reduce the mediator which then undergoes an electron transfer reaction with the NAD^+. (b) The thermodynamic potential of the mediator must be lower than that of the NAD^+/NADH couple but higher than the potential at which direct substrate reduction at the electrode occurs. A smaller overpotential is required for this mediated electrochemical step in comparison to direct NAD^+ reduction.

Immobilised mediators to enable efficient NAD^+ reduction with low overpotentials without introducing extra components into solution have been widely sought. These systems can be described as heterogeneous catalytic systems for generation of NADH and combine the advantages of direct electrochemical steps (‘reagentless’) and mediated electrochemical steps (higher selectivity, lower overpotentials). One example of this is the use of a poly(Neutral Red) modified electrode.[143] In other examples the mediators are trapped in close proximity to the electrode using polymer gels. In many reports, metal complexes (commonly rhodium) are used as mediators.[141] Hoellrigl *et al.* used a Rh complex for mediated cofactor regeneration[144] to supply a thermophile alcohol dehydrogenase for reduction of *rac*-3-methylcyclohexanone to (1*S*,3*S*)-3-methylcyclohexanol with current efficiencies between 70-85 % and 96 % *diasteriomeric excess*. They used *in situ* product extraction to increase the productivity.

However the selectivity of these systems is still not perfect and a significant overpotential is normally required. For these reasons, none of these mediated electrochemical systems have

been used on an industrial scale for the reduction of NAD^+ to NADH. In fact, at present there are no industrial systems utilising electrochemical NADH regeneration for chemical synthesis,[119] although there are an increasing number of patents and publications in this area.[145]

Electro-enzymatic NAD^+ reduction

There are previous reports in the literature of electro-enzymatic NADH generation that is, combining the theoretical simplicity of electrochemical NAD^+ reduction with the selectivity and efficiency of enzyme catalysis. These techniques have had limited success for a range of reasons.

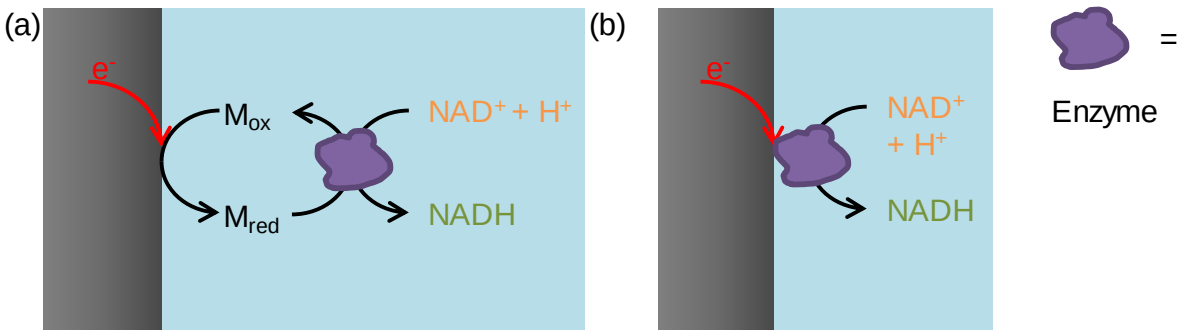

Figure 1-11: An enzyme can be used for selective reduction of NAD^+ to NADH. (a) There are examples of enzymes that can use electrons from mediators for NAD^+ reduction. (b) Some enzymes can be immobilised on an electrode and use electrons directly for the reduction of NAD^+ to NADH.

In 1989 Durliat *et al.* patented an electro-enzymatic approach for regeneration of NADH.[146] This used a Pt electrode with an NAD^+-reducing enzyme from *Ralstonia eutropha* in solution as a mediator / electron relay between the electrode and the cofactor.[147] This operated between -0.65 and -0.75 V *vs* SHE. Further papers by Cantet *et al.* in 1992 and 1996 characterised the kinetics of this system[148] and demonstrated NADH supply to glutamate dehydrogenase.[149] However, Bergel *et al.* reported high instability of the enzyme and in 1990 used a Pt electrode with flavin and an oxidoreductase (e.g. formate dehydrogenase) in solution, in a thin film electrochemical batch reactor instead, Figure 1-11(a).[150] In this system,

the flavin acts as an electron mediator to supply electrons to an oxidoreductase for NAD^+ reduction. This slightly decreased the overpotential (by 0.1 V in comparison to direct reduction at the Pt electrode) and substantially decreased the concentration of cofactor dimer produced.

More recently there have been reports of direct electron transfer between an immobilised NAD^+-reducing enzyme and an electrode for selective reduction of NAD^+ to enzyme-active NADH, Figure 1-11(b). The Vincent Group demonstrated the use of an NAD^+-reductase moiety from *Ralstonia eutropha* (*R. e*)[151] and Hirst *et al.* used the NADH oxidising subunits of complex I, Section 1.5.2.[152,153] These investigations were carried out in order to characterise the enzymes and were not directed towards application in cofactor recycling.

1.4.3 H_2-driven cofactor regeneration

Since the reduction of a ketone to an alcohol equates to the addition of H_2 across a double bond, use of H_2 as a reducing equivalent would provide a 100 % atom efficient process, Figure 1-12. This is also holds true for other hydrogenation reactions including reduction of activated alkenes and imines. This is already exploited in traditional hydrogenation reactions where metal catalysts are supplied with high H_2 partial pressures for catalytic hydrogenation using H_2 as the reducing equivalent (Section 1.1.2).

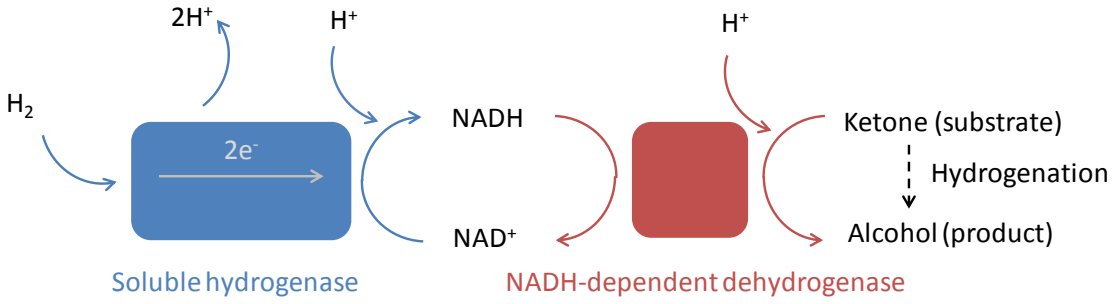

Figure 1-12: H_2-driven NADH regeneration using a soluble hydrogenase offers 100 % atom efficiency and high selectivity. The soluble hydrogenase (blue) is able to couple H_2 oxidation (producing two electrons and two protons) to NAD^+ reduction. One proton and two electrons are used for the reduction of NAD^+. The NADH-dependent enzyme (red) uses NADH and the second proton for a selective hydrogenation reaction. Overall both electrons and protons from H_2 are incorporated into the final product.

Some organisms produce an enzyme that is able to couple the oxidation of H_2 to protons and electrons to the reduction of NAD^+ to NADH. There are examples in the literature of such soluble hydrogenases (SH) being used as catalysts for H_2-driven NADH regeneration. Lauterbach *et al.* have recently reviewed the hydrogenases suitable for NAD(P)H regeneration.[154] In 1983, Payen *et al.* used the SH from *R. e* immobilised on corn stover particles for H_2-driven supply of NADH to *L*-lactate dehydrogenase.[155] More recently, Ratzka *et al.* have demonstrated the same SH for NADH supply to a carbonyl reductase (alcohol dehydrogenase) and have achieved total turnover numbers > 140,000 (number of product per SH enzyme), in comparison to 1700 using formate dehydrogenase.[156,157] Another particularly successful demonstration used *Pyrococcus furiosus* hydrogenase I, a thermophile SH for NADPH generation for NADPH supply a thermophile ADH for acetophenone reduction to phenylethanol with a yield >99 %.[158] This was tested in comparison to a substrate coupled approach (with acetone as the sacrificial substrate); the H_2-driven system gave greater conversion probably due to the presence of a thermodynamic driving force, provided by an atmosphere of H_2 in comparison to a thermodynamic equilibrium between substrate, product, sacrificial substrate and waste product. However, this enzyme is considered too O_2-sensitive[159] for application.

However, the application of hydrogenase enzymes in chemical synthesis has been limited by the stability and activity of the SH as well as the low solubility of H_2 in water. For this reason, there are no examples of the SH being used for industrial cofactor regeneration. Other strategies for H_2-driven NADH recycling use whole cells containing both the SH and an NADH-dependent dehydrogenase; this has been demonstrated for reduction of a range of carboxylic acids,[160] but again has not been followed up industrially.

Inspired by these SH enzymes, there are some reports of transition metal complexes for H_2-driven NADH generation, however these do not achieve the degree of selectivity and

therefore total turnover numbers necessary for further application.[161–163]

Although enzymatic H_2-driven NADH generation could offer the efficiency and selectivity required for a viable biocatalytic process, the present techniques are not yet competitive and thus are not utilised on an industrial scale.

1.4.4 Artificial cofactors

The final approach to utilising cofactor-dependent enzymes considered here is the use of artificial cofactors (see recent review by Paul *et al.*[164]). It is possible that less expensive synthetic nicotinamide cofactor analogues could be used in the future to support cofactor-dependent chemical synthesis. However, viable recycling systems are still required to prevent generation of substantial waste and contamination of the final product. The mNADH molecules can also provide mechanistic information into the nature of the hydride transfer[165] (Section 2.8.3).

In the study of NADH mimics, either the NADH-dependent enzyme can use the mimic directly for reduction of substrates or the cofactor mimic can be used to recycle a catalytic quantity of NADH. The nature of the cofactor mimic (Figure 1-13) changes the redox potential of the redox couple thus affecting the electron donor/acceptor ability of the molecules.[164]

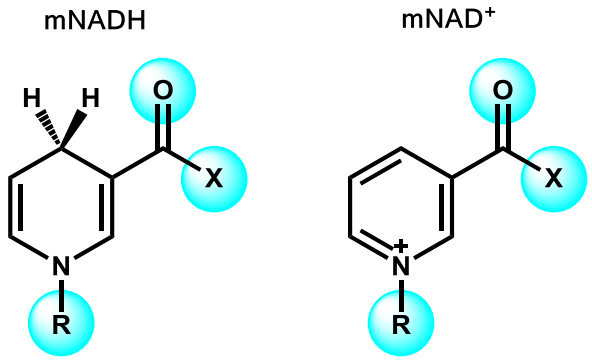

Figure 1-13: Most common sites of substitution for nicotinamide cofactor mimics.

Jones and co-workers used an mNADH where X=Me and R=β-TAG-3-acetylpyridine (E^o = -222 mV compared to $E^o(NAD^+/NADH)$ = -320 mV). This mNADH was used for

regeneration of NADH coupled to cyclohexanone reduction by horse liver ADH with a turnover number of 25 (moles product generated per mole cofactor used).[166] Knox *et al.* demonstrated use of a nitroreductase enzyme that can use either NADH or NADPH for the reduction of substrates including menadione. This enzyme was also able to use a cofactor derivative, 1-methylnicotinamide (reduced) with no change to the reduction products.[167]

1.4.5 Is the 'cofactor challenge' still present?

Overall, some consider the 'cofactor challenge' solved[168] as there are a range of NADH recycling approaches available. Despite this, the number of industrial synthetic pathways using NADH-dependent enzymes does not reflect the incredible catalytic selectivity on offer. These 'solutions' to cofactor recycling are still not environmentally sufficient for many applications due to the generation of carbon based waste. Furthermore, the need to carefully optimise the regeneration enzymes, research optimal sacrificial substrate loadings and develop product isolation protocols for each synthetic step adds to research and development time and therefore increases costs associated with implementing cofactor-dependent synthesis. For these reasons traditional methods for ketone reductions (and other relevant reactions) still tend to win-out since they are more easily translated from one synthesis to another. However, genetic engineering is rapidly advancing and allows production of 'designer enzymes' for biotransformations on highly non-natural substrates. New, easily adaptable, methods for environmentally and economically viable cofactor regeneration would provide more incentive for uptake of NADH-dependent chemical synthesis in the future. This work seeks to address this need by exploiting redox enzymes that can exchange electrons directly with a conducting surface to build systems for clean, efficient cofactor-dependent chemical synthesis using electrons from either H_2 or an electrode. The next section discusses how some organisms can use H_2 as an energy source, the enzymes involved and methods for analysing them before Section 1.6 introduces the systems developed in this work.

1.5 The enzymes used in this work

The work in this Thesis focuses on enzymes that are able to exchange electrons with a carbon surface, either an electrode or an electronically conducting carbon particle. This section introduces such redox enzymes that are able to cycle $2H^+/H_2$ or NAD^+/NADH, and the techniques for analysing them under direct potential control. A general introduction is given, further information into the structure and methods for analysis of these enzymes will be provided in the following chapters as appropriate.

1.5.1 Hydrogen cycling enzymes

A number of micro-organisms contain hydrogenase enzymes which are able to catalyse the simplest chemical reaction, oxidation of H_2 with production of protons and electrons, or the reverse, proton reduction to generate H_2, Equation [1-3].[169,170]

$$H_2 \leftrightarrow 2H^+ + 2e^- \qquad [1\text{-}3]$$

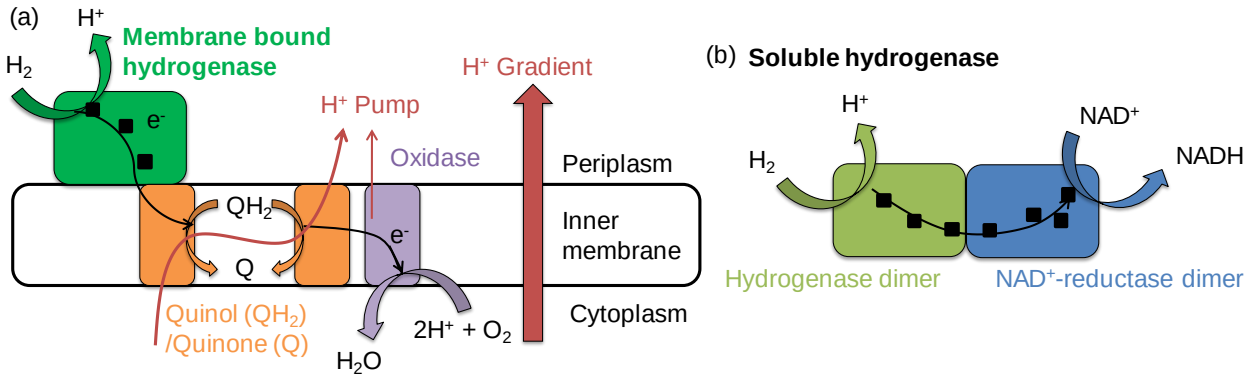

Figure 1-14: Two examples of enzymes that can obtain energy from H_2. (a) Some bacterial cells store energy from H_2 as a proton gradient *via* a cycle of enzymes; a Membrane Bound Hydrogenase (MBH) oxidises H_2 to H^+ and the electrons released are transported though the lipid membrane by quinol (QH_2) / quinone (Q). An oxidase uses the electrons to reduce O_2 to water whilst simultaneously pumping protons into the periplasm.[171] (b) A soluble hydrogenase (SH) exists in the cytoplasm of some organisms; electrons from H_2 oxidation are used for the reduction of NAD^+ to generate reducing equivalents (NADH). In each case, the black squares correspond to the electron relay centres.

The method of electron transfer depends on the cellular location and function of the particular enzyme. Some hydrogenases are bound to a membrane and are the start of an electron chain

which can eventually reduce a terminal electron acceptor, for example O_2 often alongside creation of a proton gradient, Figure 1-14(a). Other hydrogenases are soluble (i.e. not associated with a membrane) and transfer electrons to a soluble electron acceptor or a redox partner protein Figure 1-14(b).

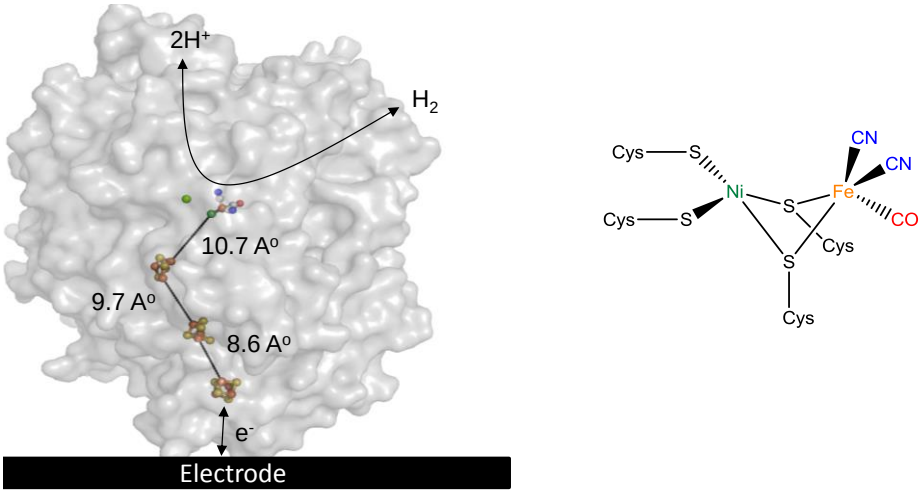

Figure 1-15: A hydrogenase enzyme is able to transfer electrons between the active-site and the electrode. These electrons are used for the interconversion of H_2 and H^+. The protein shell is shown in grey; the active-site is shown in coloured spheres. The FeS clusters for electron transfer are shown in elemental colours with the spacing between them. Figure prepared using PyMol. Hydrogenase PDB code 3UQY, membrane bound hydrogenase from *E. coli*.[172]

Hydrogenases have received much attention due to the ability of some to catalyse H_2 oxidation or production with very high efficiency and activity under very mild conditions. Advantageously, these enzymes contain either Fe or Fe and Ni in their active-site;[173,174] these metals compare favourably with traditional H_2 oxidation catalysts such as Pt which are rare and expensive. The [NiFe] hydrogenases are more commonly utilised for H_2 oxidation and [FeFe] for H_2 production.[175] Unlike the case for the NADH-dependent dehydrogenases and most other redox enzymes relevant to chemical, hydrogenases are specially equipped for electron transfer with partner proteins or membranes and are also able exchange electrons directly with an electrode and be used as electrocatalysts for $2H^+/H_2$ cycling, Figure 1-15(a). This thesis only discusses [NiFe] hydrogenases, many of which have resolved crystal structures;[176–179] the standard active-site is shown in Figure 1-15(b). The protein structure shown in Figure 1-15 is for a membrane bound hydrogenase (MBH) from *E. coli* however the

presence of FeS clusters and an active-site buried within a protein shell is standard to all hydrogenases.

There are extensive reports on the catalytic pathway for H_2 oxidation by hydrogenases (Chapter 5). It is hoped that better understanding will lead to enzyme mimics that use cheap, abundant metals for efficient H_2 oxidation. The most significant methods for this work are protein film electrochemistry where a hydrogenase is immobilised onto an electrode and the activity measured as a function of either time or potential,[174] IR spectroscopy which gives insight into the electronic configuration of the [NiFe] active site by probing the CO and CN^- ligands,[180] and EPR spectroscopy which has provided insight into the FeS electron relay centres.[181] The hydrogenases used in this work will be introduced in the results Chapters.

The protein shell is essential to how the enzyme functions, it plays many roles, many of which are not fully understood. Hydrophobic channels connecting the active site of some [NiFe] hydrogenases to the edge of the protein shell have been identified using crystallographic methods.[177] It has been suggested that these facilitate the rapid transport of H_2 and protons through the protein shell. There are reports in the literature of hydrogenase activity being manipulated by making amino acid changes to these gateways with a particular goal being improved O_2 tolerance.[182,183]

1.5.2 Soluble NAD^+-reducing hydrogenase

The bacterium *Ralstonia eutropha* is able to use H_2 as its sole energy source.[184] It contains a number of hydrogenases; of particular interest for this work is the soluble hydrogenase (SH). In its native form the SH is hexameric comprising subunits $HoxHYFUI_2$.[185] This enzyme is able to couple H_2 oxidation to the reduction of NAD^+,[186,187] thus supplying the cell with the reducing equivalent, NADH. In fact, the intact SH has been used for H_2-driven cofactor regeneration (Section 1.4.3) and has been shown to be able to supply NADH to a cofactor-dependent enzyme both *in vitro* and *in vivo*.[154,156,188,189] The SH contains five FeS clusters and two bound FMN cofactors.[186,190]

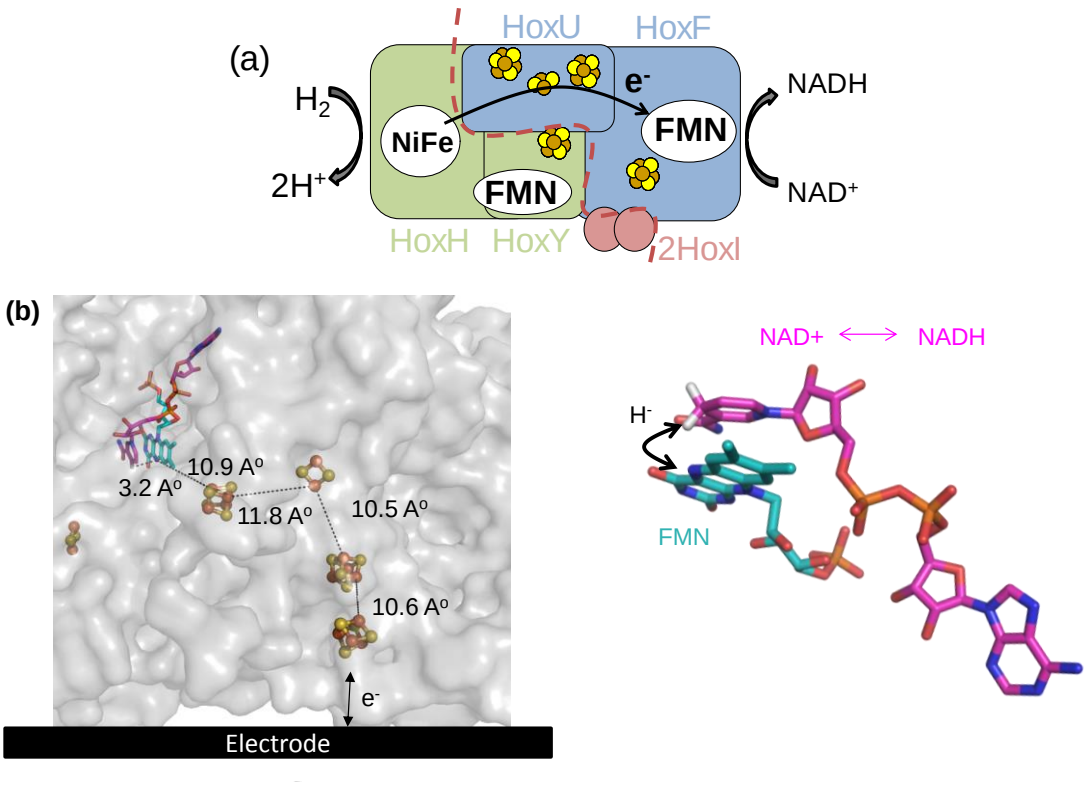

Figure 1-16: (a) A schematic representation of the Soluble Hydrogenase from *Ralstonia eutropha*. The NAD^+-reducing subunits (HoxFU) are shown in blue and the hydrogenase subunits (HoxHY) are green. The red dotted line represents where the enzyme can be split. The HoxFU catalytic portion can be produced alone. The HoxI subunits shown in red easily dissociate (especially at high ionic strength), and are of unknown function. (b) The NAD^+-reductase is able to collect two electrons from an electrode at FMN in the active site and transfer them, with a proton, as a hydride for the reduction of NAD^+ to NADH (and vice versa for NADH oxidation). Figure prepared using PyMol; NAD^+-reductase homology structure discussed in Section 3.1. The FeS clusters are shown as spheres in elemental colours, the FMN active site and the NADH cofactor are shown as blue and pink lines respectively. A close up of the FMN and NADH interaction is shown on the right hand side.

The NAD^+-reductase contains an FMN active-site; this is able to collect two electrons to form a reduced state. These electrons can be transferred selectively to NAD^+ with a proton to generate only 1,4-NADH.

Since the NAD^+-reductase portion (HoxFU) in nature uses the electrons from H_2 transferred from the hydrogenase dimer as an electron source it is appropriately set-up to allow direct electron transfer to or from an external source such as an electrode. In this way the enzyme moiety can be analysed using protein film electrochemistry (PFE) techniques.[151] Since electrons are a cheap reducing equivalent, an electrochemical route to NADH recycling will be investigated. However, for some industrial applications an electrochemical system

may not be desirable; therefore a second system that uses electrons and protons from H_2 will also be developed.

Previous electrochemical characterisation within the Vincent Group has demonstrated that the $2H^+/H_2$ cycling portion of the this enzyme (the hydrogenase dimer) is less stable and less active than the NAD^+/NADH cycling portion (the NAD^+-reductase dimer) likely due to the labile FMN in HoxY. The work in this Thesis makes use of the NAD^+-reducing subunits of the soluble hydrogenase, coupling them to H_2 oxidation by a more robust, active hydrogenase in a novel cofactor regeneration system, Section 1.6.

1.6 Cofactor regeneration systems developed in this project

The simplest reducing equivalents are electricity and H_2; systems that can use electrons either from an electrode or from H_2 to reduce NAD^+ and efficiently supply NADH to a range of cofactor-dependent dehydrogenase enzymes will therefore be investigated. In each case an NAD^+-reductase enzyme will be used to convert an electron source into a hydride source (NADH). These systems fit into the existing cofactor regeneration landscape as shown in Scheme 1-2(a).

In Chapter 3 the development of a high surface area electrode system for electro-enzymatic NADH generation will be discussed. In Chapter 4 a new NAD^+-reductase enzyme moiety will be electrochemically characterised for the first time. In Chapter 5 the NAD^+-reductase will be coupled to a range of robust hydrogenases *via* electronically conducting surfaces for development of a modular system for H_2-driven NADH generation. In Chapter 6, the electro-enzymatic and H_2-driven NADH generation systems will be explored for NADH supply to alcohol dehydrogenase enzymes for ketone reduction reactions; the approaches will be compared to the existing cofactor regeneration strategies introduced in Section 1.4 and metal catalysed hydrogenation reactions outlined in Section 1.1.2.

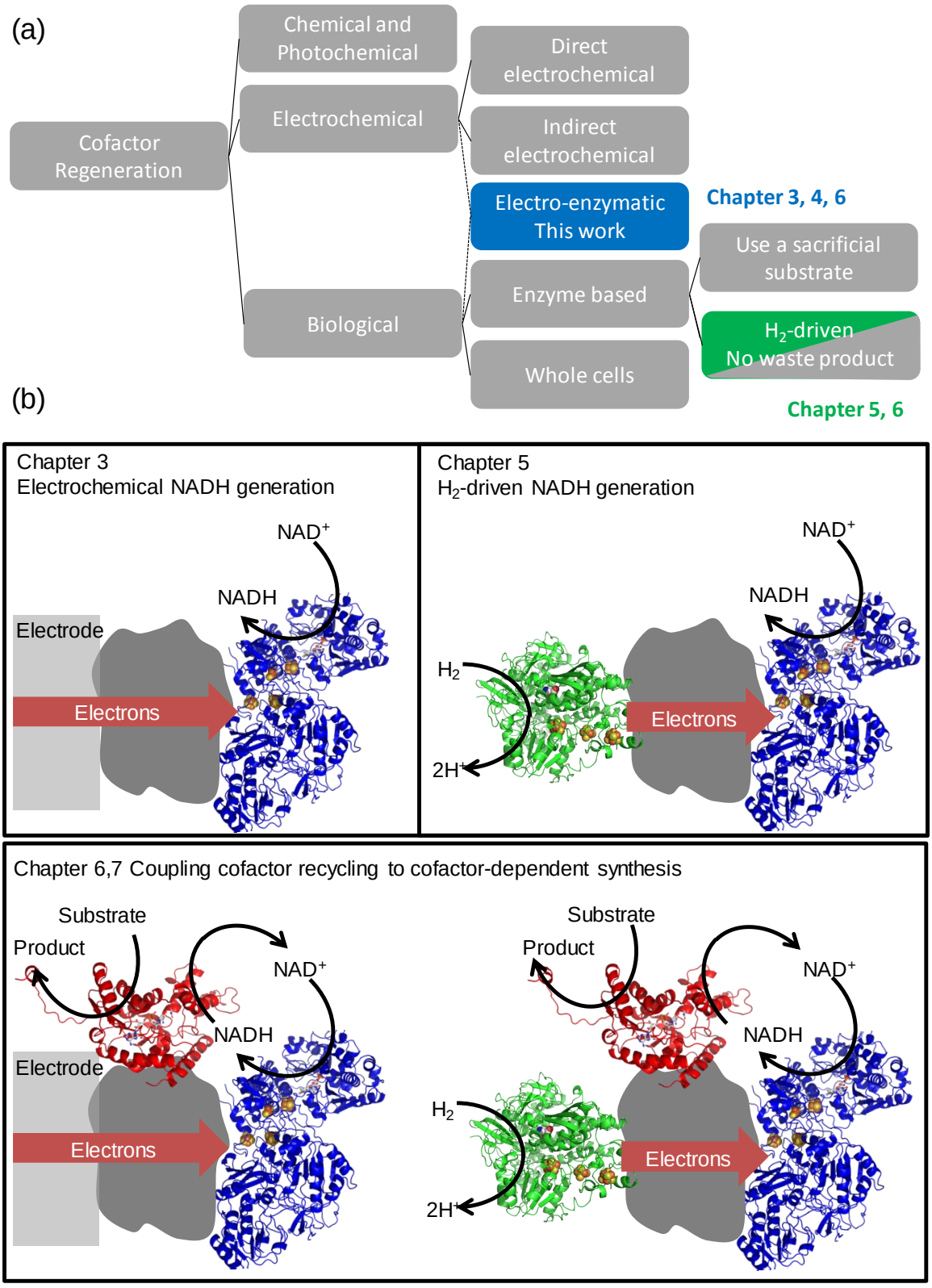

Scheme 1-2: (a) Overview of the existing cofactor regeneration methods[120] and the methods developed in this work, electro-enzymatic (blue) and H_2-driven (green). (b) Schematic representations of the NADH generation and NADH recycling strategies developed in this Thesis.

The test systems chosen are lactate dehydrogenase (LDH) for the reduction of pyruvate to *L*-lactate and an alcohol dehydrogenase (ADH) for the reduction of acetophenone to (*S*)-phenylethanol. The H_2-driven system will be adapted for NADH supply in the presence of O_2 for cofactor supply to a monooxygenase enzyme in Chapter 7. The test enzyme here is a biphenyl-2-ol 3 monooxygenase (HbpA) for the oxidation of biphenyl-2-ol to 2, 3-dihydroxy biphenyl. A schematic overview of the approaches developed in Chapters 3 to 7 is shown in Scheme 1-2. The electrodes developed for electrochemically driven synthesis will be further developed to make a proof-of-concept cofactor-dependent biosensor and fuel cell in Chapter 8.

Chapter 2 Theory and Methods

This work uses a range of different techniques to analyse or exploit redox enzyme catalysis. In this Chapter some of the more general theory and methods will be discussed. Each of the results chapters expands upon these concepts as required and details the non-standard experimental procedures developed as part of this work.

2.1 Electrochemistry

Electrochemistry is a powerful tool for understanding redox reactions. The potential of an electrode dictates the energy of the available electrons. This energy in comparison to that of a molecules highest occupied molecular orbital (HOMO) and lowest unoccupied molecular orbital (LUMO) provides the driving force for a reduction or oxidation reaction to occur. During electrosynthesis, electrons are transferred between the electrode and the molecule of interest; this flow of electrons is recorded as a current. The faster reaction occurs, the higher the magnitude of the current observed. However, having an electorn source or sink of the right energy does not necessarily mean a reaction will occur. If there is a kinetic barrier associated with the redox reaction additional energy is required to drive the reaction at an

appreciable rate, and this equates to an overpotential (Section 1.4.2); thus the onset of catalytic current is not always observed at the thermodynamic potential. Electrochemical techniques can therefore provide information on both the kinetics and thermodynamics of a redox system.

2.1.1 The Nernst equation

The Nernst equation[191] can be used to determine the potential of redox couple under a particular set of conditions. For the reaction:

$$Ox + ne^- \rightleftharpoons Red \qquad [2\text{-}1]$$

the Nernst equation is written as:

$$E = E^0 + \frac{RT}{nF} ln \frac{[Ox]_{eq}}{[Red]_{eq}} \qquad [2\text{-}2]$$

where E is the thermodynamic potential, E^0 is the standard reduction potential of the redox couple (under standard conditions), *R* is the gas constant, *T* is the absolute temperature, *F* is the Faraday constant and *n* is the number of electrons. An overall redox reaction must consist of both a reduction and an oxidation half reaction to enable a flow of electrons. If the reduction and oxidation reactions are happening at separate electrodes, the difference between the equilibrium electrode potentials can be measured as a potential difference (voltage). The standard reduction potential for a redox couple can thus be determined experimentally relative to an electrode of known or defined potential – a reference electrode – for example the Standard Hydrogen Electrode (SHE).

$$2H^+_{(aq)} + 2e^- \rightleftarrows H_{2\,(g)} \qquad [2\text{-}3]$$

The SHE is defined to be 0 V at all temperatures at 1 bar H_2 with protons at unit activity. In practice, a reference electrode that does not require H_2 gas is used (Section 2.1.5).

2.1.2 Protein Film Electrochemistry[192,193]

Protein Film Electrochemistry (PFE) refers to a suite of techniques that use a redox enzyme

immobilised on a working electrode at mono- or sub-monolayer coverage. This allows analysis of a very small sample of enzyme, typically in the order of picomoles.[174] These techniques require the enzyme to be 'wired' to the electrode and are thus only applicable to a small set of redox enzymes that are stable upon adsorption and that have accessible redox centres. Hydrogenase and NAD^+-reductase enzymes were introduced in Section 1.5, in both cases the enzymes are naturally 'wired' to a redox partner (either a membrane or a partner protein) *via* appropriately spaced FeS clusters in their structures. Electrons are shuttled between the buried active-site and the edge of the protein shell; assuming a short distance (<14 A^o) rapid electron transfer from the external FeS cluster to electrode can occur, Figure 2-1. These enzymes are therefore appropriately set-up for electron exchange with an electrode and have previously been studied extensively in this way.[151,152,175,194–198]

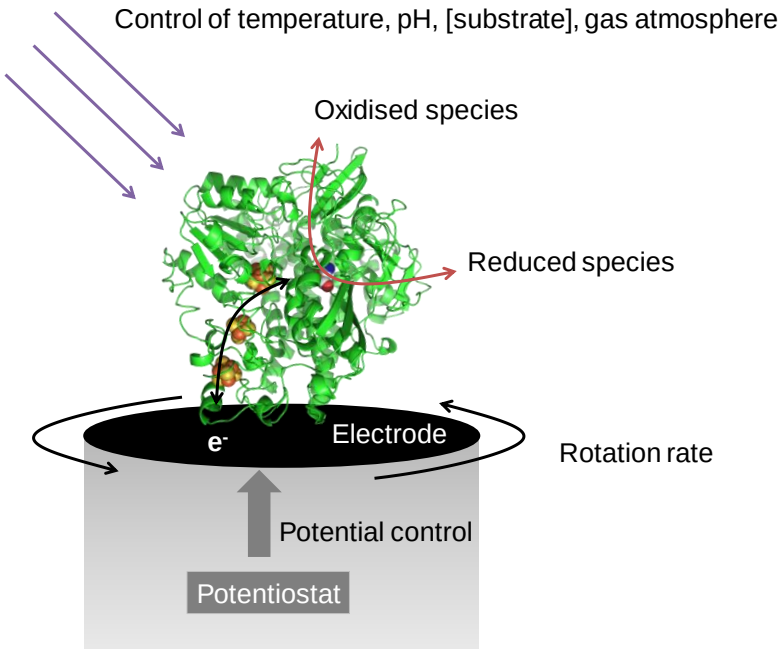

Figure 2-1: Cartoon representation of an adsorbed enzyme on a working electrode. Direct electron transfer can occur *via* a chain of FeS clusters, or other redox centres. The electrode can be rotated to ensure the solution at the electrode surface is the same as the bulk solution. The environment the enzyme is in can be carefully controlled.

The magnitude of the current recorded is related to the rate of transport of substrate to the electrode, the rate of catalysis by the enzyme and the rate of interfacial electron transfer between the enzyme and the electrode.[174,196] Since it is the rate of catalysis that is of interest

the other ‘resistive’ contributions should be minimised. Rapid rotation of the working electrode prevents mass transport limitations by bringing fresh solution to the electrode surface, Section 2.1.4. The rate of interfacial electron transfer depends on the interaction between the electrode and the enzyme, Section 2.1.9.

Since the enzyme of interest is immobilised on the electrode, the gas and liquid environment can be altered during the course of an experiment without loss of the protein. This enables the effect of substrate concentration, inhibitor concentration, gas atmosphere and temperature to be probed on a constant quantity of enzyme and thus the change in activity to be monitored.

2.1.3 Electrochemical setup

Electrochemical experiments in this Thesis use a three electrode system. The enzyme film is prepared on the working electrode (WE), and during an experiment a potential is applied between this electrode and a reference electrode (RE) of constant known potential. This allows precise control of the working electrode potential. Assuming electron transfer occurs, a current will flow; to maintain a constant potential at the reference electrode, most of the current generated at the working electrode passes through a counter electrode (CE).

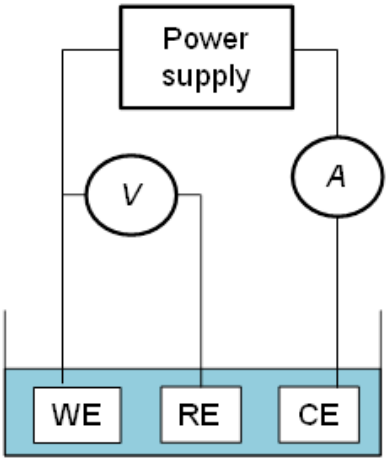

Figure 2-2: A schematic diagram for the three electrode system used in this Thesis. A potential is applied between the working electrode (WE) and the reference electrode (RE), the current generated at the WE is passed through the counter electrode (CE).

The standard electrochemical setup is shown in Figure 2-2. A potentiostat (Autolab PGstat128N with ECD module running on GPES software, EcoChemie, The Netherlands) was used to both control the applied potentials and record the current.

2.1.4 Working electrodes – for analytical electrochemistry

For analytical electrochemistry the enzyme films were prepared on a pyrolytic graphite edge (PGE) working electrode. This has been shown to be a suitable electrode material for enzyme immobilisation and in contrast to many metals does not lead to denaturation of the enzyme (often by unfolding of the protein structure). Furthermore, carbon electrodes are 'electrochemically silent' in water in the biologically relevant potential window used in this Thesis (-0.6 to +0.5 V *vs* SHE); this simplifies analysis of electrochemical data.[199] However, since O_2 reduction occurs at carbon electrodes at *ca* -0.2 V, all electrochemical experiments were performed in a N_2 atmosphere using a glove box (MBraun or Glove Box Technology Ltd, < 0.1 ppm O_2) to prevent complication of catalytic currents by direct O_2 reduction at the electrode.

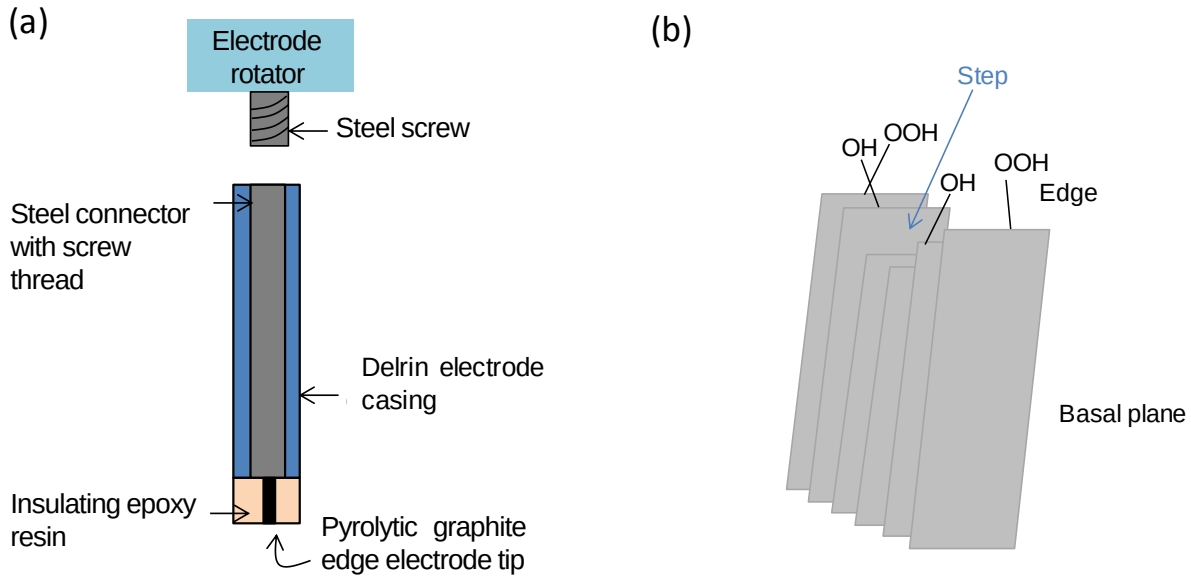

Figure 2-3: (a) Schematic representation of the pyrolytic graphite edge (PGE) rotating disk electrodes (RDE) used for experiments in this Thesis. (b) Cartoon structure of pyrolytic graphite shown the edge and basal plane. Fresh preparation of the PGE surface forms polar functional groups and 'steps' which aid enzyme adsorption.

The working electrode cases were prepared ‘in-house’ by either Mr Charlie Jones of Mr Charlie Evans. A cylindrical pyrolytic graphite rod (Momentive Performance Materials) with an edge surface area of 0.03 cm^2 was sealed into a Delrin rotating disk electrode case using silver loaded epoxy glue (RS) such that *ca* 0.5 cm protruded from the end. Insulating epoxy resin (Aradur hardener and Araldite resin, Robnor Resins) was prepared and used to coat the edge of the PGE as shown in Figure 2-3(a) so that only the ‘edge’ surface of the PG tip was exposed (b). The electrode was connected to an electrode rotator (EG&G model 636).

The electrode surface was freshly prepared before each electrochemical experiment. First the electrode was polished using an alumina (1 µm, Beuhler) slurry on cotton wool. This generates a rough ‘stepped’ surface with a range of polar functionalities, Figure 2-3(b). It is widely accepted that this facilitates enzyme adsorbption.[196,200] The electrode was then washed by sonication in MilliQ water for at least 30 seconds to ensure any loose carbon or alumina was removed. The electrode was allowed to dry or was dried gently using a dust free tissue. In some cases the electrode was then abraded using sand paper to create an electrode finish more similar to a pyrolytic graphite particle, this was followed by further sonication (at least 30 seconds) and drying.

To prepare the enzyme film an aliquot of enzyme solution (~ 0.5 µL) was spotted onto the PGE electrode tip. This was then allowed to partially dry for approximately 15 seconds (depending on the enzyme and the concentration of the solution). In most cases the electrode was then attached to the electrode rotator and immersed into buffered solution. The electrode rotator was connected to the potentiostat allowing electrochemical control over the working electrode. High surface area electrodes were developed for electrode-driven biotransformations and are discussed in Section 2.2.

2.1.5 Reference electrodes

For analytical electrochemical experiments a saturated calomel electrode (SCE, ALS) was

used as a reference and the potential corrected to SHE using Equation [2-4]. This was corrected depending on the temperature the reference electrode experienced during an experiment using a linear correction of - 67 mV / ^{o}C.[201]

$$E_{SHE} = E_{SCE} + 0.244\,V\ at\ 25\,°C \quad [2\text{-}4]$$

For experiments where a smaller reference electrode was required, a Ag Ag/Cl reference was made. A length of silver wire (Surepure Chemetals, 99.95 %, 0.4 mm diameter) was electrochemically coated with AgCl by holding at a constant current of +0.3 mA in HCl (1 M) for 10 minutes before sealing into a polyether ether ketone (PEEK) tube containing 3 M AgCl solution. One end of the tube was sealed with a molecular sieve to allow a flow of ions, but prevent large molecules (NAD^{+}, NADH etc.) from interacting with the Ag electrode. The other was sealed with a rubber septum through which the Ag wire was connected to the potentiostat. The potential of these electrodes were regularly tested against standard reference electrodes and the Ag/AgCl solution was replenished before each use.

$$E_{SHE} = E_{Ag/AgCl} + 0.205\,V\ at\ 25\,°C \quad [2\text{-}5]$$

Potentials were converted to SHE using Equation [2-5] and corrected for the temperature using a linear correction of - 0.73 mV / ^{o}C.[201]

2.1.6 Counter electrode

The counter electrode, a platinum wire (Surepure Chemetals, 99.95 %, 0.4 mm diameter), takes the current from the working electrode to complete the circuit. A redox reaction must therefore be taking place at the counter electrode. For analytic electrochemical reactions, this reaction was not a concern; the reaction times were short and low currents were observed. Furthermore the resulting electrolyte solution was not analysed and the buffer system prevented large changes to the pH. However, for much of this work it was the resulting solution which was of interest. It was therefore very important the counter electrode was not affecting the nature of the solution. In many cases a fritted counter electrode was used; a

molecular sieve prevented the molecules of interest from interacting with the Pt wire. This electrode set-up was made 'in house' using a molecular sieve (Sigma) and heat shrink tubing (RS Components). This was filled with high concentration buffer solution and sealed with a rubber septum; the buffer was replaced before each use. A piece of Pt wire was pressed through the septum to make contact with the solution and connected to the potentiostat using a crocodile clip. The size, and therefore surface area of the counter electrode, affects the maximum current that can flow through the electrochemical set-up. In experiments were the catalytic current recorded was high, longer lengths of counter electrode were required.

2.1.7 Electrochemical cells

Analytical electrochemical experiments were performed in either a specialised, gas tight, electrochemical cell Figure 2-4(a), or a slightly simplified version for experiments that did not require gas access (not shown).

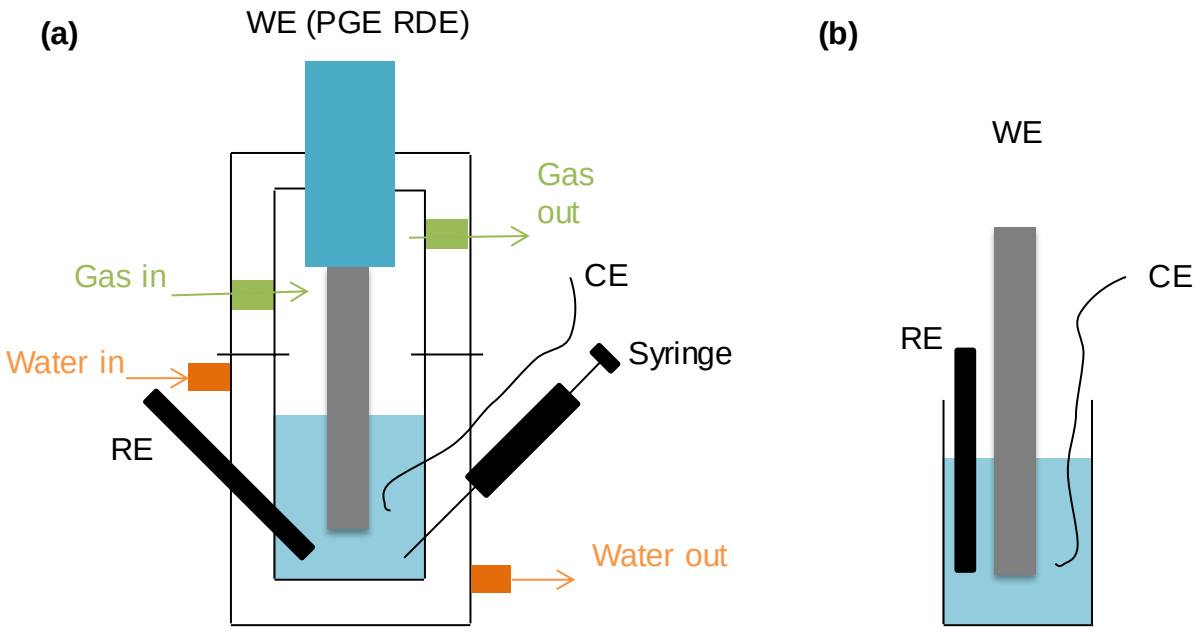

Figure 2-4: Schematic representations of the electrochemical cells used for experiments in this Thesis. (a) A gas tight glass electrochemical cell with a water jacket for temperature control and gas inlet and outlet for control of the gas atmosphere. In many experiments a precise gas mixture was controlled using mass flow controllers. The cell seals around the electrode rotator allowing use of a pyrolytic graphite edge (PGE) rotating disc electrode (RDE). Sealed side arms allow the use of a RE, CE and syringe for injecting substrates and inhibitors. (b) A simple sample vial set up with a WE, RE and CE.

Both cells allowed precise control over the temperature (*via* water jacket and water circulator), rate of rotation of the working electrode and concentration of substrate and inhibitors. Electrochemically driven biotransformations were performed in a glass vial, Figure 2-4(b). Details of the electrodes used are discussed in the results chapters. In most cases the working electrode was not rotated in these experiments, instead the solution was stirred using a magnetic stirrer.

2.1.8 Electrochemical techniques

This work made use of cyclic voltammetry and chronoamperometry to understand and characterise enzyme activity. Chronoamperometry was also used to drive enzyme catalysed redox reactions.

Cyclic voltammetry

During cyclic voltammetry, the potential of the working electrode is swept between two potentials, E_1 and E_2 (Figure 2-5(a)), and the resulting current recorded. There can be both non-Faradaic and Faradaic contributions to the current observed.

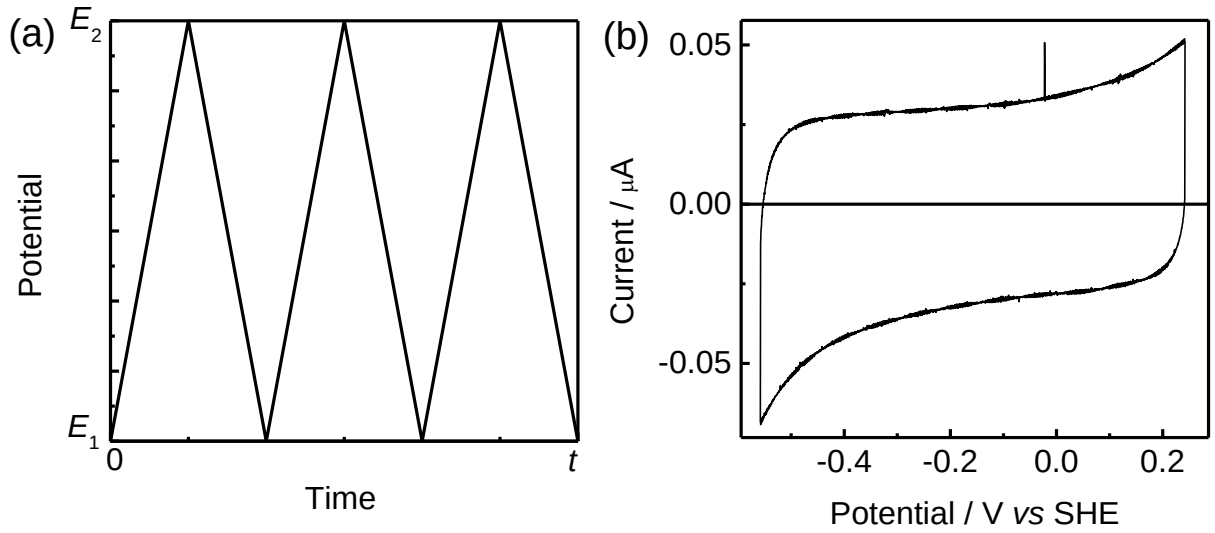

Figure 2-5: Analysis of redox enzymes using electrochemistry. (a) The variation of potential with time during cyclic voltammetry experiments. (b) The capacitive current recorded for a 'blank', unmodified, electrode at 10 mV s^{-1} where E_1 and E_2 where $^{+}$0.24 and -0.56 V *vs* SHE, respectively.

When the potential and therefore charge of an electrode is changed, the electrical double layer is changed due to rearrangement of ions in the surrounding solution the electrode leading to a flow of ions, this gives a non-redox (non-Faradaic) current. When a redox reaction occurs, electrons are transferred between the redox active species and the electrode leading to a Faradaic current.

In order to separate the two contributions, a 'blank' cyclic voltammogram is always recorded under the same conditions as the system of interest but in the absence of substrate and catalyst, Figure 2-5(b). A second blank scan is often recorded in the presence of only substrate to ensure that there is no interaction between the electrode and the substrate. When using an enzyme-modifie electrode in the presence of substate, any deviation from the 'blank' voltammogram can therefore be attributed to a Faradaic process. The magnitude of the non-Faradaic (capacitive) current is dependent on several factors including electrode surface area, scan rate and temperature. These factors were therefore kept constant between 'blank' and experimental voltammograms. As standard, cyclic voltammetry was carried out at a scan rate of 10 mV s^{-1}; when using a freshly prepared PGE electrode the capacitive current was below 0.1 μA (Figure 2-5(b)) which allowed simple analysis of enzyme films. Before each voltammogram, the potential was held at the start potential for 10 seconds, allowing the electrode and surrounding solution (double layer) to equilibrate before the current was recorded, preventing a very large initial capacitive current.

Cyclic voltammetry allows the activity of an immobilised enzyme to be assessed with respect to applied potential. The potential at which catalysis starts (often referred to as the onset potential, E_{onset}) gives insight into the thermodynamic efficiency of the enzyme. The shape of the catalytic wave gives information on potential dependent inactivation and activation steps. Not only are these properties scientifically interesting, but understanding them is essential for utilising enzymes in industrial biocatalysis.

Chronoamperometry

For a chronoamperometry experiment, the potential applied at the working electrode is kept constant with respect to time. Since the charge of the electrode does not change, there is no significant non-Faradaic contribution to the current after *ca* 10 seconds. Chronoamperometry allows the activity of the enzyme to be monitored under constant conditions (potential, temperature, gas atmosphere, rotation rate) whilst one or more parameters are changed as required (usually substrate or inhibitor concentration). This allows quick characterisation of certain enzyme parameters using very small quantities of enzyme as many different factors can be assessed on the same enzyme sample. The methods for quantification of the enzyme substrate-affinity and product-inhibition constants using chronoamperometry are discussed in Section 2.3.

Chronoamperometry was also used to drive electro-enzymatic redox catalysis; the methods for this are described in the results chapters. Advantageously, electrochemically driven biotransformations allow a continuous read out of the activity of the 'wired' enzyme (the enzyme that is transferring electrons with the electrode). By integration of the current (*I*) over time (t_i to t_f) the charge passed (Q)can be calculated and used to determine the number of electrons passed can be calculated using the Faraday constant, *F*, Equations [2-6]and [2-7]. In Equation [2-7], *e* is the charge of an electron and N_A is the Avagadro constant.

$$Q = \int_{t_i}^{t_f} I \, \mathrm{d}t \qquad [2\text{-}6]$$

$$F = eN_A = 96{,}485 \; C \; mol^{-1} \qquad [2\text{-}7]$$

This can be directly compared to the extent of substrate to product conversion and thus used to determine the current efficiency – moles of product generated per moles electrons passed. Since the reduction of NAD^+ to NADH is a two electron process, at 100 % current efficiency the number of catalytic turnovers should be equal to half the number of electrons passed.

2.1.9 Limitations and considerations

Each enzyme immobilised on the electrode undergoes many redox cycles; between 100 and 10,000 s^{-1} have been reported for H_2 oxidation by some hydrogenase enzymes.[202,203] The active site is oxidised by the electrode, reduced by H_2 during catalytic turnover and re-oxidised by the electrode, and thus the process continues. The Faradaic current recorded from an immobilised enzyme under electrochemically controlled redox catalysis is therefore a catalytic wave dependent on multiple factors including:

(1) Mass transport (of substrate to and product from the electrode)
(2) Rate of reaction at the active site
(3) Intramolecular electron transfer (between the active site and the protein shell)
(4) Interfacial electron transfer (between the enzyme and the electrode).

The rate of reaction at the active site combined with intramolecular electrons transfer is of most interest for this work.

At a stationary electrode, significant catalysis leads to depletion of substrate and build-up of product at the electrode surface, which effects the activity of the adsorbed enzyme (Section 2.3). To prevent mass transport limitations, the electrode was rotated at at rate of at least 2000 rpm. This ensured that the solute concentration at the electrode was constant and the same as that in the bulk solution; substrate was continuously supplied to the electrode and any product formed was rapidly spun away (laminar flow).[204] In practice, the rate of rotation of the working electrode was increased until no further increase in the magnitude of catalytic current was seen.

The rate of intramolecular electron transfer is assumed to be fast and therefore not rate limiting. However, the rate of interfacial electron transfer is more complicated. Electrons are transferred between the electrode and the outer-most FeS cluster, and the rate of electron transfer depends on the distance between them which in turn depends on the orientation of the enzyme. This factor has an impact on the shape of a cyclic voltammogram for a redox enzyme

in protein film electrochemistry. The magnitude of the catalytic current is proportional to the enzyme activity. It would be expected that as the overpotential (driving force) applied increases the rate of catalysis would increase until the enzyme reaches its maximum activity. At this point, the rate of reaction and therefore observed current would become limited by the enzyme. In practice, the catalytic current recorded for an immobilised enzyme under catalytic turnover continues to rise with increasing overpotential. This has been modelled by assuming a dispersion of enzyme orientations, and therefore electron transfer distances (and hence interfacial electron transfer rates). This leads to a range of different overpotential requirements to enable fast electron transfer.[205]

This orientation effect brings about another significant limitation to PFE. It is generally unclear exactly how much enzyme is immobilised on the electrode and further, how much of the enzyme is able to exchange electrons with an electrode. For this reason, two enzyme films prepared in the same way are not directly comparable. The shape of a catalytic wave (in cyclic voltammetry) tends to be consistent between films, however the exact nature of the electrode surface changes and therefore slight differences in the magnitude of catalytic current are observed. In order to electrochemically characterise a redox enzyme, methods for directly comparing multiple enzyme films are sometimes required; these are discussed in more detail in Section 2.3.

2.2 High surface area electrodes

The analytical (planar) working electrodes discussed above are essential for enzyme characterisation. They allow analysis of very small quantities of enzyme sample with high sensitivity to small catalytic currents since the electrode surface area is low, and therefore the capacitive current is much lower than the catalytic current. However, this work endeavoured to use enzyme-modified electrodes to drive enzyme-catalysed biotransformations. Although this required some enzyme characterisation, many of the experiments were instead interested

in the conversion of starting material to product. This meant that larger quantities of enzyme were employed in order to achieve detectable conversions. Much of the work in Chapters 3 and 6 made use of high surface area electrodes to enable large quantities of enzyme to be used.

A brief review of high surface area electrodes is given here alongside an introduction to some of the materials chosen and the standard protocols for enzyme adsorption onto particles. The materials and techniques for preparing high surface area electrodes were transferred to approaches for coupling a hydrogenase and an NAD^+-reductase on conducting carbon surfaces in Chapter 5.

2.2.1 Review of scale-up of hydrogenase electrodes

As discussed in Section 1.2.3, immobilised enzymes are used in industry for chemical synthesis, and a range of advantages are apparent. In the work presented in this Thesis, it is essential that the enzyme support is electronically conducting and therefore the existing strategies for enzyme immobilisation used in the chemicals sector are not relevant. Instead, this work draws upon techniques used for electrochemical devices such as enzyme-catalysed fuel cells where enzymes, for example hydrogenases, are 'wired' to high surface area electrodes such that high current densities are achieved. Only carbon based materials will be considered here since bare metals are likely to both denature immobilised enzymes and interact with organic molecules (substrates and products) and the cofactors at the potentials relevant to this work, leading to side reactions and therefore decreasing product purity. Some modified gold surfaces have proven suitable for immobilisation of active enzyme,[206] however these would likely lead to more expensive systems due to the cost of the metal and the extra modification steps.

Many research groups have developed high surface area electrodes for enzyme catalysed H^+/H_2 cycling due to the interest in enzymes or enzyme mimics for these energy relevant

reactions (H_2 production and H_2 oxidation in H_2/O_2 fuel cells). Healy *et al.* demonstrated enzyme-modified pyrolytic graphite particles (produced from the same material used to prepare the analytical electrodes described in Section 2.1.4) in electronic contact as high surface area electrodes.[207,208] Xu *et al.* used compacted mesoporous carbon electrodes modified with hydrogenase in which additional stability was achieve by 'burying' of the enzyme deep into the pores slowing down desorption.[209] Morozov *et al.* used carbon filament electrodes for adsorption of hydrogenase and demonstrated high enzyme stability (50 % activity after 1 year storage).[210] Krishnan *et al.* demonstrated a hydrogenase covalently linked to multi-walled carbon nanotubes on a PGE electrode leading to an order-of-magnitude improvement in a H_2/O_2 fuel cell.[211]

The reports above provide a good basis for utilising carbon materials to generate high surface area enzyme-modified electrodes. In this work, direct adsorption of the enzyme onto carbon materials is favoured since covalent attachment steps add time and cost to preparation of the final catalyst systems.

2.2.2 Materials used for high surface area electrodes

Carbon materials for adsorption of hydrogenase 1 from *E. coli* to form high surface area electrodes have been recently reviewed.[212] Quinson *et al.* characterised a range of both commercially available and novel synthesised carbon particles, nanopowders and nanotubes and compared the magnitude of catalytic H_2 oxidation current by an immobilised hydrogenase (*E. coli* Hyd-1). The activity was compared to the specific surface area, surface morphology and the 'graphitic' nature of the carbon materials. Overall, the highest catalytic H_2 oxidation currents were achieved using enzyme-modified carbon black - black pearls 2000 (BP, Cabot Corporation); these particles were therefore investigated in this work. Advantageously these particles are already used in a range of industries including as conducting fillers[213] and high surface area supports for fuel cell catalysis.[214] This means they are cheap and commercially

available; this is an important consideration when developing a catalytic system that is appropriate for applications in industry.

Initial experiments for both electro-enzymatic and H_2-driven NADH generation utilised pyrolytic graphite (PG) particles since both the hydrogenase and NAD^+-reductase have been extensively studied at PGE electrodes and shown to adsorb easily, without any surface modification, and undergo efficient direct electron transfer. The PG particles were freshly prepared before use since it is accepted that this aids enzyme adsorption,[196] however, this complicates direct comparison between particle preparations. In comparison to other carbon materials, PGE is relatively expensive; other carbon materials were therefore also considered.

Carbon paper has been previously used by the Vincent Group as a conductive 'sheet' to aid connectivity between enzyme-modified particles and between the particle network and a working electrode connector. In Chapters 3 and 5 carbon paper was used for direct enzyme adsorption and as an electrode support for enzyme-modified particles. Carbon paper is made from interwoven carbon fibres and is used in a range of enzyme fuel cells as well as some precious metal fuel cells.[215–217] A further set of carbon materials was considered as a conductive surface for coupling hydrogenase and NAD^+-reductase enzymes in Chapter 5 and are discussed in Section 5.4.6.

Overall, a range of carbon materials were used; a general protocol for preparing enzyme-modified particles is given here:

- Carbon particles were added to aqueous(-buffer) solution to give a concentration of *ca* 20 mg mL^{-1}.
- The particle mixture was sonicated for at least 5 minutes to aid dispersion.
- An aliquot of this was added to the required enzyme (or mixture of enzymes) sample and left at 4 ^oC for at least 30 minutes.
- In most cases, the particles were then separated by centrifugation (7,000 *g*, Eppendorf MiniSpin®) and the supernatant removed. Addition of 3 successive aliquots of fresh water-buffer solution each followed by centrifugation to remove supernatant ensures that no unabsorbed enzyme was left in solution.

The precise quantity of enzyme and particles used is detailed in the relevant results chapters.

2.2.3 How much enzyme is immobilised and how active is it?

As discussed in Section 2.1.9 it is unclear exactly how much enzyme is immobilised on an electrode and therefore how active each enzyme molecule is. This poses a further problem when analysing the current enhancement when using high surface area electrodes. An increase in magnitude of catalytic current is indicative of more catalytic turnovers per second but does not necessarily differentiate between the presence of *more* catalyst or simply *more active* catalyst. In general a large increase in catalytic current implies a higher loading of electrocatalytically active enzyme.

It is thought that some carbon materials promote increased enzyme adsorption, activity and stability due to the surface structure.[88] For example, carbon materials with large pores may trap the enzyme slowing desorption, aiding hydration and increasing the proportion of enzyme appropriately orientated for direct electron transfer. A large 'pore'-like structure also increases the surface area per g of carbon.

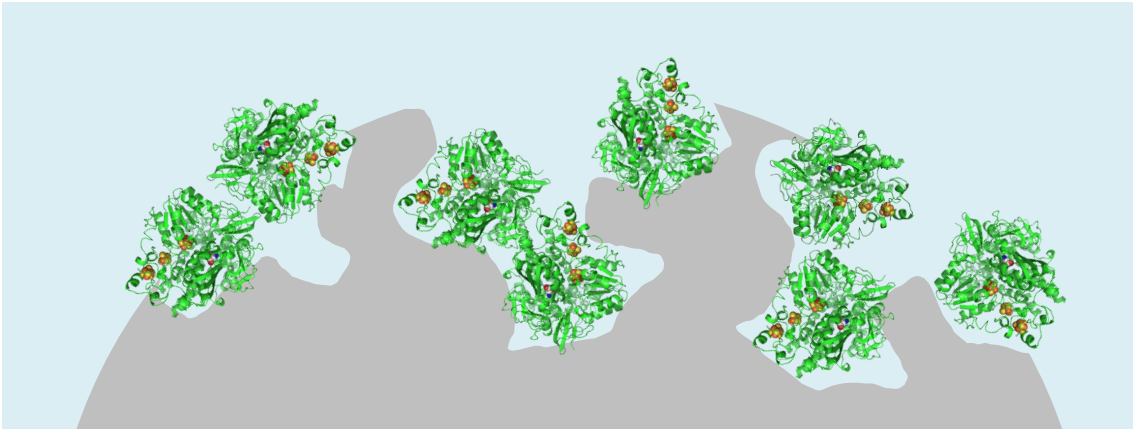

Figure 2-6: Cartoon showing that some carbon materials can offer an improvement in enzyme activity and stability due to pores on the surface. It is possible that the pores retain water aiding with hydration and that the enzyme is more likely to be orientated for direct electron transfer.

Ensuring the enzyme turnover is not mass transport limited is more difficult when using particle electrodes since the substrate must diffuse through the particle network. This is especially problematic when using bulky substrates (like NAD^+ and NADH) and is considered in the results chapters.

2.3 Enzyme kinetics and electrochemical analysis

The mechanism and therefore kinetics of enzyme reactions are complicated. Even enzymes that catalyse the same reactions (for example the hydrogenases already mentioned) behave differently under the same conditions since they have different structures and roles *in vivo*. The work presented in theis Thesis requires an understanding of enzyme kinetics in order to develop and optimise particular experiments for a range of applications. In Chapter 4 a hydrogenase and an NAD^+-reductase were electrochemically characterised for the first time and kinetic parameters determined. Here, some key models for understanding enzyme kinetics are discussed, including a brief description of electrochemical techniques for their quantification. More detailed protocols are discussed in the results chapters.

2.3.1 Affinity constant (k_M)

The Michaelis-Menten kinetic model relates the activity of an enzyme to the concentration of its substrate.[218,219] For this Michaelis and Menten described enzyme catalysis according to Equation [2-8] where an enzyme (*E*) and a substrate (*S*) form a complex (*ES*) with a rate of k_1. This complex can either dissociate with a rate constant of k_{-1} or react to form the product (*P*) with rate constant k_2.

$$E + S \underset{k_{-1}}{\overset{k_1}{\rightleftharpoons}} ES \xrightarrow{k_2} E + P \qquad [2\text{-}8]$$

If the formation of the product is the rate limiting step the rate of reaction (v) is equivalent to Equation [2-9].

$$v = k_2[ES] \qquad [2\text{-}9]$$

If the formation and dissociation of [*ES*] occur at equal rates the steady-state approximation can be applied to the enzyme-substrate complex (Equation [2-10]) and a constant, the Michaelis constant (k_M), derived, Equation [2-11]. Throughout a reaction the total enzyme

concentration ($[E_{total}]$) is equal to $[E]$ + $[ES]$, by substituting for $[E]$ the equation can be re-written to give Equation [2-12].

$$\frac{d[ES]}{dt} = k_1[E][S] - (k_{-1} + k_2)[ES] = 0 \quad [2\text{-}10]$$

$$[ES] = \frac{k_1[E][S]}{k_{-1} + k_2} = \frac{[E][S]}{k_{\mathrm{M}}}, k_M = \frac{k_{-1} + k_2}{k_1} \quad [2\text{-}11]$$

$$[ES] = \frac{([E_{total}] - [ES])\,[S]}{k_{\mathrm{M}}}, [ES] = \frac{[E_{total}][S]}{(k_{\mathrm{M}} + [S])} \quad [2\text{-}12]$$

At the maximum rate of reaction, v_{max}, all of the enzyme will have substrate bound meaning $[ES]$ is equivalent to $[E_{total}]$, Equation [2-13].

$$v_{max} = k_2[E]_{total} \quad [2\text{-}13]$$

By substituting the expression for $[ES]$ from Equation [2-12] into Equation [2-9] and combining with Equation [2-13] the Michaelis-Menten equation is reached:

$$v = \frac{v_{max}[S]}{[S] + k_{\mathrm{M}}} \quad [2\text{-}14]$$

From Equation [2-14] it can be seen that when the substrate concentration is equal to the k_{M}, the rate is half the maximum. Simplified, this means that k_{M} is equal to the concentration at which half of the enzyme forms the substrate-bound complex $[ES]$. The Michaelis constant therefore indicates the affinity of an enzyme for a particular substrate. An enzyme with a low k_{M} requires less substrate to reach its maximum activity compared to an enzyme with a high k_{M}. The cartoons in Figure 2-7 demonstrate the relationship between $[E]$, $[S]$ and $[ES]$ at substrate concentrations (A) below, (B) at, and (C) above k_{M}. A typical plot of rate *vs* substrate concentration is shown in (D).

The k_{M} for an enzyme can be determined electrochemically (Section 4.2.3). The current is recorded at constant potential (chronoamperometry) whilst aliquots of substrate are injected into the electrolyte. Since current is proportional to the rate of catalytic turnover by the enzyme the current at each substrate concentration can be plotted and fitted to the Michaelis-

Menten Equation. Advantageously this electrochemical technique is independent of the amount of enzyme used, thus the problems with knowing exactly how much enzyme is electrocatalytically active on the electrode are negated. The value of k_M can be compared across multiple enzyme films to obtain an average.

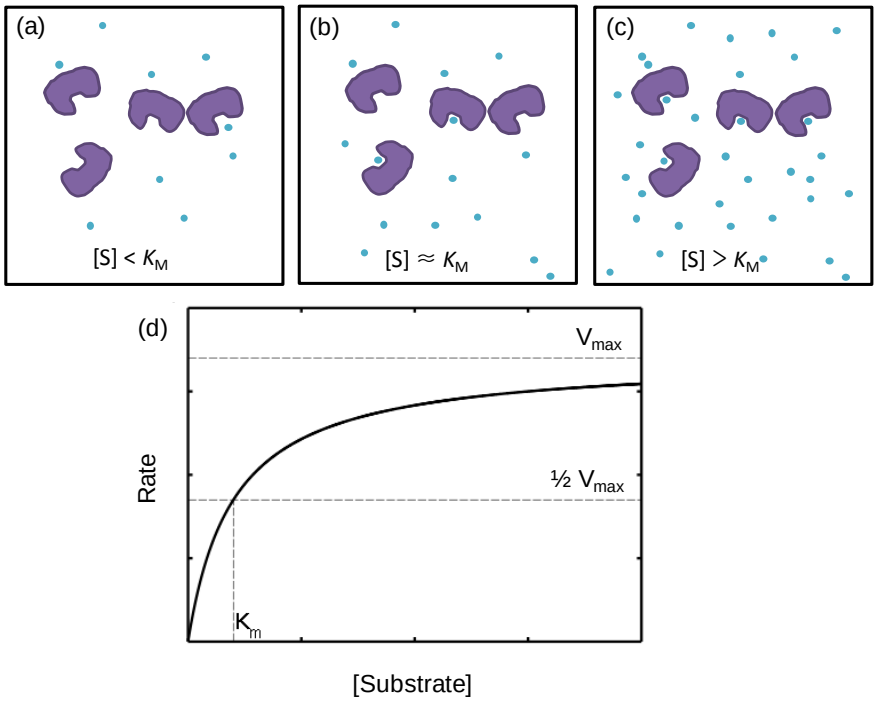

Figure 2-7: The effect of substrate concentration on the rate of an enzyme catalysed reaction. Cartoons showing the relationship between substrate (blue dots) and enzyme (purple) at different concentrations. At low substrate concentration (A) very little substrate is associated with the enzyme active site; at k_M (B) half the enzyme active sites contain substrate. At high substrate concentration (C) almost all the enzyme is involved in an enzyme substrate complex and therefore the rate is at its maximum. (D) An idealised curve showing the relationship between rate of reaction and substrate concentration.

This discussion of Michaelis-Menten kinetics is important as it aids choice of substrate concentration for a particular experiment. In general, for an enzyme to work at a rate near its maximum, a substrate concentration of 10 × k_M is used. The k_M of NAD^+ for the NAD^+-reductase (HoxFU) from *Ralstonia eutropha* is *ca* 197 μM.[151] For experiments requiring highly active NAD^+-reductase an NAD^+ concentration between 1 and 2 mM were therefore used. In cases where a change in activity was more important a concentration just below k_M is more useful (since the change of rate with [S] is most sensitive here and therefore changes in the current more significant).

2.3.2 Inhibition constant (k_I)

Enzymes can be inhibited by a range of substances; the inhibition is either competitive, uncompetitive or a mixture of the two. This depends on whether the inhibitor binds to the free enzyme, the enzyme substrate complex or to both.

An important subsection of inhibition is product inhibition. This is the effect of the product of a reaction (NADH) on the rate of reaction (NAD^+ reduction) and occurs when the product binds to the active site preventing further reaction with the substrate. Previous electrochemical analysis confirms that the NAD^+-reductase from *Ralstonia eutropha* is product inhibited for both NAD^+ reduction and NADH oxidation. This had an impact on experiments in the following chapters since a build-up of product decreases the rate of reaction. The type of inhibition and the value of the inhibition constant, k_I, can be determined electrochemically (Section 4.2.4) using similar techniques as for determination of k_M.

A Cornish-Bowden plot can be used to determine the type of inhibition (competitive, mixed or uncompetitive). A plot of the ratio of [substrate] and rate (current) against [inhibitor] at a range of substrate concentrations gives a set of straight lines. The lines are parallel for competitive inhibition and intersect at a positive or negative value for mixed or uncompetitive inhibition, respectively. This is described in more detail in Chapter 4.

Dixon proposed a slight change to the Michaelis-Menten equation to determine the inhibition constant for competitive inhibition, Equation [2-15].

$$v = \frac{v_{max}[S]}{[S] + k_M(1 + \frac{[inhibitor]}{k_I})} \qquad [2\text{-}15]$$

A Dixon plot of 1 / rate (current) against [inhibitor] a range of substrate concentrations leads to a number of lines that intersect at $-k_I$.

In contrast to electrochemical determination of k_M, to determine k_I multiple experiments, and therefore multiple enzyme films, at a range of substrate concentrations must be directly

compared. Due to the differences in catalytic current due to the range of enzyme orientations (Section 2.1.9) a control substrate injection at a particular concentration was used to normalise the current across multiple chronoamperometry experiments.

2.4 Ultraviolet-visible spectroscopy

Solutions of NAD^+ and NADH are commonly studied using ultraviolet–visible (UV-vis) spectroscopy. This absorbance spectroscopy uses light in the UV-vis region (200-800 nm). The adsorptions in this region are due to electronic transitions – the excitation of electrons from an occupied to an unoccupied molecular orbital. The energy required relates to the type of electronic transition, in general:

$$\sigma \rightarrow \sigma^* > n \rightarrow \sigma^* > \pi \rightarrow \pi^* > n \rightarrow \pi^* \qquad [2\text{-}16]$$

The $\sigma \rightarrow \sigma^*$ transitions tend to be too high in energy to see in the UV-vis region. However, UV-vis spectroscopy is a particularly important technique for studying molecules that contain conjugated systems and aromatic rings, where the $\pi \rightarrow \pi^*$ and $n \rightarrow \pi^*$ transitions tend to be in the UV-vis region.

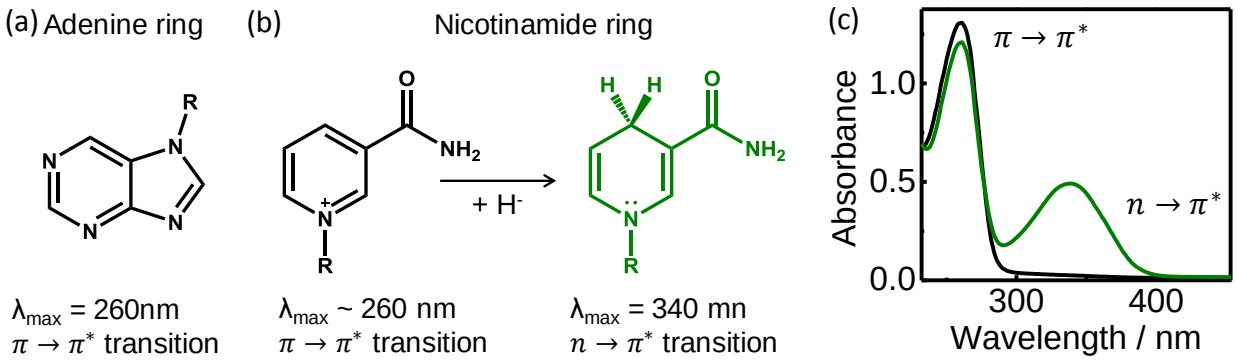

Figure 2-8: The UV-vis active portions of the nicotinamide cofactors. (a) The adenine ring gives a strong absorbance band at 260 nm due to a $\boldsymbol{\pi \rightarrow \pi^*}$ transition. (b) The oxidised nicotinamide ring has a weak $\boldsymbol{\pi \rightarrow \pi^*}$ transition around 260 nm which is lost on reduction *via* hydride addition. The introduction of two additional electrons leads to a $\boldsymbol{n \rightarrow \pi^*}$ transition at 340 nm. (c) UV-vis spectra of NAD^+ (black) and NADH (green) at concentrations of 77 µM in a UV-vis cuvette of 1 cm path length.

The $\pi \rightarrow \pi^*$ transition in the adenine portion of the nicotinamide cofactors leads to a conserved absorbance between 240-275 nm with λ_{max} = 260 nm, Figure 2-8(a).[220] The

reduced and oxidised cofactors can be distinguished by the presence or absence of absorbance with λ_{max} = 340 nm, respectively, Figure 2-8(b). This is due to a $n \rightarrow \pi^*$ transition in the reduced cofactors involving the non-bonding nitrogen electrons and the carboxyamide group. A UV-vis spectrum of NAD^+ (black) and NADH (green) are shown in Figure 2-8(c).

UV-vis spectroscopy was routinely used in this work either to determine the concentration of NADH or the concentration ratio of NAD^+ and NADH.

2.4.1 Concentration determination using UV-vis spectroscopy

The extinction coefficient at a particular wavelength can be used to determine the concentration of a molecule using the Beer-Lambert Law, Equation [2-17]. There are literature values for the extinction coefficient (ε) of NAD^+ at 260 nm and NADH at 260 and 340 nm, Table 2-1.[221]

Table 2-1: Comparison of literature[221] and typical experimental extinction coefficients (ε) for the NAD^+ and NADH cofactors.

Sample	Literature[221] / mM^{-1} cm^{-1}		Experimental[222] / mM^{-1} cm^{-1}	
	$\varepsilon_{260\ nm}$	$\varepsilon_{340\ nm}$	$\varepsilon_{260\ nm}$	$\varepsilon_{340\ nm}$
NAD^+	17.4	N/A	15.1	N/A
NADH	14.1	6.22	*nd*	5.5

However, when standard samples of NAD^+ and NADH were analysed experimentally the extinction coefficients are consistently lower than these values, Table 2-1. This is likely due to interaction of the cofactor with different buffer systems.[223] Original 'in house' extinction coefficients were determined by Dr Z. Idris[222] (Table 2-1) and were routinely confirmed under the reaction conditions utilised. UV-vis spectra of known concentrations were recorded and the absorbance (*A*) at a particular wavelength plotted with respect to the concentration (*c*). According to the Beer-Lambert Law (Equation [2-17]) the gradient of the line is equal to the extinction coefficient (ε) multiplied by the path length (*l*) and therefore the concentration of an unknown sample was then determined from the UV-vis spectra.

$$A = \varepsilon c l \quad [2\text{-}17]$$

UV-vis spectroscopy can also be used to determine the ratio of NAD^+ and NADH in samples to give an indication of the extent of NAD^+ to NADH conversion. This was particularly important in systems where the total cofactor concentration did not remain constant, for example if solution was lost due to evaporation, samples were diluted or cofactor was adsorbed onto a carbon material. A plot of $[NAD^+]/[NADH]$ *vs* $A_{260\,nm} / A_{340\,nm}$ gives a straight line, thus the concentration ratio can be determined from the ratio of absorbance at 260 and 340 nm, Appendix A. Assuming the initial concentration of cofactor is known the individual NAD^+ and NADH concentrations can be calculated.

2.4.2 UV-vis spectrophotometers and experimental methods

Two UV-vis spectrophotometers were used in this work. The first (Cary 60, Aglient) uses the sample in a UV-vis cuvette (Hellma) of well-defined path length (1 cm) and thus allows quantitative analysis of a samples concentration using the Beer-Lambert Law. A cell holder (Agilent) incorporating magnetic stirring and a peltier element was used such that experiments could be performed in the UV-vis cuvette and monitored *in situ* with constant temperature and stirring to ensure good transport of substrate to the catalyst system. In general the buffer systems used give a strong absorbance below *ca* 210 nm. For this reason, a baseline was always recorded in the presence of buffer and subsequent spectra of solutions containing cofactor recorded using this baseline to remove any contributions from the buffer. The maximum absorbance (A) that can be detected using the Cary 60 spectrometer is ± 4 A, including contributions from the buffer. However, in general only absorbance below 1 A was used quantitatively. Using the literature extinction coefficients this means the maximum concentrations of NAD^+ (detected at 260 nm) and NADH (detected at 340 nm) than can be detected are 57 µM and 160 µM, respectively using a 1 cm path length cuvette. However, since much of this work monitors the generation of NADH from NAD^+, only the absorbance

at 340 nm was required to calculate the activity of a system and initial activities of the NADH generation systems could be monitored *in situ* in this way. The absorbance at 340 nm was recorded as a function of time (A min^{-1}) and converted into the change in concentration over time using the Beer-Lambert equation. In the literature, this tends to be converted to µmoles min^{-1} per mg of enzyme (abbreviated to Units mg^{-1} or U mg^{-1}) to allow direct comparison to different systems.

The second UV-vis spectrophotometer was a NanoVue^{TM} plus (GE healthcare) which advantageously enables analysis of very small sample volumes (2 µL) with a low path length (0.02 or 0.05 cm). This analytical method was therefore crucial in initial experiments where very low reaction volumes were used as many time points could still be taken. According to the Beer-Lambert equation, as the path length decreases, the absorbance for a particular concentration also decreases. The NanoVue therefore allowed *ex situ* monitoring of more concentrated samples without dilution. However, the path length is less well-defined; therefore this UV-vis spectrophotometer was more often used to determine the concentration ratio. In some cases, for *ex situ* analysis of reaction solutions, the samples were diluted and analysed using the Cary 60 for higher accuracy.

The methods described here were used to either determine the concentration of NADH or to monitor NAD^+ to NADH conversion. The procedures were adapted in systems where electrodes or particles were used in the solution; the methods are described in Chapters 3 to 8.

2.5 High-performance liquid chromatography

High-performance liquid chromatography (HPLC) was used to determine the final concentrations of substrate and product after either H_2-driven or electrochemically-driven cofactor-dependent chemical synthesis. HPLC enables identification and concentration determination of each component in a mixture by comparison to known standards. Molecules are separated based on their affinity for a mobile and stationary phase. The columns used and

protocols developed are detailed in Appendix E. A Shimadzu Prominence HPLC equipped with a CBM-20 system controller, LC-20AD superior solvent delivery system, SIL-20A high-throughput autosampler, CTO-10AS column oven and SPD-20A UV-vis absorbance detector was used running on LabSolutions software. UV-vis detection was carried out two wavelengths. The absorbance at 210 nm and 260 nm was recorded to enable detection of both the organic molecules and the cofactor. However, NAD^+ and NADH could not be distinguished in this way as the absorbance at 340 nm was not recorded.

When using the enzyme-modified particle system for H_2-driven cofactor supply, the overall volume of reaction mixture can change. Care was taken to avoid excessive loss of solution by using a gas bubbler for introduction of H_2 and sealing the reaction vessel; however with long reaction times there may still be slight loss. Furthermore, some substrate and product, as well as the NAD^+ and NADH may adsorb onto the particles over time thus affecting the final concentrations observed. If the molecules used are volatile, they may also be removed from the reaction mixture during the constant flow of H_2. For these reasons, a ratio of the peak areas for substrate and product was often used to determine percentage conversion of substrate to product.

A sample was prepared for HPLC analysis by first removing particles by centrifugation and then removing any enzyme in solution by centrifugation through a molecular sieve. A significant limitation of HPLC is that the reactions can not be monitored *in situ* and therefore the change activity of the systems could only be observed as a function of time by removing aliquots.

2.6 Infrared spectroscopy

Infrared (IR) spectroscopy was used for *in situ* product detection (as a complementary technique to HPLC) and to understand the nature of the electronic link between co-immobilised hydrogenase and NAD^+-reductase moieties.

2.6.1 Theory of IR spectroscopy

Infrared radiation refers to uses light with wavelengths in the region of 1-1000 µm (10-10,000 cm^{-1}) and the absorbance of IR radiation generally leads to vibrational transitions in organic molecules. The IR radiation is absorbed according to the Beer-Lambert Law (Section 2.4) and thus the absorbance is generally proportional to the sample concentration. As an approximation, a molecule can be thought of as a series of masses (nuclei) connected by springs (bonds) and thus vibrations can be modelled by Hooke's Law. The energy of an absorbance band therefore gives information on the strength of a particular bond, and the mass of the atoms involved in the vibration. This work makes use of an attenuated total reflectance (ATR) IR cell developed in the Vincent Group.[207,224] The cell was designed to allow an adsorbed-enzyme particle film to be under precise electrochemical control and to be monitored using IR spectroscopy. In Chapter 5 this allowed the hydrogenase active-site to be probed whilst immobilised on particles (although in this case electrochemical control was provided indirectly) and in Chapter 6 this simplified monitoring of an electro-enzymatically driven reaction. Infrared spectra were recorded at 4 cm^{-1} resolution on either a Bio-Rad FTS 6000 (Chapter 6) or Varian 680-IR (Chapter 5) spectrometer.

2.6.2 *In situ* product detection

Although IR spectroscopy is not a commonly used method for monitoring reactions catalysed by dehydrogenase reactions, the ATR-IR cell developed in the Vincent group enables simple analysis of small reaction volumes and precise electrochemical control over enzyme-modified particles. A schematic diagram of the cell is shown in Figure 2-9(a). The enzyme film on either carbon particles or carbon paper was placed on top of a silicon ATR prism. There are 5 inlets for the three electrodes (if required) and tubing to flow solution through the cell and prevent mass transport limitations. Difference spectra were collected: a background spectrum was taken of the starting solution, the reaction was then triggered by applying an appropriate

potential to the working electrode, and spectra were recorded relative to this background. The absorbance band for a substance that decreases in concentration is therefore seen as a negative peak and vice versa, Figure 2-9(b).

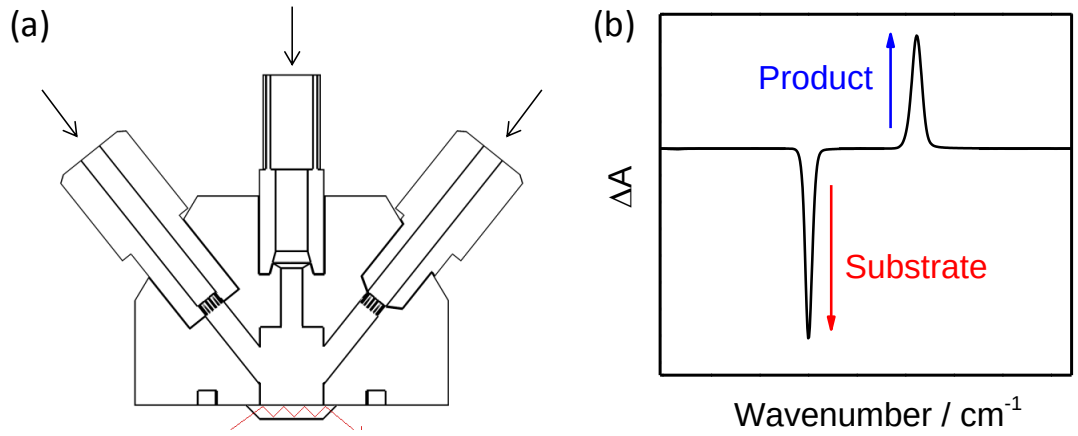

Figure 2-9: Infrared spectroctroscopy to monitor electrochemically and H_2-driven reactions. (a) Schematic representation of the IR cell, figure provided by Mr Ricardo Hidalgo-Gonzales. (b) Model of difference spectra showing loss of substrate and generation of product.

Using difference spectra allows greater sensitivity to the changes in absorbance to be detected since it negates any absorbance contributions from species that are not changing in concentration simplifying the analysis. However, since all the experiments were performed in buffered solutions, changes in the buffer absorbance complicate the spectra, particularly in the region below approximately 1100 cm^{-1}, of interest for analysis of alcohol functional groups. Since the IR beam only probes a solution depth of approximately 1 μm above the prism, only the solution directly above was monitored. In this application, the cell was set-up such that the enzyme film was not close enough to be analysed and therefore does not complicate the spectra. In order to achieve this, an aliquot of reaction mixture was dropped onto the prism and the carbon paper electrode placed on top. This approach was used to monitor electro-enzymatic NADH supply to lactate dehydrogenase for pyruvate reduction to lactate in Chapter 6.

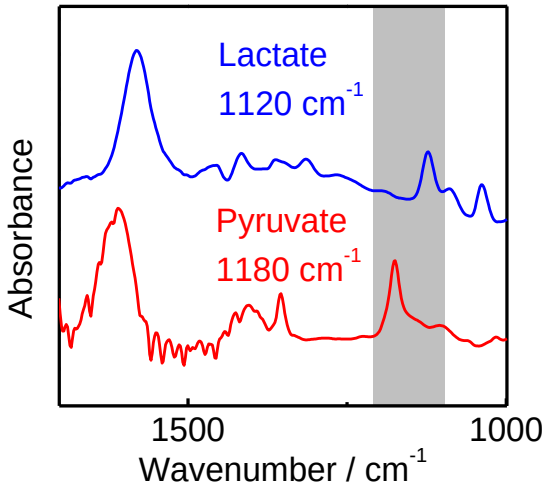

Figure 2-10: Infrared spectra of lactate and pyruvate. Spectra recoreded in water with 100 mM lactate or pyruvate using a diamond ATR accessory. The shaded region denotes the area that is not complicated by either water or buffer peaks, and contains absorbnaces unique to pyruvate and lactate.

Control IR spectra of the pyruvate (substrate) and lactate (product) taken on a diamond ATR accessory (DuraSamplIR II, SensIR Technologies) are shown in Figure 2-10. There are clear and separate peaks in the shaded region which are not compromised by either buffer or water absorbance. These peaks at 1120 and 1180 cm^{-1}, for lactate and pyruvate respectively, were used to monitor the LDH system.

2.6.3 Monitoring immobilised enzymes using IR

The ATR-IR cell was also used to understand the electronic interaction between co-immobilised hydrogenase and NAD^+-reductase enzymes. Hydrogenase enzymes have been extensively studied using IR spectroscopy due to the presence of CO and CN^- groups in their active sites (Section 1.5.1). The strength of these bonds is very sensitive to the electron density in the active site, which changes throughout catalytic turnover. By coupling electrochemical control and IR spectroscopy, a number of electronic states and their potential dependence have been identified.[225] This has enabled a clearer understanding of the catalytic pathway in a range of hydrogenases and provides a sound basis for probing the electronic link between the hydrogenase and NAD^+-reductase immobilised on particles. In this application, it

was the enzyme film that was under investigation. For that reason, the enzyme-modified particles were placed directly onto the prism such that the IR beam extended into the particle network. Electrode connections were not required since the experiments aimed to investigate if the potential of the particle could be determined by the NAD^+-reductase *via* the NAD^+/NADH concentration ratio. Again, difference spectra before and after changing the cofactor ratio were recorded to increase the sensitivity to active-site changes by removing any absorbance contributions that did not change. The positions of the active site CO absorption bands were compared to those determined previously within the Vincent Group.

2.7 Reagents

Some of the reagents and methods for their use are discussed in this Section. In most cases more detail can be found in the relevant Chapters.

2.7.1 Buffers

Nearly all of the experiments in this Thesis were performed in buffered solutions. This firstly facilitates the electrochemical experiments by increasing the conductivity of the solution but also acts to control the pH of the solution within a particular range. This is important as enzymes often have strict pH requirements and the thermodynamic potential of the $2H^+/H_2$ and NAD^+/NADH couples are related to the pH *via* the Nernst equation. The buffer used depends on the pH required by a particular system. In general a system buffers in a pH range ± 1 of the pk_a; buffer systems were chosen using Table 2-2. If a more extreme pH was required, or an experiment to determine the pH effect was carried out, a mixed buffer system was employed.

Buffers were prepared by dissolving an appropriate mass of buffer in Milli-Q water (resistivity 18.2 MΩ cm) to produce a concentration of 100 mM (unless otherwise stated). This buffer solution was then titrated to the desired pH using either concentrated HCl or KOH

using a Ag/AgCl pH electrode (Fisher) at the temperature the experiment was to be performed (unless otherwise stated). It has been shown that the NAD^+-reductase used in this work is inhibited by the presence of sodium ions[187] therefore NaOH is not used as a base for titration.

Table 2-2: Buffers used to maintain a particular pH are shown with their respective pk_a values.

pH	Buffer	pK_a (25 ^{o}C)
6	Bis-Tris	6.5
7	KPB	6.8-7.2
8	Tris-HCl	8.1
9	CHES	9.3
5-10	Mixed buffer	-

The phosphate buffer (KPB) was prepared by titrating K_2HPO_4 (Sigma, > 99 %) and KH_2PO_4 (AnalaR, > 99 %) of the same concentration together.

The mixed buffer system contained CHES, TAPS, HEPES, MES and Sodium Acetate (at 15 mM) and KCl (100 mM). The buffer was titrated to the chosen pH using KOH and HCl.

2.7.2 Cofactors

The cofactors (NAD^+, NADH, $NADP^+$ and NADPH) were all purchased from Melford and made up to 100 mM stocks in buffer or water as required. It is widely accepted that commercially available cofactors tend to contain impurities such as adenosine diphosphate ribose and adenonsine triphosphate. The effect of these impurities on the activity of the NAD^+-reductase has been previously determined within the group and shown to only be significant above ~ 1 mM.[222] In this work the cofactor concentration is never above 2 mM therefore the effect of such impurities (<1 %) will not be significant.

A more problematic contamination was of the oxidised cofactor (NAD^+ or $NADP^+$) in the reduced cofactor (NADH or NADPH, Figure 2-11). Although this trace impurity is often not identified using UV-vis spectroscopy, and therefore not noticed when studying enzymes using

most biochemical assays, the high sensitivity of electrochemical analysis means clear NAD^+ reduction by the NAD^+-reductase can be seen when using as-received NADH. For analytic experiments the NADH was therefore purified using an anion exchange column. The oxidised cofactor (NAD^+) was used as recieved.

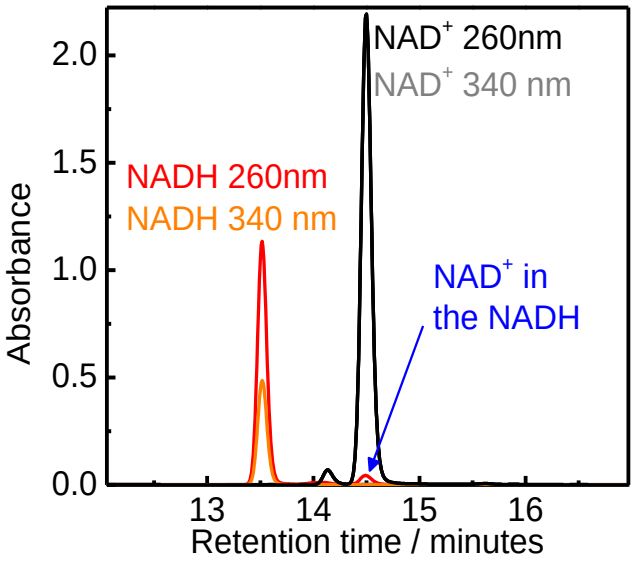

Figure 2-11: HPLC chromatogram showing the contamination of NADH with NAD^+. An aliquot of either NAD^+ or NADH was injected onto a Zic-Hilic column. At time 0 the running buffer was 20 % of 20 mM Ammonium acetate in water with 80 % of 20 mM Ammonium acetate acetonitrile at a flow rate of 1 mL/min. A gradient was applied such that after 30 minutes the mobile phase was 80 % ammonium acetate in water and 20 % ammonium acetate in acetonitrile. The column was maintained at 40 ^oC.

To purify the NADH cofactor a 1 mL AcroSep^{TM} Q Ceramic HyperD F anion exchange column (Pall) was used. The column was first cleaned with buffer (10 mL, 50 mM Tris-HCl, pH 8), a stock solution of NADH in buffer was then loaded onto the column. An aliquot of buffer (*ca* 5 mL) was then used to remove any unbound impurities and analysed using UV-vis spectroscopy to ensure that no cofactor had been removed. Low salt solution (*ca* 0.1 M) was added in 1 mL aliquots to remove the NAD^+ impurity; the eluted samples were analysed and subsequent aliquots used until no additional NAD^+ was seen. A high salt solution (0.5 M, 1 mL) was then used to elute the NADH. The eluted solution was collected in *ca* 100 µL portions and each analysed using UV-vis spectroscopy.

Each time, standards of un-purified NADH were used to construct a standard curve to

determine the concentration of purified NADH, Section 2.4. Samples of NADH were purified on the day of use and were not stored. For purification of $NADP^+$ or NADPH the method was slightly altered and aliquots of increasing salt concentration were used to elute the cofactors in the order NAD^+, NADH, $NADP^+$, NADPH and each fraction collected for analysis using UV-vis spectroscopy.

All cofactors (purified and un-purified) were made up freshly before use as they tend to be unstable. In particular, the reduced cofactors are unstable with respect to oxidation, high pH, high temperature and buffer systems.[223]

2.7.3 Gases and preparation of gas mixtures

Throughout this Thesis H_2 Premier Plus grade (Air Products), O_2 (BOC) and N_2 (BOC) were used. Details of particular experimental set-ups will be discussed in the results chapters. In some cases only one gas was required, in others precise mixtures were used. For this mass flow controllers were necessary.

Mass flow controllers (Brooks Instrument SLA Series, scontrolled using Brooks Smart Interface software) were used to prepare accurate gas mixtures and enable low and constant flow rates. Individual mass flow controllers have different flow limits and between them allow flow rates between 0.2 and 2000 mL min^{-1} to be used accurately. This was essential when low volume reactions were used to minimise loss of the solution but ensure a continuous supply of gas. Multiple mass flow controllers were used to make precise gas mixtures down to 1 % O_2 in H_2 or N_2. For such mixtures, accuracy was important since there is a well-defined limit for mixing these gases in a non-explosive ratio.

2.7.4 Other reagents

The substrates and products for the enzymes used: pyruvate, lactate, acetophenone, phenylethanol, glycerol and ethanol were all purchased from Sigma and used without further puficiation.

2.8 Enzyme samples

A range of redox enzymes are used in this work. Some of the enzymes used were commercially available, some were produced and provided by collaborators and others were made within the Vincent Group.

2.8.1 NAD^+-Reductase

**I spent a total of 2 months at Humboldt University in Berlin learning about protein purification in the group of Dr O. Lenz.*

The soluble hydrogenase (HoxHYFU) and NAD^+-reductase (HoxFU or Hox~~HY~~FU) from *Ralstonia eutropha* were produced and purified according to a published procedure by Dr Lars Lauterbach (Humboldt University, Berlin, Lenz Group).[151,226] Table 2-3 lists the NAD^+-reductase enzymes used in this work with their abbreviations.

Table 2-3: Some of the NAD^+-reductase enzymes that will be used in this work.

Abbreviation	Description
WT SH	Wild type, HoxHYFU soluble hydrogenase
HoxFU	NAD^+-reductase subunits only
Hox~~HY~~FU	HoxHYFU variant with inactive hydrogenase dimer
SE	Non-purified enzyme, crude soluble extract
Rh. o HoxFU	NAD^+-reductase subunits of SH from *Rh. opacus*
Rh. o HoxHY	Hydrogenase subunits of SH from *Rh. opacus*

The required genes (for the desired subunits i.e. HoxF) are overexpressed in a plasmid containing the *hox*FUYHWI operon. A *Strep*-tagII-encoding sequence is incorporated at the end of the *hox*F gene. This plasmid is then inserted into a variant of *Ralstonia eutropha* which prevents production of the other hydrogenases (membrane bound and regulatory). These cells are grown in a mixture of fructose, glycerol and media (minimal media H16).

This fermentation broth is analysed over time using UV-vis spectroscopy; the optical density at 436 nm is used to determine the concentration of cells. When the concentration is high

enough, the cells are harvested by centrifugation and re-suspended in buffer under an inert atmosphere (Argon). The cells are then broken apart using a French Press (1000 psi). The NAD^+-reductase is part of the soluble hydrogenase which is not membrane bound, the cell membranes can therefore be removed by ultra-centrifugation at 36000 rpm (at 4 ^oC).

The remaining solution is then passed through a *Strep*-tactin affinity and size exclusion column. This separates the *Strep* labelled protein (the NAD^+-reductase) from any other proteins. For the soluble extract (SE) samples, this purification step is not carried out. This means the extra soluble proteins are not removed, this is discussed further in Section 3.5.2).

The soluble hydrogenase from *Rhodococcus opacus* is electrochemically analysed for the first time in Chapter 4. This enzyme and its hydrogenase (HoxHY) and NAD^+-reductase (HoxFU) dimers were prepared by Ms K. Karstens (Humboldt University, Berlin, Friedrich Group).

The activity of the systems developed will be quoted in U mg^{-1} NAD^+-reductase (U = µmole min^{-1}) to simplify comparison to the literature. For this reason the quantity of NAD^+-reductase used in each experiment was stated in mass (µg). The HoxHYFU construct (with or without H_2 oxidation activity) has a mass of 177 kDa,[151] therefore 1 µg of NAD^+-reductase equates to *ca* 5.6 picomoles of enzyme.

The NAD^+-reductase from *R. eutropha* shows highest activity at 33 ^oC and highest operational stability at 25 ^oC. These two temperatures were commonly used in this work.

2.8.2 Hydrogenases

The hydrogenase enzymes used in this work are all kindly provided by collaborators or produced in house by other members of the Vincent Group. *E. coli* hydrogenase 1 (Hyd 1) and *E. coli* hydrogenase 2 (Hyd 2) are prepared by Ricardo Hidalgo and Min-Wen Chung respectively with cooperation from the Armstrong group (University of Oxford) according to estabilished procedures. The *D. vulgaris* MF hydrogenase (*D. v* MF) was provided by Prof.

Lubitz.

2.8.3 Cofactor-dependent enzymes

Lactate dehydrogenase (LDH from rabbit muscle, Sigma), yeast alcohol dehydrogenase (*y*ADH, Sigma) and glycerol dehydrogenase (GlyDH, Sorachim) were commercially available and used without further purification.

The alcohol dehydrogenase used for the reduction of acetophenone was supplied by Johnson Matthey Catalysis and Chiral Technologies and is now commercially available (X-Zyme ADH-*S*4).

The O_2 requiring cofactor-dependent enzyme used in Chapter 7 was provided as part of research collaboration. Development of a cofactor regeneration method for the flavin monooxygenase (HpbA) was carried out with Almog Bregman and Dr A. Fishman (Technion, Haifa, Israel).

Mechanism of hydride transfer in NADH-dependent enzymes

The mechanism of alcohol oxidation by liver alcohol dehydrogenase (the reverse of ketone reduction) is generally accepted as:[227,228]

(1) binding of NAD^+
(2) coordination of the alcohol to zinc
(3) deprotonation of the alcohol
(4) hydride transfer to NAD^+ generating a zinc bound ketone
(5) dissociation of NADH

as described in Figure 2-12. Acridine and acridinium derivatives have been used as NAD^+/NADH mimics to model the interconversion following a hydride transfer. Two main pathways have been proposed: a concerted hydride transfer (1 step)[229,230] or a step-wise electron-proton-electron transfer[231,232] *via* a high energy intermediate. It is likely that the exact nature of the hydride transfer depends on a range of conditions and is a mixture of the two mechanisms.[233]

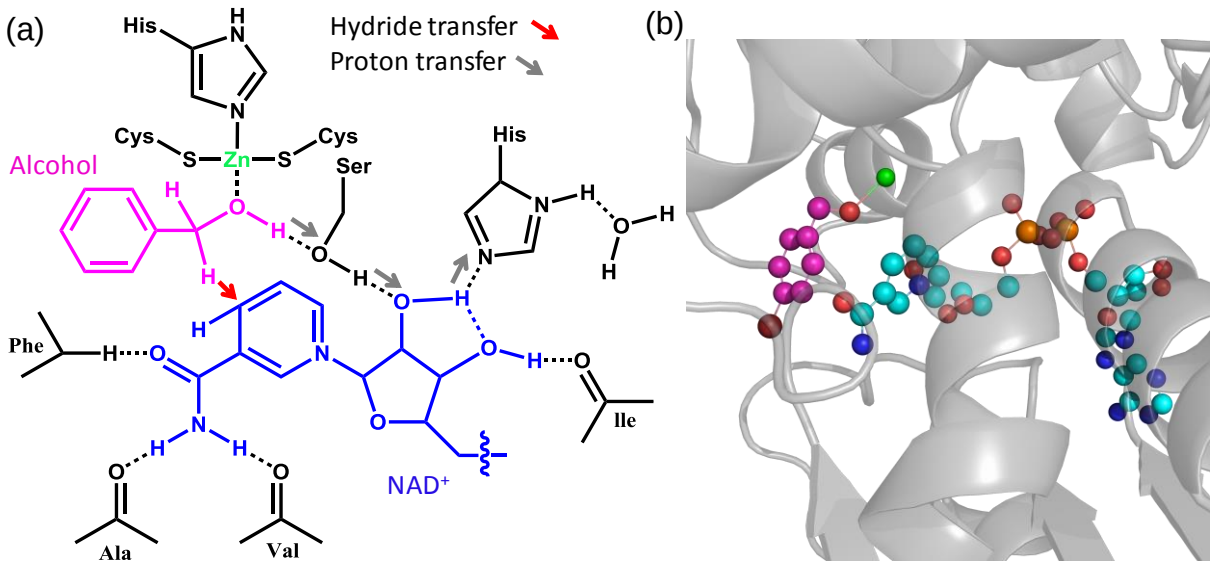

Figure 2-12: The mechanism of hydride transfer in liver alcohol dehydrogenase. (a) Structure of substrate (pink), NAD^+ (blue) and the amino acid residues (black) involved with proton transfer (grey arrows) are shown with the site of hydride transfer (red arrow). (b) The crystal structure of horse liver alcohol dehydrogenase with para-bromobenzyl alcohol (pink) and NAD^+ (blue) bound. The protein is shown as a grey cartoon, with the zinc atom shown as a green sphere. Made with PyMol, PDB code: 1HLD.[234]

2.9 Summary

This Chapter has provided information on many of the standard protocols used in this work. Due to the developmental nature of much of the work presented in this Thesis, the detailed methods used for producing and analyzing enzyme-modified electrode and particle systems are discussed at the appropriate points in Chapters 3 to 8.

Chapter 3 Electro-enzymatic NADH generation

Oxidation and reduction reactions make up a significant portion of industrial processes used in the synthesis of complex organic molecules. In particular reduction reactions can provide routes to chiral compounds, for example *via* ketone to alcohol conversion. Electrosynthesis, the use of an electrode as either a reducing or oxidising equivalent, is often considered as an 'environmentally friendly' approach to driving these redox reactions.[69] For an optimal process, an electrocatalyst is often required to prevent the need for extreme potentials (and therefore aid thermodynamic efficiency) and to increase the selectivity, Section 1.4.2.

This Chapter explores the possibility of an electro-enzymatic approach to reducing the NAD^+ cofactor to form NADH using an NAD^+-reductase as a highly selective, immobilised, electrocatalyst.

3.1 Structure and electrochemistry of the NAD^+-reductase

The whole soluble hydrogenase (SH) contains FeS clusters which, *in vivo*, shuttle electrons

between the hydrogenase dimer and the NAD^+-reducing dimer, Section 1.5.2. Although at present there is no crystal structure for the SH, there is for a related enzyme with similar function and high sequence similarity (amino acid chain);[235] it has been shown that proteins with similar function tend to have very similar geometries at their active sites even if the actual amino acid sequence similarities are low.[236] The soluble subunits of Complex I from *Thermus thermophilus* are the first step in the respiratory chain taking electrons from NADH and transferring them across a membrane along with four protons. This process creates a proton gradient, the energy from which is used for the synthesis of ATP from ADP.[237] Similarly to the NAD^+-reductase from *R. e* this enzyme also uses a bound FMN active site for the removal of a hydride from the NADH cofactor, and FeS clusters for efficient electron transfer through the protein structure. For these reasons, the crystal structure of Complex I from *Thermus thermophilus* (PDB code 2FUG)[237] provides insight into the structure of HoxFU. As such, it has been used to create a homology model, Figure 3-1(a), combing the crystal structure of Complex I with the amino acid sequence of HoxFU.

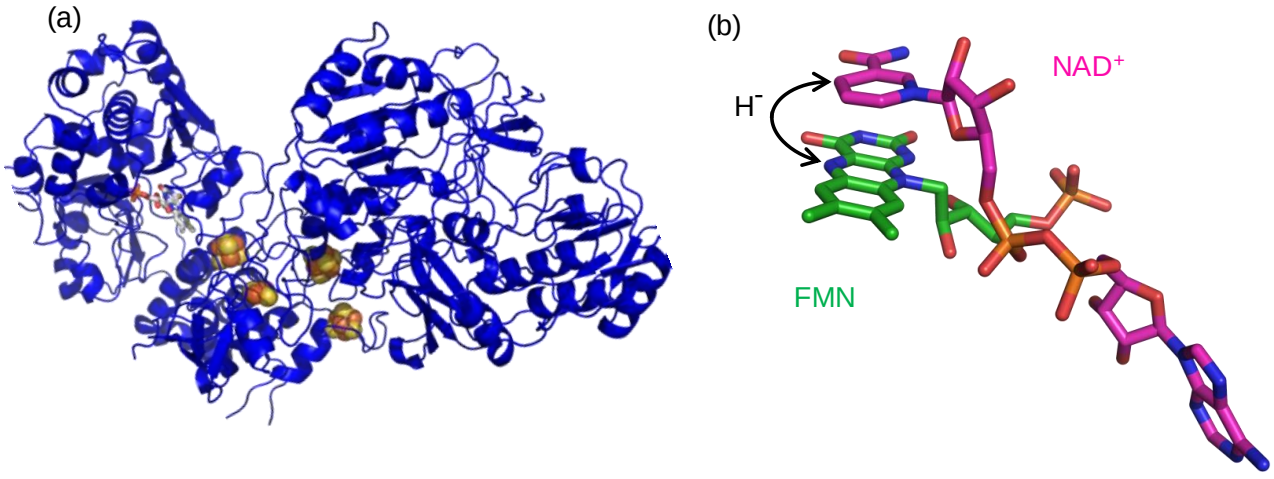

Figure 3-1: The homology model fo the NAD^+-reducing domains of the Soluble Hydrogenase (HoxFU). Panel (a) shows a cartoon representation of the protein structure with the FeS clusters as spheres (in elemental colours) and the FMN active site as sticks. Panel (b) shows the interaction between the FMN active site (green) and the NAD cofactor (pink) with the site of hydride transfer demonstrated by the arrow. Figures created using PyMol.

This homology model is particularly useful for understanding the interaction between NADH and FMN in the active site, Figure 3-1(b). The NAD^+ diffuses into the protein where it is held

in a particular orientation with respect to the FMN by surrounding protein environment. The close proximity of the FMN and NAD^+ ensures that only enzyme-active 1,4-NADH is generated.

In nature flavin cofactors are often used to meditate between one- and two-electron processes, Figure 3-2. The NAD^+-reductase contains two FMN centres:[238,239] the FMN cofactor in the hydrogenase dimer is thought to be involved with mediation between the single electron transfers at the [NiFe] hydrogenase active-site and the two electron process at the FMN active-site in the NAD^+-reductase dimer.

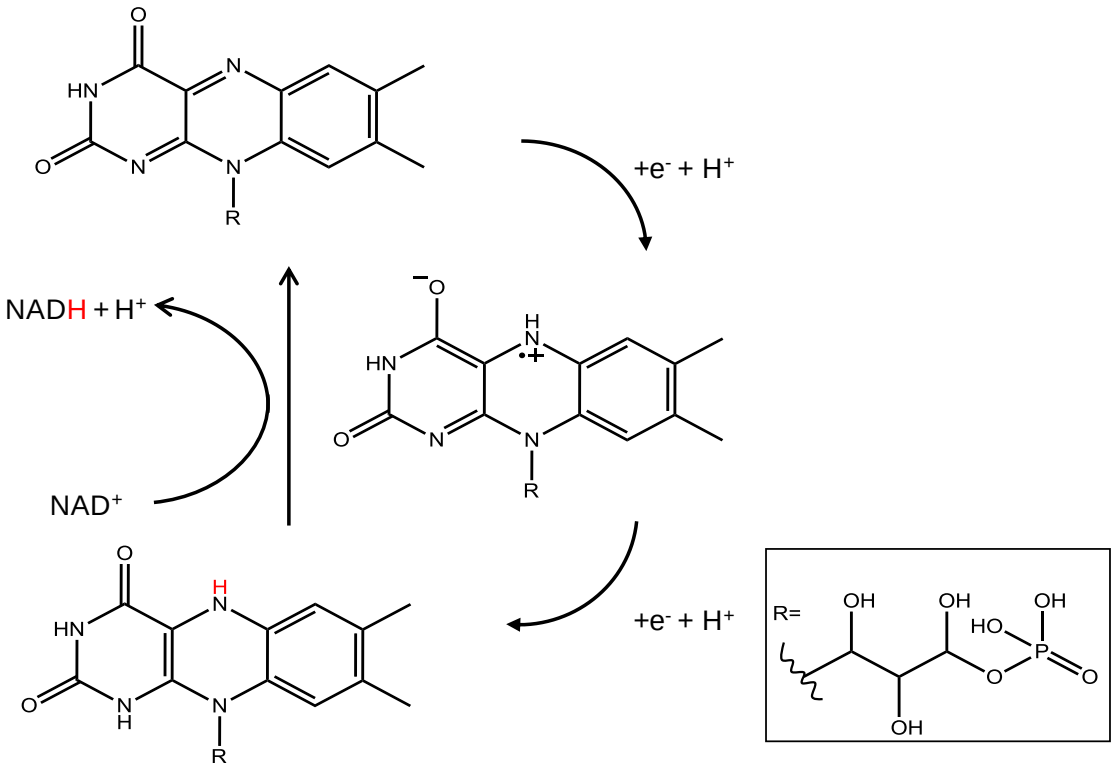

Figure 3-2: FMN is able to collect two single electrons and combine them to form a hydride using a proton from solution. This hydride can then be transferred to NAD^+ to generate NADH. This transfer occurs selectively in the active-site of the NAD^+-reductase.

The FMN in the hydrogenase dimer is known to be less tightly bound than that in HoxFU and easily dissociates from the enzyme. Changing the amount of FMN associated with the SH has been demonstrated to change the H_2:NAD^+ and H^+:NADH activity without affecting the HoxHY biochemical assays using benzyl viologen as an artificial electron donor (by-passing

HoxFU),[190] indicating that the FMN is involved with electron transfer between the two active sites. Most other [NiFe] hydrogenase enzyme do not contain this FMN cluster, instead they have two extra FeS clusters which are involved with single electron transfers.[240] It is likely that this labile FMN in the hydrogenase dimer is responsible for the enzymes instability in comparison to more standard [NiFe] hydrogenases. Approaches for using only the more stable NAD^+-reducing subunits could therefore aid development of more robust cofactor recycling systems.

3.1.1 The constructs used in this work

The soluble hydrogenase (SH) from *Ralstonia eutropha* (*R. e*) has been studied using biochemical techniques by the Lenz Group (Technical University, Berlin)[151] For this the whole SH (HoxHYFU or $HoxHYFUI_2$) was analysed using H_2 as a reducing equivalent for NAD^+ reduction allowing the enzyme to function as it does *in vivo*. The activity was monitored using UV-vis spectroscopy to follow the generation of NADH.

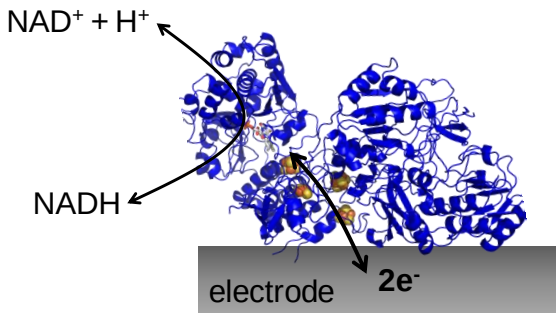

Figure 3-3: The NAD^+-reductases constructs (HoxFU and Hox~~HY~~FU) are able to use an electrode as an electron source or sink for NAD^+ reduction and NADH oxidation.

Previous work in the Vincent Group has demonstrated that the FeS clusters in the SH can also be used to transfer electrons between an electrode and the active site. If the enzyme is immobilised on an electrode, electrons can be shuttled from the electrode to the FMN active site for selective NAD^+ reduction to generate NADH. Most of the experiments in this Thesis utilise an NAD^+-reductase, either HoxFU or Hox~~HY~~FU; these constructs delete or inactive the hydrogenase dimer, respectively, and as such require and external electron source for

NAD^+ reduction to occur. For this reason it is highly advantageous to be able to use an electrode as the electron source, Figure 3-3; protein film electrochemistry has been used previously to study the hydrogenase and NAD^+-reductase dimers separately without $2H^+/H_2$ cycling complicating analysis of NAD^+/NADH activity.[151,222] This Chapter builds upon the observation that the NAD^+-reductase can use electrons from an electrode for NAD^+ reduction and aims to develop and electro-enzymatic approach to NADH generation that combines the selectivity of enzyme catalysis with the efficiency of an electrode driven system.

3.1.2 Overview of NAD^+-reductase electrochemistry

Cyclic voltammetry has been used previously to characterise the activity of the NAD^+-reductase with respect to potential and thereby give an indication of the potential at which catalysis and inactivation occur (Section 2.1.2).[151,222] The initial experiments for the work in this Chapter, used a pyrolytic graphite edge (PGE) electrode since it has been demonstrated as a good surface for adsorbing enzymes and it is also chemically inert over a wide potential window, Figure 3-4(a) grey line.

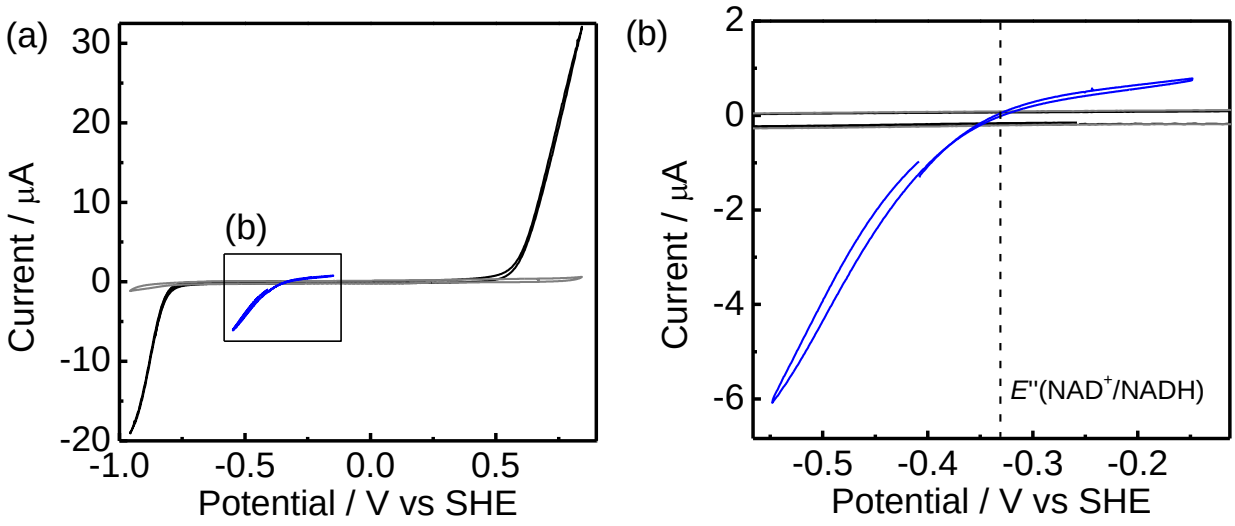

Figure 3-4: Cyclic voltammograms showing NAD^+ reduction and NADH oxidation by an unmodified carbon electrode (black) and an electrode modified with NAD^+-reductase (blue). The scans were performed in phosphate buffer pH 7 containing NAD^+ (1 mM) and NADH (1 mM). The cyclic voltammograms shown in grey corresponds to an unmodified electrode in the absence of NAD^+ and NADH. In each case the electrode rotation rate was 2000 rpm. Panel (b) shows the boxed region from (a) in more detail.

The cyclic voltammogram of a PGE electrode modified with an NAD^+-reductase (blue line) shows a negative current below the thermodynamic potential corresponding to NAD^+ reduction and a positive current for NADH oxidation above the thermodynamic potential. The current crosses the *x*-axis at the thermodynamic potential for the NAD^+/NADH couple under these conditions. In contrast the unmodified carbon electrode requires a large overpotential for both NAD^+ reduction and NADH oxidation (black line, Figure 3-4(a)).

The NAD^+-reductase is recognised as a good electrocatalyst for electrochemical cofactor conversion and carbon is identified as a suitable electrode material since it offers good enzyme adsorption and does not significantly interact with the cofactors in the relevant potential window.

3.2 Development of high-surface area electrodes

This Chapter uses the NAD^+-reductase as an electrocatalyst for NADH generation. Analytical electrochemical experiments to aid characterisation or direct comparisons were performed using a pyrolytic graphite edge (PGE) rotating disk electrode (RDE) with very small quantities of enzyme (typically < 1 pmole). In experiments where high conversion of NAD^+ to NADH was desired, larger quantities of enzyme needed to be used. For this, it was necessary to build high surface area electrodes. Section 2.2 provided some introduction into the materials used, protocols developed and literature precedents for the formation of high surface area electrodes.

3.2.1 Preparation of high surface area electrodes

Two approaches for development of high surface area electrodes were considered, using the NAD^+-reductase immobilised on either carbon paper or carbon particles. Advantageously, carbon paper can be cut to any desired shape or size allowing electrode systems of consistent geometrical surface area to be used. In the second approach, the NAD^+-reductase was

adsorbed onto carbon particles, and these enzyme-modified particles deposited onto a carbon paper electrode or PGE RDE support. This approach should increase the enzyme loading per geometrical area but is likely to be less consistent between experiments, Section 2.2.3.

Cyclic voltammetry was used to analyse the NAD^+-reductase-modified electrodes. It was important to determine if there was any change to the potential dependence of catalysis by the NAD^+-reductase on incorporation into these high surface area electrodes. This was achieved by comparing the shape of the cyclic voltammograms to those recorded using a NAD^+-reductase-modified PGE RDE. Previous electrochemical characterisation of the NAD^+-reductase (using a PGE RDE) gave similar results to the biochemical characterisation providing evidence that the electrode-immobilised enzyme operates similarly to the enzyme in solution.[151] The cyclic voltammograms provide information on the onset potential for catalysis and potential-dependent inactivation. If the shape of the cyclic voltammogram does not change when the enzyme is incorportated into different electrode systems, it is likely that the enzyme is not damaged. The cyclic voltammograms were also used to obtain information on the increase in enzyme loading. If all experiments were performed under the same conditions and mass transport was not limiting, a higher current provides evidence that more enzyme molecules were under direct electrochemical control. Although it was not possible to completely separate the activity of each enzyme from the overall activity (and therefore the amount of immobilised enzyme), the magnitude of catalytic current is proportional to the rate of NAD^+ reduction and therefore NADH generation (Section 2.2.3). As such, a large increase in catalytic current demonstrates that an electrode is more suitable for electro-enzymatic NAD^+ to NADH conversion.

3.2.2 Carbon paper electrodes

In Section 2.1.4 the preparation of enzyme films on the PGE electrodes for analytical electrochemistry was discussed. Briefly, NAD^+-reductase (HoxFU, *ca* 0.5 μg) was spotted

onto a freshly prepared electrode and allowed to adsorb over 30 seconds. The electrode was then immersed into an electrolyte solution containing NAD^+ (1 mM in Bis-Tris buffer, pH 6.3). The cyclic voltammogram was recorded by sweeping the potential between +0.24 and -0.46 V *vs* SHE and measuring the resulting current. A typical cyclic voltammogram is shown in Figure 3-5(a). The thermodynamic potential of the NAD^+/NADH couple under these conditions (assuming NAD^+/NADH > 1000) is marked by the dashed line.

For the high surface area electrode, carbon paper was cut to size such that *ca* 1 cm^2 could be suspended into solution. A piece of gold wire was used to make an electrical connection to the potentiostat *via* a crocodile clip. Care was taken such that the gold wire was not incontact with the solution to prevent any redox activity from the gold wire contributing to the catalytic current observed. A cyclic voltammogram of the unmodified carbon paper electrode in the presence of NAD^+ (1 mM, Bis-Tris buffer, pH 6.3) is shown in Figure 3-5(b), grey line. The shape of the carbon paper voltammogram is as expected, showing no redox activity. However the capacitive current (non-catalytic) from the 'blank', unmodified carbon paper electrode was much greater than for the 'blank' PGE electrode (grey lines) since the surface area was much higher.

The carbon paper used in this Thesis is hydrophobic; if enzyme was spotted straight onto dry carbon paper the solution droplet did not soak into the paper, preventing efficient enzyme adsorption. For this experiment the carbon paper was pre-soaked in buffer for *ca*1 hour and then dried before use (using N_2 gas flow). An aliquot of NAD^+-reductase (HoxFU, 5 µg) was then spread across the carbon paper and allowed to partially dry. Since the carbon paper cannot be rotated, a different electrochemical set-up was used. This consisted of a small glass vial with a magnetic stirrer bar. The three electrodes were then immersed into the electrolyte; care was taken to prevent contact between the electrodes and the magnetic stirrer as this would cause spikes in the current response. Incorporation of the stirrer was essential to

prevent build-up of NADH or depletion of NAD^+ at the electrode surface which would lead to product inhibition and mass transport limitation, respectively.

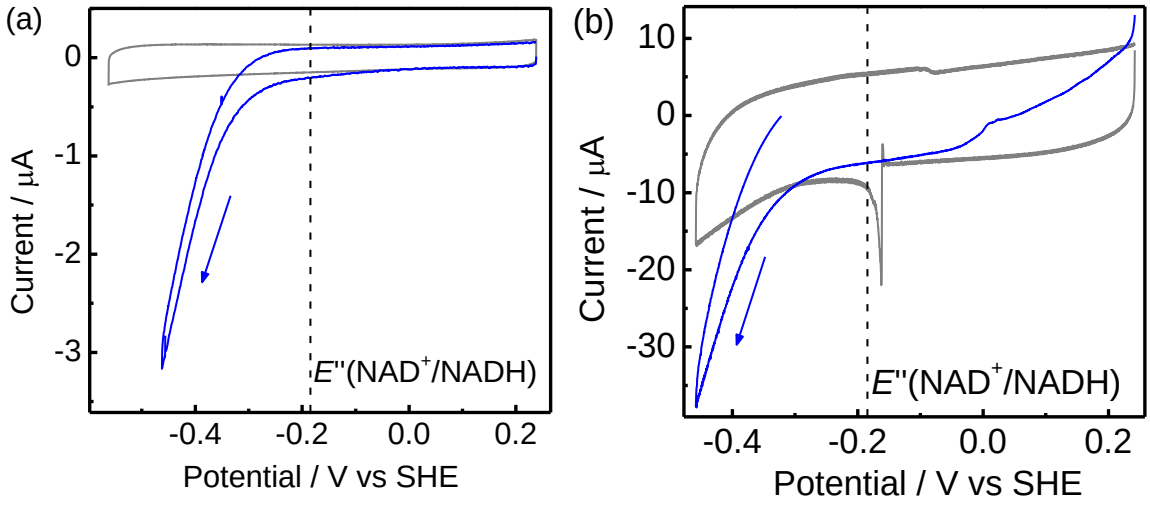

Figure 3-5: Cyclic voltammograms demonstrating that the NAD^+-reductase can be immobilised on carbon paper and is electrocatalytically active. The NAD^+-reductase (HoxFU) immobilised on (a) a PGE electrode and (b) a carbon paper electrode immersed in buffer (Bis-Tris pH 6.3) containing NAD^+ (1.1 mM). In each case a 'blank' scan of the unmodified electrode is shown in grey. The PGE RDE was rotated at 2000 rpm. The carbon paper electrode was not rotated but the solution was stirred using a magnetic stirrer to ensure that mass transport of NAD^+ to the electrode was not limiting. The potential of the NAD^+/NADH couple under the experimental conditions is shown by the black dotted line.

The cyclic voltammograms in Figure 3-5 compare the catalytic activity of NAD^+-reductase immobilised on (a) a PGE RDE and (b) carbon paper. The catalytic current from the immobilised NAD^+-reductase shown in Figure 3-5 (blue lines) confirms that the onset potential for NAD^+ reduction was not significantly altered by changing the electrode material. In each case, the onset of catalysis occurred just below the thermodynamic potential under the conditions used and there was a significant NAD^+ reduction current at -0.42 V *vs* SHE. This suggests that the activity of the NAD^+-reductase was not significantly affected after immobilisation on carbon paper in comparison to the PGE RDE. Furthermore the rate of NAD^+ reduction (moles of electrons used per second) was improved using the carbon paper electrode as evidenced by the increase in the magnitude of the catalytic current. The magnitude of the catalytic reduction current at -0.42 V *vs* SHE (taken as the midpoint between

the current on the forward and reverse scan compared to the midpoint of the blank scan at the same potential) in Figure 3-5(b) is *ca* 8 times higher than that in Figure 3-5(a).

These results confirm that carbon paper is a suitable electrode material; the blank electrode (Figure 3-5, grey line) did not show any electrochemical activity and the NAD^+-reductase was readily immobilised and used for NAD^+ reduction with no observed effect on its catalytic behaviour.

3.2.3 Carbon particle electrodes

**This experiment was performed by Ms Chloe Tomlinson, Part II student, under my supervision.*

This section investigates using carbon particles modified with NAD^+-reductase 'stuck' onto a PGE electrode as a way to further increase the enzyme loading without increasing the geometrical surface area of the electrode. Carbon black (Black Pearls 2000 Section 2.2.2) have a very large surface area, *ca* 1487 $m^2\ g^{-1}$, which means they should support high enzyme loading per g of particles.[241] In order to investigate whether high surface area electrodes can be developed using NAD^+-reductase-modified carbon particles, initial experiments were performed using enzyme-modified particles deposited on a PGE RDE. This allows direct comparison of enzyme immobilised on the electrode *vs* using the enzyme-modified particle electrode system with a consistent electrode geometrical surface area.

Cyclic voltammetry for NAD^+-reductase (0.5 μg) immobilised on the planar PGE electrode was carried out as previously described. The enzyme-modified particles were prepared by firstly dispersing a suspension of BP particles (20 mg mL^{-1}) in buffer (KPB, pH 7) by sonication. An aliquot of the particles (1 μL) was mixed with NAD^+-reductase (Hox~~HY~~FU, 10 μg) and left at 4 ^oC for 30 minutes. The particles were then separated by centrifugation (7,000 × *g*), the supernatant removed and the particles re-suspended in *ca* 10 μL of buffer. A portion of this mixture (2 μL containing *ca* 1.2 μg of BP particles and 1 μg Hox~~HY~~FU) was then spotted onto a freshly prepared PGE electrode and allowed to partially dry for *ca*

5 minutes. The electrode was then immersed in buffer containing NAD^+ (1 mM) and rotated at 3000 rpm; faster rotation rates led to loss of particles from the electrode surface. This rotation rate provided a compromise between mass transport and film stability.

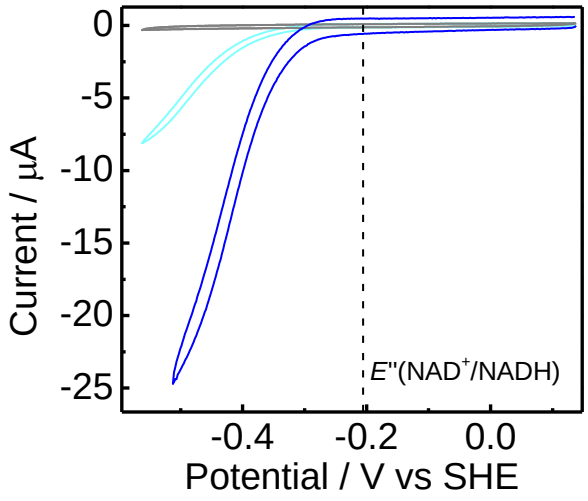

Figure 3-6: Cyclic voltammograms showing the increase in NAD^+ reduction current when using NAD^+-reductase (Hox~~HY~~FU)-modified carbon particles on a PGE electrode (dark blue) in comparison to NAD^+-reductase (Hox~~HY~~FU) immobilised onto the planar PGE electrode (light blue). A cyclic voltammogram of the unmodified electrode is shown in grey. The experiments were performed in buffer (KPB, pH 7) with NAD^+ (1 mM) at 30 °C. The electrode was rotating at 2000 rpm (grey, light blue) or 3000 rpm (dark blue) to prevent mass transport limiting the catalytic current.

The cyclic voltammograms in Figure 3-6 show that enzyme-modified particles can be used to increase the quantity of NAD^+-reductase under electrochemical control. The cyclic voltammogram for the enzyme-modified particle electrode (dark blue) shows a similar shape to enzyme adsorbed directly onto the electrode. Catalysis starts at the same potential, again indicating that the carbon particles are a suitable electrode material for use with the NAD^+-reductase and that the catalytic behaviour is not significantly affected. The catalytic reduction current at -0.40 V *vs* SHE for the enzyme-modified particle electrode is > 6 times the magnitude of the enzyme modified planar electrode. Overall *ca* 2 times as much NAD^+-reductase was used on the particle electrode compared to on the PGE RDE, however using the PGE RDE, no more than a monolayer of enzyme can be used over the 0.03 cm^2 geometricla surface area. In contrast the particle electrode allows much more enzyme to be in

electronic contact with the electrode by creating an electronically conducing network of enzyme-modified particles. This result indicates that more NAD^+-reductase was under direct electrochemical control on the particle electrode and that the particle networks are a viable approach for electrode scale-up. It is likely that using NAD^+-reductase of a higher concentration with longer adsorption times will further enhance the catalytic current of these high surface area electrodes.

3.2.4 Comparison of the catalytic activity per geometrical electrode area

Although there was a clear enhancement in the catalytic current for NAD^+ reduction using NAD^+-reductase immobilised either on carbon paper or particles, for better understanding of the high surface area electrodes constructed the catalytic current was compared per geometrical electrode area and by specific surface area of the carbon materials.[212] For this, the current response from the previous experiments was divided by either the geometrical electrode surface area (RDE: 0.03 cm^{-2}, Carbon paper: 1 cm^{-2}) or the specific surface are of the carbon particles (BP particles, 1 µL aliquot, *ca* 1.2 µg BP, 24 cm^2).

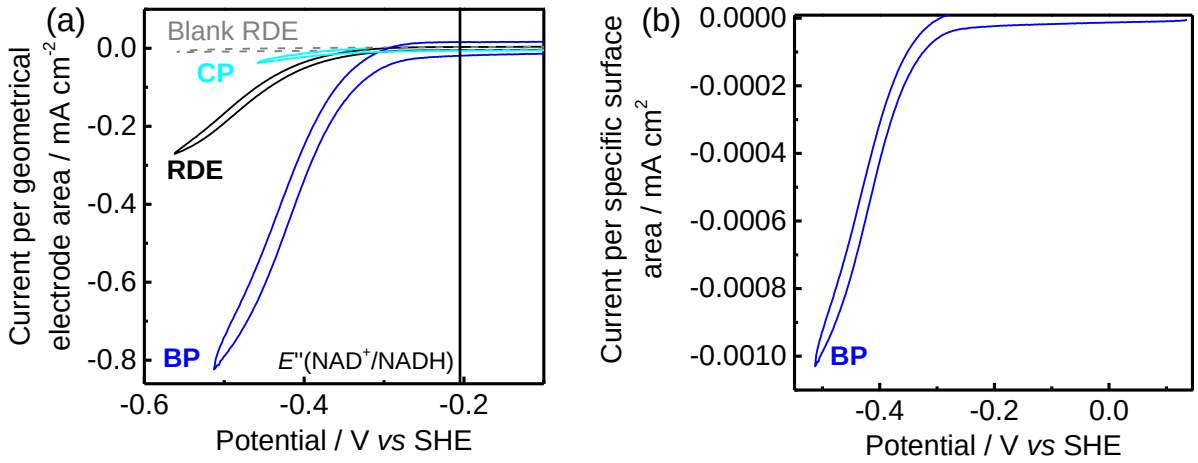

Figure 3-7: Comparison of the catalytic NAD^+ reduction current by electrodes modified with NAD^+-reductase. (a) Cyclic voltammograms recorded with a RDE (black), carbon paper (light blue) and BP particles on RDE (dark blue) modified electrode displaying the current per geometrical area. (b) The NAD^+ reduction current from NAD^+-reductase immobilised on BP particles on the RDE electrode is displayed per surface area of the particles.

The previous results suggest that the catalytic enhancements in comparison to the PGE RDE were 6 and 8 times for the BP particles and carbon paper high surface area electrodes, respectively when *ca* 2 and 10 times the amount of NAD^+-reductase was used (i.e. there was greater amount of catalytically active NAD^+-reductase on the carbon paper electrode but much higher activity per NAD^+-reductase on particles). The cyclic voltammograms in Figure 3-7(a) further show that the magnitude of catalytic current per geometrical area was much higher for the BP particle electrode in comparison to the carbon paper electrode, this is as expected due to the more '3D' nature of the particle electrode allowing greater than monolayer coverage.

Figure 3-7 (b) shows the catalytic activity per specific surface area of the BP particles. This is approximately 3 orders of magnitude lower than the activity per geometrical area and demonstrates that only a small percentage of the BP particle surface area has active enzyme adsorbed. Furthermore, the catalytic wave curves at low potentials suggesting that the enzyme is partially mass transport limited. This is in agreement with the findings by Quinson *et al*. where it was suggested that there is slow diffusion of substrate through the particle networks.[212]

In conclusion, the NAD^+-reductase electrochemical behaviour is not noticeably affected on different carbon materials. Carbon paper is a useful way to increase the geometrical surface area of the electrode systems but to achieve highest catalytic current per geometrical area particle electrodes will be most beneficial.

3.3 Electro-enzymatic NADH generation

The concept of electro-enzymatic NADH generation is simple: the NAD^+-reductase is immobilised on an electrode and supplied with electrons which are used for the selective reduction of NAD^+ to NADH. This section assesses the viability of the electro-enzymatic system introduced for NADH generation. Key areas for investigation include the potential at

which the electrode should be held, analysis of the reduction products, scale-up of the electrode system and enzyme stability improvements.

3.3.1 Investigating a suitable potential for NAD^+ reduction

In general all potentials lower than the thermodynamic potential should lead to reduction of NAD^+ by the NAD^+-reductase. As the potential becomes more negative in comparison to the thermodynamic potential of the NAD^+/NADH couple (Figure 3-8(a), blue arrow), the driving force for NAD^+ reduction increases and a faster rate of NAD^+ reduction should be possible. At potentials significantly lower than -0.5 V *vs* SHE, the NAD^+-reductase can be inactivated over time, especially if the concentration of NAD^+ is low.[222] Three different potentials were investigated; -0.41, -0.46 and -0.51 V *vs* SHE corresponding to overpotentials of 0.18, 0.23 and 0.28 V respectively at pH 8 (assuming a constant NAD^+/NADH ratio of *ca* 1000).

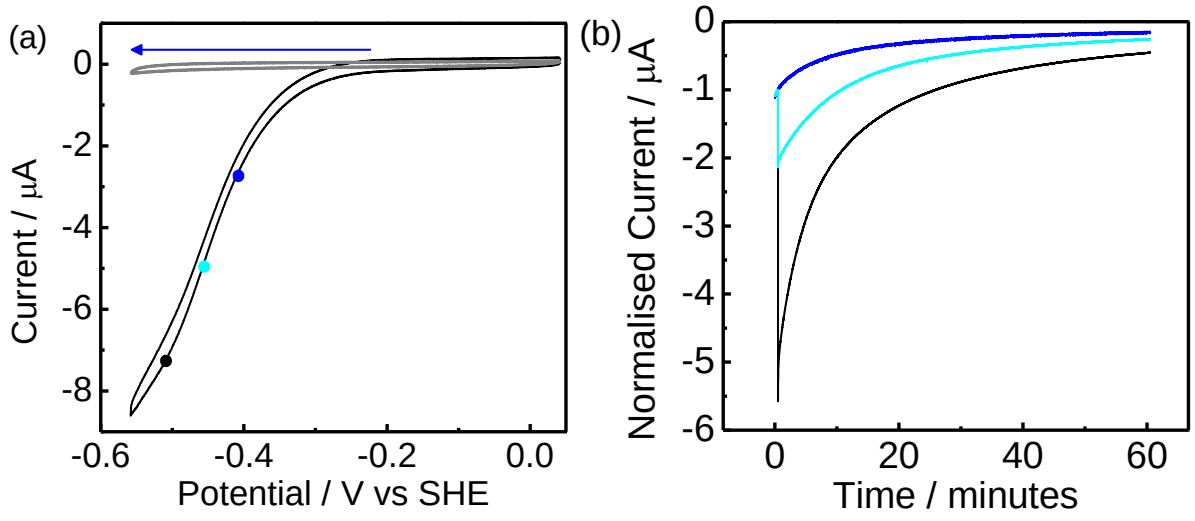

Figure 3-8: Electrochemical experiments to determine the potential at which electro-enzymatic NADH generation should be performed. Panel (a) shows a cyclic voltammogram of NAD^+ reduction by a PGE electrode modified with NAD^+-reductase (Hox~~HY~~FU). The blue arrow indicates the increase in applied overpotential for NAD^+ reduction; the dots indicate the potentials at which the half-life of the NAD^+-reductase will be determined. Panel (b) shows the results from three chronoamperometry experiments where an NAD^+-reductase modified PGE electrode was held at -0.41 (dark blue), -0.46 (light blue) or -0.51 (black) V *vs* SHE in the presence of NAD^+ (1 mM). In each case the electrode was poised at -0.41 V *vs* SHE for 30 seconds and then changed to the required potential for 1 hour. The current was normalised to the current at -0.41 V *vs* SHE in each case for easy comparison. All experiments were performed in Tris buffer (pH 8) at 22 ^oC, with electrode rotation of 2500 rpm.

At each potential chronoamperometry was used to observe how the current changed over time whilst catalysis was occurring and to calculate the half-life of the immobilised enzyme system. The calculations will assume that there was no significant change to the NAD^+/NADH ratio during the experiments; this assumption holds when using a relatively large volume of NAD^+ and a small quantity of NAD^+-reductase thus preventing large-scale conversion of NAD^+ to NADH. The coloured dots in Figure 3-8(a) correspond to the potential at which chronoamperometry experiments were carried out, Figure 3-8(b). For each chronoamperometry experiment a new enzyme film was prepared. The chronoamperometry experiments all started at -0.41 V *vs* SHE and were held at this potential for 30 seconds. After this time the potential was set to -0.41, -0.46 or -0.51 V *vs* SHE. In each case the current was normalised to the initial value at -0.41 V to negate the effect of using different enzyme films. This step in potential led to a large capacitive current (the magnitude of which is dependent on the size of the step) which decayed over the first few minutes.

The half-life of the enzyme system is the time taken for the activity to drop by half. Since the drop in current is due to the half-life of the enzyme, possible inactivation of the enzyme, loss of the enzyme from the electrode or denaturation, it is not trivial to model the change in current. As a rough calculation, the time taken for the current to drop to half of the value at 6 minutes was recorded (since the initial capacitive current is likely to have completely decayed); the results are shown in Table 3-1.

Table 3-1: Comparing the stability and activity of the NAD^+-reductase at a range of potentials to determine a potential suitable for electro-enzymatic NADH generation.

Potential / V *vs* SHE	**Half-life / minutes**	**NADH generated / nmoles**
-0.41	21.0	6.1
-0.46	20.0	11.9
-0.51	18.5	23.1

The results in Table 3-1 show that there was very little effect on the stability of the enzyme at the range of potentials investigated. Integration of the current over the whole hour was used to determine the theoretical concentration of NADH produced from the number of electrons passed (Section 2.1.8); these are also shown in the table. It is likely that the increase in current and therefore rate of NADH generation compensates for the slight decrease in NAD^+-reductase half-life at lower potentials. Since the NAD^+-reductase has been shown to become inactivated at lower potentials at low NAD^+ concentration, the potential used will depend on the concentration of NAD^+. Using NAD^+ at 1 mM, all of the potentials investigated are suitable for NADH generation.

3.3.2 Initial 'proof-of-concept' NADH generation

High surface area electrodes modified with NAD^+-reductase were used to generate NADH. The *in situ* UV-vis spectroelectrochemical approach (introduced in Section 2.4.2) was used to follow the conversion of NAD^+ to NADH in solution; the cartoon in Figure 3-9(a) shows the experimental set-up. The UV-vis cuvette holder was able to control the temperature of the sample, this was set to 33 ^oC and supplied with water (30 ^oC) from a water circulator. The carbon paper electrode was modified with Hox~~HY~~FU (7.5 µg) and immersed into a UV-vis cuvette containing NAD^+ (0.75 mM, Tris-HCl buffer, pH 8) such that it did not block the path of the UV-vis light. A small Ag/AgCl reference electrode and a fritted counter electrode were also used (Sections 2.1.5 and 2.1.6) and a stirrer bar incorporated to minimise mass transport limitations and a build up of NADH at the electrode surface, in close proximity to the NAD^+-reductase. The enzyme-modified electrode was poised at +0.24 V *vs* SHE for 20 seconds, since no NAD^+ reduction occurs at this potential the current was approximately 0 µA. The potential was then stepped to an NAD^+-reducing potential of -0.46 V *vs* SHE. Initially a large capacitive current was observed, this quickly decayed leaving a catalytic current. This current was recorded over time and is shown in Figure 3-9(b).

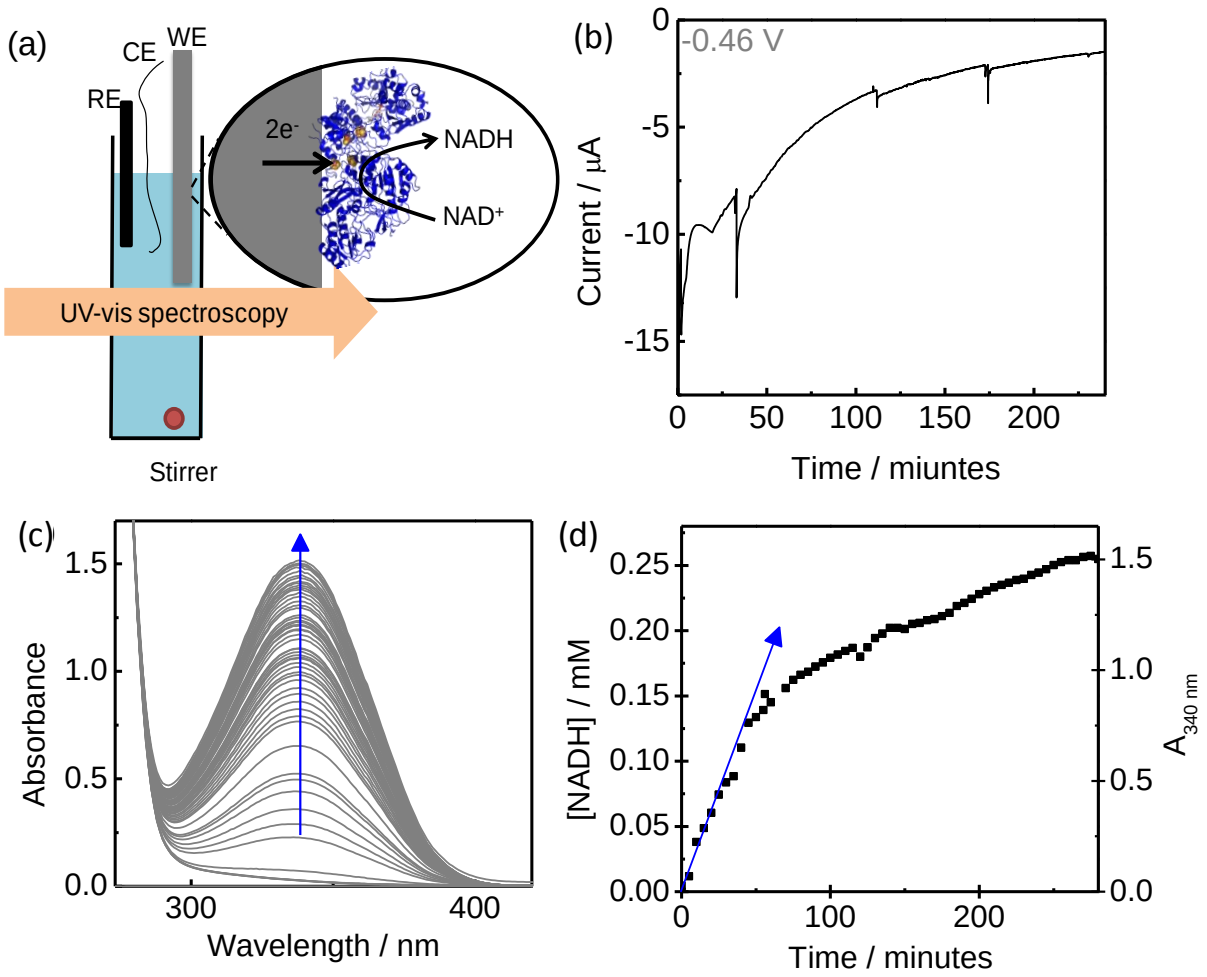

Figure 3-9: Electro-enzymatic NADH generation using an NAD^+-reductase-modified carbon paper electrode. (a) Cartoon representation of the UV-vis spectroelectrochemsitry technique used to investigate the reduction of NAD^+ to NADH by an working electrode modified with NAD^+-reductase. (b) A chronoamperometry trace for a high surface area electrode in the presence of NAD^+ (0.75 mM) poised at -0.46 V *vs* SHE in buffer (Tris-HCl buffer, pH 8) at 33 ^oC. UV-vis spectra (c) and absorbance at 340 nm (d) as a function of time show generation of NADH.

The chronoamperometric trace in Figure 3-9(b) shows a fairly constant, negative current corresponding to NAD^+ reduction by the NAD^+-reductase. The large drop at *ca* 40 minutes is due to an increase in the speed of stirring and a corresponding change to the capacitive current. Integration current recorded allowed calculation of the moles of electrons passed and therefore the maximum number of moles and concentration of NADH that could have been generated. From this calculation the number of electrons passed equated to an NADH concentration of *ca* 0.34 mM over 4.5 hours.

UV-vis spectra were recorded every 5 minutes during the experiment and are shown in Figure 3-9(c). The spectra show an increase in the absorbance at 340 nm and therefore confirm the generation of NADH over time. Figure 3-9(d) shows a plot of the absorbance at 340 nm over time; this was then converted into a concentration of NADH as previously discussed, Section 2.4.1. From the data in Figure 3-9(d) the rate of NADH generation was calculated. Often, enzyme activities are quoted in U mg^{-1}, defined as μmole of substrate converted per minute (μmole min^{-1} = U) per mg of enzyme. In order to relate the activity of the electro-enzymatic system to the activity of enzymes in solution, the activity was calculated in units per mg of NAD^+-reductase applied to the electrode. The initial rate of NADH generation (Figure 3-9(d), blue arrow) was calculated to be 6.4 ± 1.1 μmole min^1 per mg NAD^+-reductase. (This equates to a turnover frequency of 19 s^{-1} or > 68,00 h^{-1} per NAD^+-reductase molecule.) This is much lower than the activity of the natural SH using H_2 as reducing equivalent. However, it is likely that not all of the NAD^+-reductase supplied in solution was adsorbed onto the electrode, that only some of the NAD^+-reductase that was adsorbed is in the correct orientation to exchange electrons with the electrode and that mass transport to the planar electrode is less efficient than to an enzyme in solution. For this reason the activity calculated per mg of NAD^+-reductase is likely to be an underestimate of the actual activity. There is some evidence in the literature that NAD^+ and NADH adsorb onto carbon materials; however the adsorbance at 280 nm is fairly constant throughout this experiment suggesting that there was no significant adsorption over the course of this experiment.

Using 5.9 mM^{-1} cm^{-1} as the extinction coefficient for NADH at 340 nm (Section 2.4.1), the end solution contained NADH at a concentration of 0.26 ± 0.02 mM. This is less that the concentration predicted from the current passed. This could be explained by the significant residual capacitive current at this high surface area electrode. Overall, the current efficiency of this electrode system was 74 %. This extent of conversion requires each NAD^+-reductase to

have turned over > 6000 molecules of cofactor.

The activity of the system decreased substantially after *ca* 50 minutes, corresponding to the time at which > 10 % conversion of NAD^+ to NADH had occurred. This can be explained by a decrease the applied overpotential since 10 % conversion of NAD^+ to NADH will have led to a > 30 mV decrease in the thermodynamic potential of the NAD^+/NADH couple (assuming an initial NAD^+/NADH ratio of 1000).

3.3.3 Confirming the electrochemically generated NADH is enzyme-active

The experiments detailed so far demonstrated that an NAD^+-reductase modified electrode is able to electrochemically drive NADH generation. However, many electrochemical NADH generation methods produce enzyme-inactive forms of the cofactor by forming NAD radicals, dimers and 1,2- or 1,6-NADH, Section 1.4.2. Investigations into the nature of the electro-enzymatically derived NADH were therefore undertaken. For this, an NADH-dependent lactate dehydrogenase (LDH) enzyme and its substrate (pyruvate) were used: in the presence of NADH the LDH is able to reduce pyruvate to lactate and generate NAD^+ according to Equation [3-1].

$$Pyruvate + NADH \xrightarrow{LDH} Lactate + NAD^+ \qquad [3\text{-}1]$$

Again, this reaction can be monitored using UV-vis spectroscopy; a loss in absorbance at 340 nm corresponds to a decrease in the concentration of NADH. This will only occur if the NADH is enzyme-active and able to be consumed by the LDH.

This experiment was performed directly after the electrochemical experiment in Section 3.3.2. Lactate dehydrogenase (20 μg) and an aliquot of pyruvate to give a final concentration of 2 mM were added into the solution containing the electrochemically produced NADH. UV-vis spectra were recorded every 1 minute after the injection and are shown in Figure 3-10.

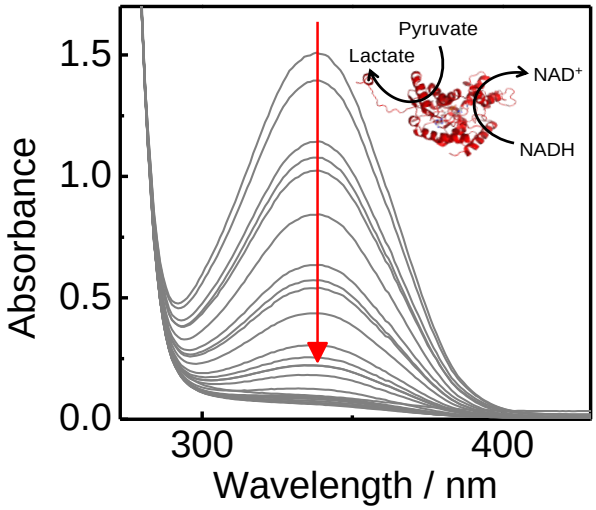

Figure 3-10: UV-Vis spectra showing that the electrochemically derived NADH is enzyme-active. UV-vis spectra recorded after addition of LDH (20 µg) and pyruvate (2 mM) to the end solution from Figure 3-9. Spectra were recorded every 1 minutes, all other conditions remained the same.

The UV-vis spectra show a loss of absorbance at 340 nm (Figure 3-10) and therefore indicate the consumption of NADH after addition of LDH and pyruvate. This confirms that the NADH contributing to absorbance at 340 nm has been used by the LDH and is therefore enzyme-active. This will be further investigated in Chapter 6 where the NAD^+-reductase and a NADH-dependent enzyme are co-immobilised on an electrode for further characterisation.

3.3.4 Scale-up of the electro-enzymatic NADH generation system

The stability of the NAD^+-reductase on BP particles during electro-enzymatic NADH generation was considered. An aliquot of BP particles were dispersed by sonication in buffer (20 mg mL^{-1}, 50 µL, KPB, pH 7) and mixed with NAD^+-reductase (Hox~~HY~~FU, 25 µg). This sample was left at 4 ^oC for 15 minutes. The entire mixture was then spotted onto carbon paper and allowed to partially dry for 15 minutes. This electrode along with an Ag/AgCl reference electrode and a fritted counter electrode were placed into a glass vial containing 11 mL of NAD^+ solution (2 mM in KPB pH 7). A stirrer bar was included to prevent diffusion limitation or product inhibition following build-up of NADH at the electrode surface in close proximity to the NAD^+-reductase. The large reaction volume prevented significant conversion

of NAD^+ to NADH, particularly over the first few hours and therefore allowed the enzyme stability to be analysed with minimised effects from the change in NAD^+/NADH ratio and therefore thermodynamic potential (and thus the applied driving force).

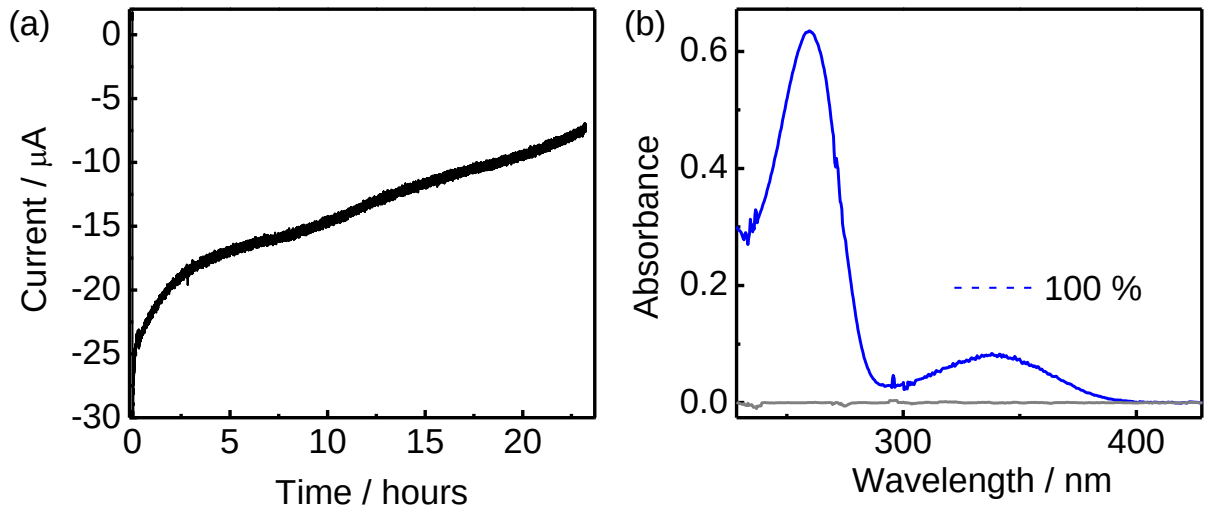

Figure 3-11: Electrochemically driven NADH generation using NAD^+-reductase (Hox~~HY~~FU) modified BP particles on carbon paper. (a) Chronoamperometry trace of the enzyme-modified electrode. (b) A UV-Vis spectrum of the resulting solution confirms 26 % conversion of NAD^+ to NADH. The dotted line represents the expected absorbance at 340 nm for complete conversion. Experiment performed in 11 mL pH 7 KPB buffer with NAD^+ (2 mM). The solution was continuously stirred and the electrode held at -0.41 V *vs* SHE at 22 ^oC.

Using the chronoamperometry trace shown in Figure 3-11(a) the half-life of NAD^+-reductase absorbed onto carbon particles was 16 hours. If true, this suggests that the BP particles have increased the stability of the immobilised enzyme by ~ 48 times compared to the NAD^+-reductase on a PGE electrode. It is possible that the pores on the surface of the BP particles are of a suitable size for stabilisation of the NAD^+-reductase. It is possible that this half-life is an underestimate, as over the course of 16 hours, there was a significant change in the NAD^+/NADH concentration ratio. By integration of the current over this time, the number of electrons passed equates to *ca* 0.55 mM NADH.

A UV-vis spectrum of the resulting solution is shown in Figure 3-11(b) and indicates formation of 0.55 ± 0.03 mM NADH equating to 26 % conversion. This suggests that the current efficiency is approaching 100 % since all of the electrons calculated to have passed

through the electrode were used for reduction of NAD^+. Overall *ca* 6 μmoles of NADH were generated. This equates to a turn over number > 40,000 (NADH molecules generated per NAD^+-reductase) over the course of the experiment. Further improvements to this system were considered in the next Sections.

3.4 Improving the stability of the electro-enzymatic system

It is clear that NAD^+-reductase-modified carbon electrodes can be used for the generation of NADH from NAD^+. Due to the much higher expense of NADH in comparison to NAD^+ this could be developed into an industrially relevant system. However, the carbon paper electrodes are hard to handle (they easily tear) and do not give very reproducible results. Methods to build robust electrodes with uniform surface area were therefore investigated. Other methods that help to stabilise the NAD^+-reductase were also considered. In general a stabilisation method that does not increase the cost of, or time for, electrode preparation is desirable.

3.4.1 Building robust, uniform electrodes from carbon paper

A method was explored whereby the carbon paper electrode was placed between sheets of laminating paper. A carbon fibre connector was used to provide an electronic link between the carbon paper and the potentiostat; the whole system was sealed using a soldering iron. This had the effect of creating a strong coating for the carbon paper with a flexible conducting carbon linker. 'Holes' of a uniform size were made in the laminating paper before sealing, such that a well-defined area of carbon paper was exposed to solution. Carbon paper electrodes with any number of these 'holes' could be created allowing for simple, reproducible scale-up. The laminated carbon paper electrode was placed across the UV-vis cuvette such that it did not block the light. This system was analysed using an adapted version of the UV-vis spectroelectrochemistry set-up developed earlier (Figure 3-9); the results are displayed in Figure 3-12.

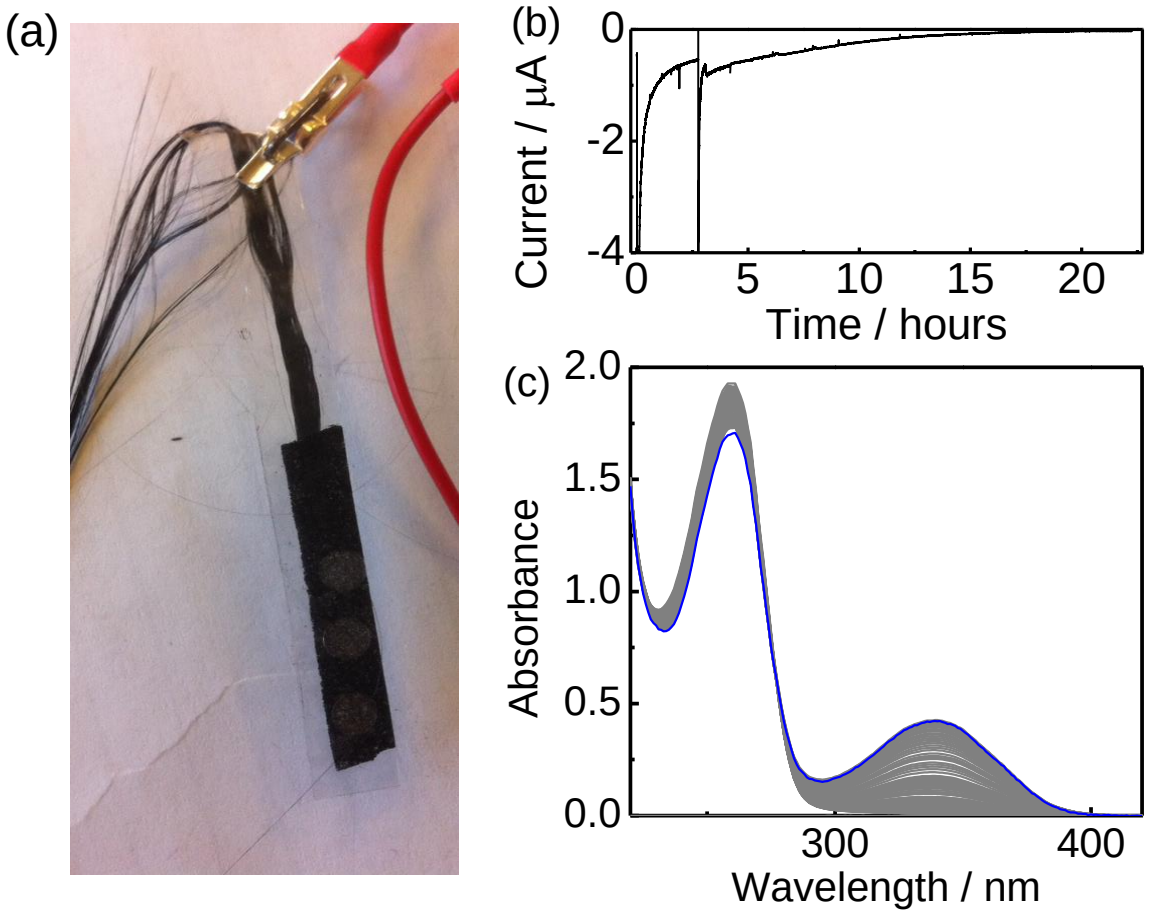

Figure 3-12: The NAD^+-reductase modified electrode systems can be designed in order to improve their usability and viability on a large scale. (a) The carbon paper was laminated to improve the stability of the electrode system. Holes of a uniform size allow good control of the surface area used for enzyme adsorption.The electrochemistry (b) and UV-vis spectra (c) recorded over time in response to an NAD^+-reductase modified carbon paper electrode. The electrode was poised at -0.41 V *vs* SHE in the presence of NAD^+ (0.11 mM, KPB, pH 7).

The picture in Figure 3-12(a) shows a typical laminated carbon electrode. In this example there are three holes on either side allowing a large quantity of enzyme to be used. A sample of BP particles were modified with NAD^+-reductase (30 µg) and spotted onto the carbon paper and allowed to partially dry for *ca* 15 minutes. The electrode was then placed in the UV-vis cuvette containing NAD^+ (0.11 mM). The working electrode was poised at -0.41 V *vs* SHE, and the current, Figure 3-12(b), and UV-vis spectra (c) were recorded simultaneously. The results show 80 % conversion of NAD^+ to NADH with an enzyme half-life of 3.6 hours. This is much less than the half-life calculated in the previous section; however the high conversion of NAD^+ to NADH will have significantly changed the thermodynamic potential

of the NAD^+/NADH couple to a more negative potential. Since the potential of the electrode was not changed, the effective overpotential is decreased and therefore the expected activity of the NAD^+-reductase will be lower. The loss in current over time is therefore partially due to the half-life of the NAD^+-reductase but also due to the change in solution redox potential and therefore NAD^+-reductase activity. For this reason it is likely that the half-life observed was substantially lower than the actual half-life of the immobilised enzyme. The overall current of the system is lower than might be expected. It is possible that the enzyme did not adsorb effectively to the particles. The results confirm that the electrode system is viable. Laminated NAD^+-reductase modified electrodes act as a good starting point for further developments.

3.4.2 Using a Nafion polymer to increase the enzyme stability

Immobilisation on BP particles was shown to increase the stability of the NAD^+-reductase enzyme. Another possible method for increasing the stability of the enzyme-modified electrode to use a coating to prevent desorption of the enzyme. Here, pH neutralised Nafion was used as a polymer electrolyte to 'trap' the protein at the electrode. Again the half-life of the enzyme can be measured as the time taken for the catalytic current to drop by half. The use of a Nafion polymer layer may stabilise the protein films by preventing desorption, by keeping the enzyme hydrated during immobilisation on the electrode and possibly also by preventing denaturing of the enzyme.[242]

In order to test the effect of Nafion on the NAD^+-reductase, a PGE RDE was used rather than a high surface area electrode. This increased the sensitivity to changes in the catalytic current and increased reproducibility by maintaining a well-defined electrode surface area. In Figure 3-13, a PGE RDE modified with NAD^+-reductase is compared to a similar enzyme-modified electrode with an aliquot of Nafion (1 μL, pH 7) spotted on after 30 seconds, and allowed to dry for *ca* 1 minute to leave a partially hydrated film. These scans

are both shown against the current recorded at a blank, unmodified electrode (grey) in the same solution.

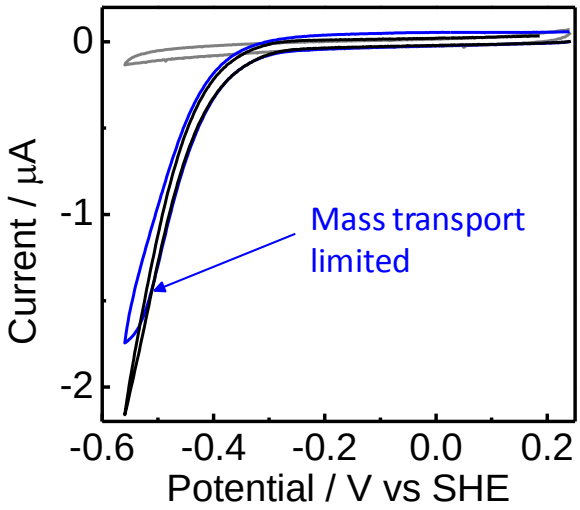

Figure 3-13: Cyclic voltammetry comparing a blank electrode (grey) an NAD^+-reductase modified electrode (black) and NAD^+-reductase and Nafion modified electrode (blue). The experiments were performed using a PGE RDE rotating at 2000 rpm in buffer (KPB, pH 7, 0.1 M) containing NAD^+ (1 mM).

The cyclic voltammograms in Figure 3-13 demonstrate that the NAD^+-reductase is able to sustain catalysis in the presence of Nafion. It is clear that catalysis starts at the same potential with and without Nafion and that up until -0.5 V there is no significant effect on the enzyme activity. However, at more negative potentials the magnitude of the catalytic current was lower at the electrode comprising enzyme coated in Nafion and the catalytic wave at this electrode has a more curved shape, indicative of the enzyme being mass transport limited. This may be due to the difficulty of a large NAD^+ molecule diffusing through the Nafion layer. Some NADH oxidation current can also be seen on the reverse scan at more positive potentials suggesting that it is not spun away from the electrode but instead trapped at the electrode surface. The use of Nafion to trap cofactor at the electrode surface may have positive implications for some industrial applications where methods that allow use of lower cofactor concentrations by maintaining a sufficient cofactor concentration in close proximity to an enzyme cascade is crucial.

Chronoamperometry experiments to determine the half-life suggest that some

improvement was observed (increased from *ca* 20 minutes to *ca* 37 minutes). Although this was not a huge increase in stability, the approach may offer advantages in applications where keeping the cofactor localised at the electrode surface is important.

3.4.3 Methoxy-poly(ethylene) glycol (mPEG) modification

There are many other literature techniques for stabilising enzymes that could be applied to this NAD^+-reductase modified electrode system, some require an immobilised enzyme and some do not.

One particular method which has been investigated for increasing the stability of the NAD^+-reductase (HoxHYFU) from *Ralstonia eutropha* is using a methoxy-poly(ethylene) glycol (mPEG) modification.[156,157] This has been carried out using the whole SH and tested in biochemical solution activity assays. The protein surface is chemically modified with a polymer layer (in this case using mPEG). This has been demonstrated to increase stability towards a range of solvents and inhibitors. A brief test as to the effect of an mPEG modification to NAD^+-reductase immobilised on PG particles showed that although there was no significant decrease in activity, there was also no particular increase in stability.

3.5 Other NAD^+-reducing enzymes and constructs

An electro-enzymatic approach for NADH generation has been demonstrated and some methods for scale-up identified. In Chapter 6 these electrodes will be further developed for cofactor recycling, that is, electrochemically-driven NADH supply to a NADH-dependent enzyme.

One significant limitation of using NADH-dependent enzymes at present is the need to develop a cofactor regeneration system for each desired application. The research and development is therefore time intensive and expensive. It would be desirable to access a cofactor regeneration system that can be easily modified to suit any reaction conditions; this

would include a range of pH and temperature environments as well as different solvent mixtures, high substrate loadings and different reactor set-ups. This Section explores the possibility of substituting the NAD^+-reductase for other NAD^+-reducing enzymes either to enable NAD^+ reduction in different conditions or to produce a more economically viable NAD^+-reductase construct. Electrochemical characterisation of NAD^+-reducing enzymes and constructs in this Thesis will follow the methods previously used by Dr Z. Idris[151,222] where possible. Complete characterisation of an NAD^+-reductase enzyme from *Rhodococcus opacus* will be described in Chapter 4.

3.5.1 A note on industrial scale enzyme preparation

Here, a few notes are included as to how an enzyme can be produced in an industrially viable way. This includes ensuring that the enzyme is produced cheaply, without waste and optimised for the application.

Work so far has focused on using either *Ralstonia eutropha* Hox~~HY~~FU or HoxFU for electro-enzymatic NAD^+ reduction since in each case the only active catalytic domain is the NAD^+-reductase moiety. The Hox~~HY~~FU construct contains the hydrogenase dimer but it is not catalytically active. This sample is most often used since it is easier to produce in large quantities by collaborators in Berlin (Lenz Group, Technical University, Berlin). However, for industrial scale preparation it would be beneficial not to include the hydrogenase dimer since it contains a complicated [NiFe] centre – adding unnecessary expense to the growth media, since a Ni source is required. There is ongoing work in the Lenz Group to improve the yield of the HoxFU dimer and its activity and stability.

Highly purified NAD^+-reductase samples have been used so far and are prepared using affinity columns and a *Strep* protein tag, Section 2.8.1. Although purified enzyme samples are used on an industrial scale they tend to be prepared using partial purification techniques, for example by precipitation or separation based on size. A more useful NAD^+-reductase sample

would have fewer or no purification steps.

The NAD^+-reductase from *R. e* has been demonstrated in this Chapter as a good electro-catalyst for NAD^+ reduction. However, other enzymes may be able to collect electrons from an electrode and use them for selective production of NADH and may offer different advantages. For this reason other NAD^+-reducing enzymes and constructs will be considered. In general their ability to use an electrode as an electron source is analysed, and if successful this is followed by characterisation techniques to determine the activity of NAD^+ reduction, the overpotential requirement, the affinity of the enzyme for NAD^+ and the inhibition of NAD^+ reduction by the product, NADH. An ideal NAD^+-reducing enzyme would operate with negligible overpotential, have a high affinity for NAD^+, high activity and little inhibition by NADH. Furthermore, enzymes that can operate in more varied temperature and pH ranges would have advantages in some experimental set ups and applications.

3.5.2 Crude extract

At present, the methods for production and purification of the NAD^+-reductase are time- and labour-intensive. Here, the possibility of using a non-purified enzyme sample was investigated.

The *R. eutropha* NAD^+-reductase samples are prepared by over-expression of the soluble hydrogenase (with or without mutations). Once the sample has reached the desired optical density the cells are broken apart using a French press. The mixture is then subject to centrifugation to separate the cell membranes from the soluble portion. Here, the un-purified, *crude* soluble extract of SH (HoxHYFU with active hydrogenase dimer) was tested. This soluble extract also contains a range of other proteins and these may compete to adsorb onto the electrode, and this may affect the adsorption of the NAD^+-reductase. Time was taken to find the best way of creating an enzyme film of crude extract on the electrode. When the enzyme film was prepared as normal (by spotting 0.5 μL of a sample onto the PGE electrode

and allowing it to partially dry) no NAD^+ reduction was seen. However NAD^+-reductase activity was seen when ~ 1 µL of the sample was spotted onto the PGE electrode and immediately removed using a pipette. The same aliquot of sampled was added and removed in this way at least 5 times before the electrode was immersed into a solution containing NAD^+ for electrochemical analysis. It is possible that this 'on/off' technique only allows the proteins that most favour adsorption to become immobilised on the electrode and that this includes the NAD^+-reductase.

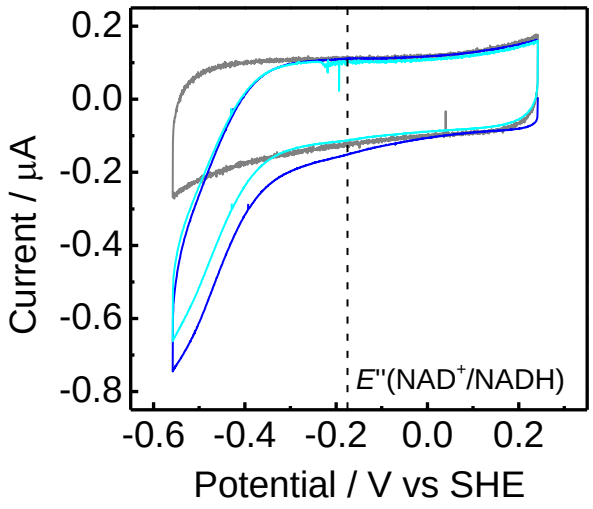

Figure 3-14: Cyclic voltammograms showing the response of a PGE electrode modified with crude soluble extract from an NAD^+-reductase (HoxHYFU) culture. The experiment was performed in Bis-Tris buffer (pH 6) containing NAD^+ (1 mM), the electrode was rotating at 3000 rpm. The first (dark blue) and second (light blue) scans are shown, as is the response of the unmodified electrode (grey).

The cyclic voltammogram in Figure 3-14 confirms that a PGE electrode modified with crude extract of NAD^+-reductase (Hox~~HY~~FU) in this way is able to reduce NAD^+. This required that the NAD^+-reductase had been 'picked' out of the sample by the electrode. However, the electrocatalytic activity was much lower than that of a purified sample, likely due to co-adsorption of other proteins onto the electrode. No other redox processes were observed over this potential window used. Overall this is a significant finding for developing industrially relevant enzyme since the use of this crude extract would considerably decrease the cost of enzyme preparation in comparison to the purified samples.

3.5.3 *Rhodococcus opacus* soluble hydrogenase

Ralstonia eutropha is not the only species with a soluble hydrogenase. Work by Ms. K. Karstens (Lenz Group, Humboldt Univeristy, Berlin) has led to isolation and biochemical analysis of the soluble hydrogenase from *Rhodococcus opacus*. The next chapter will electrochemically characterise this enzyme for the first time and discuss is activity in comparison to the NAD^+-reductase from *R. e* and it's compatibility for electro-enzymatic NADH generation.

3.5.4 Variants of the SH for electro-enzymatic NADPH generation

It would be hugely advantageous to develop the electro-enzymatic system to generate NADPH from $NADP^+$ since this reaction is harder to achieve and the cost of NADPH is even greater than NADH. In their natural roles the functions of NADH and NADPH are different; NADH is involved with energy transfer and storage, making ATP, and NADPH is used for reductive biosynthesis.[219,243] Thus there is a wide library of NADPH-dependent enzymes that would be useful for chemical synthesis. For this reason the Group of Dr Lenz (Technical University, Berlin) is carrying out mutagenesis on the NAD^+-reductase from *R. e* to change the selectivity from the NAD cofactors to the NADP cofactors. These variants are then tested biochemically (by the Lenz Group) and electrochemically (by the Vincent Group). Previous work in the Vincent group has characterised a range of these mutants.[222,244]

Rational mutagenesis was used to change the binding pocket of the NAD^+-reductase to favour the larger and more negatively charged NADP cofactors by the Lenz Group. The homology model (Section 3.1) of HoxF, Figure 3-15, was used by the Lenz team to design mutation sites. The amino acid residues picked for mutagenesis range from residues that are directly hydrogen bonded to the NAD cofactor in the active site to residues much further away that may have an effect on substrate access channels or protein folding. In general, the mutations aimed to allow more space for the large NADP cofactor and to decrease the negative charge

to prevent repulsion of the additional negative charge (for the extra phosphate group). After identification of viable mutation sites, a round of random mutagenesis was carried out to produce variants A1, A5 and A12.

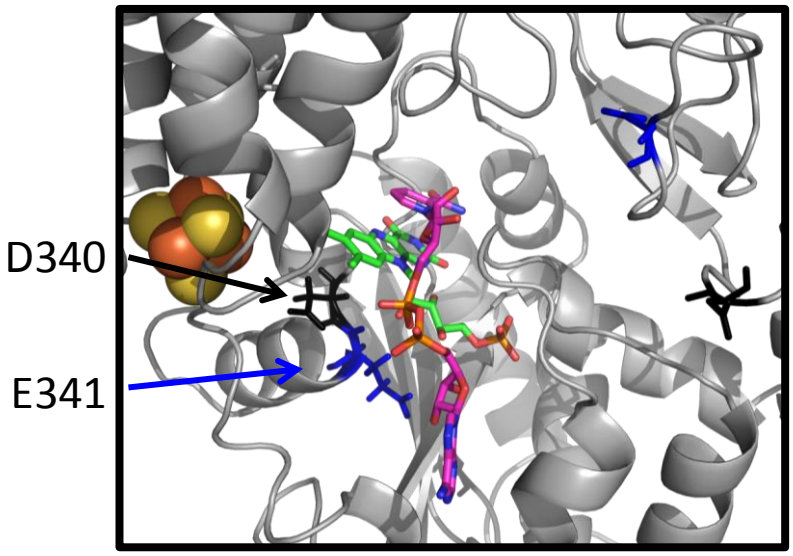

Figure 3-15: A homology model of HoxF with the sites chosen for mutation. The FMN (green) NADH (pink) and amino acids mutated (blue and black) are shown as sticks. The FeS cluster is shown as spheres and the protein back bone as a grey cartoon.

Table 3-2: Characterisation of new variants compared to the wild type (WT)

Variant	k_M NAD^+ / μM	k_M $NADP^+$ / μM	k_i NADH / μM
WT (HoxFU)*	197	8300	100-300
D467S/ E341A* (HoxHYFU)	710	300	-
(A1)**	35	46	-
(A5)**	210	84	300-800
(A12)**	220	100	1500-2000
Rhodococcus opacus SH***	102	> 1000	600
Rhodococcus opacus HoxFU (Chapter 4)	131	-	700

*Previously characterised by Dr Zulkifli Idris[151,222]

**A1, 5 and 12 are variants of D467S/E341A after a round of random mutagenesis and electrochemically analysed by Mr Thomas Lonsdale (Part II) and Ms Janina Preissler (Visiting Masters Student, Humboldt University, Berlin) under my supervision.

****Rhodococcus opacus* SH was electrochemically characterised by Ms Jenny Bradley, Part II student, under my supervision.

- not determined due to low activity

Here, a selection of the latest variants were analysed using electrochemical techniques to determine the k_M values for NAD^+ reduction and $NADP^+$ reduction and a k_i value for inhibition of NAD^+ reduction by NADH (Section 2.3). These are compared to the wild type (WT) data collected previously by Dr Idris in Table 3-2. (A more detailed description of electrochemical experiments for enzyme characterisation is provided in Chapter 4 where the SH from *Rhodococcus opacus* was characterised for the first time.)

The variants analysed electrochemically show very high affinity for $NADP^+$ in comparison to the wild type (in some cases 2 orders of magnitude better) and the variants previously characterised although the overall activity and stability of these variants is low (so low that further electrochemical characterisation was not possible). The exact origin of this low affinity constant is not yet known and further research in this area is ongoing. However, these results are encouraging and with further mutagenesis it is hoped that an active and stable variant will be generated such that the electro-enzymatic approach can be extended to NADPH generation.

3.5.5 Can other types of NAD^+-reducing enzymes be used?

In contrast to the NAD^+-reductase from *Rh. o* which has high similarity to the NAD^+-reductase from *R. e*, other enzymes that can reduce $NAD(P)^+$ occur in nature. Some contain FeS clusters for fast electron transfer to a redox partner, making it possible that they are well-suited for electron transfer to a carbon electrode. It is possible that some of these enzymes will be appropriate for electro-enzymatic $NAD(P)^+$ reduction and may offer some benefits over the soluble hydrogenase NAD^+-reductase dimers. In particular many of these enzymes catalyse interconversion of the NADP cofactors which at present is not feasible with variants of the NAD^+-reductase from the SH.

Ferrodoxin $NADP^+$-reductase (FNR)

Ferrodoxin $NADP^+$-reductase (FNR) catalyses the reduction of $NADP^+$ to NADPH using

electrons from 2 reduced ferredoxin molecules according to Equation [3-2].

$$2\ ferrodoxin_{red} + NADP^{+} + H^{+} \xrightarrow{FNR} 2\ ferrodoxin_{ox} + NADPH \quad [3\text{-}2]$$

The ferrodoxin in Equation [3-2] is a single electron carrier protein containing a FeS cluster. The ferredoxin is able to transfer electrons to the FNR protein which has a flavin active-site (flavin adenine dinucleotide, FAD – similar to FMN found in the NAD^+-reductase). The FAD molecule is able to collect 2 electrons from 2 equivalents of ferrodoxin, combine them with a proton and transfer them to $NADP^+$. In nature, this enzyme is involved in photosynthesis storing electrons from water oxidation as the reduced cofactor, NADPH. Since in nature the enzyme is able to accept electrons from a second soluble protein, the distance between the active-site and the protein surface is likely to be appropriate for electron transfer to an electrode.

This enzyme, FNR, was immobilised on a PGE electrode according to the previously described methods however no enzyme-catalysed $NADP^+$ reduction was observed. This is probably due to the absence of FeS clusters in the FNR itself preventing the electrode from acting as the electron source. It is likely the interaction between the protein and the electrode is not similar enough to that with the ferredoxin molecule or that a structural change is involved with the physiological electron transfer which is prevented by adsorption onto the electrode.

Phthalate dioxygenase reductase (PDR)

Phthalate dioxygenase reductase (PDR) is an enzyme related to FNR which is able to oxidise NAD(P)H and transfer the electrons to an electron carrier protein. This enzyme naturally works in the oxidation direction meaning it could be an alternative to the NAD^+-reductase from *Ralstonia eutropha* for generation of the oxidised cofactor.

This enzyme was tested on the electrode and a small catalytic current was observed for NADH oxidation however a large over potential was required (Figure 3-16(b), *ca* 300 mV)

despite the observation of flavin peaks (active-site) around -0.2 V *vs* SHE, Figure 3-16(a). It is possible that the FMN was lost from the active site and adsorbed directly onto the electrode and that high potentials required to see any catalytic activity further denatured the protein. This, alongside complications with NAD(P)H oxidation at the bare electrode above 0.25 V prevented further characterisation of this enzyme.

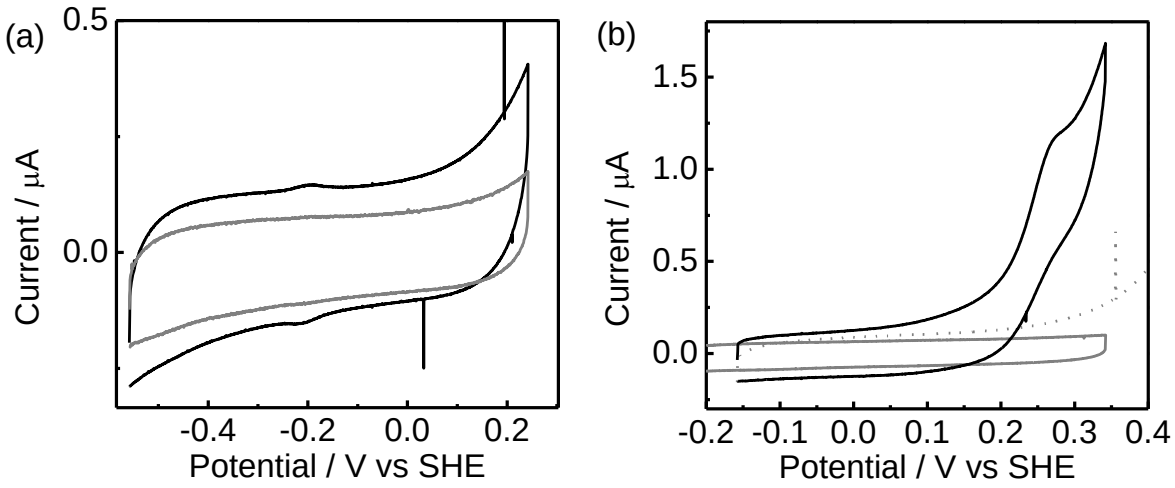

Figure 3-16: Cyclic voltammetry showing the current response to an electrode modified with PDR in the absence (a) and presence (b) of NADH (10 mM). The experiments were performed using a PGE electrode rotating at 2000 rpm in buffer (Bis-tris, pH 6, 0.1 M). In each case a scan recorded at an unmodified electrode is shown (grey) and in (b) an unmodified electrode was used in the presence of NADH (grey dotted line).

Overall this enzyme is not suitable to replace the NAD^+-reductase enzymes. However, it is possible that other NAD^+-reducing enzymes might be. In particular the NAD^+-reducing domains of other soluble hydrogenase enzymes may be used more easily, one such enzyme is considered in the next Chapter.

3.6 Summary and outlook

This work in this Chapter has demonstrated that the NAD^+-reductase from *Ralstonia eutropha* is a good electrocatalyst for (re-)generation of the reduced cofactor, NADH. Catalysis occurs at an appreciable rate even at a very mild overpotential and only enzyme-active cofactor has been detected. Activities of *ca* 6 μmoles min^{-1} per mg of NAD^+-reductase were achieved equating to a turnover frequency (moles of NADH per mole of NAD^+-reductase) of *ca* 19 s^{-1}.

This system could be developed for industrial production of NADH from NAD^+, but here is used as a starting point for the development of immobilised enzyme cascades for electrochemically-driven cofactor-dependent synthesis which is detailed in Chapter 6. Further work extending this to the production of NADPH is ongoing. The ability to use unpurified crude extract containing NAD^+-reductase is an important finding and is likely to aid development of an industrially viable system. Some other NAD^+-reducing enzymes have been tested electrochemically and a full electrochemical characterisation of the NAD^+-reducing soluble hydrogenase from *Rhodococcus opacus* is described in Chapter 4.

One disadvantage of the electro-enzymatic approach is that only solution in contact with the electrode surface will engage in catalysis; constant stirring of the solution is therefore needed. In an industrial reactor it may be hard to prevent mass transport limiting the electrochemical process, especially where a high enzyme loading is achieved using particle electrode systems. Furthermore, for each catalytic turnover, the NAD^+-reductase is using a proton; this means that the solution becomes more basic over time. To compensate either strong buffering systems are required or constant monitoring and adjustment of the pH by addition of acid is required to prevent changing the thermodynamics of the system or inactivating the enzyme. Furthermore, if used on an industrial scale, the oxidative process occurring at the counter electrode must be considered. In the small-scale set-ups described in this Chapter a Pt counter electrode was used to catalyse an oxidation, possibly water oxidation. Although this is acceptable on a small scale, it would not be practical if scaled-up. In an ideal electrochemical system, the reduction of NAD^+ would be coupled to a useful oxidation reaction that occurs at lower potential such that the two redox half equations occur spontaneously and two desirable products are generated. This would mean that electricity is not needed to drive the reactions thereby lowering costs associated with the system.

In the next Chapter, an alternative SH from *Rhodococcus opacus* is electrochemically

characterised and compared to the *R. e* SH. In Chapter 5 a particle system that exploits the electro-catalytic activity of the NAD^+-reductase will be investigated. Instead of using electrons from an electrode, the electrons will be extracted from H_2.

Chapter 4 Electrochemical characterisation of SH from *Rhodococcus opacus*

The previous Chapter developed an electro-enzymatic approach for NADH generation using a construct of the soluble hydrogenase from *Ralstonia eutropha* (*R. e* SH) as an electrocatalyst. Here the NAD^+-reductase (HoxFU) from a related soluble hydrogenase from *Rhodococcus opacus* (*Rh. o*) was electrochemically analysed for the first time. It is possible that this enzyme may have subtle differences in Michaelis-Menten kinetics, activity or stability in comparison to the NAD^+-reductase from *R.e* which may in turn offer advantages for particular applications. The hydrogenase moiety (HoxHY) will also be electrochemically analysed providing context for Chapter 5, where enzyme-modified particles for H_2-driven NADH generation are developed and a range of hydrogenases discussed. This chapter also aims to demonstrate that the techniques previously reported by Vincent and co-workers for

electrochemical characterisation of *R. e* NAD^+-reductase[151,222] are applicable to other NAD^+-reducing enzymes.

4.1 Introduction

Ralstonia eutropha is not the only organism to produce a soluble hydrogenase. Other species, including a number of cyanobacteria,[245] contain an NAD^+-reducing hydrogenase with high sequence homology and similar function. It could therefore be possible to substitute the *R. e* NAD^+-reductase for another NAD^+-reducing enzyme. Chapter 3 gave some insight as to the information that can be taken from electrochemical techniques; here the catalytic current was monitored following injections of cofactor to quantify the substrate affinity and product inhibition constants. These constants will provide insight into the differences between the two SH enzymes and their applicability to cofactor recycling.

4.1.1 The SH from *Rhodococcus opacus*

Rhodococcus opacus (formerly known as *Nocardia opaca*) and *Ralstonia eutropha* (formerly known as *Alcaligenes eutrophus*) are gram-positive and gram-negative, respectively. Despite this, their bidirectional cytoplasmic SH enzymes are very closely related with 71-86 % amino acid similarity across four subunits (HoxHYFU).[246] It has been previously reported using biochemical techniques that the two enzymes are partially identical.[247]

Gros *et al.* demonstrated a thin-layer cell with a platinum working electrode and *Rh. o* SH in solution to study the mechanism of NAD^+ reduction.[248] They reported two pathways: at potentials just negative of the thermodynamic potential for the NAD^+/NADH couple direct electron transfer between the Pt electrode and the SH occurred with low catalytic turnover to generate NADH whereas at more negative potentials than -0.42 V *vs* SHE, H_2 generated at the electrode was used by the hydrogenase dimer followed by intramolecular electron transfer to the NAD^+-reductase for NADH generation. The second pathway led to much faster NADH

generation (> 34 times faster), likely due to the faster diffusion of H_2 to the enzyme than enzyme to the electrode.

Despite this example of direct electron transfer to *Rh. o* in solution, there are no examples of protein film electrochemistry of the enzyme and thus no quantitative electrochemical characterisation similar to that reported for the *R. e* SH.[151]

4.1.2 Isolation of the HoxHY and HoxFU moieties

The *Rh. o* HoxHY and HoxFU samples were prepared by Ms. Katja Karstens (Lenz Group, Humboldt University, Berlin). Separate expression of HoxHY or HoxFU led to very low yeilds, therefore the whole SH was grown and the two dimers separated using an anion exchange column. Since *Rh. o* only grows under chemolithoautotrophic conditions (using explosive H_2/O_2 gas mixtures) a heterologous expression system in *R. e* was previously established.[246] Here, this was extended to include a *Strep*-tag to HoxF to enable purificiaton on a *Strep*-tactin affinity column.[249] The HoxHY and HoxFU dimers were separated on a anion exhange column by fast protein liqud chromotography (FPLC) with a salt (KCl) gradient from 250 to 320 mM using a protocol based on that by Zaborosch *et al*.[250,251] In this Thesis, these samples were used for protein film electrochemistry with no further purification.

4.2 Electrochemical analysis of the NAD^+-reducing subunits, HoxFU

The NAD^+-reducing subunits (HoxFU) of the SH from *Rh. o* were studied electrochemically and compared to the related HoxFU subunits from *R. e* SH. The whole SH (HoxHYFU) from *Rh. o* was also characterised (by Ms J. Bradley, part II, under my supervision), the data will not be shown but the results will be added into the discussion when appropriate. Many of the experiments in this section used purified NADH since the as-received samples contain NAD^+ impurities which would significantly affect the affinity and inhibition constants determined.

The methods for this were described in Section 2.7.2.

4.2.1 HoxFU for NAD^+/NADH cycling

Initial experiments were performed to confirm that the NAD^+-reductase was able to exchange electrons with an electrode and catalyse both the oxidation of NADH and the reduction of NAD^+. For each experiment, an aliquot of enzyme (0.5 µg) was spotted onto a freshly prepared PGE RDE and allowed to partially dry for a few seconds. This enzyme-modified electrode was then immersed into buffer containing either NAD^+ or purified NADH. The potential was swept from a value where no catalysis was expected to a potential where significant catalysis was thermodynamically favourable. Analogous experiments were also performed in the presence of H_2 and absence of NAD^+/NADH; no H_2 oxidation or H^+ reduction activity was seen confirming that the enzyme sample did not contain any active hydrogenase dimer (black lines in Figure 4-1). This indicated that any catalytic current observed was due to NAD^+/NADH cycling by the NAD^+-reductase.

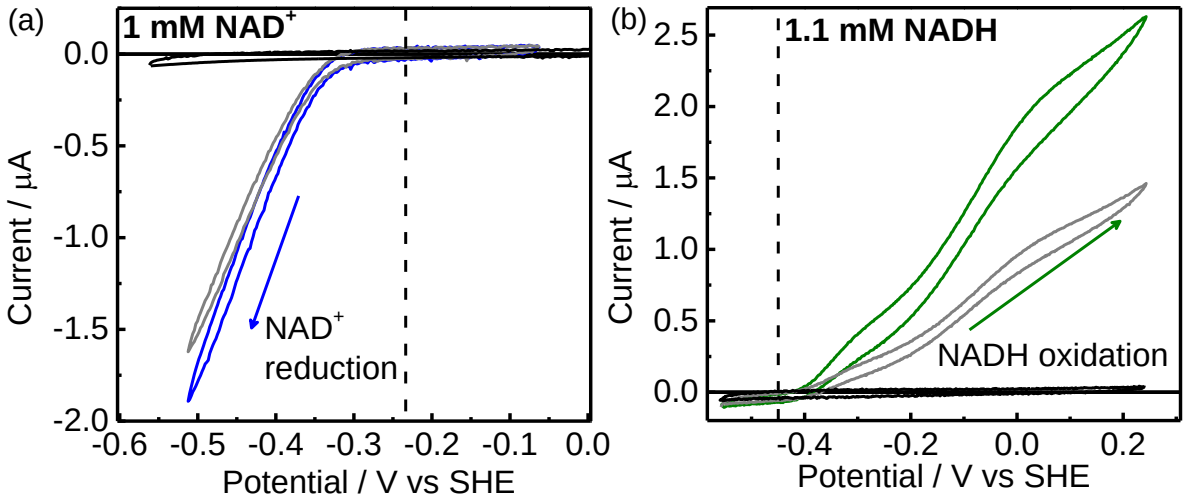

Figure 4-1: Cyclic voltammetry confirming that the NAD^+-reductase (HoxFU) from *Rh. o* is able to catalyse the reduction of NAD^+ and the oxidation of NADH. Experiments performed in Tris-HCl buffer, pH 8, at 33 °C in the presence of (a) NAD^+ (1 mM) or (b) NADH (1.1 mM). The arrows denote the direction of the first potential sweep. In each case the second scan is shown in grey. A scan in the absence of cofactor and presence of H_2 (1 bar) is shown in black. The electrode was rotated at 2000 rpm to prevent mass transport limitations. The dotted lines denote the thermodynamic potential for the NAD^+/NADH couple under the conditions used assuming NAD^+/NADH is (a) 1000 and (b) 0.0001.

The cyclic voltammograms in Figure 4-1 show that the NAD^+-reductase (HoxFU) was able to reduce NAD^+ (a) and oxidise NADH (b) by exchanging electrons with an electrode. The catalytic waves for NAD^+ reduction and NADH oxidation commence at *ca* -0.280 V and -0.450 V *vs* SHE respectively, these are the same as the values observed for HoxFU from *R. e* under the same conditions.[151]

4.2.2 Catalytic bias

Cyclic voltammetry was used to determine the catalytic bias of the NAD^+-reductase. The current response of an enzyme-modified electrode was recorded in the presence of different NAD^+/NADH concentrations, in each case the total cofactor concentration was maintained at 2 mM. The cyclic voltammograms commenced at *ca* -0.22 V *vs* SHE and the first electrochemical sweep was towards high potenital.

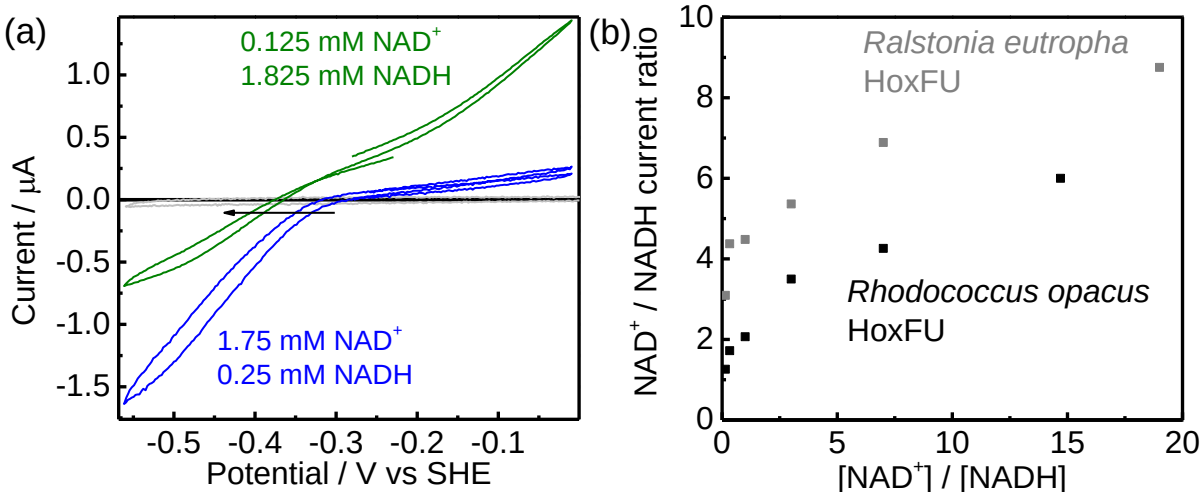

Figure 4-2: Cyclic voltammetry experiments to determine the catalytic bias of HoxFU from *Rh. o.* (a) The current response of a HoFU-modified electrode at high (blue) and low (green) $[NAD^+]/[NADH]$ ratios. The response of an unmodified electrode is also shown (grey). (b) The current ratio ±140 mV from the *x*-intercept is plotted as a function of $[NAD^+]/[NADH]$. Each experiment was performed at a total cofactor concentration of 2 mM, in Tris-HCl, pH 8, 30 °C, 10 mV s^{-1} with an electrode rotation rate of 2000 rpm. The *R. e* HoxFU data in Panel (b) was recorded by Dr Z. Idris under analogous conditions.[151,222]

The cyclic voltammograms in Figure 4-2(a) show clear NAD^+ reduction and NADH oxidation under both high and low $[NAD^+]/[NADH]$ conditions. The cyclic voltammograms crossed the *x*-axis sharply at the thermodynamic potential under the conditions used demonstrating very high

thermodynamic efficiency for NAD^+/NADH cycling. The current ratio for NAD^+ reduction and NADH oxidation ± 140 mV from this potential was plotted against the concentration ratio and compared to the analogous data for *R. e* HoxFU.

The potential at which the current crosses the *x*-axis decreases (black arrow) as the [NAD^+]/[NADH] ratio decreases as expected using the Nernst equation (Section 2.1.1). The plot in Figure 4-2(b) shows the current ratio as a function of the concentration ratio in comparison to previous results for *R. e* HoxFU.[151] The data sets show the same trend of bias towards NAD^+ reduction with similar absolute values but suggests that the *Rh. o* NAD^+-reductase is slightly less biased towards NAD^+ reduction. This may be beneficial in applications where NADH oxidation is required (Chapter 8).

4.2.3 Determination of the affinity constants for NAD^+ and NADH

Chronoamperometric techniques were used to determine the affinity of the NAD^+-reductase towards NAD^+ and NADH. The techniques for characterising affinity constants electrochemically were introduced in Section 2.3. A low k_M value means that an enzyme has high affinity for the substrate and therefore that high activity can be achieved at a low substrate concentration; this would be beneficial for many applications for two reasons. Firstly the cofactors are expensive and therefore ways of minimising the concentration are economically beneficial and secondly, if catalytic cofactor (< 0.1 mole % of the product) is used additional product purification steps could be prevented.

The cyclic voltammogram in Figure 4-3(a) was recorded at a PGE electrode modified with NAD^+-reductase in NAD^+ solution (1 mM) and shows the potential at which the chronoamperometry experiments were performed (-0.41 V *vs* SHE). At this potential there is significant current for NAD^+ reduction and no other redox reactions occur at the PGE electrode. A typical chronoamperometry trace to determine k_M^{NAD+} is shown in Figure 4-3 (b); at the start the current is close to 0 A since there is no substrate present in solution. The

current observed was due to residual capacitance and this value was subtracted from the electrochemical data before use to give an adjusted current. After each injection of NAD^+ there was an increase in magnitude of the current. This catalytic current is directly proportional to the activity of the enzyme; a plot of the current *vs* the concentration of NAD^+ can be used to determine the k_M for NAD^+ by fitting to the Michaelis-Menten Equation, Section 2.3.1. A typical plot is shown in Figure 4-3(c).

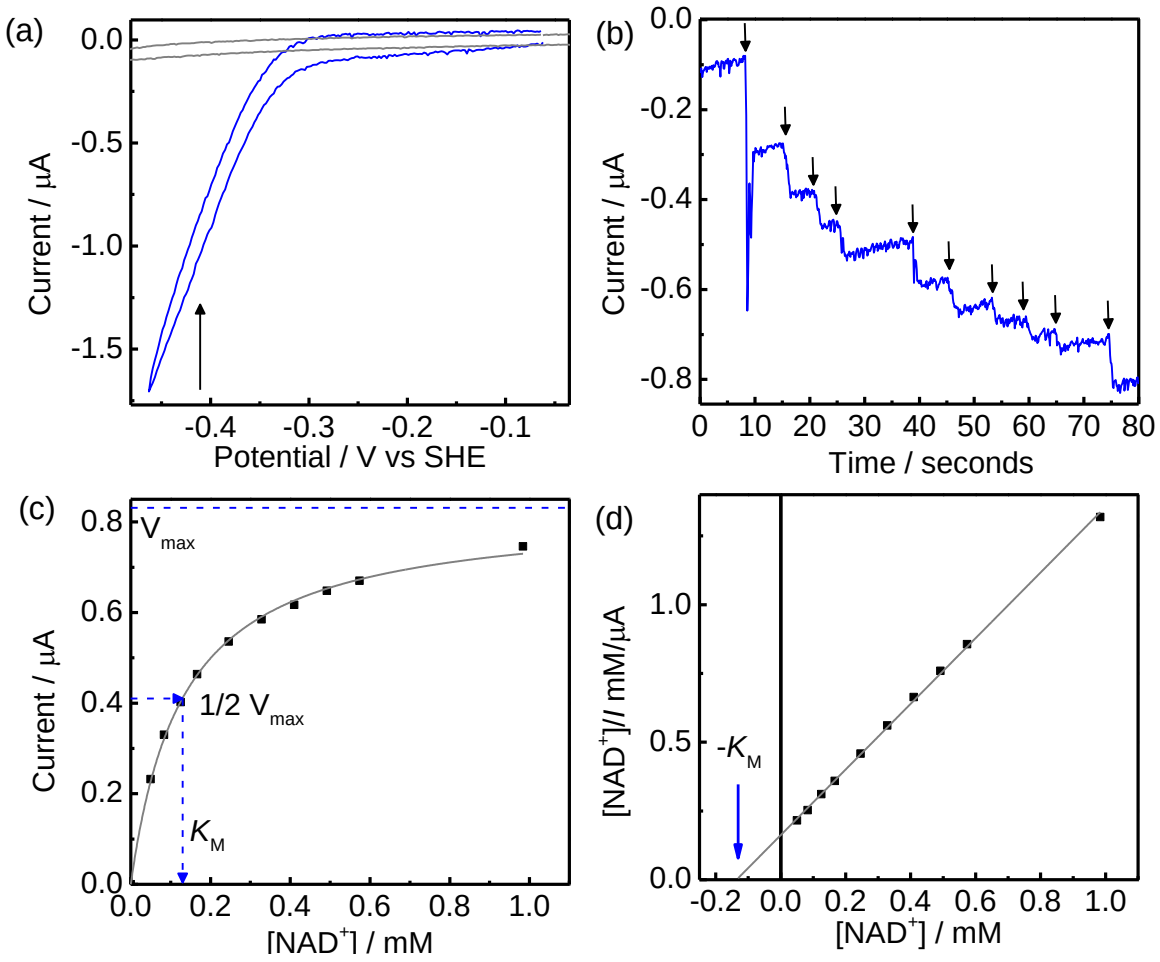

Figure 4-3: Electrochemical techniques were used to determine k_M^{NAD+} of the NAD^+-reductase (HoxFU) from *Rh. o.* (a) Cyclic voltammetry using an electrode modified with NAD^+-reductase in the presence of NAD^+ (blue) or H_2 (grey). (b) The NAD^+-reductase modified electrode was poised at -0.41 V *vs* SHE, aliquots of NAD^+ were injected over time and the current recorded. (c) The current can be plotted *vs* the concentration of NAD^+ and analysed to give the k_M for NAD^+. (d) A Hanes-Woolf plot can be used to give a more accurate calculation of k_M. Experiments performed in Tris-HCl, pH 8 at 30 °C with electrode rotation of 2000 rpm.

Alternatively a Hanes-Woolf plot can be constructed as shown in Figure 4-3(d). Using the plots in Figure 4-3(c) and (d), k_M^{NAD+} was determined to be 131 µM for this single

measurement. From 5 similar chronoamperometry traces, each using a separate enzyme film, an average k_M^{NAD+} of 131 ± 17 μM was determined. This value is very similar to the K_M^{NAD+} for the *R. e* NAD^+-reductase which has been electrochemically determined to be 197 ± 28 μM by Dr Idris. Similar experiments were also performed on the whole HoxHYFU from *Rh. o.* This enzyme did show some H^+ reduction current (as expected due to the presence of an active hydrogenase domain) however it was considered negligible in comparison to the NAD^+ reduction current. The k_M^{NAD+} for *Rh. o* HoxHYFU was determined to be 102 ± 33 μM.[252] This value is within experimental error of the k_M value determined for the HoxFU subunits.

The k_M^{NADH} value was also determined using chronoamperometry. The enzyme-modified electrode was poised at -0.1 V *vs* SHE (an NADH oxidising potential) and aliquots of NADH injected over time; the resulting current after each NADH addition was recorded.

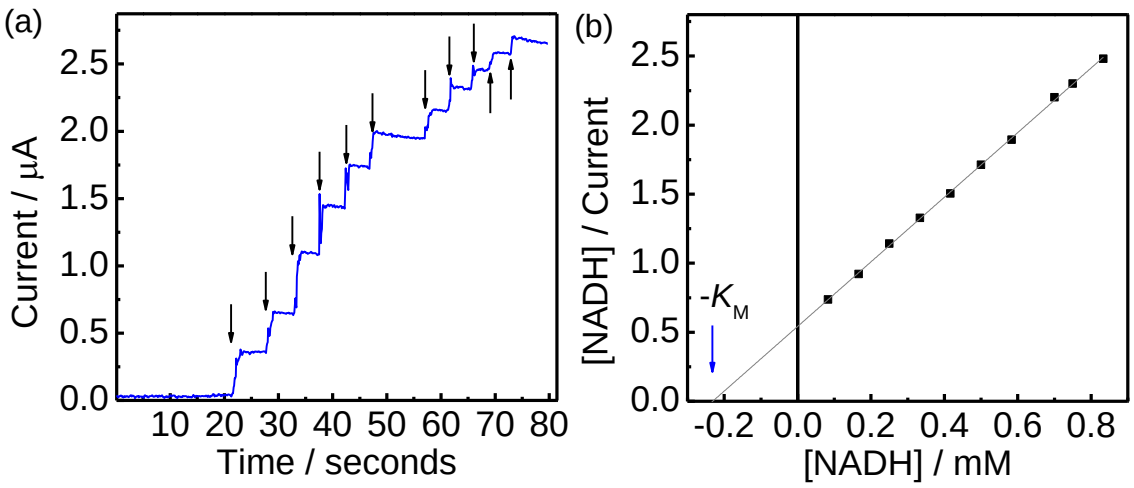

Figure 4-4: Electrochemical experiments to determine the k_M for NADH. (a) Typical chronoamperometric measurement for an NAD^+-reductase (*Rh. o.* HoxFU) modified electrode poised at -0.01 V *vs* SHE with injections of NADH over time. (b) Hanes-Woolf plot constructed to determine the value of k_M^{NADH}. Experiments performed in Tris-HCl, pH 8 at 30 °C with electrode rotation of 2000 rpm.

A typical chronoamperometric trace for k_M^{NADH} determination is shown in Figure 4-4(a). The data was analysed as a Hanes-Woolf plot, Figure 4-4(b). Using an average of 6 datasets the k_M^{NADH} was calculated to be 311 ± 92 μM. This is very close to the value determined for *Rh. o* HoxHYFU, 307 ± 127 μM, but much higher than the value for *R. e* HoxFU (56 ± 18 μM).

Although this enzyme shows less affinity for NADH than the NAD^+-reductase from *R. e*, its activity in the NADH oxidation direction is comparable.

4.2.4 Product inhibition constants

As previously mentioned, the NAD^+-reductase from *Ralstonia eutropha* is subject to product inhibition in both directions; this can be quantified electrochemically.

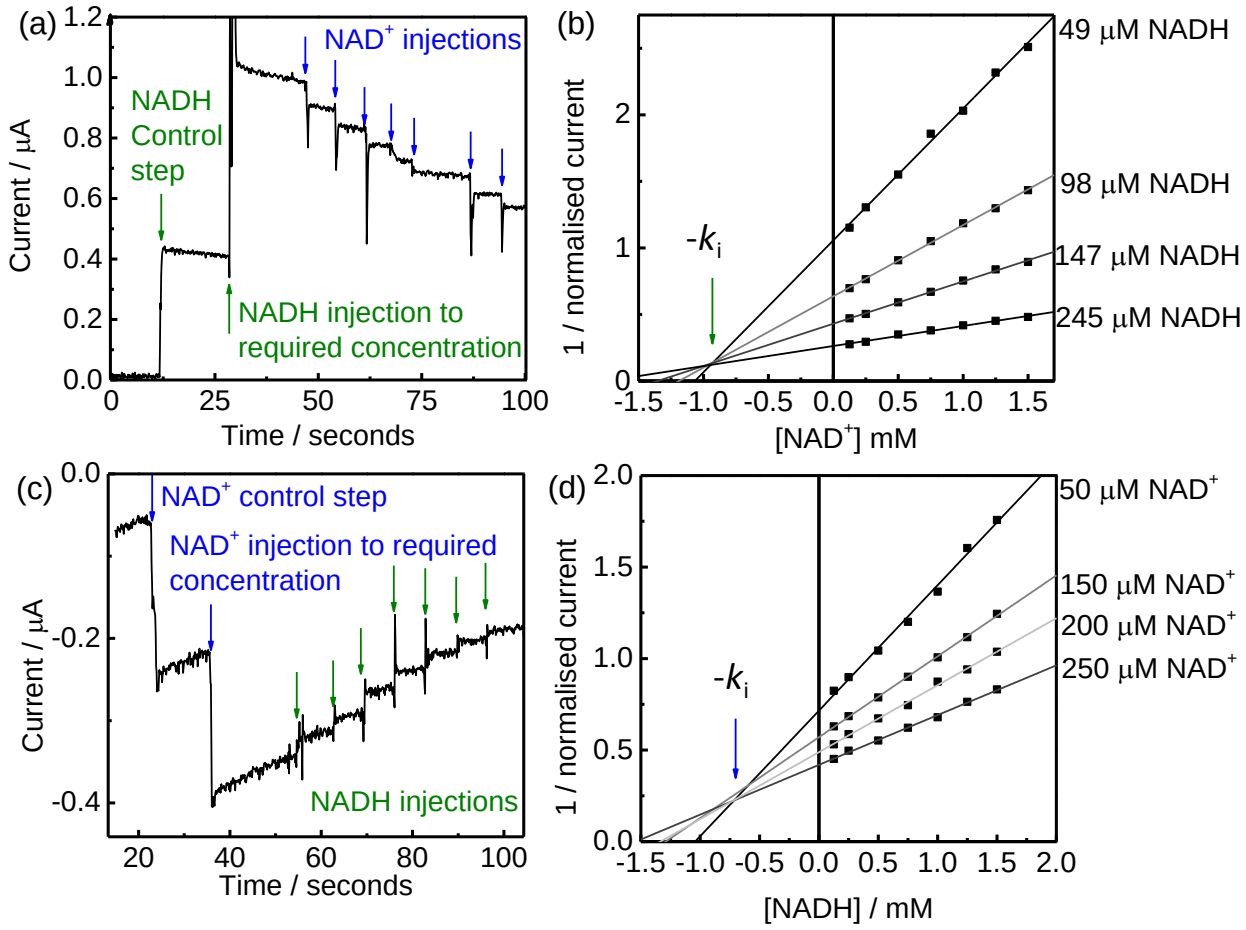

Figure 4-5: Chronoamperometry experiments to determine the product inhibition constant, k_i, for *Rh. o* HoxFU of NAD^+ and NADH. (a) The enzyme-modified electrode was poised at -0.01 V *vs* SHE and an aliquot of NADH was injected, (49 µM NADH, green arrow) followed by a second substrate injection to give the desired NADH concentration (green arrow). Aliquots of NAD^+ (blue arrows) were injected to inhibit NADH oxidation by HoxFU. The current after each cofactor injection was recorded and the residual current substrate. (b) A Dixon plot of 1/normalised current *vs* inhibitor concentration to determine the k_I. (c) The enzyme-modified electrode was poised at -0.46 V *vs* SHE and the current recorded during a series of substrate (NAD^+) and inhibitor (NADH) injections. (d) A Dixon plot to determine k_I for NADH inhibition of NAD^+ reduction.

To determine the inhibition constant (k_I), experiments must be carried out at a range of substrate concentrations. In order to directly compare datasets, a control substrate injection

step was used followed by a second injection to give a desired substrate concentration. Each chronoamperometric trace was then normalised to the current after the control step to allow direct comparison between different enzyme films. Additions of product were then injected and the resulting current recorded. To ensure that the change in catalytic current was not due to dilution of the substrate, the inhibitor solution contained substrate at the required concentration for each experiment.

Typical chronoamperometric traces for the inhibition of NADH oxidation or NAD^+ reduction by their products are shown in Figure 4-5(a) and (c), respectively. As expected, initial injections of substrate led to an increase in the catalytic current in each case. Subsequent additions of inhibitor (product) caused a decrease in the magnitude of the catalytic current.

A Dixon plot was constructed by plotting 1 / normalised current *vs* inhibitor concentration at each substrate concentration (Section 2.3.2). First, the residual capacitive current was subtracted from the chronoamperometric traces (as for Section 4.2.3) before they were normalised to the current after the control step. For competitive inhibition (Appendix B), the inhibition constant is equal to -[inhibitor] at the point where the lines intersect. The Dixon plots for k_I^{NAD+} and k_I^{NADH} are shown in Figure 4-5(b) and (d) and give values of *ca* 0.9 mM and *ca* 0.7 mM, respectively. These are higher than the values for the NAD^+-reductase from *R. e* (0.2-0.3 mM and 0.1-0.3 mM) suggesting the *Rh. o* NAD^+-reductase is less product inhibited. This may be beneficial for some applications where substantial conversion of NAD^+ to NADH or *vice versa* is required.

4.3 Soluble hydrogenase HoxHY dimer

The SH from *R. e* is able to sustain H_2-driven NAD^+ reduction in the presence of O_2 and is therefore categorised as an O_2-tolerant hydrogenase. This section will analyse the hydrogenase dimer (HoxHY) from *Rh. o* electrochemically for the first time and compare the

results to HoxHY from *R. e*. The *R. e* HoxHY dimer was previously characterised electrochemically in the Vincent Group and the same protocols will be used here for simple comparison.[226,253]

4.3.1 Determination of E_{switch} for *Rh. o* HoxHY

The HoxHY dimer from *R. e* is isolated in a state that is inactive towards H_2 oxidation. On sweeping an enzyme modified electrode from a high potential (*ca* 0 V *vs* SHE) to a more negative potential a reactivation peak is observed. This means that at a certain potential, H_2 oxidation by this enzyme becomes possible and that the enzyme is put into an active state. Shortly after, the potential is swept below the thermodynamic potential for the H^+/H_2 couple and H^+ reduction begins leading to a negative current. On the return scan, the oxidative sweep, clear H_2 oxidation is seen at potentials positive of the thermodynamic potential. The second scan shows H_2 oxidation and H^+ reduction with no reactivation peak at the potential seen in the first scan showing that the as-isolated, inactive, state is not reformed. The potential at which this reactivation peak is observed depends on the pH of the solution and the scan rate of the cyclic voltammogram. The potential at which the increase in current is at a maximum has been termed E_{switch} by Armstrong and co-workers and can be easily determined using a plot of the differential of the current as a function of potential.[254] For HoxHY from *R. e* E_{switch} is *ca* -220 – -330 mV between pH 6 and 8 at a scan rate of 1 mV/s. There is a linear relationship between pH and E_{switch} for this enzyme which is indicative of a proton coupled process and from the gradient of this line the recovery of as-isolated HoxHY is determined to be a $1H^+/1e^-$ process. A similar set of experiments were carried out for the analogous protein, HoxHY from *Rh. o* in order to compare the two enzymes.

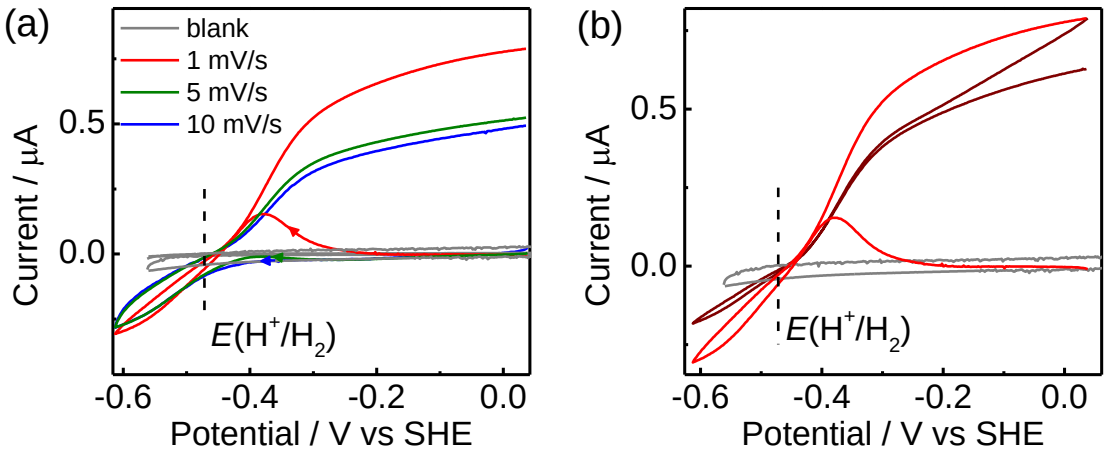

Figure 4-6: Cyclic voltammetry was used to analyse H^+/H_2 cycling of the hydrogenase dimer (HoxHY) from *Rh. o.* An electrode modified with HoxHY was put into the electrochemical cell and the current was recorded with respect to potential. (a) The scans were performed with different scan rates and are shown compared to an unmodified electrode at 10 mV/s. (b) The first scan at 1 mV/s is compared to the second scan. All scans performed with a stationary electrode in 50 mM Tris buffer-HCl pH 8 with 1 bar H_2 flowing through the sealed cell at 22 ^oC. In each, the current response is shown for an unmodified electrode (grey).

The cyclic voltammograms in Figure 4-6(a) show that *Rh. o* HoxHY is able to exchange electrons with an electrode and catalyse both H_2 oxidation and H^+ reduction. The cyclic voltammograms in Figure 4-6(a) started at +0.03 V *vs* SHE and showed no catalytic activity for H_2 oxidation. The potential of the electrode was then swept to more negative potentials (at 1 mV s^{-1}, red), at around -0.3 V, the current started to increase, indicative of H_2 oxidation. This reductive reactivation is consistent with that observed for HoxHY from *R. e.* The current soon started to drop as the thermodynamic potential for the H^+/H_2 couple was reached due to the driving force for H_2 oxidation decreasing. At potentials below this value, a negative current was seen due to H^+ reduction. On the reverse scan, H_2 oxidation was seen at all potentials above the thermodynamic potential, and no inactivation was seen at higher potentials. In Figure 4-6(b) the second scan at 1 mV s^{-1} is shown in comparison to the first. The second scan is consistent with the enzyme being active throughout, with no reductive reactivation. On both the reductive and oxidative sweeps, a positive current was recorded at higher potentials, and a negative current at lower potentials.

This experiment was also performed at different scan rates: 5 mV s^{-1} (green) and 10 mV s^{-1} (blue). These cyclic voltammograms look similar, although the size and potential of the reductive activation peak is different.

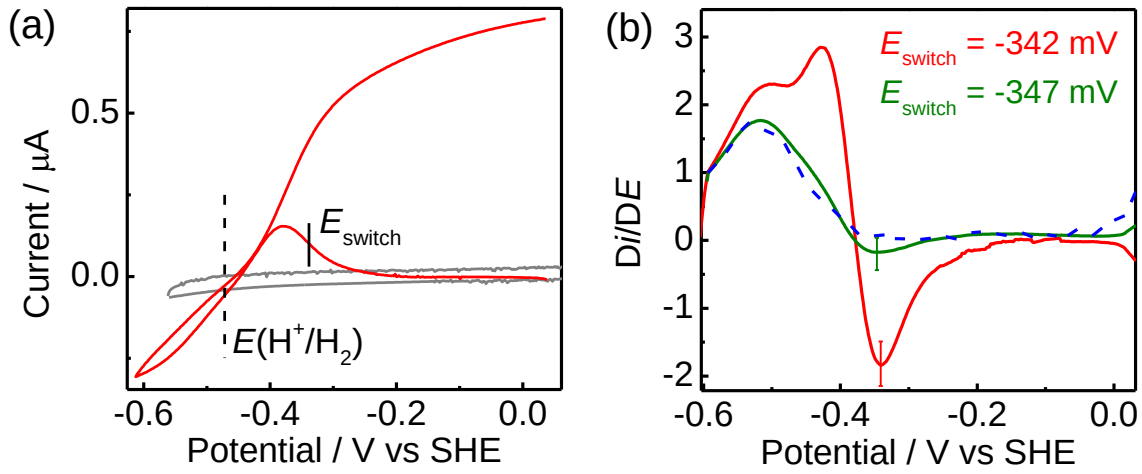

Figure 4-7: (a) Reproduced from Figure 4-6, scan at 1 mV/s. The maximum gradient of the current for the reductive reactivation peak is marked, E_{swtich}. (b) The derivative of the current from the HoxHY modified electrode on the initial reductive sweep from high potential to low potential, from which the value for E_{switch} can be determined. This is shown for different scan rates: 1 mV s^{-1} (Red), 5 mV s^{-1} (green) and 10 mV s^{-1} (blue, dotted).

The potential and magnitude of the reactivation peak is shown to be dependent on the scan rate. The results in Figure 4-7 show the determination of E_{switch} for HoxHY from *Rh. o*. Panel (a) shows a scan at 1 mV s^{-1} reproduced from Figure 4-6(a). Figure 4-7(b) shows the derivative of the current on the initial reductive sweep (red). The derivatives of the current on the reductive sweeps at a 5 mV s^{-1} (green) and 10 mV s^{-1} (blue) are also displayed. It is observed that the magnitude of reactivation decreased and that the potential shifted to a more negative value with increasing scan rate. At a scan rate of 10 mV s^{-1}, no reactivation peak was seen. At 1 mV s^{-1} the value of E_{switch} was determined as -342 mV and at 5 mV s^{-1} as -347 mV. These results are in agreement with the results for *R. e* HoxHY; the absolute values are very similar (at 1 mV/s, E_{switch}= -345 mV at pH 8).[226,253]

4.3.2 Stability of HoxHY from *Rh. o*

The experiments to determine E_{switch} where carried out using a stationary electrode. This

allowed direct comparison with the electrochemistry carried out on the *R. e* HoxHY[151] which is not very stable on the electrode especially at high rotation rates. The stability of HoxHY from *Rh. o* on a rotating electrode was also investigated here.

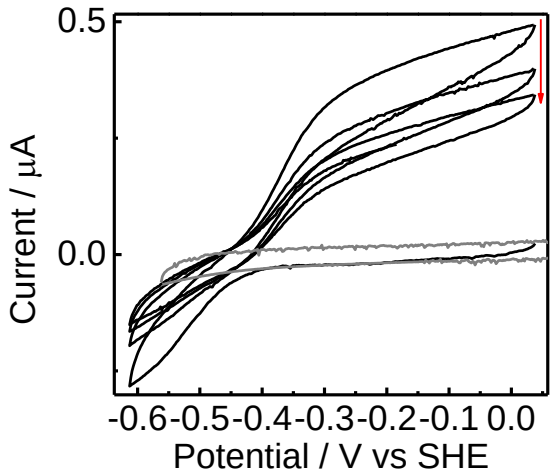

Figure 4-8: Cyclic voltammograms to show the instability of *Rh. o* HoxHY on an electrode rotating at 1000 rpm. Experiment performed in Tris-HCl, pH 8 with 1 bar H_2 at 10 mV s^{-1}.

The cyclic voltammograms in Figure 4-8 show four successive scans with HoxHY on a RDE rotating at 1000 rpm. There is a clear drop in both H_2 oxidation and H^+ reduction current over time (red arrow). This demonstrates the instability of the enzyme film on the electrode. However, this enzyme appears to be more active and more stable than HoxHY from *R. e* which tends to have a maximum H_2 oxidation current of ca 50 nA under the same conditions.

4.3.3 Electrochemical analysis of the O_2-tolerance of HoxHY from *Rh. o*

The O_2-tolerance of HoxHY was probed using similar electrochemical protocols to those used for *R. e* HoxHY. Chronoamperometry was used to moitor the current response of an enzyme-modified electrode while the gas atmosphere in the electrochemical cell was changed over time.[226,253] An aliquot of HoxHY (0.5 µL) was spotted onto a freshly polished electrode and allowed to adsorb over *ca* 30 seconds. This working electrode was placed into a gas tight, and rotated at 2000 rpm to provide efficient equilibration of the cell solution with the gas atmosphere.

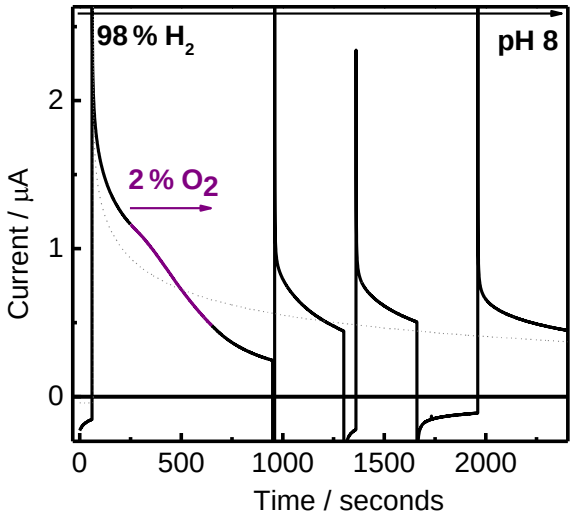

Figure 4-9: Chronoamperometry to monitor the inhibition of HoxHY by O_2 during catalysis of H_2 oxidation and the extent of reductive reactivation. The enzyme was first reductively activated at -0.46 for 60 seconds, then the potential was changed to 0.26 V with 98 % H_2 : 2 % N_2 flowing through the headspace of the electrochemical cell (1 L min^{-1}). At 250 seconds, the gas mixture was exchanged for 98 % H_2 : 2 % O_2 for a total of 400 seconds (corresponding to the purple line). Reductive poises at -0.46 V were carried out at 950, 1300 and 1650 seconds for 10, 60 and 300 seconds, respectively. An enzyme-modified film in the presence of 98 % H_2 : 2 % N_2 over the same time period is also shown for comparison. The experiment was performed at 22 ^oC in Tris-HCl, pH 8 with electrode rotation rate of 2000 rpm.

The chronoamperometric trace in Figure 4-9 shows the effect of introducing 2 % O_2 on the catalytic H_2 oxidation current for HoxHY. Since the enzyme is isolated in an inactive state, the electrode was first poised at -0.46 V *vs* SHE for 60 seconds in the presence of 98 % H_2 : 2 % N_2 to activate the enzyme. A negative current corresponding to H^+ reduction was seen at this time, although it was very small due to the high H_2 partial pressure (leading to significant product inhibition). The electrode was then poised at a H_2 oxidation potential, -0.26 V *vs* SHE. A spike in the current was observed due to reorganisation of electrolyte at the electrode after this fast change in potential (Faradaic current). The current then settled at a positive value (*ca* 1 µA) corresponding to H_2 oxidation by HoxHY.

At 250 seconds the gas mixture was exchanged for 98 % H_2 : 2 % O_2 such that the H_2 partial pressure was not changed. A similar chronoamperometry trace was recorded for an electrode modified with HoxHY in the presence of 2 % N_2 in 99 % H_2 for comparison (dotted line). The decrease in magnitude of the catalytic current on introduction of O_2 (purple section)

indicates that there was less H_2 oxidation occurring in the presence of O_2. At 650 seconds the gas atmosphere was returned to the starting mixture; the current appeared to level off at *ca* 0.25 μA. The catalytic current dropped slowly demonstrating that the enzyme can sustain H_2 oxidation in the presence of O_2 and is therefore O_2-tolerant. However it is clear that some of enzyme was inactivated over this period, hence the lower magnitude of catalytic current. The effect of reductive reactivation was therefore considered.

At 950, 1300 and 1650 seconds the potential of the electrode was dropped to -0.46 V for 10, 60 and 300 seconds respectively before returning to -0.26 V. In each case there was a capacitive 'spike' in the current recorded on changing potential. There was clear recovery of the catalytic current after each reductive poise, demonstrating that HoxHY can be reductively reactivated from the O_2-induced state. It appeared that most of the hydrogenase was reactivated after a very short, 10 second, period at low potential. It is not clear if all of the enzyme activity has returned due to the complication of film loss; however, there is still significant H_2 oxidation current after 2000 seconds suggesting that a large portion of the hydrogenase is in an active state.

The analogous chronoamperometry experiment cannot be performed to determine the effect of O_2 on H^+ reduction as direct O_2 reduction occurs at the electrode at the potential required, therefore complicating interpretation of the electrochemistry. For this experiment, the inhibition of H^+ reduction in the absence and presence of O_2 was compared. Since H^+ reduction is inhibited by the presence of H_2, the effect of changing the gas mixture from 2 % O_2 : 98 % N_2 to 2 % O_2 : 98 % H_2 can be used to determine if any H^+ reduction is occurring in the presence of O_2. The same procedures as in the previous experiment were used, however, reductive activation of HoxHY was not required since the electrode was poised at a H^+ reducing potential, -0.46 V for the entire experiment. The electrochemistry was carried out in Bis-tris buffer, pH 6 since HoxHY is much more active for H^+ reduction

under these slightly acidic conditions at this potential.

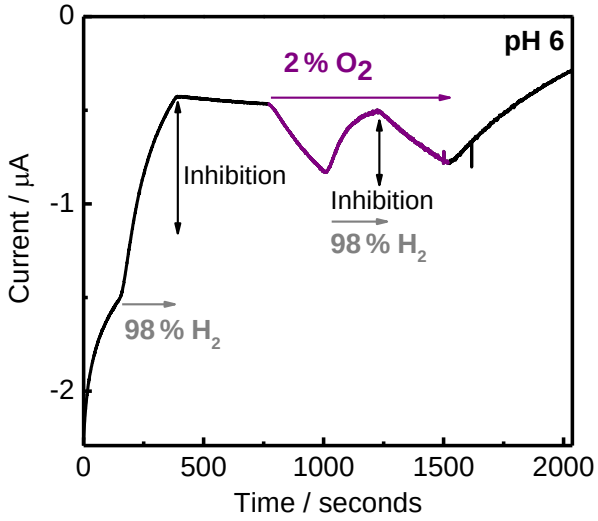

Figure 4-10: Chronoamperometry to monitor the inhibition of HoxHY by O_2 during catalysis of H^+ reduction. Initially 100 % N_2 was flowing through the headspace (1 L min^{-1}) and a clear H^+ reduction current observed. At 150 seconds the gas mixture was changed to 98 % H_2 : 2 % N_2 for a total of 225 seconds to inhibit H^+ reduction by HoxHY and then returned to 100 % N_2. At 760 seconds, 2 % O_2 in N_2 was introduced into the electrochemical cell (purple). Again, 98 % H_2 was introduced at 1000 seconds for 200 seconds but with 2 % O_2 still flowing. The H_2 was replaced by N_2 at 1500 seconds, and the gas mixture changed to 100 % N_2 at 2100 seconds. The experiment was performed at 22 ^oC, in Bis-Tris, pH 6 with electrode rotation of 2000 rpm.

The chronoamperometry trace in Figure 4-10 analyses the extent of product inhibition of H^+ reduction by HoxHY in the absence (black) and presence (purple) of O_2. At the start of the experiment a clear H^+ reduction current was observed; introduction of 98 % H_2 led to a decrease in the magnitude of this current as expected, due to product inhibition of HoxHY. On removal of this H_2, some of the catalytic current was restored. The original catalytic current was not restored, and this is likely to be due to film loss at high rotation rates.

The gas mixture was then changed to 2 % O_2 : 98 % N_2 (purple line) and shows a clear increase in the magnitude of reduction current due to direct O_2 reduction at the electrode. However, it is not clear whether there is any contribution of HoxHY catalysed H^+ reduction to this current. For this reason the gas mixture was changed to 2 % O_2 : 98 % H_2. This does not have an effect on the extent of O_2 reduction therefore any change to the current recorded necessarily comes from a change in catalysis by HoxHY. This led to a decrease in magnitude of the current suggesting that HoxHY is becoming product inhibited by the presence of H_2.

This is further supported by the increase in magnitude of current on removal of the H_2 as product inhibition decreases and the activity of HoxHY increases. Overall, this results shows that there is significant inhibition of H^+ reduction by HoxHY in the presence and absence of O_2 and therefore demonstrates that HoxHY is active for H^+ reduction in the presence of O_2. This behaviour is in agreement with the data previously recorded for *R. e* HoxHY.[226]

4.4 Summary

This Chapter has detailed the first electrochemical characterisation of the NAD^+-reductase and hydrogenase dimers from *Rh. o* SH. The results show that HoxHY and HoxFU from *Rh. o,* like the hydrogenase and NAD^+-reductase dimers from *R.e* can be directly controlled using an electrode and reversibly catalyse the $2H^+/H_2$ and NAD^+/NADH couples, respectively. The results are very similar to those for the *R. e* dimers, although there are slight differences in the affinity and product inhibition constants. Significantly, the *Rh. o* NAD^+-reductase (HoxFU) shows slightly lower catalytic bias towards NAD^+ reduction compared with NADH oxidation and thus may be more productive for NADH oxidation; this will be exploited further in Chapter 8.

The *Rh. o* hydrogenase dimer was characterised as O_2-tolerant using the electrochemical techniques, however, like the *R. e* hydrogenase dimer, it is also very unstable on the electrode. As previously discussed, it is known that FMN in the hydrogenase dimer is labile and that this contributes to the low stability of the whole SH, Section 3.1. However, an enzymatic H_2-driven NADH oxidation system is highly appealing. In the next Chapter, a H_2-driven NADH generation system using enzymes immobilised on carbon particles is developed, with the aim of coupling the NAD^+-reductase to a more active and more robust hydrogenase yielding an adaptable, modular, approach to NADH regeneration.

Chapter 5 H_2-driven NADH generation

Chapter 3 described the development an electro-enzymatic approach to NADH generation using an immobilised NAD^+-reductase. However, there are a range of limitations to this electrochemical approach, the most significant being that only solution in contact with the electrode is available to the catalyst. Driving NADH generation using a suspension of particles could improve mass transport compared to the electro-enzymatic approach due to a higher surface area being accessible to the solution. However, in the absence of an electrode, an alternative source of electrons is required. Here, inspired by nature (and the family of $NAD(P)^+$ reducing soluble hydrogenases), H_2 will be used as an electron source. The particular benefits of this will become apparent in Chapter 6 when the system is coupled with cofactor-dependent enzymes since the selective hydrogenation reactions performed by many NADH-dependent enzymes are equivalent to the addition of H_2 across a double bond. In this

way, H_2 is used as a 2-electron 2-proton source and provides a 100 % atom efficient hydrogenation process. This has important implications for industrial use of NADH-dependent enzymes where H_2-driven NADH recycling should simplify product isolation procedures, prevent generation of waste products and could have the effect of lowering overall production costs since sacrificial substrates are not required (Section 1.4.1).

This Chapter explores the possibility of coupling a hydrogenase and an NAD^+-reductase *via* electronically conducting particles for efficient generation of NADH using H_2 as the reducing equivalent. In effect this re-assembles the catalytic functionality of the soluble hydrogenase but using a more robust and more active hydrogenase enzyme. Furthermore, the ability to select a hydrogenase and NAD^+-reductase appropriate for a particular set of reaction conditions allows the particle system to be tuned for a desired reaction. Here, a range of hydrogenase enzymes will be discussed and their advantages for H_2-driven NADH generation considered. The system will then be tested, developed and characterised.

5.1 Introduction

Previous work by Armstrong and co-workers has shown that catalysis by two redox enzymes can be coupled by co-immobilising the enzymes on carbon particles. The particle acts as electron source for one enzyme and an electron sink for the other and thus electronically links the two redox centres. Provided that there is a thermodynamic driving force to couple the enzyme-catalysed half-reactions, electrons will flow through the particle from one enzyme (catalysing an oxidation reaction) to another (catalysing a reduction reaction).

In one example, the oxidation of H_2 by a hydrogenase was coupled to the reduction of nitrate by nitrate reductase, Figure 5-1(a).[255] The product, nitrite, was only detected when the hydrogenase and nitrate reductase were co-immobilised on the carbon particles, Figure 5-1(b). In another example, the water gas shift reaction was shown; H^+ reduction by a hydrogenase was coupled to CO oxidation by a carbon monoxide dehydrogenase, Figure 5-1(c).[256]

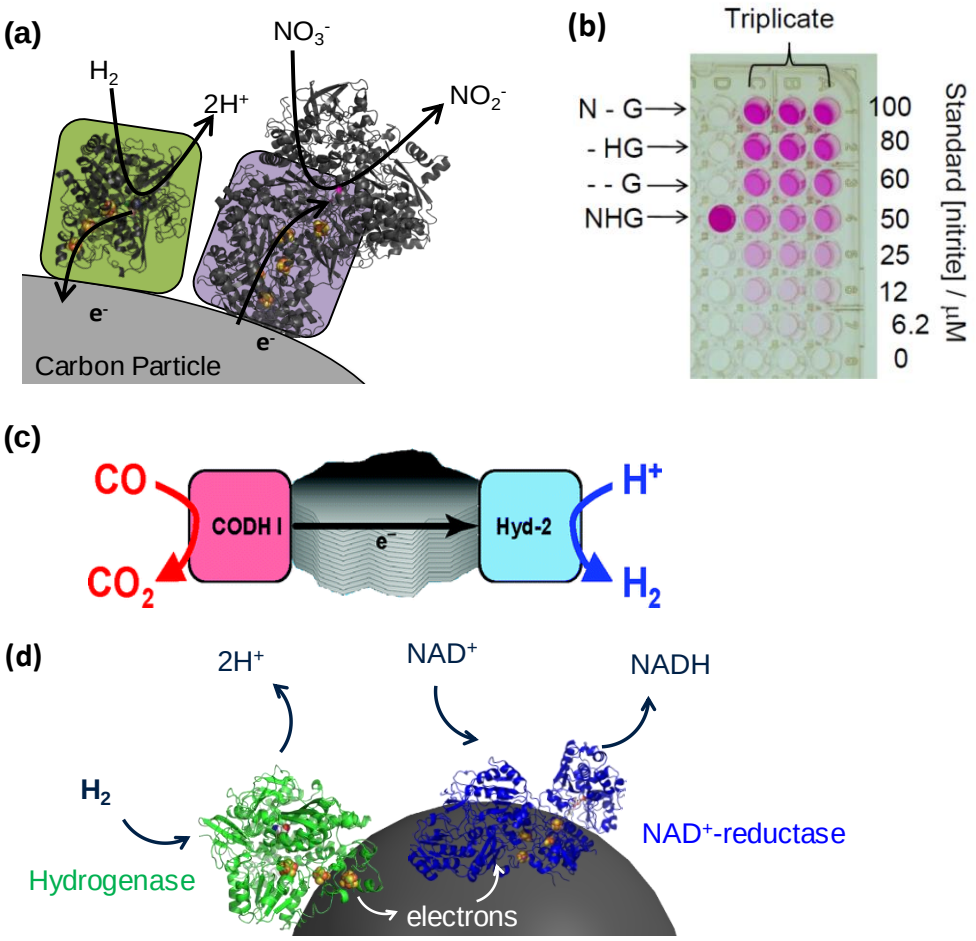

Figure 5-1: The concept of coupled enzyme redox catalysis on graphite particles. (a) Schematic representation of enzyme modified particles for coupling H_2 oxidation to nitrate reduction. A hydrogenase and a nitrate reductase are electronically linked *via* a conducting carbon particle. (b) Colourimetric assays showed nitrite formation by graphite particles modified with both *Allochromatium vinosum* [NiFe] membrane bound hydrogenase and *Escherichia coli* nitrate reductase (NHG). Also shown are control experiments omitting hydrogenase (N-G), nitrate reductase (-HG) or both enzymes (--G); no nitrite was detected for these experiments.[255] Reprinted by permission from Macmillan Publishers Ltd: Nature Chemical Biology (K. A. Vincent *et al.*, *Nat Chem Biol*, 2007, **3**, 761–762, copyright 2007. (c) The oxidation of CO to CO_2 (by carbon monoxide dehydrogenase) was coupled to H^+ reduction (by a hydrogenase) via pyrolytic graphite particles.[256] Reprinted with permission from (O. Lazarus *et al.*, *J. Am. Chem. Soc.*, 2009, **131**, 14154.). Copyright 2009 American Chemical Society. (d) Schematic representation of the enzyme-modified carbon particles developed for H_2-driven NADH generation in this Thesis. A hydrogenase (green) and an NAD^+-reductase (blue) are co-adsorbed onto a carbon particle. The enzymes are shown using cartoon structures and were made using PyMol.

The work described in this Chapter develops a system where H_2 oxidation by a hydrogenase is coupled to NAD^+ reduction by an NAD^+-reductase, Figure 5-1(d).[257] The enzymes are electronically linked by the conducting carbon particles following the same principles as the above examples. The extent of H_2-driven NADH generation is governed by many factors

including enzyme loading and the potential difference between the $2H^+/H_2$ and NAD^+/NADH couples under a given set of conditions. This potential difference can be calculated using the Nernst equations for the two couples. The Nernst equation was introduced in Section 2.1.1 and is reproduced below, Equation [5-1].

$$E = E^0 + \frac{RT}{nF} ln \frac{[Ox]_{eq}}{[Red]_{eq}} \quad [5\text{-}1]$$

The standard reduction potentials of the NAD^+/NADH and $2H^+/H_2$ couples are -0.113 V and 0 V, respectively. As such the Nernst equations for the two reactions are shown below:

$$E = -0.113 - 2.303 \times \frac{RT}{2F}(pH - log \frac{[NAD^+]}{[NADH]}) \quad [5\text{-}2]$$

$$E = -2.303 \times \frac{RT}{2F}(2pH + log[H_2]) \quad [5\text{-}3]$$

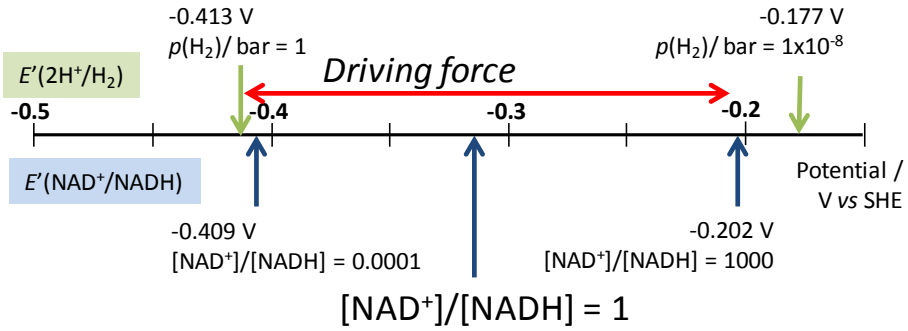

Scheme 5-1: The thermodynamic potentials of the NAD^+/NADH and $2H^+/H_2$ couples at pH 7, 25 °C. The red line denotes the driving force for coupling H_2 oxidation and NAD^+ reduction at 1 bar H_2 with a large excess of NAD^+.

The standard reduction potentials for H_2 oxidation and NAD^+ reduction are close in energy, Scheme 5-1. At pH 7, 25 °C with 1 bar H_2 the potential of the $2H^+/H_2$ and NAD^+/NADH couples are -413 mV and -320 mV respectively. This provides a 93 mV driving force for H_2-driven NADH generation. However, this assumes that the concentration of NAD^+ and NADH are equal. Due to the high expense of NADH compared to NAD^+ it is more economical to start a reaction with the oxidised cofactor, NAD^+. If the ratio of NAD^+/NADH is 1000, the potential of the NAD^+/NADH couple is -202 mV providing a driving force of

ca 207 mV to couple the two half reactions. This equates to an energy gap of *ca* -40 kJ mol^{-1}.

As discussed in Section 1.4.2, although a redox couple has a particular thermodynamic potential, electron transfer may not occur at a useful rate at this potential even with an electrocatalyst; an overpotential may be required. Due to the close spacing of the $2H^+/H_2$ and NAD^+/NADH couples it is clear that a substantial overpotential requirement for either half-reaction would prevent H_2-driven NADH generation occurring. However, if both H_2 oxidation and NAD^+ reduction can be catalysed with significant activity at minimal overpotential, Scheme 5-1 shows that NADH could theoretically be generated using electrons from H_2 until only 0.1 % NAD^+ remains. This 'NAD^+ contamination' would be well within acceptable purity limits; the NAD^+ sold by many companies contains at least this amount of NADH, Section 2.7.2.

The previous Chapters demonstrated that the NAD^+-reductase enzyme is a suitable catalyst for NAD^+ reduction and operates with significant activity at low overpotential. There are a range of electrocatalysts available for H_2 oxidation based around precious metals such as platinum; however, platinum is expensive and easily poisoned by trace CO and sulphur species. Furthermore, platinum also catalyses a range of other redox reactions such as O_2 reduction and is likely to interact with the cofactors. Such redox reactions may compete with NAD^+ reduction and could lead to side products and therefore contamination of the desired product (NADH). Platinised carbon particles modified with NAD^+-reductase were successfully trialled as a test system for H_2-driven NADH generation[222,258] but here, a range of hydrogenase enzymes that are able to oxidise H_2 with little or no overpotential are discussed as electrocatalysts. Comparisons between hydrogenases and platinum as electrocatalysts have been reported in the literature and the maximal current densities[254,259] and turnover frequencies per active site[174,260] calculated to be similar under the same conditions.

5.2 Electrochemistry of hydrogenases

In order to couple H_2 oxidation to NAD^+ reduction on particles, the hydrogenase must adsorb onto a carbon surface, exchange electrons with the carbon and catalyse the oxidation of H_2, preferably with little or no overpotential and high activity.

Hydrogenases have a complicated catalytic pathway which has been studied using a variety of different techniques including electrochemistry,[174] IR spectroelectrochemistry,[180] EPR spectroscopy[261] and X-ray crystallography.[262] The active site consists of Ni and Fe co-ordinated by CO, CN^- and cysteine ligands. It is suggested that during heterolytic cleavage of H_2 the Ni cycles +1, +2 and +3 oxidation states whilst the Fe remains in the $^+2$ oxidation state.[263] The catalytically active redox states of most [NiFe] hydrogenases correspond to the active site being in its more reduced electronic state. At high potentials, or in the presence of O_2, the active site of many hydrogenases is oxidised and the enzyme may become inactive. Different hydrogenases form different inactive states, at different potentials, which in turn have different kinetics and potential requirements for re-activation. It is important in this work, for H_2-driven NADH generation, that the hydrogenases used are not inactivated in the potential regions accessed, which is expected to be between *ca* -400 and -200 mV at pH 7, Scheme 5-1. This section will compare three different hydrogenases and the potential windows over which they remain active. The activity and stability of the hydrogenases will also be considered.

The [NiFe] hydrogenase dimer (HoxHY) from *Rh. o* was characterised in Chapter 4 and compared to *R.e* HoxHY. These hydrogenases both require low potential electrons for activation from the as-isolated state. In nature, these electrons are provided by the presence of NADH however, addition of NADH is not desirable due to its expense. Furthermore, the enzymes showed low activity and stability on the electrode. Here, another two [NiFe] hydrogenases are discussed; *D. vulgaris* MF [NiFe] hydrogenase (*D. v* MF)[264] and *E. coli*

hydrogenase 2 (Hyd-2),[265] the advantages and limitations of these enzymes will be analysed with respect to the 'ideal' requirements for H_2-driven NADH generation.

5.2.1 *Desulfovibrio vulgaris* MF [NiFe] hydrogenase

Desulfovibrio vulgaris is a gram-negative sulphate reducing bacterium which obtains energy from H_2 and sulphate. Sulphate is used as the terminal electron acceptor in place of O_2, which is more commonly used.[266] This enables anaerobic respiration using H_2 and sulphate, releasing hydrogen sulphide. It is thought that this type of bacteria date back over 3.5 billion years. The [NiFe] hydrogenase from *D. v* MF is a heterodimeric protein of 89 kDa.[176] The enzyme consists of a small and a large subunit which contain 3 FeS clusters and a NiFe active site, respectively. The enzyme structure has been determined to high resolution in a range of redox states and has been characterised extensively.[267–269] This hydrogenase is able to oxidise H_2 at high potentials and reduce H^+ at low potentials.

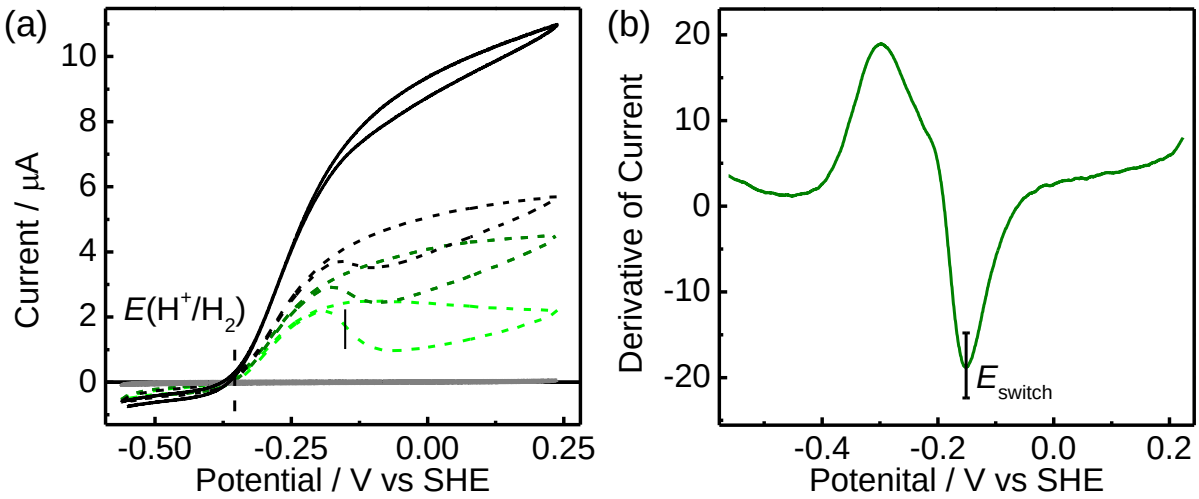

Figure 5-2: (a) Cyclic voltammograms of *D. v* MF hydrogenase at a PGE RDE modified with hydrogenase in the presence of 1 bar H_2. The first (light green), second (dark green) and third (black) scans are shown as dotted lines. A scan following 300 s activation at -0.65 V is also shown (black, solid line, no further activation was seen). All experiments performed in Bis-tris buffer, pH 6 with 1 bar H_2 in the headspace at 22 ^oC with rotation of 2500 rpm at 10 mV s^{-1}. (b) The derivative of the current from scan 1 was used to determine E_{switch} under these conditions.

Here, simple electrochemistry is carried out and used to compare the activity of this hydrogenase to that of HoxHY from *R. e* and *Rh. o.* Cyclic voltammograms were recorded

using a *D. v* MF hydrogenase-modified PGE electrode (using procedures discussed in Section 2.1.4). The cyclic voltammograms in Figure 5-2(a) show that *D. v* MF hydrogenase is able to catalyse H_2 oxidation using the electrode as an electron sink. The current cuts the *x*-axis at the thermodynamic potential for the H^+/H_2 couple under these conditions and a slight proton reduction current was observed demonstrating that this enzyme cycles H^+/H_2 with no significant overpotential. The first 3 scans are shown in dotted lines; an increase in activity between subsequent scans was observed. This was due to some of the enzyme being initially in an inactive state; the sweeps to low potential led to reductive activation. Before the final scan (black solid line) the electrode was poised at -0.65 V for 300 seconds. The final cyclic voltammogram shows a very large catalytic current for H_2 oxidation (higher currents were not achieved with further activation times). The *D. v* MF hydrogenase can also be activated from the as-isolated state using H_2 gas. This is advantageous since for the particle system developed in this Chapter where it is not possible to use an electrode to active the hydrogenase.

At high potential the *D. v* MF hydrogenase is inactivated as can be seen by the decrease in gradient of the catalytic current potentials above *ca* -0.2 V *vs* SHE. The value for reactivation from this state, E_{switch}, is calculated as -0.15 V *vs* SHE Figure 5-2(b) at pH 6 and a scan rate of 10 mV s^{-1}. This is much more positive than *ca* -0.35 V *vs* SHE for HoxHY (at pH 6 at a scan rate of 1 mV s^{-1}). Importantly, the hydrogenase is not in an inactive state within the potential window available from coupling to $E_{NAD+/NADH}$, Scheme 5-1.

From Figure 5-2(a), clear advantages to being able to couple this enzyme rather than HoxHY, to NAD^+ reduction can be seen, the most obvious being the much higher activity.

5.2.2 *E. coli* hydrogenase 2

The bacterium *E. coli* contains a suite of hydrogenases with different functions and therefore behaviours. In particular hydrogenase 2 (Hyd-2) is able to catalyse both oxidation of H_2 and

reduction of H^+ with no significant overpotential.[265] The electrochemistry of Hyd-2 is very similar to that of the *D. v* MF hydrogenase: H_2 oxidation is catalysed with high activity and the enzyme shows high stability on the electrode. This enzyme will therefore be used interchangeably with *D. v* MF hydrogenase.

5.3 Methods and experimental design

Methods for preparing enzyme-modified carbon particles were discussed in Chapters 2 and 3. The specific details for each experiment are provided in the results sections since many parameters were changed throughout development of the H_2-driven NADH generation system. Here, the more general protocols used in this Chapter are discussed along with the developmental experiments.

5.3.1 Using electrochemistry to balance H_2 oxidation and NAD^+ reduction

In the work described so far, redox enzymes catalysing half reactions have been analysed separately using protein film electrochemistry. Here, two enzymes were co-adsorbed onto an electrode and studied electrochemically such that suitable conditions for coupling them could be identified. It is important that both enzymes operate efficiently under the same conditions and that the two enzymes can be affectively co-immobilised (i.e. that one does not 'block' the electrode surface from the other). This is essential for coupled catalysis on carbon particles since the enzymes provide an electron source and sink for each other. Protein film electrochemistry was carried out using a PGE RDE and similar procedures to those previously discussed. Briefly, an enzyme mixture containing hydrogenase (*D. v* MF, 0.5 μg, *ca* 7 pmoles) and NAD^+-reductase (Hox~~HY~~FU, 0.5 μg, *ca* 3 pmoles) was spotted onto a freshly polished PGE electrode tip and allowed to partially dry over *ca* 30 seconds. The electrode was then placed into an electrochemical cell containing mixed buffer (pH 7) and NAD^+ (1 mM) with

1 bar H_2 flowing through the headspace. Electrodes modified with only one enzyme, either hydrogenase (0.5 µg) or NAD^+-reductase (0.5 µg) were also prepared for comparison.

The cyclic voltammograms in Figure 5-3 show the current response of an electrode modified with a mixture of NAD^+-reductase and hydrogenase in the presence of H_2 and NAD^+ (black line). Clear NAD^+ reduction and H_2 oxidation were seen at similar activity to that of either a hydrogenase (green) or an NAD^+-reductase (blue) film under the same conditions, demonstrating that substantial amounts of each enzyme were adsorbed and were catalytically active. The current trace cuts the *x*-axis at approximately the mid-point between the onset potentials at which H_2 oxidation and NAD^+ reduction are observed (grey region). This shows that the activity of the hydrogenase and NAD^+-reductase are appropriately matched at this potential (-0.33 V *vs* SHE) and that significant (*ca* 0.5 µA) and equal amounts of H_2 oxidation and NAD^+ reduction are occurring.

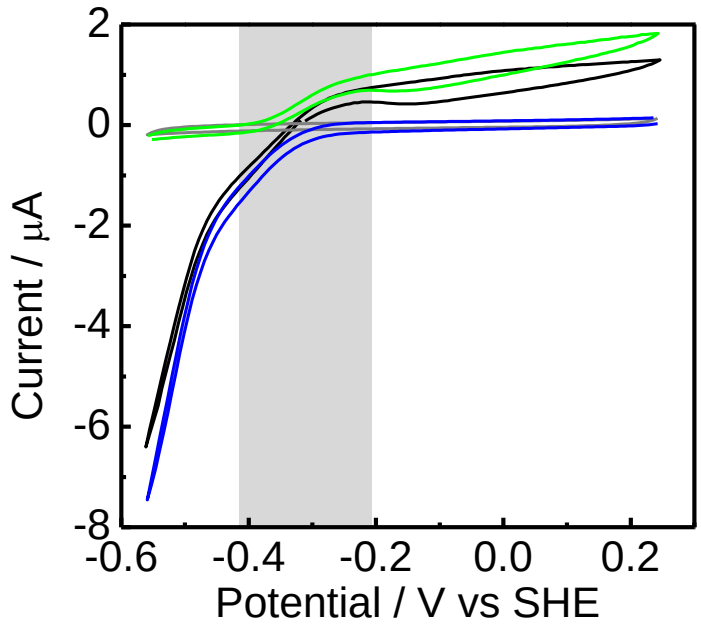

Figure 5-3: A hydrogenase and an NAD^+-reductase can be co-immobilised on a PGE electrode and remain catalytically active. Cyclic voltammograms of *D. v* MF hydrogenase (green), the NAD^+-reductase (Hox~~HY~~FU, blue) and a mixture of the two (black) immobilised on a PGE electrode in the presence of 1 bar H_2 and NAD^+ (1 mM). The response of an unmodified electrode in the same conditions is also shown (grey). In each case the electrode was rotated at 2000 rpm and the electrochemical cell contained mixed buffer (pH 7, 22 °C). The grey box shows the region in which it is thermodynamically favourable to couple H_2 oxidation and NAD^+ reduction under these conditions.

In this particular example the quantity of the two enzymes by mass is equal, equating to approximately twice as many moles of hydrogenase compared to NAD^+-reductase. However, this is not always the case for optimal coupling. In some cases substantially more moles of one enzyme would be required, this depends on the activity of a particular enzyme preparation and the conditions used compared to the enzymes pH and temperature optima as well as substrate concentrations. In some cases it may be desirable to have one enzyme working more efficiently than the other in which case the cyclic voltammogram would cross the *x*-axis more at a more positive or negative potential than the mid-point. This will be discussed further in Section 5.5.1 where the activity of the particles with different ratios of co-immobilised enzymes is considered.

In general, throughout this work, the activity of the particle system was calculated with respect to the mass of NAD^+-reductase used in μmole per minute per mg NAD^+-reductase (= U mg^{-1}). This enables direct comparison to existing cofactor regeneration methods for example formate dehydrogenase (*ca* 0.5 U mg^{-1}), malic decarboxylase (20 U mg^{-1}) and glucose dehydrogenase (15 U mg^{-1}), Section 5.8.[270]

5.3.2 Experimental set-up with *ex situ* UV-vis detection

For some experiments *ex situ* UV-vis spectroscopy was used to determine the NAD^+ and NADH concentrations over time. This was particularly necessary if reaction volumes were either too low or too high for the experiment to be carried out in a UV-vis cuvette or if many experiments were carried out in parallel. Furthermore, many enzyme systems show decreased stability when a magnetic stirrer is used and improved results are seen if the reaction is instead shaken. This is not conducive to being monitored with *in situ* spectroscopy.

These reactions were performed in 1.5 mL microcentrifuge tube, the reaction mixture was pre-saturated with H_2 and the enzyme-modified particles injected. A shaker case was designed such that gases could be flowed over the head space of the plastic tubes whilst they were

shaken to ensure a good supply of H_2 and good mixing of the particles, thus preventing mass transport limitation of the rate, Figure 5-4.

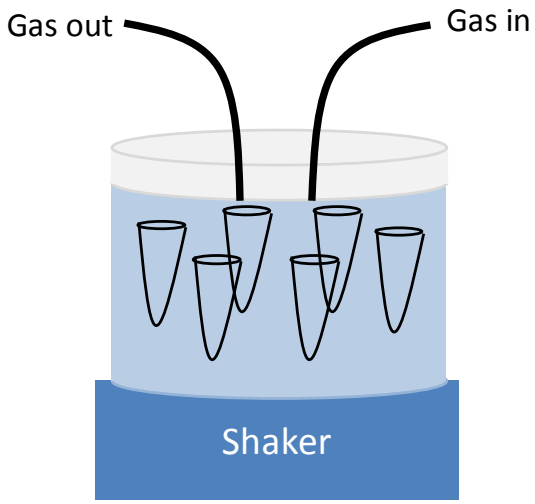

Figure 5-4: Schematic representation of the shaker case designed to run multiple reactions in parallel for *ex situ* analysis. As case was designed and built onto a shaker (IKA) such that 6 microcentrifuge tubes (1.5 mL) could be placed upright inside with the lids removed. Two threaded holes in the lid enable connections to tubing using specially designed threaded screws; this allowed the gas atmosphere to be controlled.

Aliquots of the particle suspension were removed at specific time points, particles separated by centrifugation and the supernatant solution analysed (either using the NanoVue or in a UV-vis cuvette, Section 2.4). By removing the particles, H_2-driven NADH generation is stopped. Samples recovered at a particular time point can then be stored and analysed at a later time if required. The standard methods for determining the concentration of NADH can then be used, either using the absorbance at 340 nm or using a ratio of absorbance at 260 and 340 nm as in Chapter 2.

5.3.3 Experimental set-up with *in situ* UV-vis detection

Similar UV-vis spectroscopy techniques as those used for the electro-enzymatic approach were used for *in situ* monitoring of NAD^+ conversion to NADH by enzyme-modified particles. However for the work detailed in this Chapter, carbon particles were present in the reaction mixtures; this led to scattering of the UV-vis light and therefore raised the background absorbance, to a good approximation independent of wavelength. Since the

UV-vis beam only passes through a small volume of the cuvette, small changes to the particle concentration (due to gravity or mixing) led to a large change in the extent of scattering and therefore baseline absorbance. This change in the baseline over time means that simple analysis of the UV-vis spectra using the previous techniques cannot be used since the change in absorbance will be affected by both the concentration of NADH and the concentration of particles at any given time. For this reason UV-vis spectra were recorded between 200 and 800 nm over time and a simple baseline correction carried out, Figure 5-5(a)→(c).

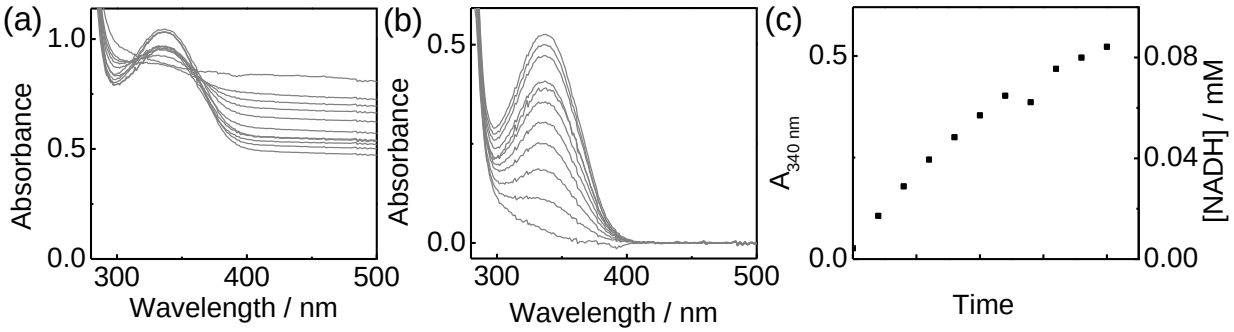

Figure 5-5: The baseline correction method used to analyse H_2-driven NADH generation using enzyme modified particles. The presence of particles causes light scattering and therefore a change to the baseline (a). This can be compensated for by subtracting the absorbance at *ca* 450 nm (b). The corrected absorbance at 340 nm can be plotted against time and used to calculate the change in NADH concentration (c).

The absorbance at 450 nm (which is clear from cofactor absorbance) was taken as a 'zero value' and used to determine a baseline to subtract from the entire spectra, Figure 5-5(a)→(b). UV-vis spectra were recorded over time and the absorbance at 340 nm after baseline correction plotted, Figure 5-5(c). These results can then be analysed using the same methods as previously described. Although this technique allowed analysis of solutions containing low loadings of particles, if the baseline absorbance was too high (>1 O.D.) the UV-vis spectra were compromised and the data could not be used. In general, *in situ* experiments therefore used a maximum particle loading of 0.1 mg mL^{-1}.

The *in situ* experiments were performed in a UV-vis cuvette (1 mL, 1 cm path length) unless otherwise stated. A rubber septum was used to seal the cuvette. In most experiments the reaction mixture was pre-saturated with H_2 and the gas mixture was further bubbled

throughout the experiment using an inlet and outlet needle through the septum. The enzyme-modified particles were injected into the UV-vis cuvette using a syringe. A magnetic stirrer was included to prevent sedimentation of the particles and to prevent mass transport limitation, although in general enzymes are sensitive to being stirred. This *in situ* approach was most commonly used to analyse the initial rate of reaction before a high percent of conversion has been achieved, so the reaction times tend to be short and therefore the effect of stirring was not problematic. In some cases bubbling of H_2 was used to perturb the solution instead of stirring, care was taken such that this did not lead to bubbles in the path of the UV-vis light. The temperature of the UV-vis cuvette was controlled using a water jacket and peltier element.

In most of the experiments in this Chapter, the enzyme-modified particles were prepared in the absence of H_2. On exposure of the particles to H_2, the hydrogenase is likely to put electrons from H_2 oxidation into the particle. This would shift the potential of the particle to a more negative value, and since it is known that the NAD^+-reductase is unstable at low potentials, particularly when there is no NAD^+ present, this could act to inactive the NAD^+-reductase. For this reason, the particles were usually injected into H_2-saturated solution containing NAD^+.

5.4 H_2-driven NADH generation

Initial experiments to consider the feasibility of a H_2-driven cofactor regeneration system were conducted using pyrolytic graphite (PG) as the electronically conducting surface since the interaction of a PG surface with hydrogenase and NAD^+-reductase enzymes is well established from protein film electrochemistry.

Freshly prepared PG particles were dispersed by sonication in buffer (KPB, pH 7) and an aliquot (containing 0.4 mg) was added to a mixture of NAD^+-reductase (HoxFU, *ca* 4.5 µg) and hydrogenase (Hyd-2, 2 µg). This solution was left at 4 ^oC for 20 minutes and the excess

liquid containing any un-adsorbed enzyme was removed by centrifugation. The particles were added to the H_2-saturated reaction mixture (60 µL) containing NAD^+ (1 mM). The reaction was monitored using *ex situ* UV-vis spectroscopy due to the low total volume. At each time point 10 µL of solution was removed, the particles separated and the supernatant diluted (100-fold) for analysis by UV-vis spectroscopy.

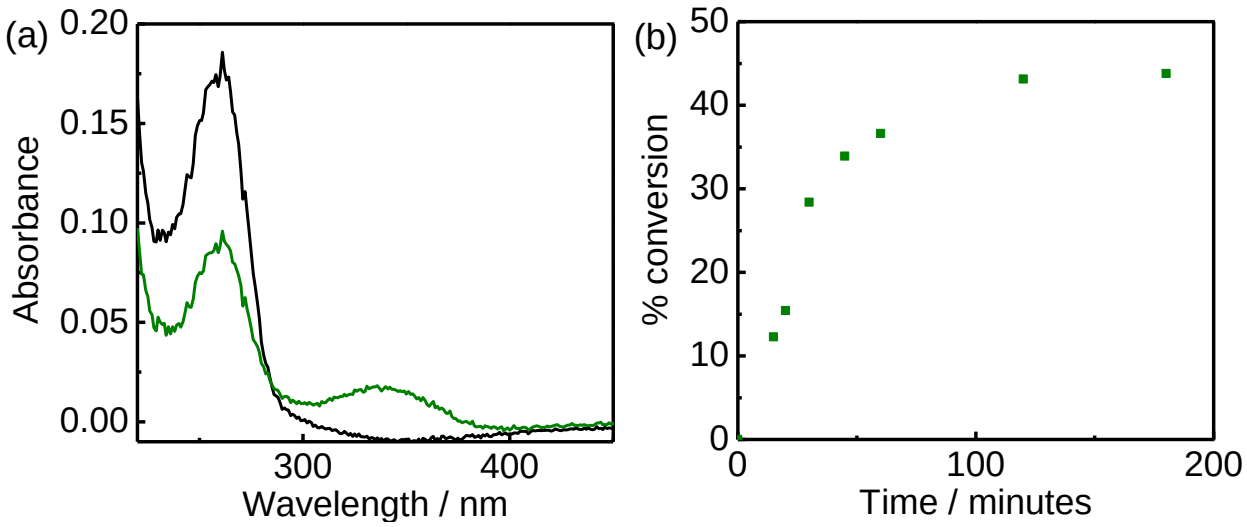

Figure 5-6: Cofactor regeneration by NAD^+-reductase (HoxFU) and hydrogenase (Hyd-2) modified PG particles. (a) UV-vis spectra of the initial (black) and final (green) reaction mixture. (b) Time series showing the amount of NAD^+ to NADH conversion over time, calculated using a ratio of the absorbance at 260 and 340 nm. Experiment performed in 50 mM KPB, pH 7 at 21 ^oC.

The spectra from the starting (black) and finishing (green) solutions in Figure 5-6(a) confirm that NADH has been generated. Using the ratio of abosrbance at 260 and 340 nm the extent of conversion of NAD^+ to NADH was calculated and is plotted in Figure 5-6 (b). The data shows that particles modified with a hydrogenase and an NAD^+-reductase are able to catalyse H_2-driven NADH generation. This requires electrons from H_2 to have been passed through the particles to the NAD^+-reductase for NAD^+ reduction. However, the overall cofactor concentration has dropped over this time – observed as a significant drop in absorbance at 260 nm, Figure 5-6(a). If 50 % conversion of NAD^+ to NADH had occurred, the expected drop in absorbance at 260 nm would be *ca* 0.01 (assuming identical dilution). This loss of cofactor is likely to be due to adsorption onto the particles. The time series in Figure 5-6(b)

shows that the particles initially operated with high activity, which was lost over time.

For experiments in the next Sections, it was important to ensure that the cofactor concentrations analysed are accurate to enable calculation of the activity of the particles. This required a trade off since to ensure that there was minimal 'empty' space on the particles for cofactor adsorption, an excess of enzymes could be used. This may prevent complete uptake of the enzyme onto the particles and therefore the calculations of activity per mg NAD^+-reductase are likely to be an underestimate of the true activity per immobilised NAD^+-reductase.

5.4.1 Towards *in situ* UV-vis detection

As discussed in Section 5.3.3, an *in situ* UV-vis set-up was developed for monitoring H_2-driven NADH generation by enzyme-modified particles. First, a similar set-up to the electro-enzymatic system was employed to prevent complication by particles in solution. For this, a piece of carbon paper was used instead of carbon particles. It is already known that hydrogenase (Section 2.2.1) and the NAD^+-reductase (Chapter 3) are able to carry out catalysis using carbon paper as an electrode material. Therefore, there should be no reason why carbon paper cannot be used to electronically link the two enzymes. Although this would have the same mass transport limitations as the electro-enzymatic system, a piece of carbon paper can be incorporated into a UV-vis cuvette without compromising the UV-vis spectra recorded. For this experiment a piece of carbon paper was pre-soaked in water and then soaked in a mixture of NAD^+-reductase (HoxFU, 10 μg) and hydrogenase (*D. v* MF, 10 μg) for 20 minutes at 4 ^oC. This was then placed into a UV-vis cuvette containing NAD^+ (77 μM) in KPB, pH 7. Spectra were then recorded over time whilst H_2 was continuously bubbled into the solution. There was no change to the baseline using this method and therefore no baseline correction was required.

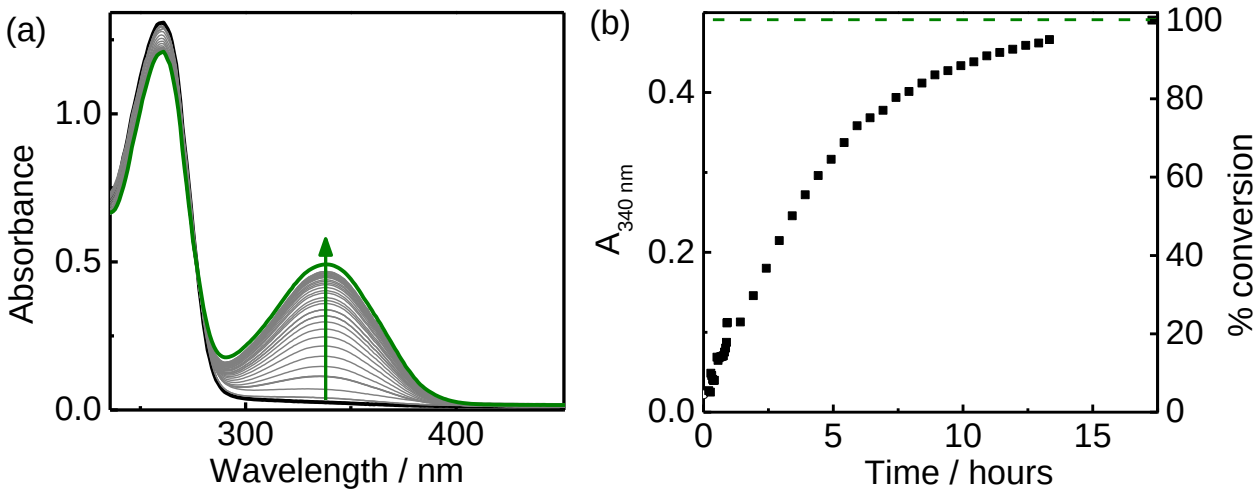

Figure 5-7: Formation of NADH by carbon paper modified with *D. v* MF hydrogenase and NAD^+-reductase (HoxFU). (a) UV -vis spectra taken over time with the first shown in black and the last in green. (b) The absorbance at 340 nm is plotted as a function of time; the corresponding percent conversion is also shown, calculated from the absorbance at 340 nm. Experiment performed in H_2 saturated NAD^+ (77 µM in 50 mM KPB, pH 7). H_2 was continuously bubbling and the temperature maintained at 22 ^oC.

The results in Figure 5-7 show an increase in absorbance at 340 nm over time, indicating that H_2-driven NADH generation using enzyme-modified carbon paper is possible. Furthermore, the *in situ* UV-vis method provided improved insight as to the kinetics of the system and demonstrates that there was no loss of cofactor from solution. From the spectra in panel (a) a clear increase in absorbance at 340 nm can be seen as well as a decrease at 260 nm. This is exactly as expected for conversion of NAD^+ to NADH. Using the extinction coefficients for NAD^+ at 260 nm and NADH at 340 nm, the concentrations in the final and starting solutions can be determined as 77 ± 4 µM NAD^+ and 78 ± 3 µM NADH respectively. This result demonstrates that near complete conversion of NAD^+ to NADH is possible. The initial activity for the experiment was very low, < 0.3 µmole min^{-1} per mg NAD^+-reductase. One reason for this may be the low concentration of NAD^+ used (77 µM); this is much lower than the k_M for the enzyme and therefore prevents high activity of the NAD^+-reductase. Another reason for the low activity may be use of a carbon paper support; only the solution in close proximity to the carbon paper is available to the catalyst.

5.4.2 Enzyme-modified particles for H_2-driven NADH generation with *in situ* UV-vis detection

The *in situ* approach was used to follow H_2-driven NADH generation by enzyme-modified particles. For this experiment an aliquot of freshly prepared PG particles dispersed in buffer (50 µL) by sonication were added to a mixture of NAD^+-reductase (Hox~~HY~~FU, 5 µg) and hydrogenase (*D. v* MF, 30 µg). The particles were left at 4 ^oC for *ca* 15 minutes. An aliquot of the enzyme-particle mixture (10 µL) was then injected into a UV-vis cuvette containing NAD^+ (1 mM) in Bis-tris buffer (pH 6). This concentration of NAD^+ is *ca* five-times higher than k_M for the NAD^+-reductase meaning that the activity of the NAD^+-reductase should be higer than in the previous experiment (assuming there are no mass transport limitations). Due to the high concentration of cofactor, the absorbance at 260 nm could not be monitored. The cell temperature was maintained at 33 ^oC, H_2 was bubbled in and the solution was stirred with a magnetic stirrer.

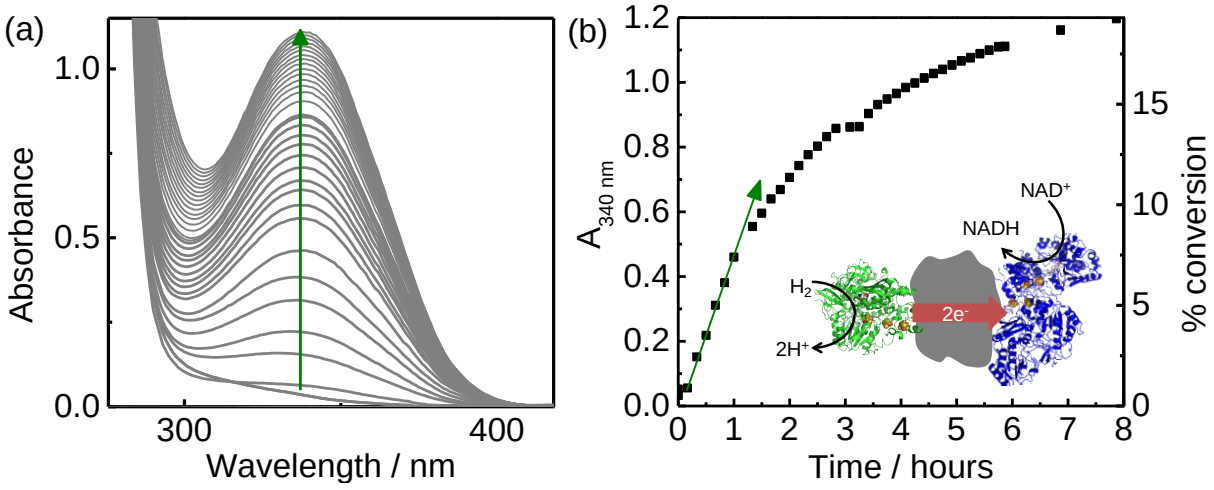

Figure 5-8: H_2-driven NADH generation using particles modified with NAD^+-reductase (Hox~~HY~~FU) and hydrogenase (*D. v* MF). (a) UV-vis spectra and (b) the absorbance at 340 nm over time after injection of enzyme-modified particles into a H_2-saturated solution containing NAD^+ (1 mM), pH 6, 33 ^oC with continuous stirring.

UV-vis spectra were recorded every 10 minutes over 6 hours and additional spectra recorded after 7 and 8 hours. A simple baseline correction was carried out on each spectrum to account for light scattering by the carbon particles, as described in Section 5.3.3. The spectra in Figure

5-8(a) show an increase in absorbance at 340 nm over time, indicative of NADH generation. Although the absorbance at 260 nm cannot be monitored using this system (as it is too high), there was no evidence that large quantities of cofactor are adsorbing onto the particles – the absorbance at *ca* 280 nm remained fairly constant.

Using a plot of the absorbance at 340 nm over time, Figure 5-8(b), the initial activity of the particles was calculated (green arrow) and determined to be 2.3 μmole min^{-1} per mg NAD^+-reductase. This is equates to a cofactor turnover frequency of *ca* 7 s^{-1} per NAD^+-reductase. This is a huge improvement in comparison to the result in Section 5.4.1. This is aided by the use of a higher NAD^+ concentration but is likely also to be dependent on a range of other factors, for example better mass transport when using the particle system in comparison to the enzyme-modified carbon paper and possibly immobilisation of more enzyme due the higher surface area available.

5.4.3 Factors affecting the kinetics of H_2-driven NADH generation

All of the *in situ* and *ex situ* plots showing NADH generation in this Section had a similar shape, fast initial activity for NADH generation which slowed down over time. There are a range of reasons for this effect: the decrease in driving force as NAD^+ is converted to NADH, the decrease in substrate concentration (Michaelis-Menten kinetics), the increase in product concentration (and therefore product inhibition), the instability of the particle systems by enzyme desorption and general loss of activity of the enzymes over time.

The data in Figure 5-9 was calculated using the Equations in Section 5.1 and demonstrates the effect that conversion of NAD^+ to NADH has on the driving force for H_2-driven NADH generation. It is clear that the high initial driving force provided by the potential difference between the $2H^+/H_2$ and NAD^+/NADH couples in the absence of NADH drops off quickly up to *ca* 10 % conversion, and then more slowly up to *ca* 90 % conversion. This provides some understanding as to the shape of the NADH generation plots, especially once the effect of

increasing product inhibition (due to NADH generation) on the activity of the NAD^+-reductase is taken into account. However, these factors complicate determination of the stability of the particle systems.

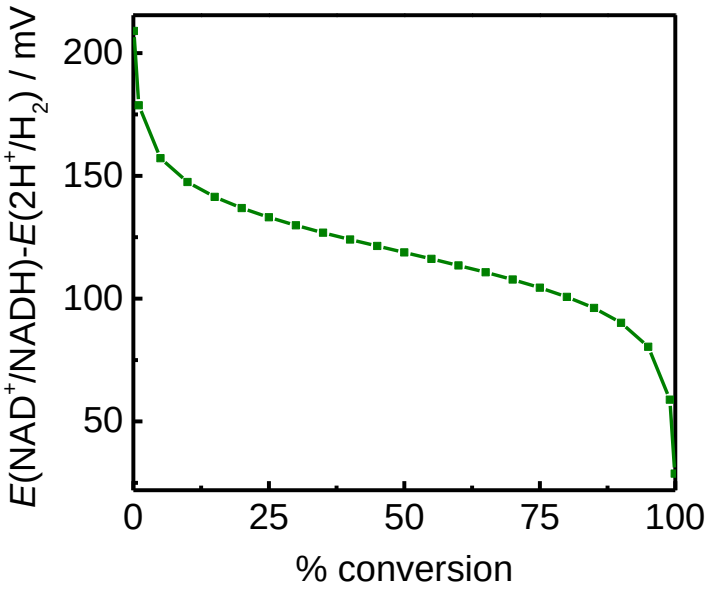

Figure 5-9: The effect of NAD^+ to NADH conversion on the driving force for H_2-driven NADH generation. A more positive value demonstrates a higher driving force. This data is calculated at pH 8, 1 bar H_2 at 25 ^oC.

Through out the rest of this Chapter, that the initial activity will be used to compare the enzyme-modified particles system under a range of different conditions.

5.4.4 Analysis of the cofactor produced

The nature of the NADH generated was investigated using HPLC. Particles were made by addition of NAD^+-reductase (Hox~~HY~~FU, 15 μg) and hydrogenase (*D. v* MF, 35 μg) to BP particles (0.12 mg). Aliquots were injected into H_2-saturated solution containing NAD^+ (0.5 or 5 mM), and left in a shaker with a flow of H_2 through the headspace (200 mL min^{-1}) for 20 hours, Section 5.3.2. The solutions were analysed after *ca* 20 hours using UV-vis spectroscopy and HPLC to determine the amount of conversion from NAD^+ to NADH. Using the ratio of absorbance at 260 nm and 340 nm the conversion was calculated to be *ca* 95 % and 80 % for the 0.5 mM and 5 mM samples, respectively.

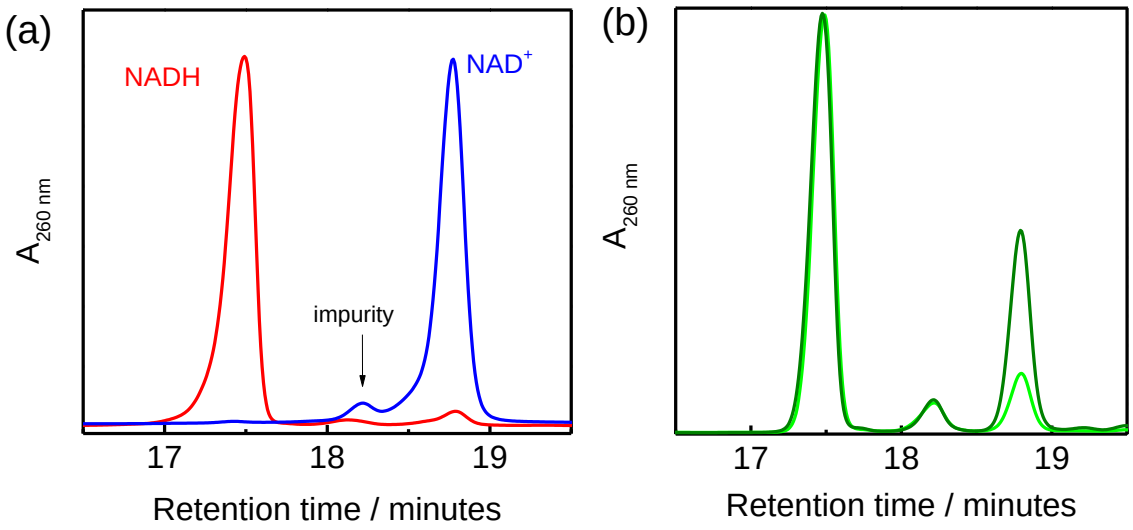

Figure 5-10: Chromatograms to confirm the conversion of NAD^+ to NADH by particles modified with *D. v* MF hydrogenase and NAD^+-reductase (Hox~~HY~~FU). Samples of (a) NAD^+ (blue) and NADH (red) and (b) end solutions after enzyme modified particles were left in NAD^+ (0.5 mM, light green and 5 mM, dark green) for *ca* 20 hours were analysed. A Zic-HILIC column was used and an acetonitrile to water gradient used for separation. The aqueous solution contained ammonium acetate buffer (pH 8).

The chromatogram shown in Figure 5-10(a) demonstrates that the as-provided NAD^+ (Melford, blue) contains an impurity (retention time ~ 18.25 minutes) and that the NADH (red) contains a significant quantity of NAD^+. The chromatograms for the two experiment samples (b) were normalised to the NADH peak for simplified comparison; both show good conversion of NAD^+ to NADH. The chromatograms are otherwise clear of peaks in this region each case demonstrating that no other cofactor forms were generated by the enzyme-modified particles (the whole chromatograms up to 27 miuntes are shown in Appendix D and further confirm that no ther UV-vis active molecules were generated). This is crucial when coupling to NADH-dependent synthesis since for a system to be viable, each cofactor must go through many cycles and it is therefore important that other, potentially enzyme-inactive forms of the cofactor are not produced.

The experiment conducted with an NAD^+ concentration of 5 mM generated *ca* 4 mM NADH, this equates to a total turnover number of >100,000 NADH per NAD^+-reductase. This value is much better than many other enzyme systems and is competitive with that of the

wild type whole SH enzyme (*ca* 140,000 NADH per SH).[154]

5.4.5 Control experiments

Control experiments were carried out to confirm that all components, the hydrogenase, NAD^+-reductase and conductive carbon particles, were required for H_2-driven NADH generation. A solution containing NAD^+ (1 mM) in Tris-HCl, pH 8 was saturated with H_2. To an aliquot of this (1 mL) different enzymes or enzyme mixtures were added and the samples were monitored using UV-vis spectroscopy. The hydrogenase used was Hyd-2 (2 µg) and the NAD^+-reductase was Hox~~HY~~FU (3.2 µg). The UV-vis cuvette was sealed to prevent loss of the H_2 and the mixtures were stirred using a magnetic stirrer. The UV-vis spectra after 30 minutes are shown in Figure 5-11, the experimental set-ups are detailed in Table 5-1.

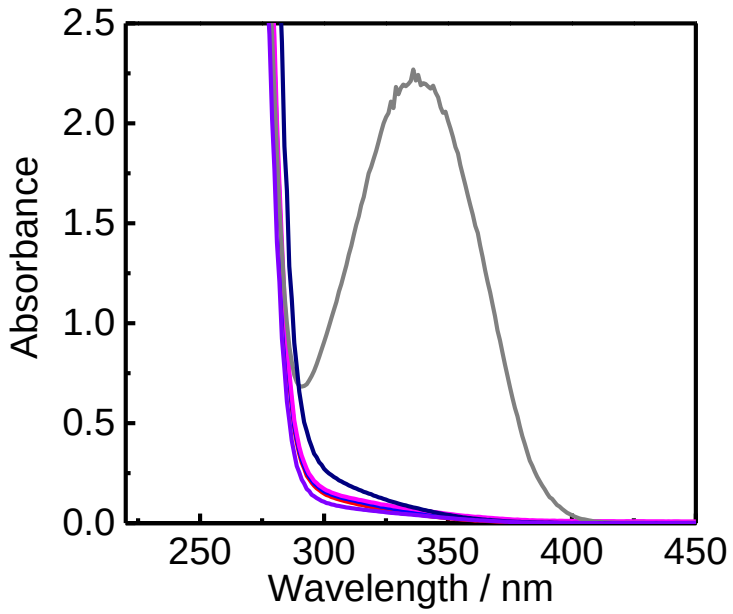

Figure 5-11: UV-vis spectra to confirm that hydrogenase, NAD^+-reductase and carbon particles are all required for H_2-drivenNADH generation. All experiments performed in H_2-saturated Tris-HCl, pH 8 at 30 ^oC with NAD^+ (1 mM). Details of each experiment are recorded in Table 5-1. Only the experiment using particles modified with hydrogenase and NAD^+-reductase (grey) produced NADH.

The UV-vis spectra in Figure 5-11 show that only one set-up generated NADH after 30 minutes. This corresponds to the enzyme-modified carbon particles (grey). None of the control reactions generated any NADH on this time-scale.

Table 5-1: Details of the control experiments run and the concentration of NADH generated after 30 minutes.

Experimental set-up	NADH generated / mM
No enzyme added	-
Hydrogenase only	-
NAD^+-reductase only	-
Hydrogenase and NAD^+-reductase added successively	-
Hydrogenase and NAD^+-reductase premixed and injected together	-
Enzyme-modified particles	0.37 ± 0.2

These results confirm that the hydrogenase and NAD^+-reductase must be in direct electronic contract to be able to transfer electrons and therefore reduce NAD^+ in the presence of H_2.

5.4.6 Other carbon materials

Although pyrolytic graphite particles and carbon paper have been shown to be good surfaces to electronically couple the enzyme moieties, other conducting materials were also explored. To be useful the materials must allow adsorption of the hydrogenase and NAD^+-reductase, have minimal interaction with the cofactor, and allow electron transfer to provide an electronic link between the two enzymes. In general, many carbon based materials were considered and each may offer different advantages for H_2-driven NADH generation. Here, results for carbon paper, carbon nanotubes and commercially available carbon nanopowder are presented. Carbon nanotubes were investigated since there are many reports of using them for immobilisation of enzymes[271,272] and many functionalisation methods[273] which can be used to enable covalent enzyme attachment. Other methods of using that carbon nanotubes will be considered in Section 5.6.4. The pyrolytic graphite particles used for the preliminary results were freshly prepared under anaerobic conditions to provide an exposed surface comparable to that of the PGE electrodes used for enzyme characterisation. This means that

the specific surface area of particles is not known and is therefore not consistent across reactions, complicating standard protocols to characterise the particles. For this reason, being able to utilise commercial carbon particles, as-provided, would be very advantageous.

A mixture of hydrogenase (*D. v* MF) and NAD^+-reductase (HoxFU) was split into aliquots and the same volume added to each set of carbon material. To each, a solution of NAD^+ (20 µL, 2 mM) was added and the mixture was saturated with H_2. The reactions were left for *ca* 5 hours and the resulting solutions analysed using UV-vis spectroscopy after removal of the carbon materials by centrifugation.

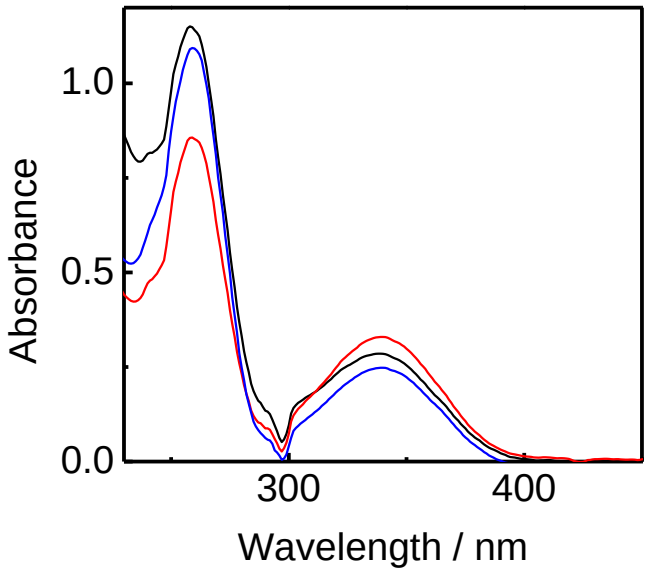

Figure 5-12: UV-Vis spectra confirming that a range of carbon materials modified with both *D. v* MF hydrogenase and HoxFU are able to catalyse H_2-driven NADH generation. For each experiment the carbon material was first exposed to a mixture of hydrogenase and HoxFU before addition to H_2 saturated NAD^+ (2 mM in mixed buffer pH 7). Spectra were recorded after 5 hours. Carbon materials used: carbon paper (black), carbon nanotubes (red) and carbon nanopowder (blue).

The spectra in Figure 5-12 show that a significant portion of NAD^+ was converted into NADH in each case. The same concentration of NAD^+ was added to each sample however, the final cofactor concentration (NAD^+ + NADH) differs for each material. Since each carbon material has different surface area properties, optimisation of each to prevent adsorption of the cofactor would be necessary, for example the concentration of the cofactor in solution in contact with the carbon nanotubes has decreased in comparison to the other experiments

suggesting that more cofactor is adsorbed. The UV-vis spectra in Figure 5-12 suggest the final mixture after exposure to enzyme-modified carbon paper, carbon nanotubes and carbon nanopowder contained *ca* 70 %, >99 % and *ca* 65 % NADH, respectively after the same length of time. The extent of NAD^+ and NADH adsorption on each material was not investigated; as such these values can not be used to give a true indication of the ativity of H_2-driven NADH generation. It is likely that there is scope for optimising H_2-driven NADH generation using each of these carbon materials; for example, near complete conversion of NAD^+ to NADH has been achieved using carbon paper as the electronically conducting material in an experiment described earlier (Figure 5-7).

The results demonstrate that a range of carbon materials can be used for H_2-driven NADH generation; this could enable a range of different experimental set-ups to be employed. For example carbon paper could be used to line a flow cell. Different carbon particles have different properties that can be exploited: in applications where having a dispersed catalyst is essential, nm scale particles can be used (i.e. nanopowder), however if easy separation by sedimentation is more important, larger μm scale particles can be employed (for example the PG particles).

5.5 Characterisation using carbon black particles

The ability of the BP particles (Section 2.2.2) to couple a hydrogenase and a NAD^+-reductase was examined. An aliquot of BP particles (0.1 mg) was added to a mixture of hydrogenase (*D. v* MF, 15 μg) and NAD^+-reductase (Hox~~HY~~FU, 2.5 μg) and left at 4 ^oC for *ca* 30 minutes. These enzyme-modified particles were then injected into a H_2-saturated solution containing NAD^+ (1 mM) in buffer (KPB, pH 7). This was analysed using *in situ* UV-vis spectroscopy with H_2 bubbling and spectra recorded every 4 minutes.

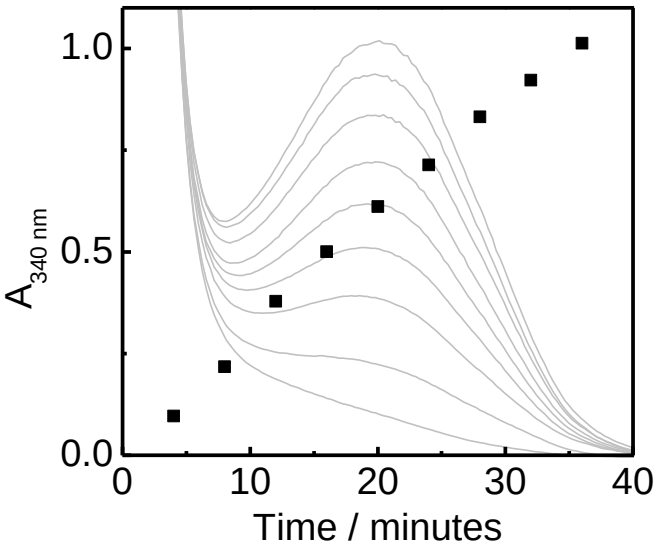

Figure 5-13: Absorbance at 340 nm (■) and UV-vis spectra (grey lines) confirming that BP particles modified with *D. v* MF hydrogenase (15 µg) and NAD^+-reductase (Hox~~HY~~FU, 2.5 µg) are able to generate NADH from H_2-saturated NAD^+ (2 mM in KPB pH 7). The experiment was performed in a UV-vis cuvette (1 mL) with continuous H_2 bubbling at 33 ^oC.

Clear NADH generation is indicated by an increase the absorbance at 340 nm in Figure 5-13. A simple baseline correction was used to correct for light scattering by the particles in solution, Section 5.3.3. The initial rate of NADH generation calculated from the increase in absorbance at 340 nm was 7.8 ± 0.5 µmole min^{-1} per mg NAD^+-reductase. This is a significant improvement from the fastest rate obtained using PG particles (2.3 µmole min^{-1} per mg NAD^+-reductase) and is competitive with existing cofactor regeneration enzymes (Section 5.8). This is as expected since the BP particles offer a higher surface area (and therefore higher enzyme loading) and possibly a more favourable particle-protein interaction leading to improved enzyme adsorption (Section 2.2.3). Furthermore, whereas the PG particles have to be prepared by freshly sanding a plate of PG, the BP particles do not have to be prepared freshly; therefore more quantitative experiments are possible using stock particle suspensions.

5.5.1 Changing the ratio of enzymes on the particles

The rate of NADH generation has been calculated per mg of NAD^+-reductase to enable a direct comparison to existing enzyme-based cofactor regeneration methods and traditional

metal catalysts. This Section explores the effect of changing the ratio of hydrogenase to NAD^+-reductase on the activity of H_2-driven NADH generation.

In the presence of H_2 and NAD^+, the particles modified with hydrogenase and NAD^+-reductase generate NADH. In effect the particle acts as an electrode for each half reaction, H_2 oxidation and NAD^+ reduction. The nature of this is investigated in Section 5.7 when the potential of the particle is approximated under different NAD^+/NADH conditions using IR spectroscopy to probe the hydrogenase active site. It is likely that both the experimental conditions and the loading of each catalyst act to change the equilibrium potential of the particle and therefore the availability of electrons for NAD^+ reduction.

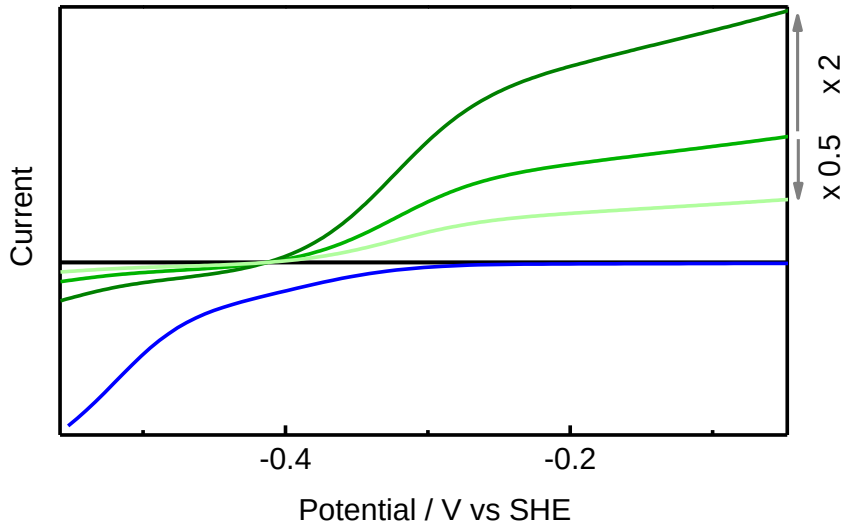

Figure 5-14: Current response of an oxidative sweep with a hydrogenase (*D. v* MF, green) modified electrode compared to a reductive sweep of a NAD^+-reductase (Hox~~HY~~FU, blue) modified electrode. The green lines demonstrate the effect of 'increasing hydrogenase loading' and correspond to simple multiplications of the original scan (as indicated by the grey arrows). The original scans were performed at 10 mV s^{-1} in the presence of 1 bar H_2 and NAD^+ (1 mM) at pH 8.

As a simple demonstration, the effect of increasing the hydrogenase loading in comparison to NAD^+-reductase is considered using electrochemistry. The electrochemical sweeps in Figure 5-14 demonstrate the effect of increasing the amount of hydrogenase (by simple multiplication of the current response, green) and compare the current response to that of an electrode modified with NAD^+-reductase (blue). As the hydrogenase loading increases, the

potential at which the H_2 oxidation and NAD^+ reduction current are matched moves to a more negative potential. It is therefore likely that this has the effect of decreasing the potential of the enzyme-modified particle thus subjecting the NAD^+-reductase to an increased 'overpotential'. This would be expected to increase the rate of NAD^+ reduction per mg of NAD^+-reductase (Section 3.3.1).

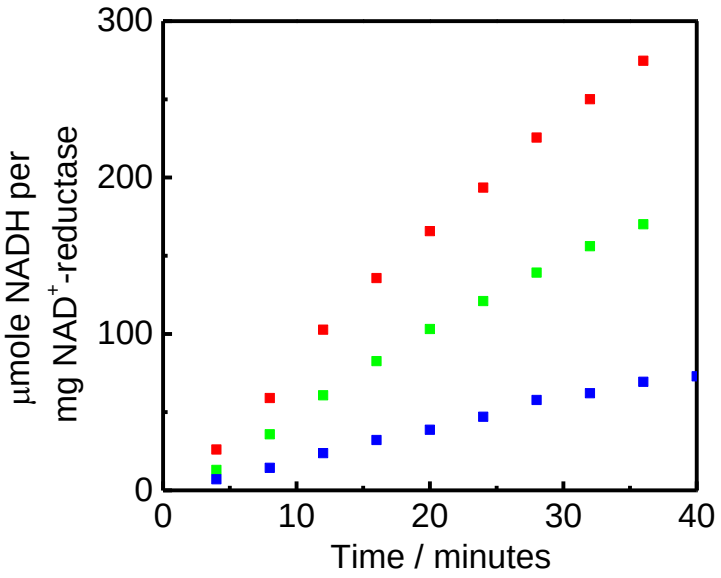

Figure 5-15: Comparison of the rate of H_2-driven NADH generation for different ratios of hydrogenase and NAD^+-reductase co-immobilised on BP particles. The amount of NADH generated per mg NAD^+-reductase over time by BP particles modified with hydrogenase (*D. v* MF) and NAD^+-reductase (Hox~~HY~~FU). The ratio of hydrogenase and NAD^+-reductase by weight is 0.66 (blue), 2 (red) and 6 (green). The experiments were performed in NAD^+ (2 mM in KPB pH 7) in a UV-Vis cuvette (1 mL) with continuous H_2 bubbling at 33 ^oC.

A set of BP particles (20 mg mL^{-1}) were dispersed in buffer (KPB, pH 7) by sonication. To equal aliquots of particles, different ratios of NAD^+-reductase (Hox~~HY~~FU) and hydrogenase (*D. v* MF) were added. For each experiment, the enzyme-modified particles were injected into a H_2-saturated solution containing NAD^+ (2 mM) and UV-vis spectra were recorded every 5 minutes with continuous H_2 bubbling.

The results in Figure 5-15 show the amount of NADH generated per mg of NAD^+-reductase over time. The rate of H_2-driven NADH generation per mg NAD^+-reductase was highest with the largest hydrogenase loading (red), and slowest with the least hydrogenase (blue). This is indicative of more electrons derived from H_2 being transferred

into the particle and therefore more electrons being available for NAD^+ reduction with higher relative loadings of hydrogenase, as predicted in Figure 5-14.

Table 5-2: The activity and turnover frequency of the NAD^+-reductase immobilised on particles with different hydrogenase to NAD^+-reductase loadings.

Mass hydrogenase / Mass NAD^+-reductase	Activity / µmole min^{-1} per mg NAD^+-reductase	TOF / s^{-1}
0.67	2.0 ± 0.1	6.3 ± 0.4
2.00	4.9 ± 0.3	14.5 ± 1.0
6.00	7.8 ± 0.5	24.6 ± 1.6

For each sample the initial activity and turnover frequency per NAD^+-reductase was calculated, the results are displayed in Table 5-2. The turnover frequency at the highest hydrogenase loading was > 24 s^{-1} equal to 8.6×10^4 h^{-1} which compares favourable to some of the values discussed for metal catalysis in Section 1.1.2.

5.5.2 Effect of pH on H_2-driven NADH generation

The driving force for H_2-driven NADH generation is dependent on pH according to the Nernst Equations, 5.1. The potential difference between the two couples at 1 bar H_2 can be compared at a range of pH values and different NAD^+/NADH ratios.

A driving force for coupling the $2H^+/H_2$ and NAD^+/NADH couples is indicated by a positive value for $E(NAD^+/NADH)$-$E(2H^+/H_2)$ since the potential for NAD^+ reduction must be more positive than the potential for H_2 oxidation in order to give a favourable ΔG. The graph in Figure 5-16(a) demonstrates that there is a higher thermodynamic driving force for H_2-driven NADH generation at higher pH values at any given NAD^+/NADH ratio. However, due to the effect of pH on the activity of the hydrogenase and NAD^+-reductase enzymes, a higher driving force does not mean that the activity will correlate so simply with pH.

This section compares the activity of particles in different pH environments. In each case the enzyme-modified particles were taken from the same preparation and therefore facilitate

direct comparison of the activity. Each experiment used 7 µL of an enzyme-particle mixture injected into H_2-saturated buffer (1 mL) containing NAD^+ (1 mM). Each particle aliquot contained 70 µg BP particles, *ca* 1 µg NAD^+-reductase (Hox~~HY~~FU) and *ca* 2.7 µg hydrogenase (*D. v* MF). The experiments were performed in a UV-vis cuvette at 33 °C with continuous H_2 bubbling and a magnetic stirrer was also incorporated. Spectra were recorded every 4 minutes and the baseline subtracted using the methods described in Section 5.3.3.

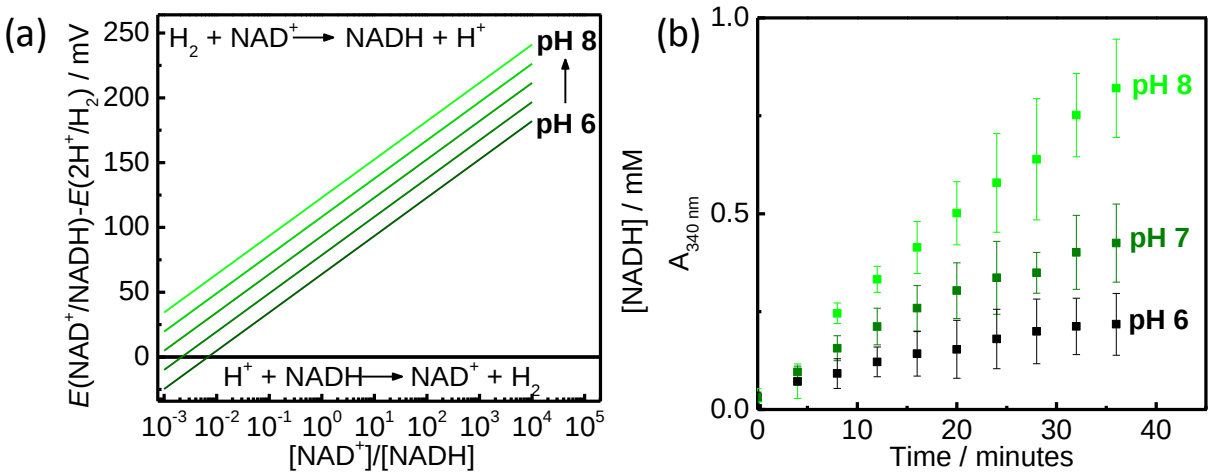

Figure 5-16: The effect of pH on H_2-driven NADH generation by enzyme-modified particles. (a) The difference in the potential of the NAD^+/NADH and $2H^+/H_2$ couples is plotted *vs* the NAD^+/NADH ratio at 298 K, 1 bar H_2 at different pH values. (b) Aliquots of enzyme-modified particles in H_2-saturated buffer containing NAD^+ (1 mM) in a UV-vis cuvette (1 cm path length). Buffers: KPB, pH 6, 50 mM (black); KPB, pH 7, 10 mM (dark green); Tris-HCl, pH 8, 50 mM (light green). All other conditions identical, carried out at 33 °C. Each time series is an average of two experiments at that pH each using fresh particles.

The time series in Figure 5-16(b) demonstrate the effect of pH on H_2-driven NADH generation by enzyme-modified particles. Two time-series were recorded at each pH (each using fresh particles). The experiments were all carried out within *ca* 4 hours to minimise the effect of the enzymes losing activity over time. The results show that H_2-driven NADH generation can be carried out between pH 6 and pH 8 and that the activity increases with pH.

An aliquot of the same particles were also analysed in water using the same enzyme-particle mixture and the same method. Overall, H_2-driven NADH generation produces 1 extra proton per NADH molecule and therefore the pH should change over time.

When the entire H_2-driven NADH dependent enzyme system is assembled in Chapter 6, the extra proton will be used by the cofactor-dependent enzyme so this will not be a problem.

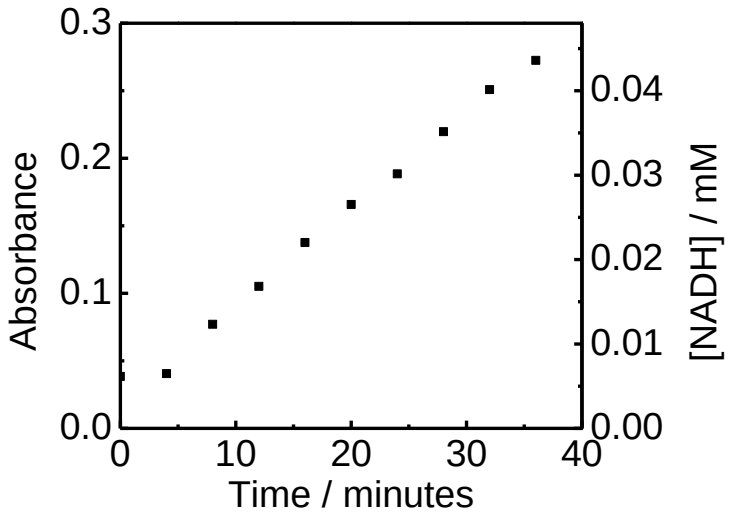

Figure 5-17: Enzyme-modified particles can sustain H_2-driven NADH generation in H_2-saturated water with NAD^+ (1 mM). Particles from the same batch as for Figure 5-16 (modified with *D. v* MF and Hox~~HY~~FU), performed at 33 ^oC.

The time series in Figure 5-17 shows that H_2-driven NADH generation is possible in water (MilliQ) with NAD^+ (1 mM) and H_2. During this experiment *ca* 40 μmoles NADH were generated therefore the concentration of H^+ will also have changed by this amount.

$$pH = -log_{10}[H^+] \quad [5\text{-}4]$$

Over the course of this experiment the pH should have changed from 7 to *ca* 4.4 using Equation [5-4]. However, there was no significant change to the activity of the particles. There is some evidence in the literature that immobilised enzymes are less affected by reaction conditions and for example many show improved solvent tolerance. It is thought that the enzymes are protected by the solution trapped inside pores in the surface where enzyme is located and the bulk solution does not substantially change this environment. The surface of the carbon particles probably contain pH-sensitive groups including carboxylate/carbonxylic acid that act to 'self-buffer' the particle system. These effects may prevent the immobilised enzymes from becoming inhibited by the acidic conditions.

The results in this section confirm that H_2-driven NADH generation can be carried out

between pH 6 and 8, and that non-buffered systems can also be used. A comparison of the initial activity in each pH system can be made.

Table 5-3: A comparison of the initial activity of H_2-driven NADH generation in solutions of different pH.

pH	Activity (μmole / min per mg NAD^+-reductase)
6	0.8
7	1.9
8	3.4
water	1.0

The results in Table 5-3 show a clear trend of increasing activity with pH. This may be in part due to a greater driving force for coupling H_2 oxidation and NAD^+ reduction but also due to different catalytic activity of the enzyme moieties at this pH. The generation of NADH in a non-buffered system is promising as it may enable H_2-driven synthesis using a NADH-dependent enzyme in a non-buffered system, further simplifying isolation of the desired product and decreasing the costs and waste associated with buffering systems.

5.5.3 H_2-driven NADH generation at low H_2 partial pressure

The effect of changing the partial pressure of H_2 was investigated, corresponding to change in the concentration of H_2 in solution. The potential of the NAD^+/NADH couple will remain constant but the potential of the $2H^+/H_2$ couple will change. Again the potential difference between the two couples can be plotted as a function of NAD^+/NADH ratio for different H_2 partial pressures at pH 8, 25 ^oC. A positive value means that H_2-driven NADH generation is favourable.

The graph in Figure 5-18(a) demonstrates the driving force for coupling H_2 oxidation and NAD^+ reduction. At 1 bar H_2, the driving force is highest and near complete conversion to NADH can occur (*ca* 99.99 %) assuming both H_2 oxidation and NAD^+ reduction occur at their thermodynamic potentials. At lower H_2 pressure, the driving force is lower and less

NAD^+ to NADH conversion is expected (the lines cross the *x*-axis at increasingly high NAD^+/NADH values as the H_2 partial pressure decreases).

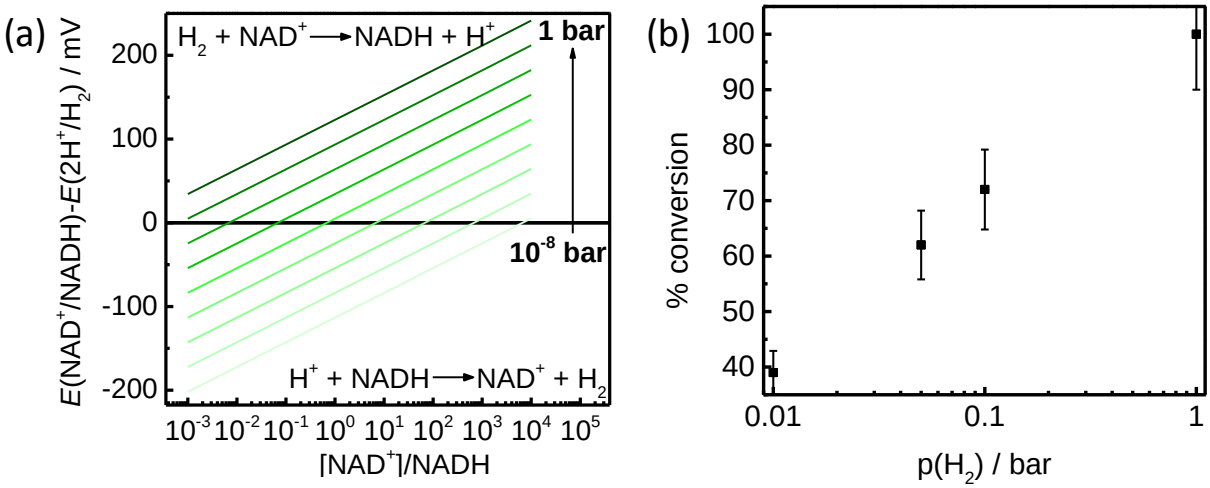

Figure 5-18: The extent of H_2-driven NAD^+ conversion to NADH in the presence of different H_2 partial pressures. (a) The potential difference between the $2H^+/H_2$ and NAD^+/NADH couples is plotted *vs* the NAD^+/NADH ratio. (b) Particles modified with hydrogenase (Hyd-2) and NAD^+-reductase (HoxFU) were added to a solution containing NAD^+ (1 mM) and saturated with different H_2:N_2 mixtures. After 1 hour, the particles were removed by centrifugation and the solution monitored using UV-vis spectroscopy. Experiments performed in Tris-HCl buffer, pH 8, 22 ^oC.

Experiments were performed to investigate whether enzyme-modified carbon particles can sustain H_2-driven NADH generation in the presence of low partial pressures of H_2. It was not possible to monitor these reaction using the *in situ* method developed since the gas flow rates required for low H_2:N_2 ratios were too high. The *ex situ* method was therefore utilised. Particles of PG were freshly prepared and dispersed in water by sonication. An aliquot of the particles (*ca* 0.1 mg) was added to a mixture of Hyd-2 (5 µg) and NAD^+-reductase (HoxFU, 5 µg) and left at 4 ^oC for 30 minutes. The particles were then washed *via* centrifugation to remove any unadsorbed enzyme. The enzyme-modified particles were split into 4 aliquots and to each a solution containing NAD^+ (1 mM) was added (50 µL). Each reaction was saturated with a different H_2:N_2 mixture using mass flow controllers or by injection of H_2 into the pre-N_2-saturated reaction mixture. After approximately 60 minutes the particles were removed by centrifugation and the remaining solution analysed using UV-vis spectroscopy (NanoVue,

Section 2.4.1). A ratio of the peaks at 260 and 340 nm was used to determine the extent of conversion. Error bars were calculated at 10 % due to slight inconsistencies in the time the experiments were left for. The data is plotted as a function of H_2 partial pressure and assumes 100, 10, 5 and 1 % H_2 equate to 1, 0.1, 0.05 and 0.01 bar, respectively.

The results in Figure 5-18(b) demonstrate that the enzyme-modified particles are able to operate even at a H_2 partial pressure of 0.01 bar in N_2 and that substantial catalysis occured (40 % conversion compared to 100 % at 1 bar H_2). Although it was not possible to reliably quantify the activity of the particles in each set-up, it is very advantageous that the particles can operate under such low H_2 partial pressures. This is in contrast to many metal hydrogenation catalysts which require in excess of 80 bar H_2 for operation (as discussed in Section 1.1.2).

5.5.4 Reusing the particles

The effect of removing the enzyme-modified particles from solution and reusing them was investigated. An aliquot of BP particles (0.2 mg) were modified with NAD^+-reductase (Hox~~HY~~FU, 4.8 µg) and hydrogenase (Hyd-2, 3 µg) at 4 ^oC for 1 hour. The enzyme-modified particles were injected into a H_2-saturated solution containing NAD^+ (1 mM, Tris-HCl, pH 8), stirred using a magnetic stirrer and monitored using the previously described *in situ* UV-vis spectroscopy approach, Section 5.3.3. After 30 minutes, the entire particle suspension was sedimented by centrifugation (7,000 *g*, 8 minutes) and the supernatant removed. The particles were washed in fresh buffer (500 µL) and injected into a fresh, H_2-saturated solution of NAD^+ (1 mM) and monitored in the same way. After another 30 minutes, this process was repeated.

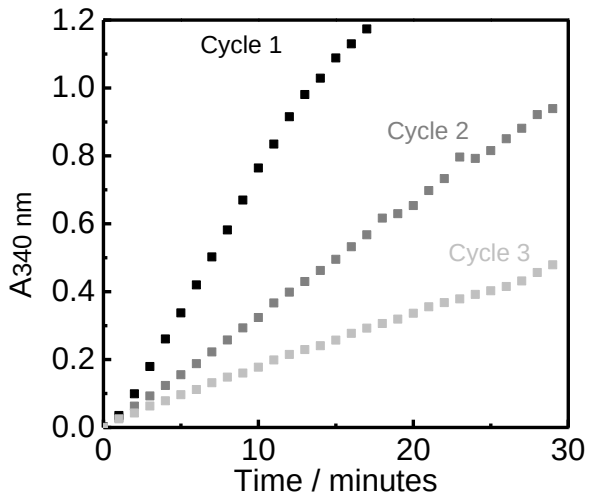

Figure 5-19: The effect on activity of reusing enzyme-modified particles for H_2-driven NADH generation. Particles modified with NAD^+-reductase (Hox~~HY~~FU) and hydrogenase (Hyd-2) were injected into H_2-saturated NAD^+ (1 mM) solution containing Tris-HCl buffer, pH 8. Between cycles the particles were collected and washed by centrifugation. Experiments performed at 33 ^oC.

The time series in Figure 5-19 demonstrate that the particles remain active for H_2-driven NADH generation over repeated cycles. The initial activity of the particles was 2.8 ± 0.13 µmole min^{-1} per mg NAD^+-reductase. The activity on the 2^{nd} and 3^{rd} cycles was > 43 % and > 20 % of the original activity, respectively. However, these activities are likely to be an underestimate since some of the particles were lost during the washing cycles. The ability to reuse the enzyme-modified particles is a significant advantage of the immobilised enzyme system.

5.6 Modularity of the system

A considerable advantage of the H_2-driven particle system is its modularity. A range of different NAD^+-reductase enzymes (as discussed in Chapter 3) and hydrogenase enzymes can be used depending on the conditions required. Furthermore, different carbon materials can be used to electronically link the enzymes which may facilitate a range of reactor designs; PG, BP, carbon paper, carbon nanotubes and carbon nanopowder have all ben demonstrated.

5.6.1 Changing the hydrogenase

In this Chapter, two hydrogenases have been used interchangeably. Enzyme-modified carbon materials with either *E. coli* hydrogenase 2 or *D. v* MF hydrogenase and the NAD^+-reductase were demonstrated and shown to achieve high conversion of NAD^+ to NADH in a range of conditions. In Chapter 7, the modularity of the system will be further tested and the enzyme-modified particles will be developed for H_2-driven NADH generation in the presence of O_2 by substituting the hydrogenase for an O_2-tolerant hydrogenase.

5.6.2 Changing the NAD^+-reductase

The experiments in this Chapter have used the NAD^+-reductase from *R. e*, either HoxFU or Hox~~HY~~FU. Here, the soluble extract containing NAD^+-reductase (Hox~~HY~~FU) and a purified NAD^+-reductase variant for $NADP^+$ reduction were used instead. These enzyme constructs were studied electrochemically in Chapter 3 and demonstrated to be appropriate for electro-enzymatic $NAD(P)^+$ reduction.

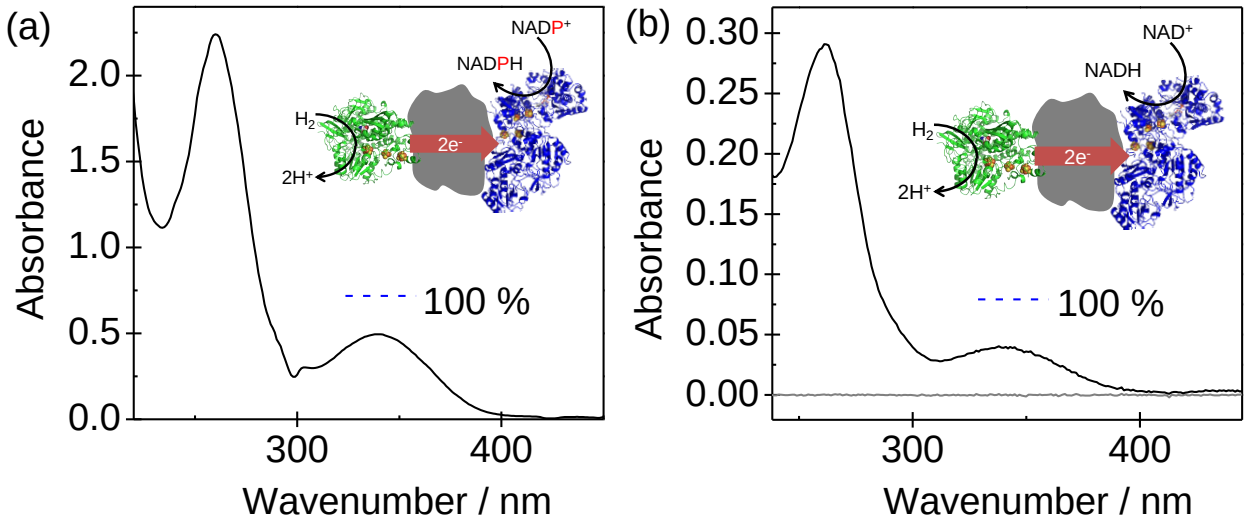

Figure 5-20: (a) UV-Vis spectrum showing the production of NADPH. Pyrolytic graphite particles modified with a D467S E341A variant of HoxHYFU (9.5 µg) and *D. v* MF hydrogenase (2 µg) were added to H_2 saturated $NADP^+$ (2 mM), the spectra was recorded after 1.5 hours. (b) UV-vis spectrum showing H_2-driven NADH generation from NAD^+ (1 mM) by particles modified with hydrogenase (*D. v* MF) and crude extract of NAD^+-reductase (Hox~~HY~~FU). Experiments performed in Bis-Tris pH 6. The dotted line in each represents the expected absorbance at 340 nm for complete conversion.

The UV-vis spectrum in Figure 5-20(a) displays results for H_2-driven NADPH generation. A variant of the SH (D467S E341A, HoxHYFU) and hydrogenase (*D. v* MF) were co-immobilised on PG particles ad placed into H_2-saturated solution of $NADP^+$ (2 mM). This was analysed using *ex situ* UV-vis spectroscopy and gave 65 % conversion of $NADP^+$ to NADPH. (N.B. the HoxHYFU variant has an active hydrogenase dimer and therefore the electrons will not necessarily pass through the particle).This result provides evidence that the enzyme-modified particle system can be extended to regeneration of the NADPH cofactor.

Next the soluble extract containing over expressed NAD^+-reductase (Hox~~HY~~FU) was trialled. The crude soluble extract and *D. v* MF hydrogenase were immobilised on PG particles and added to a H_2-saturated solution of NAD^+ (1 mM). The UV-vis spectrum in Figure 5-20(b) confirms 50 % conversion of NAD^+ to NADH.

Overall, these results show that NAD^+-reductase constructs that have been analysed electrochemically can be easily substituted into the particle system and confirms that the electrochemical techniques can be used to determine the suitability of an NAD^+-reducing enzyme for incorporation into the particle cofactor recycling system. Successful use of the crude extract may enable development of a cheaper enzyme-modified particle system and the initial result for H_2-driven NAD**P**H generation indicates that the particles can be tuned for a greater range of applications.

5.6.3 Operation in reverse for NAD^+ generation

The NAD^+-reductase is bidirectional. A catalytic wave for NADH oxidation was observed using electrochemistry in Chapter 4 at an electrode modified with *Rh. o* HoxFU in the presence of NADH (reproduced in Figure 5-21(a), blue line). Many hydrogenases are also bidirectional; both Hyd-2 and *D. v* MF hydrogenase are able to catalyse H^+ reduction, particularly in the absence of H_2 (Figure 5-21(a), green line). Under low H_2 conditions at high $NADH/NAD^+$ ratio there is a significant driving force to couple NADH oxidation to H^+

reduction thus generating NAD^+ and H_2 (approximated by the shaded area). It should therefore be possible to use hydrogenase and NAD^+-reductase modified particles for generation of the oxidised cofactor NAD^+.

Particles (PG) were prepared and modified with NAD^+-reductase (*R. e* HoxFU, 2.5 µL) and hydrogenase (Hyd-2, 1 µg). A solution containing NADH (1 mM) was added to the particles and the reaction left in a N_2 atmosphere. The reaction was monitored using the *ex situ* UV-vis spectroscopic method and the ratio of absorbance at 260 and 340 nm used to determine the NADH concentration over time.

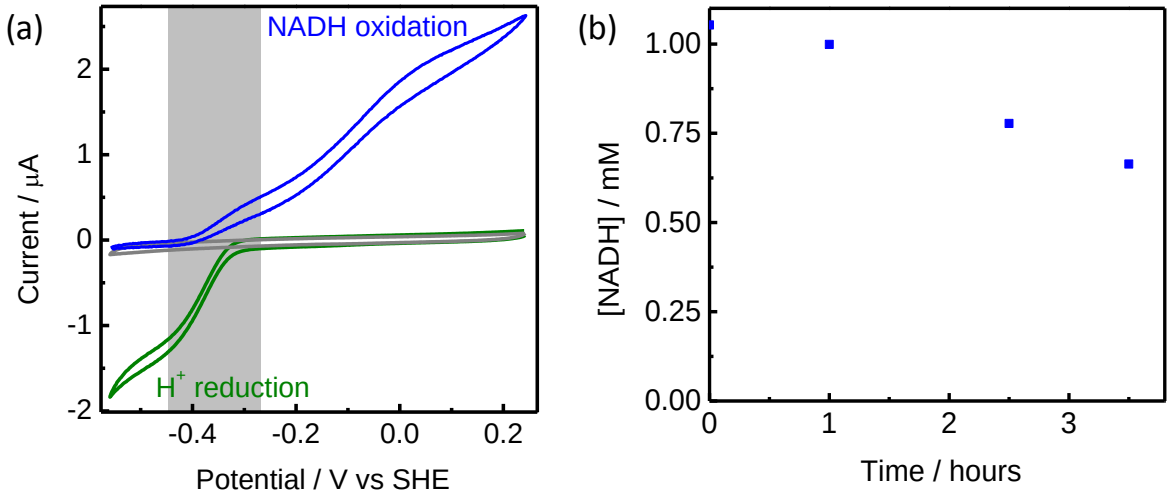

Figure 5-21: Enzyme-modified particles can be used for generation of NAD^+. (a) Cyclic voltammetry showing the potential window available to couple NADH oxidation and H^+ reduction. The current response of a PGE electrode modified with either NAD^+-reductase (*Rh. o* HoxFU, blue) in the presence of NADH (1 mM) or hydrogenase (*D. v* MF, green) in the absence of H_2. Experiments performed in Tris-HCl, pH 8 buffer. The shaded area highlights the potential window available to couple for H^+-driven NADH oxidation. (b) Pyrolytic graphite particles modified with NAD^+-reductase (*R. e* HoxFU) and hydrogenase (Hyd-2) were added to N_2-satureated buffer containing NADH (1 mM). UV-vis spectra were used to determine the concentration of NADH in solution over time. Experiment performed in KPB buffer, pH 7 at 22 °C.

The result in Figure 5-21(b) demonstrates that the particles can operate in reverse for H^+-driven NADH oxidation in the absence of H_2. Although the generation of NAD^+ from NADH is not useful in itself, recycling of the oxidised cofactor for supply to an NAD^+-dependent enzyme for selective oxidation of a primary alcohol to an aldehyde would be beneficial. This result further demonstrates the modularity and adaptability of the particle system.

5.6.4 H_2-driven NADH generation in a novel flow system

**This work is carried out in collaboration with the Grobert Group (Materials, Oxford) and in particular with Mr Jonathan Quinson (Grobert/Vincent Groups).*

Synthesis in industry is moving more towards continuous catalysis, i.e. catalysis in flow rather than batch systems. This H_2-driven system lends its self to operation in this way since both of the enzymes are immobilised. Here, a novel experimental set-up using tubes of carbon nanotubes was developed.

Carbon nanotubes were identified as a suitable carbon support for H_2-driven NADH generation in Section 5.4.6. Jonathan Quinson (Materials, Grobert Group) has been able to grow multiwall carbon nanotubes inside quartz tubes, and this 'column' can be sealed into a flow set up. Using this carbon nanotubes column (CNC) the hydrogenase and NAD^+-reductase were immobilised and solution cycled through, Figure 5-22(a). For this a peristaltic pump was used; H_2 saturated NAD^+ solution was pumped through the tube and into a small volume UV-vis cuvette (100 μL minimum volume, 1 cm path length) in which H_2 was continuously bubbled. In this way, the solution was continuously monitored in an extension to the existing *in situ* technique.

Before use, buffer was cycled through the column, this is consistent with the methods when using carbon nanotubes or carbon paper where pre-soaking was required before enzyme immobilisation. For an initial experiment, a mixture of *D. v* MF hydrogenase (35 μg) and NAD^+-reductase (Hox~~HY~~FU, 40 μg) was pumped into the column and left at 4 ^oC for 30 minutes. The column was then rinsed by pumping through 5 mL of fresh buffer (Bis-tris, pH 6, 10 mM) to remove any un-adsorbed enzyme. Next, the entire system was filled with H_2 saturated NAD^+ (0.5 mM) and an additional 200 μL of solution put into the UV-vis cuvette. This gave a total reaction volume of *ca* 1.2 mL. UV-vis spectra were recorded every 15 minutes and the flow rate was *ca* 25 μL min^{-1}; this set-up was left for 21 hours. Throughout this time, some of the reaction mixture was lost from the system complicating analysis of the

UV-vis spectra however, the final NADH concentration was found to be *ca* 0.2 mM (*ca* 40 % conversion). The solution was replaced with fresh H_2-saturated NAD^+ (0.5 mM) so that more UV-vis kinetics could be taken starting from optimal conditions (high NAD^+ and H_2).

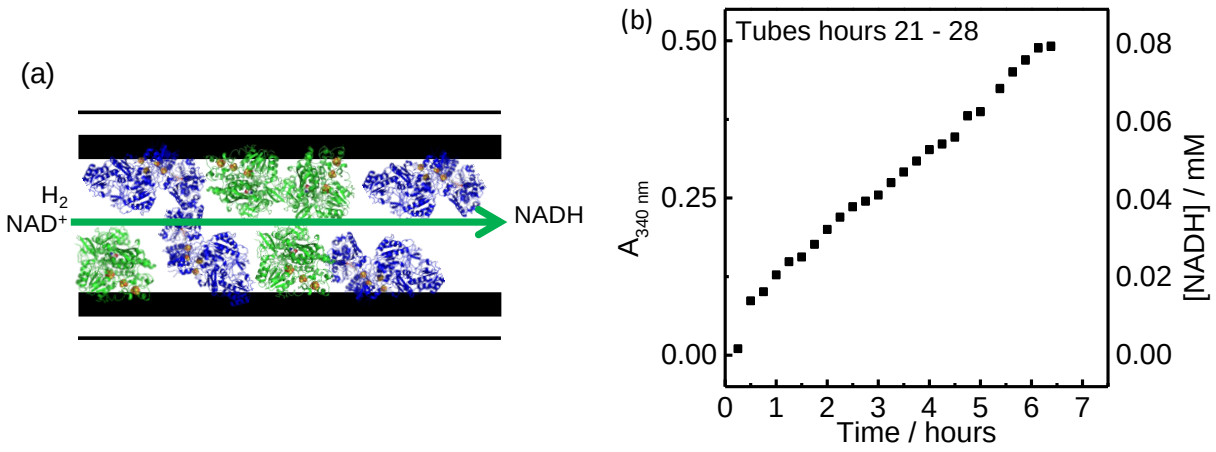

Figure 5-22: Carbon nanotube column for H_2-driven NADH generation in a continuous flow set-up. (a) Schematic representation of the CNC. (b) UV-vis spectroscopy shows generation of NADH over time.

The time course in Figure 5-22(b) shows clear NADH generation over time. Time 0 actually corresponds to fresh NAD^+ solution being used after 21 operational hours of the column (not shown as discussed above). Although it was not possible to determine how the activity of the enzymes has changed over the entire time course the fact that the CNC is still generating NADH at an appreciable rate after 28 operational hours suggests that the set-up has aided enzyme stability. This novel set-up will be further investigated for carrying out a H_2-driven biotransformation in Chapter 6.

5.7 Infrared spectroscopy to probe the electron transfer

Particles modified with hydrogenase and NAD^+-reductase were monitored using infrared spectroscopy. Many hydrogenases have been studied using IR spectroscopy, and a range of inactive and active states identified.[225] Here, the effect of changing the NAD^+/NADH ratio and possibly therefore the potential the hydrogenase is experiencing *via* the particle and the electronic connection to the NAD^+-reductase will be investigated.

The active sites of the hydrogenases used in this work consist of a NiFe centre with intrinsic CO and CN^- ligands, Figure 5-23. These ligands have well-defined, sharp absorbance bands in an otherwise empty portion of the IR spectrum and the energy of their absorbance offers insight as to the electron density of the metal centres.

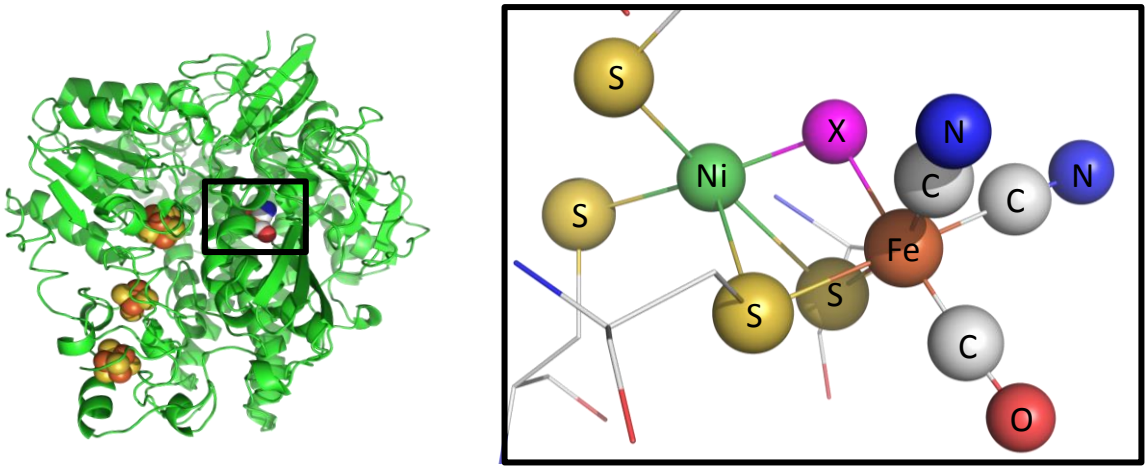

Figure 5-23: The active-site of a typical NiFe hydrogenase. The Fe atom is coordinated by two cyanide and one carbon monoxide ligands as well as the sulphur from 2 cystine residues.

The Vincent Group have previously carried out IR spectroelectrochemical characterisation of the O_2-tolerant hydrogenase-1 from *E. coli* (Hyd-1).[242] Briefly, a high surface area electrode incorporating the hydrogenase immobilised on carbon particles is prepared on an attenuated total reflectance (ATR) prism, Section 2.6.3, and the active site of the hydrogenase is monitored as a function of applied potential. The hydrogenase can be reduced either by applying a low potential (Section 5.2.1) or using H_2 gas before commencing such a potential titration. As the applied potential is changed, electrons are removed from or added to the hydrogenase active site leading to changes in the metal-ligand bonds and corresponding shifts in the CO and CN^- stretching frequencies and a set of clear potential-dependent states have been identified.

In this Section, carbon particles were exposed to hydrogenase (Hyd-1 for simple comparison) and left at 4 ^oC for 4 days in order to achieve a very high enzyme loading. The Hyd-1-modified particles were then exposed to H_2 for 15 minutes to activate the hydrogenase

before returning to a N_2 atmosphere. The particles were then washed *via* centrifugation to remove any unadsorbed enzyme. An aliquot of the hydrogenase-modified particles (2 µL) was then drop-cast onto the ATR prism. A piece of carbon paper approximately the same size as the particle film was modified with NAD^+-reductase and left at 4 °C for 10 minutes. This piece of carbon paper was placed on top of the hydrogenase particle film such that it was in electronic contact. The cell was then assembled and filled with buffer (Tris-HCl, pH 8). The active site of Hyd-1 was monitored before and after addition of NAD^+ (1 mM, by flow). Any changes to the electronic state of the hydrogenase indicate a change in the potential experienced by the hydrogenase in the particle-carbon paper network.

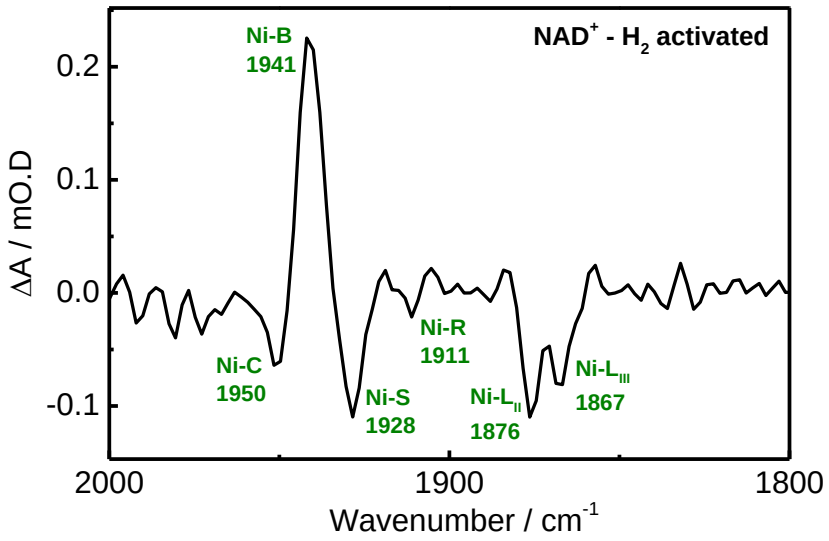

Figure 5-24: Difference spectrum recorded after addition of NAD^+ (1 mM) to particles modified with NAD^+-reductase and pre-activated hydrogenase. The spectrum shows a large increase in absorbance at 1941cm^{-1} (Ni-B) and losses at 1950, 1928, 1911, 1876 and 1867 cm^{-1}. This experiment was performed with assistance from Ms Chloe Tomlinson and Dr Philip Ash.

The IR difference spectrum in Figure 5-24 shows the changes to the electronic state of the Hyd-1 after addition of NAD^+ (positive peaks) in comparison to the initial H_2-activated states (negative peaks). The spectrum indicates that a change to the potential experienced by the hydrogenase has occurred. Since there was no change to the $2H^+/H_2$ couple (no change in pH and no H_2 present) this indicates that the potential of the particles has been altered by addition of NAD^+. This change in potential must have been caused by the NAD^+-reductase response to

the addition of NAD^+.

The IR difference spectrums show that the active site of Hyd-1 has switched from more reduced states (including Ni-R, Ni-S, Ni-C, Ni-L) into more oxidised states, including some of the oxidised-inactive state Ni-B state (see Appendix C for peak positions determined by Dr A. Healy). This is consistent with the NAD^+-reductase using electrons from the particle for NAD^+ reduction and therefore shifting the potential 'applied' to the hydrogenase to a more positive, and thus more oxidising, potential. The difference spectrum in Figure 5-24 suggests that the Hyd-1 was not fully reduced into Ni-R at the start of the experiment and that a significant portion of Hyd-1 was in the Ni-C, Ni-S and Ni-L states

The results were compared to a potential titration carried out with Hyd-1 immobilised on BP particles at pH 8 in the absence of H_2 by Mr Ricardo Hidalgo. Under the starting experimental conditions used (pH 8, no cofactor present, negligible H_2) this suggests the Hyd-1 and therefore particle was resting at a potential of *ca* -0.3 V. Following the injection of NAD^+, a large portion of the Hyd-1 was observed in the Ni-B state, suggesting that the particle was resting at a potential more positive than *ca* -0.1 V. An overall increase in potential of *ca* 200 mV occurred, mediated by NAD^+ and the NAD^+-reductase.

This experiment provides evidence that the NAD^+-reductase and hydrogenase are electronically linked and further that the two enzymes set the potential of the particle. This potential depends on the thermodynamic potential of the two couples and the relative ratio of the two enzymes. Using the hydrogenase enzyme as a probe to indicate the potential of the particle, a deeper understanding of the particle system under operational conditions is now possible.

5.8 Summary

This chapter has described the development of a particle-based system for H_2-driven NADH generation that can couple the NAD^+-reductase to a robust, active hydrogenase. The activity

of the particle system can be compared to the activity of the established enzymes for NADH regeneration, Table 5-4.

Table 5-4: A comparison of enzymatic methods for recycling of the NADH cofactor. The costs of the sacrificial substrates are taken as $1/10^{th}$ of the Sigma price. The activities are taken from the Strem Chemicals technical sheet for cofactor recycling enzymes.[270]

Regeneration System	Sacrificial Substrate	By-Product	Cost (£/mole)	Activity (U/mg)
Formate Dehydrogenase	Ammonium Formate	CO_2	0.20	0.5
Alcohol Dehydrogenase	Isopropanol	Acetone	0.45	3
Catalytic beads developed	H_2	-	0.03	>7
Phosphite Dehydrogenase	Phosphorous acid	Phosphate	0.10	12
Glucose Dehydrogenase	Glucose	Gluconic Acid	0.41	15
Malic Dehydrogenase	L-(-)-Malic Acid	Pyruvate	3.50	20

The table shows that the activity of the particles (per mg NAD^+-reductase) is comparable to many of the existing enzyme based cofactor regeneration methods. As discussed throughout this Chapter, the activities calculated for the enzyme-modified particle system are likely to be a significant underestimate of the actual rate per mg of NAD^+-reductase since not all the enzyme will be immobilised. This table also makes clear the other advantages of using H_2 as the reducing equivalent, firstly, no carbon waste is generated and secondly, the cost of H_2 is relatively low per mole. At present H_2 is not a green reagent, (because it is usually produced by steam reforming of natural gas)[274] however with increasing pressure to find alternative fuels it is hoped that new methods for the production of H_2 will be established making the catalytic particles a truly green alternative to the existing methods. The partial pressures of H_2 used in this work (0.1-1 bar) are low. The combined selectivity, turnover frequencies and total turnover numbers (moles of product per mole of catalyst) using the enzyme-modified particle system compare favourably with many metal catalysis systems, Section 1.1.2. One or more of these factors is generally compromised using metal catalysts.

The enzyme-modified particles system has been characterised and shown to operate in a range of conditions. The particles can be removed from solution and reused, retaining their

catalytic activity over multiple cycles. This acts to decrease the catalyst-to-product cost. The next Chapter will describe use of these particles for H_2-driven NADH supply to NADH-dependent enzymes. Although it is important to understand that activity of the particles for generation of NADH, their activity in an entire system, coupled to a synthetic step will be different and ultimately more important.

Chapter 6 Coupling NADH recycling to cofactor-dependent enzymes

The previous Chapters have detailed the development of systems for generation of NADH either using electrons from an electrode or H_2. Generation of NADH from NAD^+ is a useful reaction in itself due to the higher expense of the reduced cofactor; however a more important application of the systems developed in this Thesis is *in situ* NADH recycling to drive catalysis by an NADH-dependent enzyme. This Chapter develops the H_2 and electrode-driven NADH generation techniques for NADH supply for enzyme catalysed hydrogenation reactions, carries out initial characterisation of the systems and compares the results to the hydrogenation methods discussed in Chapter 1.

6.1 Introduction

The electro-enzymatic system (developed in Chapter 3) could be a powerful tool for driving enzyme catalysed reduction reactions. It is possible that the potential of the electrode, and

therefore the overall driving force, could be tuned for complete conversion of substrate to product in a way that is not possible when using the standard enzymatic approaches to cofactor recycling discussed in Section 1.4.1 (where many stoichiometric equivalents of sacrificial substrate are required). The enzyme-modified particles for H_2-driven NADH supply (introduced in Chapter 5) could also offer many advantages over the existing systems since they provide a 100 % atom efficient reaction when coupled to a dehydrogenase. This is likely to simplify product isolation since there are no by-products, no changes to the pH of the system and the immobilised enzymes can be easily removed from solution. Two NADH-dependent dehydrogenases were used as test systems in this Chapter; lactate dehydrogenase and an alcohol dehydrogenase (Figure 6-1).

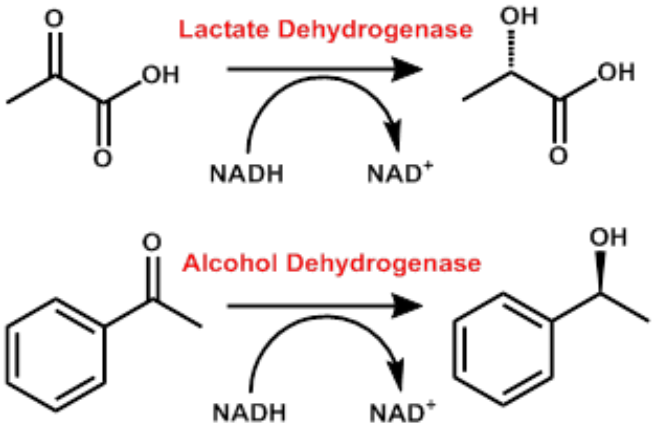

Figure 6-1: Two NADH-dependent enzymes were used as test systems in this work. A lactate dehydrogenase (LDH) catalyses the reduction of pyruvate to *L*-lactate and an alcohol dehydrogenase (ADH) catalyses reduction of acetophenone to *S*-phenylethanol.

A commercially available lactate dehydrogenase (LDH) from rabbit muscle catalyses the reduction of pyruvate to *L*-lactate and has been previously demonstrated as part of an enzyme cascade for ketone reduction to an amine using a transaminase where the LDH acts as a shifting system.[275] Here, this system is only addressed for reduction of pyruvate to lactate as a test system. An industrially used alcohol dehydrogenase (ADH) that has broad substrate specificity was used for the reduction of acetophenone to *S*-phenylethanol, which is used in production of fragrances and as an intermediate in pharmaceutical synthesis.[276] Alcohol

dehydrogenases make up a large portion of the cofactor-dependent enzymes used in industry and are equally referred to as ketone reductases in the literature since many are bidirectional. Both of the enzymes were used as-supplied with no additional purification steps.

6.2 UV-vis assays of cofactor-dependent enzymes

The activity of NADH-dependent enzymes can be monitored by measuring the rate of NADH consumption using UV-vis kinetics. The absorbance at one wavelength is recorded and plotted with respect to time. The rate of change can be used to determine the activity in U mg^{-1} (µmole min^{-1} per mg enzyme) in a similar way to the methods for calculating the rate of NADH generation in the previous Chapters.

Experiments to determine the activity of the ADH were performed in a UV-vis cuvette with a volume of 1 mL and a path length of 1 cm under aerobic conditions. A stock solution containing NADH and acetophenone (0.29 mM and 19 mM, respectively) in buffer (Tris-HCl, pH 8, 2 % DMSO) was made and 1 mL added to the UV-vis cuvette for each experiment. Aliquots of ADH (20, 30 or 40 µg) were added and the cell shaken three times before being placed into the UV-vis spectrometer. In each case the dead time between enzyme injection and UV-vis kinetics starting was *ca* 10 seconds. The activity recorded for these ADH injections were used to determine the activity per mg of ADH under these conditions. In these experiments, the solution was monitored at 380 nm as absorbance of acetophenone below this wavelength complicated interpretation of the UV-vis kinetics. An absorbance coefficient of NADH at 380 nm was calculated as 0.981 mM^{-1} cm^{-1}, Appendix F.

Table 6-1: Results from UV-vis spectroscopy to determine the activity of the ADH in the presence of NADH and acetophenone (0.29 mM and 19 mM, respectively) at pH 8.

ADH (mg)	Gradient (A min^{-1})	Activity (µmole min^{-1} mg^{-1})
0.2	0.086	0.44
0.3	0.133	0.42
0.4	0.166	0.45

The results in Table 6-1 show the quantity of ADH used and the resulting gradient recorded at 380 nm. Using the extinction coefficient calculated, the activity of the ADH under these conditions was 0.43 ± 0.02 μmole min^{-1} per mg enzyme.

The extent of ADH adsorption onto pyrolytic graphite (PG) and BP particles was investigated. A block of PG was abraded with sandpaper and the PG particles collected. Stock suspensions of BP or PG particles were prepared at 10 mg mL^{-1} in buffer and sonicated for 30 minutes to aid uniform dispersion. Aliquots of ADH (0.4 mg) were exposed to portions of the particle suspensions (0.2 mg) and left at 4 ^{o}C for 1 hour. The unadsorbed enzyme was removed by centrifugation and collected for UV-vis analysis. The particles were re-suspended in buffer (20 μL), injected into the stock solution and monitored by recording UV-vis spectra every 30 seconds and analysing using the baseline correction methods from Chapter 5.

The 'enzyme washings' were monitored using UV-vis kinetics. The gradient recorded was used to calculate the amount of unadsorbed enzyme (mg) and therefore the amount of adsorbed enzyme, Table 6-2. The activity of a portion of the particles (two thirds) was monitored by collecting whole UV-vis spectra over time. If all of the particles were used, the baseline absorbance was too high for quantitative analysis. The activity of the immobilised enzyme was determined assuming that 0.16 and 0.18 mg of ADH was immobilised on the PG and BP particles respectively. This allowed comparison between the activity of the enzyme in solution and immobilised, Table 6-2.

Table 6-2: The extent of ADH adsorption onto PG and BP particles and the activity of the immobilised enzyme. Experiments performed in the presence of NADH and acetophenone (0.29 mM and 19 mM, respectively).

	ΔA_{380nm} min^{-1} (washings)	Unadsorbed ADH (mg)	% ADH adsorbed	Immobilised ADH used (mg)	% activity
PG	0.104	0.23	43	0.106	37
BP	0.098	0.22	45	0.116	35

The results in Table 6-2 suggest the extent of adsorption of ADH onto BP or PG particles was similar and that the immobilised ADH retained significant activity. This data provided evidence that it would be possible to co-immobilise all of the enzymes required for cofactor regeneration and a ketone reduction. However, initial experiments investigate NADH supply to a cofactor dependent enzyme in solution. A HPLC protocol was established for analysis of acetophenone to phenylethanol conversion and is detailed in Appendix E.

The activity of the LDH was investigated in solutions containing NADH (1 mM) and pyruvate (5 mM) in Tris-HCl, pH 8 at 33 ^{o}C. The reactions were monitored at 365 nm where only NADH contributed to the absorbance and could be quantifiably analysed in the concentration range used.

Table 6-3: Results from UV-vis spectroscopy to determine the activity of the LDH in the presence of NADH and pyruvate (1 mM and 5 mM, respectively) at pH 8

LDH (µg)	Gradient (A min^{-1})	Activity (µmole min^{-1} mg^{-1})
5	0.91	68.2
10	2.07	75.2
20	4.16	77.9

The results are shown in Table 6-3 and give an activity of 73 ± 5 µmole min^{-1} per mg LDH under the conditions used. Following the protocols above the adsorption of LDH onto PG particles was investigated. It was found that *ca* 7 µg of LDH could be fully adsorbed onto *ca* 5 µg of particles dispersed in buffer *via* sonication and that the LDH retained significant activity. A HPLC protocol for analysis of pyruvate to lactate conversion was investigated. Although it was possible to determine the concentration of lactate, interaction between the buffer and pyruvate prevented analysis of pyruvate concentration. When probing the kinetics of the H_2-driven particle system the ADH system was therefore employed.

6.3 Electrochemical NADH supply

To develop the electro-enzymatic system for NADH supply to either LDH or ADH carbon paper electrodes were used, with or without additional carbon particles. Initial experiments used the NADH-dependent dehydrogenase in solution. The electrodes were then optimised for co-immobilising more than one enzyme and the effects of keeping the enzymes in close proximity analysed. The first experiments were performed with LDH since better adsorption and activity were observed.

6.3.1 Electrochemical cofactor cycling – LDH in solution

So far it has been demonstrated that NADH produced by the electro-enzymatic system is enzyme-active (Section 3.3.3). This section aims to cycle the cofactor between the two enzymes, to investigate if the LDH can use electrochemically derived NADH to form lactate and NAD^+, which can in turn be re-reduced by the NAD^+-reductase-modified electrode. In an initial experiment BP particles were modified with NAD^+-reductase (25 µg) and adsorbed onto a laminated carbon electrode (Section 3.4.1).

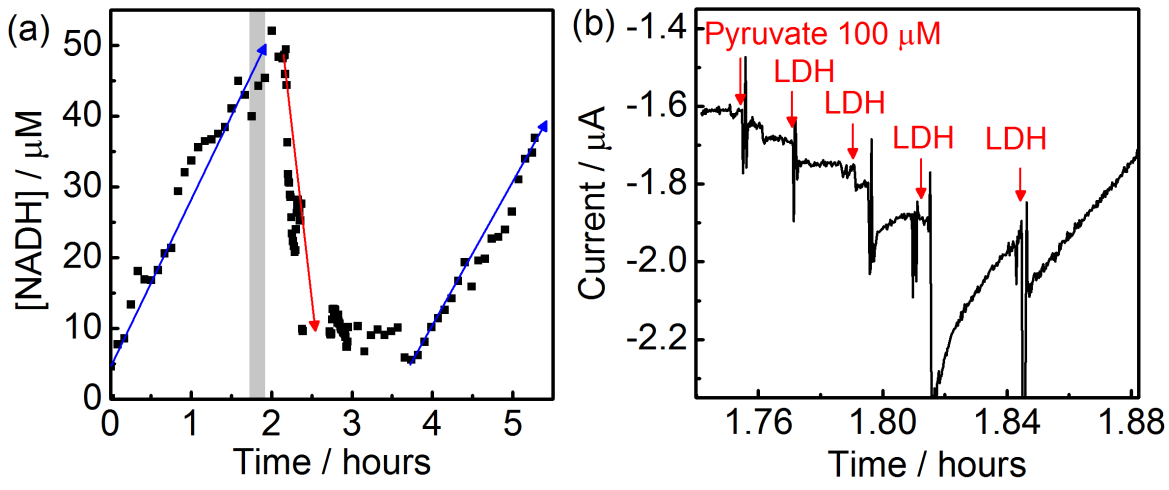

Figure 6-2: Results confirming that the electrode-immobilised NAD^+-reductase can recycle cofactor when coupled to pyruvate reduction by LDH. A carbon paper and BP particle electrode modified with NAD^+-reductase (HoxHYFU) was poised at -0.41 V *vs* SHE. The electrode was immersed in a buffered solution (KPB, pH 7) containing NAD^+ (0.75 mM) at 22 °C. At *ca* 1.76 hours, pyruvate (100 µM) was injected, followed by injections of LDH (5 µg) as indicated by arrows. Panel (a) shows the concentration of NADH over time, panel (b) shows the part of the chronoamperometric measurement corresponding to the shaded region in panel (a).

The electrode was then placed into a quartz UV-vis cuvette containing NAD^+ (0.75 mM) for spectroelectrochemical analysis using the methods developed in Section 2.4. The electrode was poised at an NAD^+-reducing potential (-0.41 V *vs* SHE) and the current monitored; UV-vis spectra were recorded every 5 minutes. The time course in Figure 6-2(a) shows an initial increase in NADH concentration (first blue arrow), calculated from the absorbance at 340 nm. After 2 hours the concentration of NADH was *ca* 50 μM. At approx. 1.76 hours pyruvate (to give a cell concentration of 100 μM) and aliquots of LDH were added to the system as indicated by red arrows in Figure 6-2(b). Shortly after this, the time course shows loss of almost all of the NADH. This is due to the LDH using the electrochemically generated NADH to reduce pyruvate to lactate. After another 2 hours (total of ~ 4 hours) another increase in the concentration of NADH was seen, suggesting that a total of 100 μM NADH has been produced and that near complete conversion of pyruvate to lactate had occurred. Therefore the NADH generated was no longer immediately used and an increase in absorbance at 340 m was observed again.

The chronoamperometry in Figure 6-2(b) corresponds to the shaded region in (a) and shows the response of the NAD^+-reductase modified electrode to injections of pyruvate (100 μM) and LDH (total of 20 μg). Following these injections of pyruvate and LDH the magnitude of the NAD^+ reduction current increased, suggesting that there was a higher concentration of NAD^+ at the electrode. Subsequent injections of LDH further increased the NAD^+ reduction current. However, the current appears to quickly decrease in magnitude after injections. It is likely that there is not efficient stirring in the UV-vis cuvette and therefore the system is limited by mass transport of cofactor or pyruvate between the electrode and the bulk solution.

6.3.2 Characterisation of an immobilised 'enzyme cascade'

Experiments were designed to analyse the effect of co-immobilisation of the

cofactor-dependent enzyme and the NAD^+-reductase. This section builds upon previous work from the Vincent group which demonstrated that an NAD^+-reductase and an NADH-dependent enzyme can be co-immobilised on an electrode, Figure 6-3(a).[222] To test the feasibility of this system experiments were performed on a planar PGE electrode in order to detect small changes in activity of the NAD^+-reductase and analyse the effect of mass transport by changing the electrode rotation rate.

A mixture of NAD^+-reductase (HoxFU, 0.5 µg) and LDH (0.5 µg) was spotted onto a freshly polished PGE RDE and allowed to partially dry for *ca* 20 seconds. Chronoamperometry was used to analyse the change in NAD^+-reductase activity when the co-immobilised LDH is undergoing catalytic turnover. This can be carried out in one of two ways; either the electrochemical cell can initially contain only NADH or only NAD^+. First, the case in which only NADH (0.2 mM) was in solution is discussed.

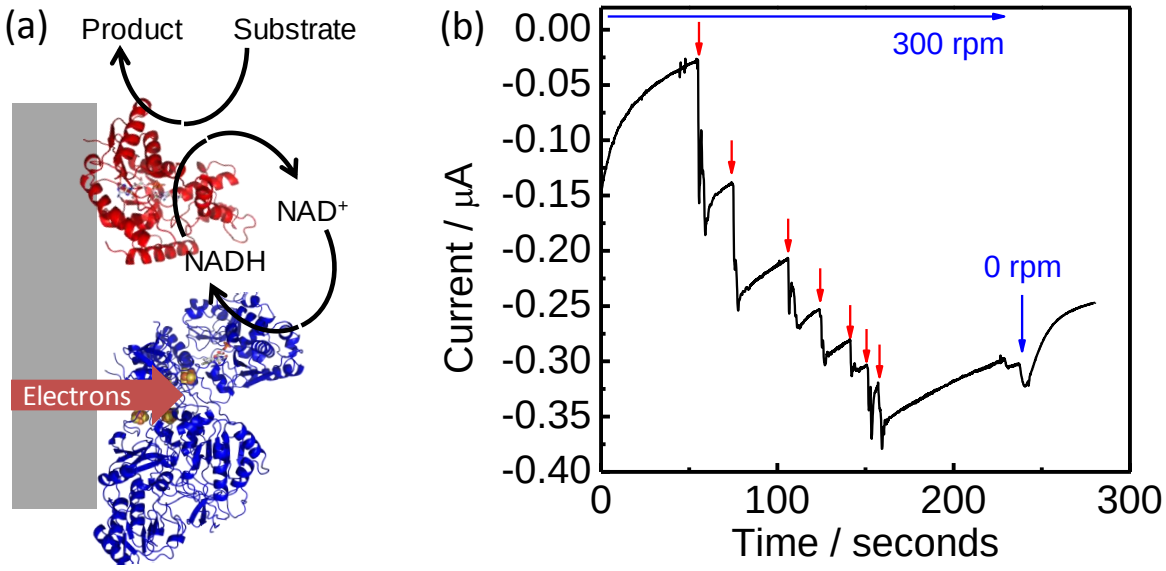

Figure 6-3: Chronoamperometry experiment to analyse the effect of co-immobilising an NAD^+-reductase and a cofactor-dependent enzyme in close proximity on a PGE electrode. (a) Schematic representation of an electro-enzymatic system for cofactor-dependent chemical synthesis. (b) Chronoamperometric trace showing the response of an electrode modified with NAD^+-reductase (HoxFU) and LDH upon injection of pyruvate (indicated by red arrows). The experiment was performed in KPB, pH 7, with only NADH (0.2 mM) present. The electrode was poised at -0.46 V *vs* SHE (an NAD^+-reducing potential) and aliquots of pyruvate injected (33 µM). The electrode was rotated at 300 rpm at the start and rotation was stopped as indicated by the blue arrow.

The electrode was poised at an NAD^+-reducing potential (-0.46 V *vs* SHE); since there was no NAD^+ present, no catalytic current was seen, Figure 6-3(b). On injection of pyruvate (33 µM, red arrow), the substrate for LDH, a large increase in negative current was observed indicating that the NAD^+-reductase was reducing NAD^+ which must have been produced by the co-immobilised LDH. Subsequent pyruvate additions led to further increase in the magnitude of the NAD^+ reduction current signifying a greater NAD^+ concentration experienced by the NAD^+-reductase. The electrode was rotated at 300 rpm in order that the pyruvate was efficiently mixed and transported to the electrode.

The effect of changing the rotation rate was investigated to provide information on the interaction between the two enzymes. There should be at least two competing effects; if the electrode is stationary, the build-up of NAD^+ at the electrode surface should be enhanced since the NAD^+ generated *in situ* by the LDH would not be spun away. However it is possible that the LDH would become limited by mass transport of pyruvate to the electrode and even product inhibition by build-up of lactate and NAD^+. Combined with these effects, it is possible that there is a complicated interplay of kinetic effects leading to generation of a localised NAD^+/NADH concentration ratio at a particular rotation rate that relies on the affinity constants and product inhibition constant for the two enzymes.

At the end of the chronoamperometry trace shown in Figure 6-3(b) the rotation was stopped; for a few seconds, the current increased in magnitude suggesting a build-up of NAD^+ had occurred however the current then quickly decreased in magnitude. It is likely that this is due to the catalytic system being limited by mass transport of pyruvate to or by a build-up of lactate at the electrode and thus the LDH is not working efficiently enough so the local NAD^+ concentration at the electrode decreased.

This experiment was then repeated using a solution containing only NAD^+ (0.02 mM). Again the electrode was poised at -0.46 V *vs* SHE. Since there was NAD^+ present from the

start, the initial current was not zero, Figure 6-4. However, the concentration of NAD^+ present was very low, approximately 10 times lower than k_M for the NAD^+-reductase, and therefore subtle changes in the NAD^+ concentration would be expected to have a significant effect on the NAD^+-reductase activity and therefore the measured catalytic current.

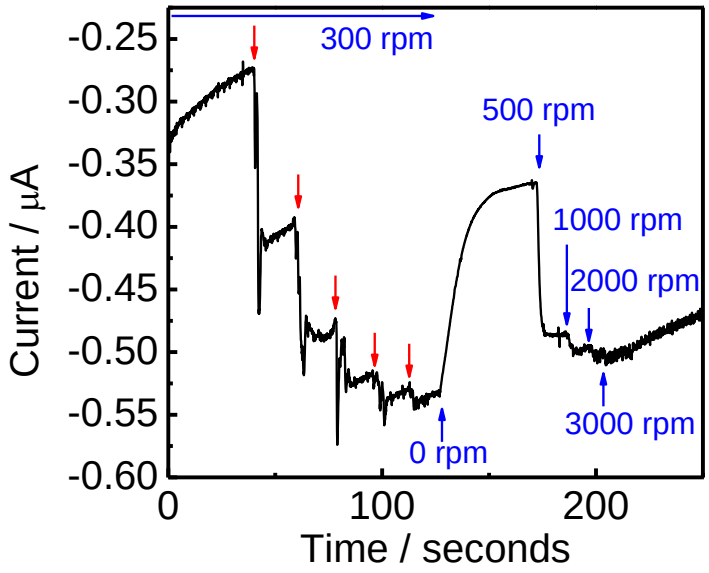

Figure 6-4: Chronoamperometric trace showing the response of an electrode modified with HoxFU and LDH on injections of pyruvate (indicated by red arrows). The experiment was performed in pH 7 KPB, with only NAD^+ (0.02 mM) present. The electrode was poised at -0.46 V *vs* SHE (an NAD^+-reducing potential) and aliquots of pyruvate were injected (33 μM). The electrode was rotated at 300 rpm at the start and was then changed as indicated to 0, 500, 1000, 2000 and 3000 rpm.

On injection of pyruvate, the LDH starts catalysing its reduction, provided there is some NADH present. An increase in magnitude of the catalytic current for the NAD^+-reductase was observed. This proves that the LDH is able to use the electrochemically derived NADH and that the NAD^+-reductase can reduce the resulting NAD^+. Again, subsequent injections of pyruvate led to an increase in the activity of the NAD^+-reductase. Since the overall concentration of NAD^+ in the cell could not have increased relative to the starting concentration, the increase in magnitude of catalytic current suggests that the cofactor has been 'concentrated' at the electrode and that co-immobilisation of the two enzymes in close proximity prevents cofactor from being spun way. Again, the effect of electrode rotation rate was investigated.

When the rotation was stopped, the catalytic current immediately decreased in magnitude, either because there was no longer enough NAD^+ or pyruvate at the electrode, or that a build-up of lactate inhibited the LDH. Furthermore, these effects act to decrease the rate of pyruvate reduction by the LDH and also decrease the rate of NADH oxidation thus leading to a high NADH concentration at the electrode, this would lead to product inhibition of the NAD^+-reductase. The magnitude of catalytic current at the stationary electrode is still higher than that at the start of the experiment suggesting that there is sufficient catalysis occurring by the LDH. The rotation rate was then increased stepwise to 3000 rpm. At this high rotation rate there is still significant increase in NAD^+ reduction current in comparison to the start of the experiment. This shows that the effect of NAD^+-reductase and LDH keeping the cofactor localised at the electrode is greater than the effect of rotation even at 3000 rpm.

These two experiments show that cofactor derived from the LDH can be used by the NAD^+-reductase and vice versa. They also demonstrate that co-immobilising both enzymes on the electrode creates a local NAD^+/NADH ratio and concentration which is maintained even at high rotation rates and further, that the two enzymes are acting to increase the cofactor concentration at the electrode. This has many important implications and it is possible that this will have the effect of increasing the rate of these immobilised catalytic systems in comparison to using the dehydrogenases in solution as the cofactor is passed back and forth between the two enzymes. This was further investigated in Section 6.4 where enzymes modified with hydrogenase, NAD^+-reductase and ADH were investigated.

6.3.3 *In situ* detection of pyruvate generation

Electrodes modified with NAD^+-reductase and LDH were used for electrochemically driven pyruvate reduction. The experiments were analysed using IR spectroscopy. A mixture of LDH (50 μg) and NAD^+-reductase (HoxFU, 10 μg) were mixed with freshly prepared PG particles and left for 1 hour at 4 ^oC to adsorb. The unwashed PG particles were then spread onto both

sides of a piece of carbon paper and used as the working electrode in in the ATR-IR cell discussed in Section 2.6.2. Briefly, the enzyme-modified carbon paper was placed onto the ATR prism, the cell was assembled and filled with reaction mixture containing NAD^+ (1 mM) and pyruvate (10 mM).

At the start of the experiment, the potential was held at -0.1 V *vs* SHE. Since NAD^+ is not reduced at this potential, the negative current can be attributed to residual capacitive current due to the large surface area of the working electrode, Figure 6-5(a). During this time an IR spectrum was recorded to be used as a background for the next scans, which will be presented as difference spectra. Difference spectra can allow analysis of small changes that are not obvious in absolute spectra (Section 2.6). The potential was then changed to -0.46 V *vs* SHE, and a large increase in current was seen corresponding to a catalytic NAD^+ reduction at the electrode by the NAD^+-reductase. The potential was held at -0.46 V *vs* SHE and IR spectra were recorded every 30 minutes.

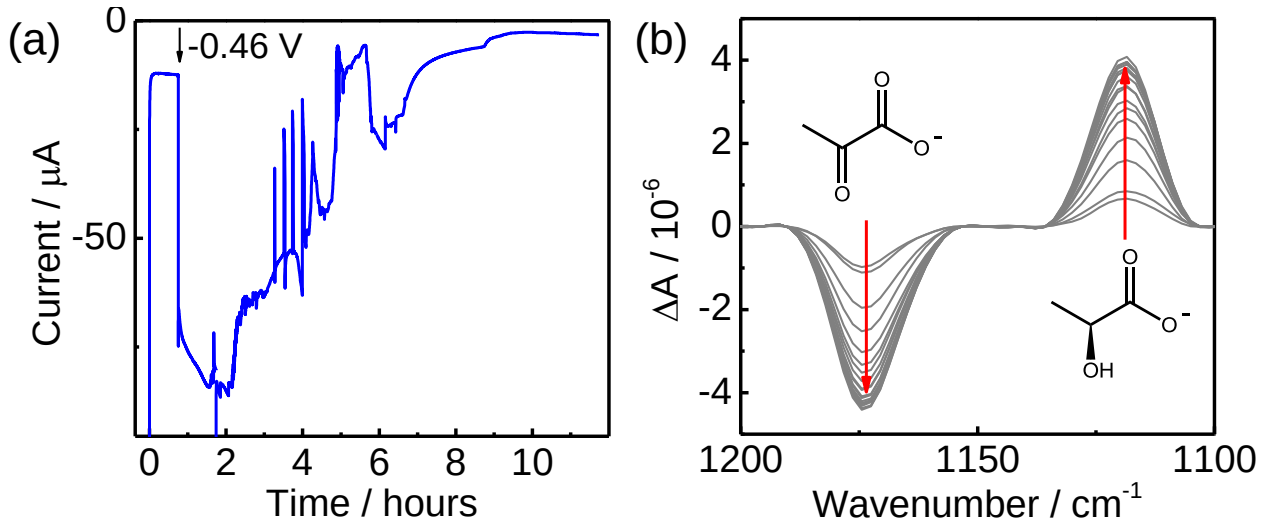

Figure 6-5: Electrochemically-driven pyruvate reduction with *in situ* detection. (a) Chronoamperometric trace from the LDH and NAD^+-reductase modified electrode in the presence of NAD^+ (1 mM) and pyruvate (10 mM). (b) *In situ* infrared detection shows pyruvate consumption (1180 cm^{-1}) and lactate production (1120 cm^{-1}). This was carried out in Bis-tris buffer, pH 6 at 22 ^oC.

At first the current had a high magnitude and was reasonably stable, however it became less stable over time, Figure 6-5(a). This may be due to loss of solution affecting the electrode

connections. Some of the oscillations in current may be due to the complicated cofactor equilibrium when using this system. Integration of the current over time suggests that 3.07 μmoles of NADH were generated. The IR difference spectra in Figure 6-5(b) confirm the loss of pyruvate (1180 cm^{-1}) and the formation of lactate (1120 cm^{-1}) using bands in a region free from overlap with components of the buffer solution. The spectra show that lactate generation starts quickly and slows over time. Both the chronoamperometry and IR spectra suggest that no further conversion was occurring after 10 hours. Assuming a cell volume of 250 μL the maximum concentration of lactate that could have been generated is 12.28 mM (calculated from the current passed), this suggests that near complete conversion may have occurred with the additional current due to residual capacitive current. Due to complications from buffer absorption below 1100 cm^{-1}, and the low relative concentrations of pyruvate and lactate in the reaction mixture, it was not possible to accurately determine the concentration of lactate and pyruvate present using IR spectroscopy.

6.3.4 *Ex situ* detection of pyruvate generation

The *in situ* IR method showed clear conversion of pyruvate to lactate but did not give quantitative data on the final concentration of lactate and therefore the extent of the reaction. In order to gain quantitative information on the conversion of pyruvate to lactate the experiment was carried out in a similar cell as to that in the previous section but with no prism. A mixture of NAD^+-reductase (Hox~~HY~~FU, 10 μg) and LDH (200 μg) were spread straight onto a carbon paper electrode. This was placed at the bottom of the cell and buffer (Bis-Tris, pH 6) containing NAD^+ (1 mM) and pyruvate (20 mM) was added, with a total volume of *ca* 1 mL. The cell was then sealed, the electrodes connected and left with the working electrode at a potential of -0.46 V *vs* SHE for 14 hours. The resulting solution was then analysed using HPLC.

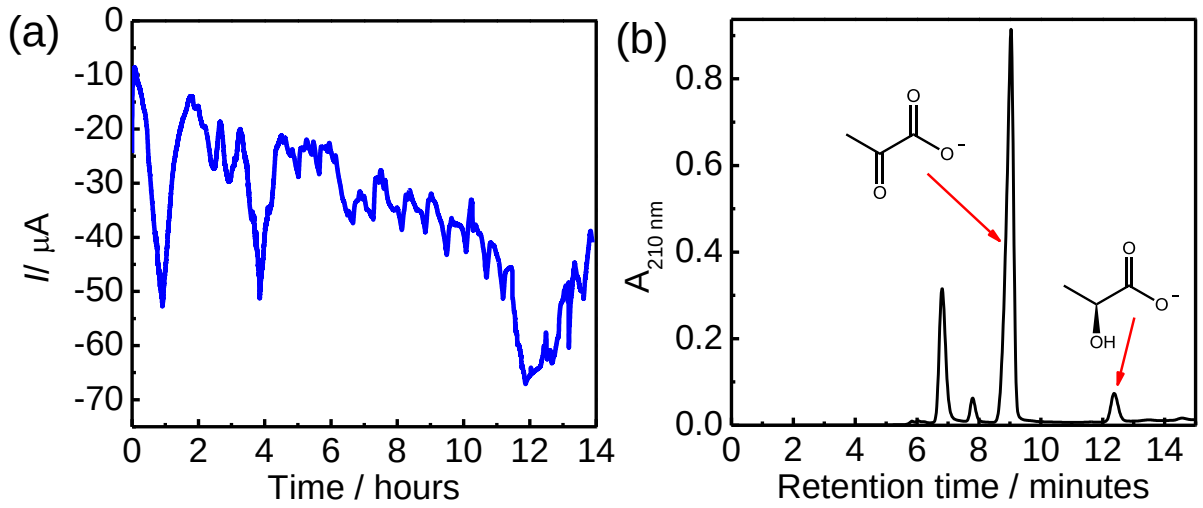

Figure 6-6: Electrochemically driven LDH with *ex situ* product detection. (a) Chronoamperometry trace showing the current response of the LDH and NAD^+-reductase modified electrode over time. (b) HPLC chromatogram shows the formation of lactate (12.53 minutes) using electrochemically derived NADH.

The chronoamperometry trace in Figure 6-6(a) shows clear NAD^+ reduction current which oscillates between *ca* -10 and – 70 µA. This oscillation may again be due to the complicated interplay between the LDH and the NAD^+-reductase, especially since the solution was not stirred. If all of the current was due to NAD^+ reduction, 50 µA of current would equates to an activity of *ca* 1.6 µmole min^{-1} per mg NAD^+-reductase. In panel (b) the end solution after this experiment was analysed using HPLC (Section 2.4), to quantify the concentration of lactate produced. In this case the final concentration of lactate was *ca* 6.2 mM equating to 33.3 % conversion of pyruvate to lactate. This result demonstrates that each cofactor molecule has been cycled at least 6 times. Integration of the current predicts formation of 9.23 mM NADH suggesting that the current efficiency was *ca* 66 %. Additional peaks in the HPLC trace correspond to the cofactor and buffer, the trace is otherwise clear of additional peaks demonstrating high selectivity of the enzyme system. The total turnover number for this system was > 100,000 moles of NADH per mole NAD^+-reductase. Overall, the enzyme-modified electrode systems are catalysing NADH-dependent biotransformations; these electrodes were adapted for electrochemical devices in Chapter 8.

6.4 Carbon particles for H_2-driven cofactor supply

Generation of NADH using a H_2-driven particle system was demonstrated in Chapter 5. Here, this system is coupled to the cofactor-dependent enzymes LDH and ADH, the overall biotransformations catalysed are 100 % atom efficient if both the electrons and protons from H_2 oxidation are incorporated into the product. Again, the cofactor-dependent enzyme can be used either in solution or co-immobilised on particles.

6.4.1 Cofactor-dependent enzyme in solution

At first, the enzyme modified particles were prepared as introduced in Chapter 5. The particles were dispersed by sonication in buffer and an aliquot of these particles was exposed to a mixture of hydrogenase and NAD^+-reductase. These were left at 4 ^oC for at least 30 minutes before addition to a H_2-saturated reaction mixture. For these experiments the reaction mixture contained the cofactor-dependent enzyme along with substrate and cofactor.

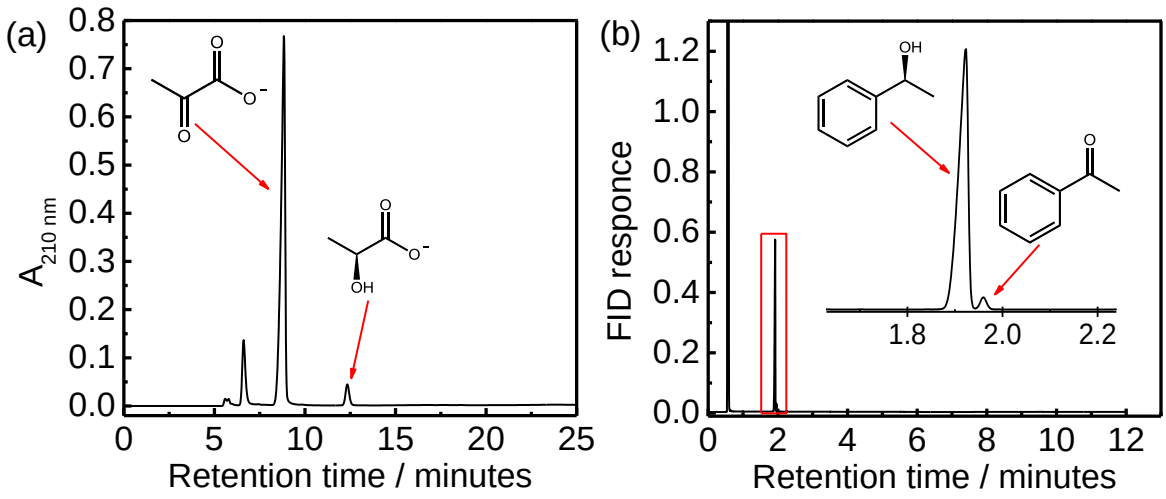

Figure 6-7: The H_2-driven catalytic particles can be used to supply cofactor to a range of NADH-dependent dehydrogenase enzymes in solution. PG particles were modified with NAD^+ reductase (Hox~~HY~~FU) and *D. v* MF hydrogenase and injected into H_2-saturated buffer containing NAD^+ (1 mM), an NADH-dependent enzyme and substrate. (a) An HPLC trace confirms the formation of lactate (12.53 minutes) from pyruvate (10 mM, *ca* 9 minutes) with *ca* 36 % conversion using LDH is solution. Experiment performed in Bis-Tris buffer, pH 6. (b) A GC trace confirming the formation of phenylethanol (9.86 mM) from acetophenone (10 mM) using ADH in solution. The boxed area is shown expanded in the inset. Experiment performed in Tris-HCl buffer, pH 8.

The chromatograms in Figure 6-7 show that the three-enzyme systems enable cofactor-dependent biotransformations to be carried out using H_2 as the reducing equivalent. In panel (a) 36 % conversion of pyruvate to lactate is shown. In panel (b) > 98 % conversion of acetophenone to phenylethanol is observed. In the latter case this requires each cofactor molecule to have been used ~ 10 times (TN = 10). It should be possible for each cofactor to be used thousands of times; for this the stability of the enzyme systems needs to be further improved and higher substrate to cofactor concentrations used. The HPLC and GC traces also confirm that no side products were formed in detectable quantities.

6.4.2 Cofactor-dependent enzyme co-immobilised

If the cofactor-dependent enzyme is used in solution, NAD^+ must diffuse to the particle where the NAD^+-reductase reduces it to NADH. This NADH must then diffuse to the cofactor-dependent enzyme (along with a substrate) where it is used for substrate conversion to product. The NAD^+ produced must then diffuse back to the particle for H_2-driven regeneration. In the case, where the cofactor-dependent enzyme is immobilised on the particles, it is possible that the cofactor is simply passed between the NAD^+-reductase and the dehydrogenase with only diffusion of substrate to and product away from the particle. As discussed in Section 6.3.2, co-immobilisation of the cofactor-dependent enzyme and the NAD^+-reductase may enable faster kinetics of a biotransformation by creating a local cofactor concentration and NAD^+/NADH ratio in close proximity to the particle surface. Here the particles for H_2-driven cofactor recycling are compared in the cases where the cofactor-dependent enzyme is either in solution or co-immobilised. These experiments were performed using ADH for acetophenone reduction to phenylethanol.

Experiments were performed in order to determine if particles modified with hydrogenase, NAD^+-reductase and a cofactor-dependent enzyme (ADH) are able to sustain H_2-driven catalysis. Particles modified with hydrogenase (*D. v* MF) and NAD^+-reductase (Hox~~HY~~FU)

were prepared according to the previously described methods and split into three equal aliquots. A solution of ADH (0.5 mg) was added to one set of particles (A) before all of the aliquots were left at 4 ^{o}C for *ca* 3 hours. One aliquot of the particles (control, C) was tested using the methods developed in Chapter 5 to confirm that the particles were active for H_2-driven NADH generation, and an activity of 0.3 µmole min^{-1} per mg NAD^+-reductase was determined. The remaining particle mixtures (A and B) were centrifuged and the supernatant containing unabsorbed enzyme removed. The particles were then re-suspended in fresh buffer (30 µL) before addition of the reaction mixture (200 µL), which consisted of NAD^+ (1 mM) and acetophenone (10 mM) in H_2-saturated Bis-Tris buffer (pH 6, 2 % DMSO). A solution of ADH (0.5 mg) was added to the set-up which did not have ADH co-immobilised (B). These were then left shaking overnight, under a flow of H_2 (100 mL min^{-1}) using the set-up described in Section 5.3.2. After 20 hours the particles were removed by centrifugation and the solutions filtered to remove enzyme in solution before analysis using HPLC, protocols in Appendix E.

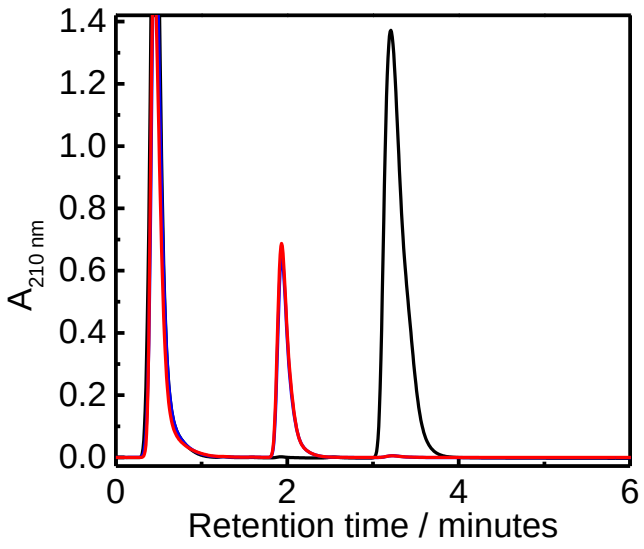

Figure 6-8: Enzyme-modified particles carry out H_2-driven acetophenone reduction. HPLC was used to analyse the starting solution (black) and the resulting solution using the ADH in solution (B, blue) or co-immobilised on particles (A, red). HPLC protocol detailed in Appendix E. Acetophenone is seen at *ca* 3.2 minutes and phenylethanol at *ca* 1.9 minutes. The large absorbance peak at *ca* 0.5 minutes is due to the cofactor.

The chromatograms in Figure 6-8 show that there was almost no acetophenone in the end solutions when the ADH was used either in solution (B, blue) or immobilised on particles (A, red) compared to the starting solution (black). Using the ratio of peak areas at 1.9 and 3.2 minutes as per the methods described in Appendix E, the concentration of phenylethanol was calculated as *ca* > 9.7 and > 9.8 mM for the ADH in solution and immobilised respectively. However, the absolute area of the phenylethanol peak is smaller than expected suggesting that although > 97 % conversion occurred in each case, the overall yield is not as high; this is likely due to some adsorption onto the particles or evaporation of the product and substrate due to the fast flow rate of H_2 overnight. These results show that it is possible to immobilise all of the enzymes required for both a biotransformation and cofactor regeneration on particles and that very high conversion can be achieved. In the next experiment a larger reaction volume was be used to prevent such a large extent of conversion and give an idea as to the effect of co-immobilising the ADH.

A stock solution of H_2-saturated reaction mixture containing NAD^+ (1.33 mM) and acetophenone (10.25 mM) was made up in Bis-tris buffer (pH 6, 7.5 mM, 2 % DMSO). Particles modified with NAD^+-reductase (Hox~~HY~~FU, 25 μg) and *D. v* MF hydrogenase (35 μg) were prepared using BP particles dispersed by sonication in buffer (1.2 mg). This enzyme-particle mixture was immediately split into two equal aliquots. To one, ADH (35 μL) was added; nothing was added to the other. Both sets of particles were then left at 4 ^oC for 1.5 hours before the reaction mixture (1 mL) was added to each set of particles; ADH (35 μL) injected into solution in the experiment where it was not previously immobilised on the particles. Both of these were then placed into a shaker under a H_2 atmosphere (100 mL min^{-1}). The experiments were left overnight and analysed after 18 hours. For this, the particles were first removed by centrifugation followed by filtration of the supernatant to remove any unadsorbed enzyme.

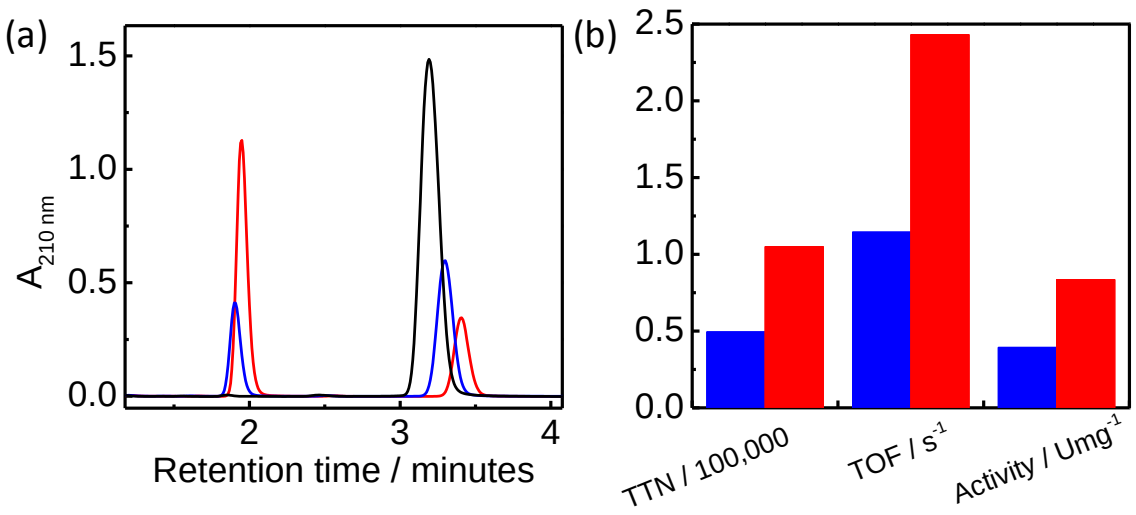

Figure 6-9: Data comparing the effect of co-immobilising the alcohol dehydrogenase (red) and using it in solution (blue). (a) HPLC traces before (black) and after the reactions. The reactions were identical except that in one all three enzymes were immobilised on the particles (red), and in the other the ADH was used in solution (blue). (b) Bar chart demonstrating the effects of immobilising all the enzymes. TTN is the total turnover number of product per enzyme, TOF is the turnover frequency of product per enzyme and the activity is the rate of product generation per minute per mg of enzyme; in each case enzyme refers to the NAD^+-reductase. Reactions performed under a H_2 atmosphere in H_2-saturated Bis-tris buffer (pH 6, 2 % DMSO) with 1 mM NAD^+ and 10 mM Acetophenone.

The HPLC traces show the initial reaction mixture (black) contained only acetophenone (*ca* 3.2 minutes) and that each of the final mixtures contained acetophenone and phenylethanol (*ca* 1.9 minutes). There was significantly less adsorption of acetophenone and phenylethanol in this experiment. Using the standard plot in Appendix E the concentration ratio of phenylethanol and acetophenone in each case was determined. In the case where all three enzymes (hydrogenase, NAD^+-reductase and alcohol dehydrogenase) were immobilised, 75 % conversion was achieved. In the experiment where ADH was used in solution only 35 % conversion was seen. These values were used to determine the total turnover number (TTN, moles product per mole NAD^+-reductase), turnover frequency (TOF) and activity per NAD^+-reductase of the two systems. A comparison of these is shown in Figure 6-9(b).

Overall the results in Figure 6-9 demonstrate that significantly more conversion occurred when using all three enzymes co-immobilised on the carbon particle. This provides further evidence that co-immobilisation may improve the activity of the cofactor-dependent enzyme

and the cofactor recycling enzyme.

So far this chapter has demonstrated a significant advantage of co-immobilising the ADH and NAD^+-reductase in close proximity. The electrochemical characterisation provided evidence that the cofactor was concentrated at the electrode and that a different NAD^+/NADH ratio is created in comparison to the bulk solution. In order to directly assess the impact of these theories, experiments were performed with different NAD^+ concentrations. If close proximity of the two enzymes does aid these effects, the effect of co-immobilising the ADH should be much more pronounced at low cofactor concentration.

Enzyme-modified particles were prepared by mixing NAD^+-reductase (Hox~~HY~~FU, 80 µg), hydrogenase (Hyd-2, 50 µg) and BP particles dispersed in buffer (0.2 mg in Tris-HCl, pH 8). These particles were split into two portions and ADH (1.1 mg) was added to one sample. Both sets of particles were left at 4 ^oC for 1 hour before they were centrifuged, the supernatant removed and the particles were re-suspended in buffer. Each set of particles was then diluted in a H_2-saturated solution (Tris-HCl, pH 8, 2 % DMSO, 3 mL) containing acetophenone (10 mM). An aliquot of ADH (1.1 mg) was added to the sample where ADH was not co-immobilised on the particles. These solutions were then split into 3 identical samples to which different concentrations of NAD^+ were injected. All of the samples where then left shaking in a H_2 atmosphere (Section 5.3.2).

At specific time points an aliquot of reaction mixture (100 µL) was removed from each sample. To each, acetonitrile was added (20 µL) to aid analysis by HPLC. The samples were then centrifuged and a portion of the supernatant was diluted with water for analysis. The area of the substrate and product peaks was recorded and a ratio of these peaks used to determine the extent of conversion, Appendix E. This data was then used to calculate the TTN, TN and TOF, Table 6-4. A direct comparison between the two sets of particles at the highest NAD^+ concentration (1 mM) is given in Figure 6-10.

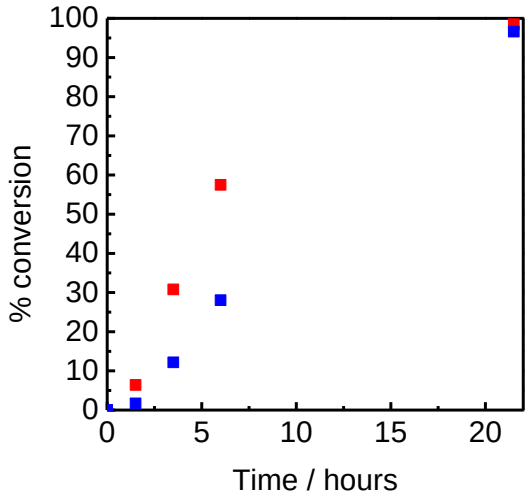

Figure 6-10: HPLC was used to determine the extent of conversion of acetophenone to phenylethanol for particles modified with hydrogenase (Hyd-2) and NAD^+-reductase (Hox~~HY~~FU) in the presence of NAD^+ (1 mM) and acetophenone (10 mM). The ADH was either co-immobilised on the particles (red) or used in solution (blue). Experiments performed in Tris-HCl, pH 8 with 2 % DMSO at 22 ^oC. The reactions were left shaking in an H_2 atmosphere.

After 21.5 hours the particles with ADH co-immobilised and in solution led to >98 % and >96 % conversion, respectively in the presence of 1 mM NAD^+. This demonstrates that there is no significant effect on the overall thermodynamic driving force for H_2-driven acetophenone reduction when using the ADH in solution *vs* co-immobilised. However, the time points recorded demonstrate that the particles with ADH in solution operated at approximately 50 % activity over the first 6 hours in comparison to using the ADH immobilised. This agrees closely with the previous experiment where the reaction with ADH in solution generated *ca* half the phenylethanol concentration compared to the co-immobilised ADH system. The HPLC data for three enzymes co-immobilised is shown in Appendix G.

When the particles modified with all three enzymes were prepared it was clear that not all of the ADH was immobilised. The ADH was prepared at high concentration (20 mg mL^{-1}) and was very yellow in colour. On separation of unadsorbed enzyme by centrifugation, the supernatant was still slightly yellow. Therefore it is even more impressive that the set-up with all enzymes immobilised operated faster than using ADH in solution.

Table 6-4: Comparison of the kinetic of acetophenone reduction by ADH co-immobilised on particles or used in solution. All experiments performed in the presence of acetophenone (10 mM), in H_2-saturated Tris-HCl buffer, pH 8 at 22 ^{o}C.

ADH	[NAD^+] / mM	% conversion				TN	TTN	TOF	TN	TTN	TOF
		1.5 hrs	3.5 hrs	6 hrs	21.5 hrs	6 hrs	6 hrs	6 hrs	21.5 hrs	21.5 hrs	21.5 hrs
Co-immobilised on carbon particles	1	6.4	30.8	57.5	98.5	5.75	$3.9x10^4$	1.5	9.85	$6.7x10^4$	0.71
	0.1	5.1	19.2	36.8	84.4	36.8	$2.5x10^4$	0.95	84.4	$5.8x10^4$	0.61
	0.01	1.5	5.3	10.7	65.5	107	$7.3x10^3$	0.28	655	$4.5x10^4$	0.47
Added into solution	1	1.7	12.2	28.0	96.6	2.8	$1.9x10^4$	0.72	9.7	$6.6x10^4$	0.69
	0.1	*	*	*	*						
	0.01	*	*	*	*						

** Significant adsorption of acetophenone and phenylethanol prevented analysis*
***TN** (turnover number) = moles product / moles cofactor, **TTN** (total turnover number) = moles product / moles NAD^+-reductase,*
***TOF** (turnover frequency) = number of product per second per NAD^+-reductase*

The data in Table 6-4 combines the activity of the particles in the presence of different cofactor concentrations. Comparing the activity of the particles with all three enzymes immobilised over the first 6 hours, the system retained *ca* 66 and 17 % activity when the cofactor concentration was decreased from 1 mM to 0.1 and 0.01 mM, respectively. This experiment further provided the first insight into the TN values that could be achieved by increasing the ratio of substrate-to-cofactor. In the previous experiments, the highest TN recorded was *ca* 10. Here, in the reaction using the lowest NAD^+ concentration (0.01 mM) the TN value was > 650 moles of product per mole of cofactor. This is a huge improvement and it is likely that further increasing the substrate loading will improve this figure in the future.

The comparison between the particles with and without ADH immobilised in Table 6-4 shows that the particles with co-immobilised ADH led to faster initial acetophenone reduction at both 1 and 0.1 mM NAD^+ compared to using the ADH in solution at 1 mM NAD^+. The analogous experiments at low cofactor concentrations using the ADH in solution led to almost complete adsorption of the acetophenone and any phenylethanol thus preventing analysis, Appendix G. It is possible that the increased protein coverage on co-immobilisation of ADH prevented this for the other reactions. However, significant adsorption was not observed at higher cofactor concentration with ADH in solution. This experiment does therefore not directly compare the effect of decreasing the cofactor concentration but does provide many useful insights into the system.

Table 6-5: Comparison of the activity and % conversion of identical sets of particles in the presence of different NAD^+ concentrations.

[NAD^+] / mM	**Activity (µmole / min per mg*)**	**% activity**	**% conversion (after 10 minutes)**
1	0.87	100	6.5
0.1	0.17	20.3	12.6
0.01	0.07	8.34	49.9

** per mg of NAD^+-reductase*

For comparison, aliquots of different enzyme-modified particles (each set utilising Hyd-2, 1.6 µg and Hox~~HY~~FU, 6.7 µg) were used for H_2-driven NADH generation in the presence of 0.01, 0.1 and 1 mM NAD^+. These particles were not coupled to an ADH; the initial activity and % conversion after 10 minutes was compared for each run, Table 6-5; the data is shown in more detail in Appendix H. The results in Table 6-5 show that only 20.3 and 8.3 % activity remained after decreasing the cofactor concentration from 1 mM to 0.1 and 0.01 mM, respectively. These values are much lower than for the whole system with all three enzymes immobilised (66 % and 17 %, respectively). The percent conversion after 10 minutes shows that there is likely to be a much higher NADH/NAD^+ ratio at the particle when lower cofactor concentrations are used. This may contribute to the increased activity of the three enzyme-immobilised system.

6.5 Carbon nanotubes columns

The use of carbon nanotubes and a carbon nanotubes column (CNC) as a material for H_2-driven NADH generation was discussed in Chapter 5. This section explores the possibility of using these CNCs as a support for the hydrogenase, NAD^+-reductase and ADH to demonstrate a flow set-up for H_2-driven biotransformations.

A CNC was incorporated into a flow system using PTFE tubing connected *via* a pair of specially machined PTFE threaded connectors, as described in Section 5.6.4. Flow was achieved using a peristaltic pump (Whatman). A solution containing concentrated hydrogenase (*E. coli* Hyd-1), NAD^+-reductase (Hox~~HY~~FU) and ADH was pumped through the tube multiple times in aerobic conditions. A N_2-saturated solution (Tris buffer, pH 8) was then flowed through (5mL) to ensure that any un-adsorbed enzyme was removed from the tube. A H_2-saturated reaction mixture containing acetophenone (8.3 mM), NAD^+ (1 mM) in buffer (Tris-HCl, pH 8) was then added to the column. This solution (5 mL) was cycled through the CNC overnight; H_2 was continuously bubbled into the reaction mixture.

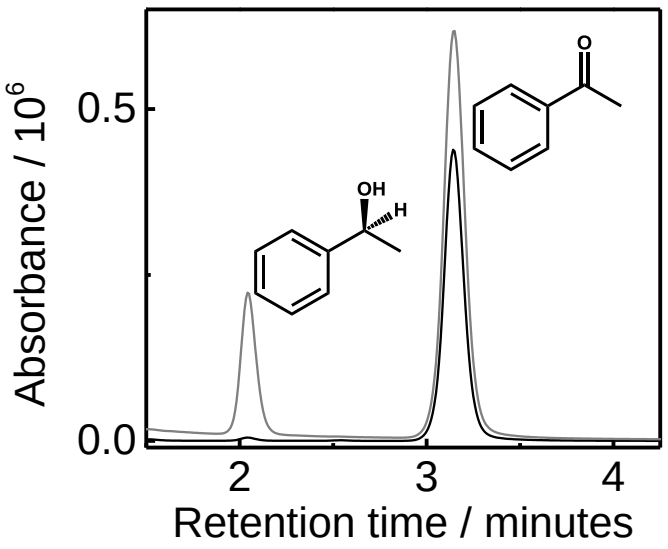

Figure 6-11: An HPLC trace showing acetophenone (3.2 minutes) and phenylethanol (2.1 minutes) in the resulting reaction mixture after repeated cycles through the enzyme modified carbon nanotubes column. The absorbance at 210 nm (grey) and 260 nm (black) are shown.

The chromatogram in Figure 6-11 shows that phenylethanol had been produced, equating to approximately 25 % conversion. Although this is not a huge conversion, the experiment was carried out in a relatively large reaction volume (5 mL) therefore a significant quantity of product has been formed, *ca*10 μmoles. Assuming that the amount of NAD^+-reductase used was *ca* 32 μg, and the reaction was occurring for 22 hours, the activity was 0.24 μmoles min^{-1} per mg NAD^+-reductase and the TTN was > 54,000 NADH per NAD^+-reductase. This system is showing much lower activity than the particle system. Firstly, it is unlikely that all of the enzymes were adsorbed onto the nanotubes and secondly it is likely that the initial maximum rate was much faster than the average calculated over 22 hours. Since the enzymes were adsorbed in the presence of O_2, there may have been a lag phase for activation of the hydrogenase. The hydrogenase used in this experiment was *E. coli* hyd-1; this enzyme will be discussed further in Chapter 7. It was chosen as it is readily available at high concentration (produced within the Vincent Group) and has been previously shown to immobilise onto a range of carbon materials with very high stability in comparison to many other enzymes.[212]

6.6 Summary

This Chapter has built upon the electro-enzymatic and H_2-driven systems for NADH generation developed in earlier chapters, and describes the use of them for NADH supply to industrially relevant enzymes for selective reduction of ketones to alcohols. Although only ketone reductions were considered, the methods and protocols should translate to a whole range of other hydrogenation reactions including C=C bond reduction, imine reduction and enzyme cascades for reductive amination by appropriate choice of hydrogenase and NAD^+-reductase.

Investigations into co-immobilisation of the NAD^+-reductase and an NADH-dependent enzyme on a PGE electrode provided evidence that the cofactor can be efficiently passed between the two enzymes and is effectively 'concentrated' at the electrode surface. This was further demonstrated by higher catalytic efficiencies for H_2-driven acetophenone reduction when all of the enzymes for cofactor recycling and the biotransformation were co-immobilised on carbon particles compared to using the ADH in solution. H_2-driven biotransformations were also demonstrated in a novel flow set up showing the versatility of the system. Turnover numbers (moles of product per mole of cofactor) up to *ca* 650 have been demonstrated. This is lower than the industrially-demanded values (10^3-10^5); higher substrate loadings would be required to achieve higher turnover numbers, but these may require two phase systems to increase the solubility of the substrates in aqueous solution and to prevent high concentrations of the substrate in the aqueous layer from inhibiting the enzymes.

The next Chapter describes work extending the H_2-driven particle approach to sustain catalysis in the presence of O_2 for NADH supply to an NADH-dependent monooxygenase.

Chapter 7 O_2-tolerant NADH recycling to supply oxygenase catalysis

**Some of the experiments in this Chapter were performed by Chloe Tomlinson, Part II, under my supervision.*

In Chapters 5 and 6 enzyme-modified particles were assessed for H_2-driven NADH generation and further coupled to cofactor-dependent enzymes for driving ketone reduction reactions. Extending this concept to other reductive biotransformations including alkene reduction to alkanes, enzyme cascades for reduction of ketones to amines, and aldehyde or nitrile reduction should only require minor changes to optimise the particles for the desired reaction conditions. Here, these systems are developed further to supply enzyme catalysed oxidation reactions, Equation [7-1], which require NADH for reductive activation of molecular O_2 (Section 1.3).

$$RH + H^+ + \tfrac{1}{2}O_2 + NADH \xrightarrow{oxygenase} ROH + H_2O + NAD^+ \qquad [7\text{-}1]$$

$$RH + O_2 + H_2 \rightarrow ROH + H_2O \qquad [7\text{-}2]$$

Again, the use of H_2 as a reducing equivalent provides a highly atom efficient reaction pathway generating only water as a waste product; the overall reaction is shown in Equation [7-2]. Specifically, this Chapter looks to supply a flavin monooxygenase (FMO) named biphenyl-2-ol 3-monooxygenase (HbpA) with NADH for the oxidation of biphenyl-2-ol to 2, 3-dihydroxybiphenyl using enzyme-modified particles for H_2-driven cofactor recycling.

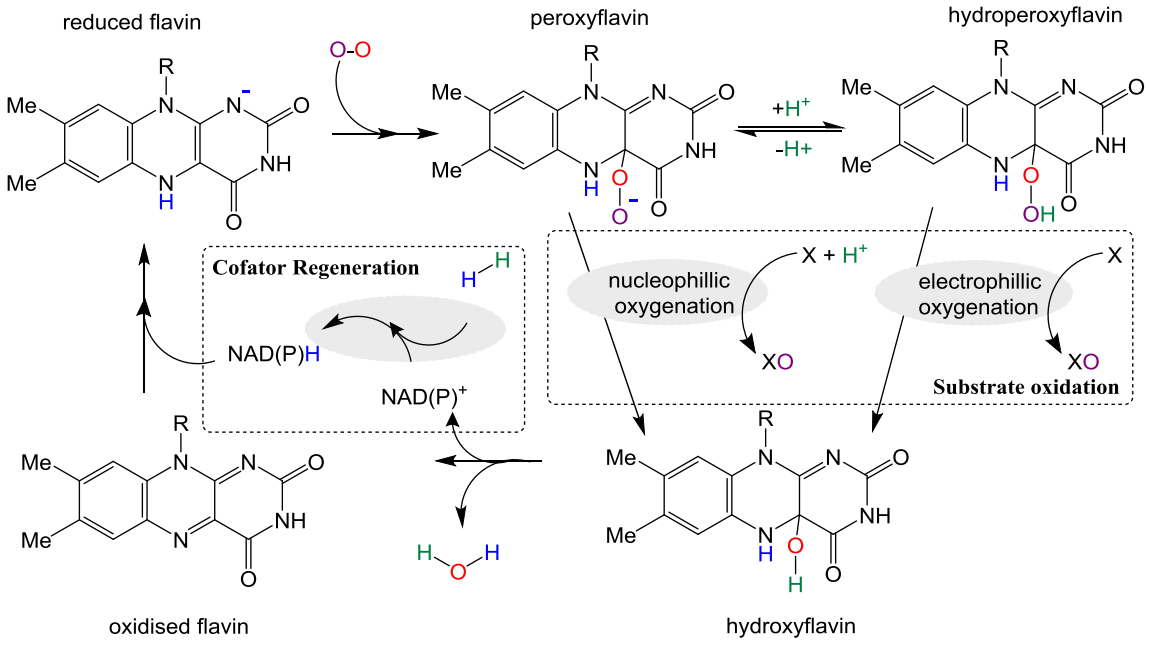

Figure 7-1: The catalytic cycle of a typical FMO coupled to H_2-driven cofactor regeneration. The FMN active site is reduced *via* hydride from NAD(P)H, O_2 is bound before substrate oxidation followed by loss of water. For clarity, the hydrogen atoms from NADH regeneration, and O atoms from O_2 are coloured.

Flavin monooxygenases, including HbpA, contain a FMN active site which is selectively reduced using electrons from NAD(P)H. Attack of O_2 leads to generation of a peroxyflavin, Figure 1-8. On diffusion of a substrate into the active site, the substrate is held within a specific orientation with respect to the FMN *via* interactions with the surrounding amino acids. This leads to a selective O atom insertion reaction leaving a hydroxyflavin after addition of a proton. Loss of water regenerates an oxidised flavin active site, which can undergo another catalytic cycle on reduction by NAD(P)H.

A significant advantage of the H_2-driven system developed in this work, is use of very mild H_2 partial pressures which enables the possibility of mixing H_2 and O_2 within safe limits. However there are technical problems to overcome:

(1) the hydrogenases used in the previous Chapters were O_2-sensitive and must therefore be replaced by O_2-tolerant hydrogenases

(2) there is little literature on oxygenases working in low levels of O_2, conditions suitable for both H_2-driven NADH generation and monooxygenase catalysis must be identified

(3) direct O_2 reduction occurs at carbon at potentials more negative than *ca* -0.2 V *vs* SHE, and this may lead to H_2 derived electrons being diverted away from NAD^+ reduction.

This Chapter introduces O_2-tolerant hydrogenases, explores the activity of enzyme-modified particles for H_2-driven NADH generation in the presence of O_2 and investigates suitable reaction conditions for supplying HbpA.

7.1 O_2-tolerant hydrogenases

A range of O_2-tolerant hydrogenases have been studied electrochemically in order to understand how they are able to catalyse the oxidation of H_2 in the presence of O_2.[277–282] This activity has led to demonstrations of their use in membrane-free enzyme-catalysed fuel cells that can operate on low levels of H_2 in air,[15,283] and provides a sound basis for this work, where H_2 oxidation in the presence of O_2 will also be required. Previous electrochemical analysis of the NAD^+-reductase (HoxFU) from *R. e* showed that it is able to sustain NAD^+ reduction catalysis in the presence of O_2 and was therefore chosen for this work.[151]

7.1.1 Thermodynamic considerations

It is known that many O_2-tolerant hydrogenases have a significant overpotential requirement

for H_2 oxidation to occur at a useful rate. In a H_2/O_2 fuel cell, where the potential window for coupling H_2 oxidation and O_2 reduction is very large, this overpotential does not significantly lower the open circuit potential, equal to the driving force (6.5 % decrease in driving force assuming an overpotential of 80 mV). In contrast, the $2H^+/H_2$ and $NAD^+/NADH$ couples are very closely spaced and thus any loss in the thermodynamic efficiency for either half reaction is likely to have a large effect on the driving force (38 % decrease assuming an overpotential of 80 mV for H_2 oxidation at pH 7 in the presence of 1 bar H_2 and a high $NAD^+/NADH$ concentration ratio). This is demonstrated schematically in Figure 7-2(a), assuming the same overpotential of *ca* 80 mV.

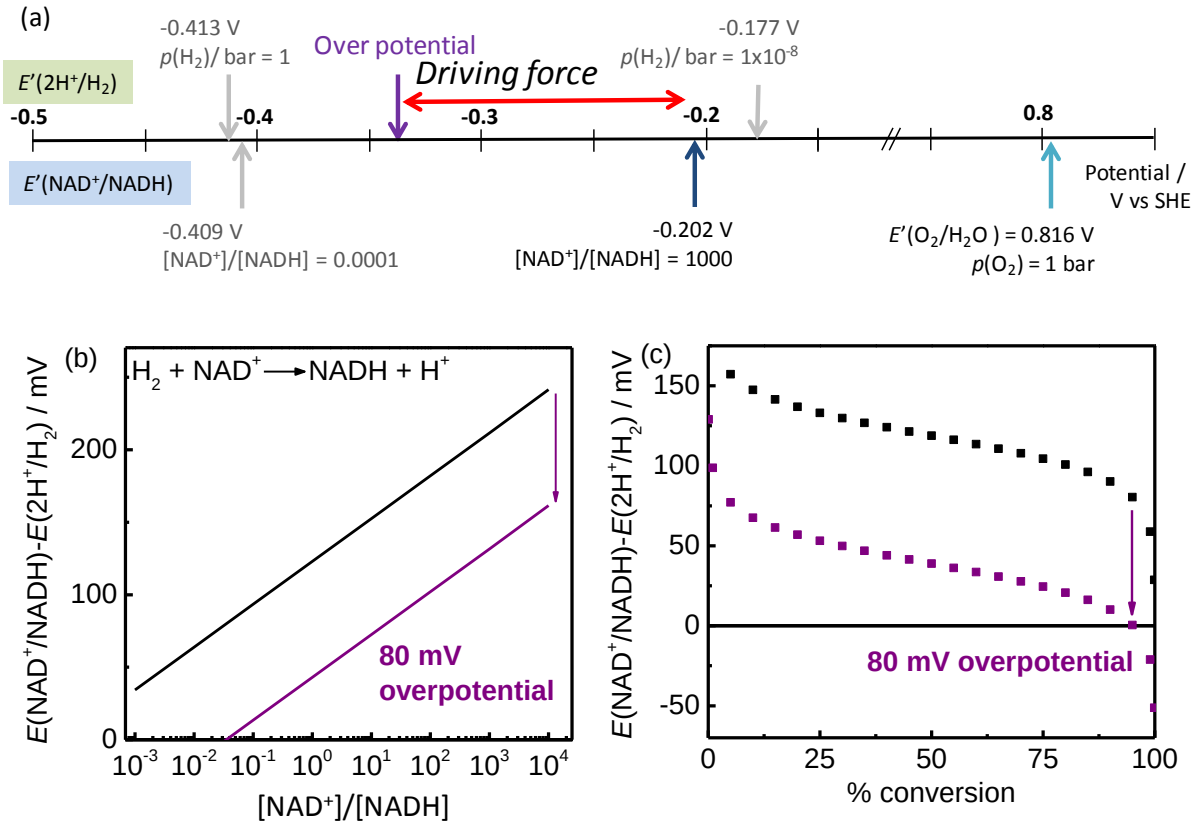

Figure 7-2: The effect of using an O_2-tolerant hydrogenase on the driving force for H_2-driven NADH generation, assuming an overpotential of 80 mV for H_2 oxidation. (a) A potential scale showing the thermodynamic potentials for the $2H^+/H_2$, $NAD^+/NADH$ and $½O_2/H_2O$ couples under the stated conditions and the theoretical decrease in driving force when using a hydrogenase with an over potential requirement. (b) The difference in potential between the $NAD^+/NADH$ and $2H^+/H_2$ couples is plotted at 1 bar H_2, 25 °C, pH 7. The black line denotes the calculated difference in thermodynamic potentials and the purple line shows the effect of an overpotential. (c) The difference in potential plotted *vs* the percentage conversion of NAD^+ to NADH using a hydrogenase with (purple) or without (black) an overpotential requirement.

Using a hydrogenase which requires an overpotential for significant H_2 oxidation catalysis, lowers the overall driving force for H_2-driven NADH generation (Figure 7-2(b)) and is also likely to prevent complete conversion of NAD^+ to NADH (Figure 7-2(c)) even in the presence of 1 bar H_2. However, a significant driving force remains and it is estimated that *ca* 95 % conversion of NAD^+ to NADH should be possible; this still provides a significant thermodynamic 'push' for high conversion when coupled to a NADH-dependent biotransformation.

The overpotential requirement for H_2 oxidation prevents the enzymes from catalysing reversible $2H^+/H_2$ cycling and has been observed for all O_2-tolerant membrane-bound hydrogenases to date.[284] Often, H^+ reduction is not seen at physiological pH even under low H_2 conditions. The FeS clusters are thought to be important in this behaviour.[181,285–289] Hexter *et al.* conclude that the overpotential and catalytic bias depend on the reduction potential of the distal FeS cluster (the point at which electrons enter and leave the protein) relative to the thermodynamic potential of the reaction.[290] This has been supported by Murphy *et al.* who demonstrated that the O_2-tolerant hydrogenase, Hyd-1, catalyses reversible $2H^+/H_2$ cycling at high proton concentrations (pH 3).[284] The thermodynamic potential of FeS clusters are generally not very pH dependent but the potential of the $2H^+/H_2$ couple decreases with pH; the difference between the two therefore decreases with decreasing pH, enabling reversibility.[284]

7.1.2 Electrochemistry

**This experiment was performed by Ms Chloe Tomlinson under my supervision*

In Chapter 5, a range of hydrogenase enzymes were introduced including Hyd-2 from *E. coli* and *D. vulgaris* MF hydrogenase. Here the O_2-tolerant hydrogenase, *E. coli* hydrogenase 1 (Hyd-1), was used instead. This enzyme has been previously reported to catalyse the oxidation of H_2 in the presence of O_2 and as such has received attention for use in applications such as membrane-less H_2/O_2 fuel cells.[283] Furthermore, the adsorption of Hyd-1 onto carbon

particles has previously been reported and occurs readily.[212]

Electrochemistry was used to determine the effect of O_2 on H_2 oxidation at potentials relevant to H_2-driven NADH generation. These experiments used the previously described protocols (Section 2.1.4). An enzyme film was adsorbed onto a PGE RDE and placed in a sealed cell. Mass flow controllers were used to precisely control the gas atmosphere in the headspace above the solution. The electrode was rotated at 3000 rpm to ensure good mass transport and the current was recorded as a function of potential. At the start of the experiment, only H_2 was used, after the first scan this was changed to include 2 % O_2.

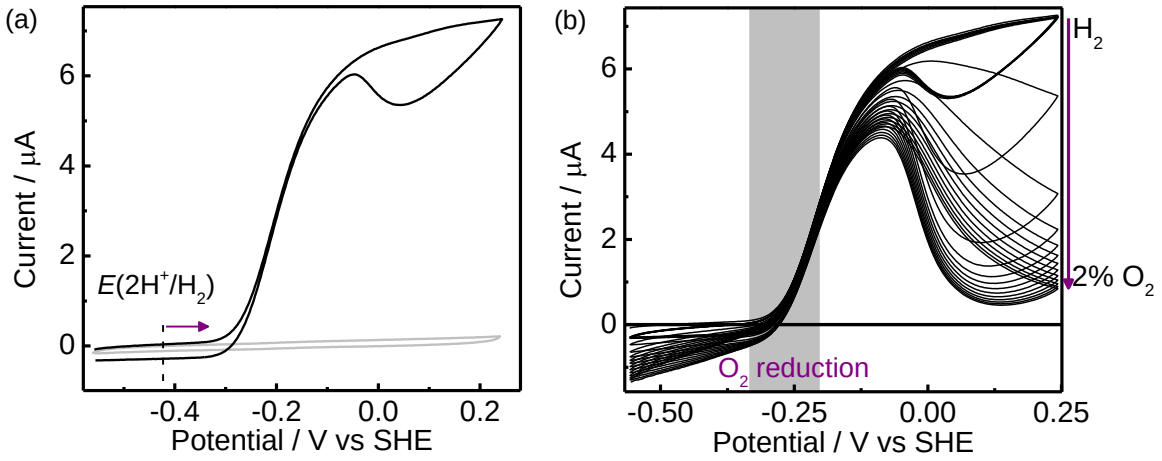

Figure 7-3: Electrochemical experiments to show the effect of O_2 on H_2 oxidation by Hyd-1. (a) Cyclic voltammogram showing the overpotential required for H_2 oxidation (purple arrow) by Hyd-1 in the presence of 1 bar H_2. (b) Cyclic voltammograms from a Hyd-1 modified electrode after changing the gas atmosphere from 100 % H_2 to 2 % O_2 in H_2. The grey shaded portion marks the region in which it is thermodynamically possible to couple H_2 oxidation and NAD^+ reduction. In each case the electrode was rotating at 3000 rpm and the solution contained 50 mM KPB, pH7. The gas mixtures were flowed through the head space at 100 mL min^{-1}.

The cyclic voltammogram in Figure 7-3(a) shows H_2 oxidation by an electrode modified with Hyd-1. A clear catalytic wave for H_2 oxidation current is seen, however this does not commence until *ca* 80 mV above the thermodynamic potential under these conditions (denoted by the dotted line), and no H^+ reduction activity is seen. On the oxidative sweep, as the potential becomes more positive than *ca* -0.1 V *vs* SHE, the catalytic current levels off. This is due to high potential inactivation of the hydrogenase. On the reductive sweep, there is a clear reactivation peak (Section 5.2.1). This is as expected and correlates well to the

literature.[265] Figure 7-3(b) shows the change in activity after the gas mixture was changed from 100 % H_2 to 2 % O_2 in H_2 (demonstrated by the arrow). The shape of the cyclic voltammogram changed in the presence of O_2; at high potentials (> -0.1 V *vs* SHE) the magnitude of the catalytic current decreased suggesting that a much larger proportion of hydrogenase enzyme had been inactivated. However, on the return scan, all of the H_2 oxidation activity was recovered below *ca* -0.15 V *vs* SHE. The shaded region in (b) denotes the approximate potentials that Hyd-1 and NAD^+-reductase modified particles access under these conditions (in the presence of 1 mM NAD^+). In this potential window there was no observed effect on H_2 oxidation activity by Hyd-1, however there was a significant reduction current due to direct O_2 reduction at the carbon electrode. In the particle system, this may lead to a decrease in the rate of H_2-driven NADH generation due to a diversion of the electrons from NAD^+ reduction towards O_2 reduction. In a recent report, Evans *et al.* provided evidence that it is the higher availability of electrons from the medial FeS cluster in O_2-tolerant hydrogenases which facilitates complete reduction and removal of O_2 from the active site and allows H_2 oxidation in the presence of O_2.[286]

Other O_2-tolerant hydrogenases from *Salmonella enterica*[179,291] and *Ralstonia eutropha*[184,278,279,292,293] have also been reported and characterised in the literature; however only *E. coli* Hyd-1 is investigated here due to the high activity and evidence of facile adsorption onto a range of carbon materials.[212]

7.1.3 Coupling H_2 oxidation and NAD^+ reduction

In Section 5.3.1 an electrode modified with a hydrogenase and an NAD^+-reductase was analysed electrochemically. Catalytic currents due to both H_2 oxidation and NAD^+ reduction were observed. Here, the same techniques were used to compare an electrode modified with NAD^+-reductase and either *D. v* MF or Hyd-1. Each cyclic voltammogram was recorded under identical conditions; H_2-saturated mixed buffer, pH 7 with NAD^+ (1 mM) at 20 ^oC.

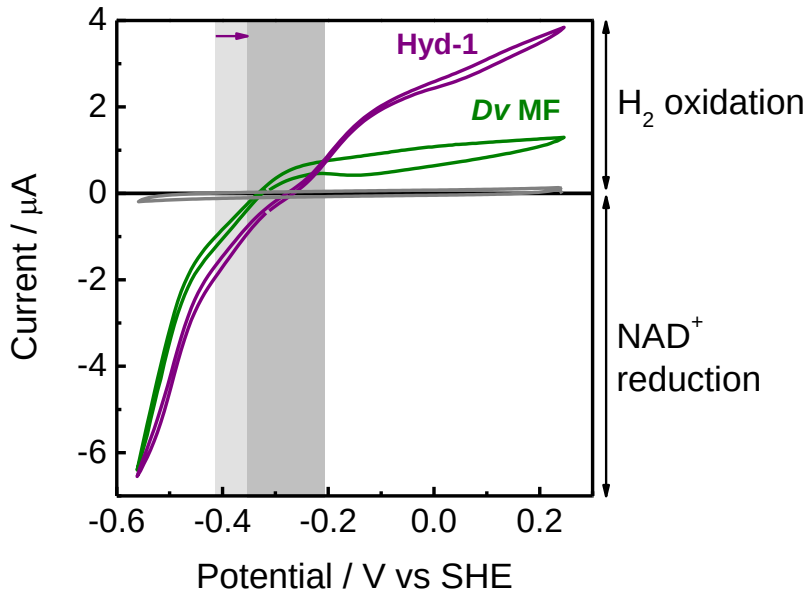

Figure 7-4: Cyclic voltammetry comparing an electrode modified with Hyd-1 and NAD^+-reductase (purple) to *D. v* MF and NAD^+-reductase (green). Experiments performed in H_2 saturated mixed buffer, pH 7, with NAD^+ (1 mM), electrode rotation rate of 2000 rpm. The shaded regions together denote the thermodynamic potentials of the $2H^+/H_2$ and NAD^+/NADH couples under these conditions. The effect of an overpotential (purple arrow) leads to a smaller potential window (dark grey) for coupling H_2 oxidation to NAD^+ reduction. The overpotential requirement for H_2 oxidation by Hyd-2 is denoted by the light grey shaded region.

The cyclic voltammogram (purple) in Figure 7-4 demonstrates that Hyd-1 and the NAD^+-reductase were both catalytically active when co-immobilised on a PGE RDE under the same conditions. Good catalytic currents for both H_2 oxidation and NAD^+ reduction were observed. The current trace cuts the *x*-axis sharply between E_{onset} for H_2 oxidation by Hyd-1 and the NAD^+/NADH couple under these conditions (dark grey box). For comparison, a cyclic voltammogram of *D. v* MF hydrogenase and NAD^+-reductase is overlaid (green); the light grey box marks the additional potential window for H_2-driven NADH generation when using *D. v* MF and the current crosses the *x*-axis close to the mid-point between the thermodynamic potentials for the redox couples (entire shaded region). It is clear that the cyclic voltammogram with Hyd-1 cuts the *x*-axis at a more positive potential than the cyclic voltammograms with *D. v* MF; this is as expected due to the overpotential for H_2 oxidation by Hyd-1. For this reason, a high ratio of hydrogenase to NAD^+-reductase may be required to increase the availability of electrons *via* the particle and thus achieve H_2-driven NADH

generation with high activity per NAD^+-reductase (see 5.5.1).

7.2 H_2-driven NADH supply in the presence of O_2

**The experiments in this section were performed by Ms Chloe Tomlinson under my supervision*

This section describes experiments for adapting the enzyme-modified particle system for H_2-driven NADH generation in the presence of O_2. The effect of different O_2 partial pressures on the rate of H_2-driven NADH generation using particles modified with Hyd-1 and NAD^+-reductase was investigated. Hyd-1 was co-immobilised on BP particles with NAD^+-reductase (Hox~~HY~~FU, 25 μg). The enzyme-particle mixture was left at 4 ^oC for 1 hour and the excess enzyme removed by centrifugation. Following the standard procedure developed in Chapter 5, *in situ* UV-vis spectroscopy was used to calculate the activity of the particle system. An aliquot of the particles (10 μL) was injected into a cuvette containing H_2-saturated buffer and NAD^+ (2 mM). UV-vis spectra were recorded every 2 minutes and the gas atmosphere changed using mass flow controllers. The spectra were baseline corrected and the absorbance at 340 nm plotted with respect to time.

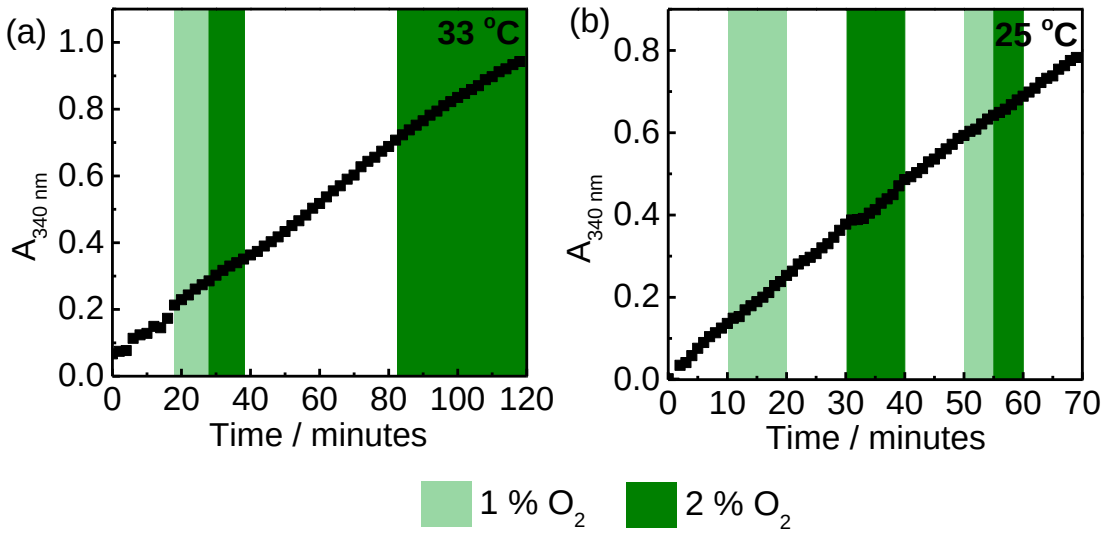

Figure 7-5: H_2-driven NADH generation in the presence of O_2. UV-vis spectra taken over time after addition of particles modified with hydrogenase (Hyd-1) and NAD^+-reductase (Hox~~HY~~FU) to a H_2-saturated solution containing NAD^+ (2 mM). The gas mixture was changed to 1 % O_2 in H_2 or 2 % O_2 in H_2 as indicated by the light and dark green regions, respectively. Experiments performed in KPB, pH 7 at 33 ^oC (a) and 25 ^oC (b).

This experiment was performed at two temperatures for comparison. The NAD^+-reductase is most active at 33 ^oC but more stable at 25 ^oC. The time series in Figure 7-5(a) shows an increase in absorbance at 340 nm after addition of the enzyme-modified particles. At the start the gas atmosphere was 100 % H_2; at well-defined times this was changed to incorporate either 1 or 2 % O_2 as indicated by light or dark green regions, respectively. It is clear that the enzyme-modified particles sustain catalysis in the presence of 2 % O_2 (within the safe limit of O_2 in H_2). In Figure 7-5(a) a slight decrease in activity was seen on addition of O_2; it is likely that this was due to H_2-derived electrons being used for direct reduction of O_2 at the particle thus decreasing the availability of electrons for NAD^+ reduction and slightly increasing the potential of the particle such that the driving force for NAD^+ reduction was lowered. The original activity seems to be restored on removal of O_2 suggesting that the availability of electrons increased and that the system was not irreversibly damaged.

Another experiment was performed at a slightly lower temperature (25 ^oC, Figure 7-5(b)) using particles prepared in the same way. The resulting time series is similar to that in Figure 7-5(a) showing an increase in absorbance at 340 nm. However, at this lower temperature there was no observable decrease in NADH generation activity. It is possible that at this lower temperature, the NAD^+-reductase is less active and therefore not limited by the availability of electrons from the particle hence the effect of O_2 reduction at the particle was less obvious. Overall, the results show clear H_2-driven NADH generation activity in the presence of low but significant O_2 partial pressures.

7.3 Use of biphenyl-2-ol 3 monooxygenase (HbpA)

There are three key examples of using HbpA for the oxidation of biphenyl-2-ol to 2,3-dihydroxybiphenyl in the literature.[294,295] These used either indirect electrochemistry (with a Rh mediator)[294] or enzymatic cofactor regeneration systems (formate/alcohol dehydrogenase).[295,296] The electrochemical system suffered from O_2 reduction by the Rh

catalyst decreasing its overall activity. Furthermore, direct O_2 reduction at the electrode lead to generation of H_2O_2 which was likely to inhibit the enzyme. To compensate for this, a large quantity of catalase was used for disproportionation of the H_2O_2 into water and O_2. The overall turnover number (TN, moles of product formed per mole of cofactor used) was 10, very low in comparison to standard enzymatic cofactor regeneration techniques, and the turnover frequency (TOF) of the mediator was 11 h^{-1} (0.003 s^{-1}). In another report, Schmid *et al.* demonstrated use of a biphasic system to improve the kinetics of the HbpA system. A decanol layer with substrate (110 mM) provided efficient product extraction; overall the aqueous layer contained a product concentration of *ca* 0.16 % of that in the organic layer. Formate dehydrogenase was used for cofactor recycling; sodium formate (160 mM) was added to the aqueous phase (40 mL), substrate (110 mM) was added *via* the organic phase (160 mL). This achieved 23 % conversion of substrate to product with TN of 506 moles of product per mole of cofactor.[296]

In this Thesis suitable protocols for H_2-driven NADH supply to biphenyl-2-ol 3 monooxygenase (HbpA) were considered. It is known that the HbpA is severely substrate and product inhibited (with 25 % inhibition at 3 mM substrate)[107] and that the product is unstable with respect to oxidation. For this reason, experiments were performed on short time scales where possible and with a maximum substrate concentration of 2 mM. A logical approach would be use of high catalyst loading, however the carbon particles used often lead to significant adsorption of some organic molecules and therefore the effect of substrate and product (biphenyl-2-ol and 2,3-dihydroxybiphenyl) adsorption onto the BP particles was investigated. The previous section demonstrated that the enzyme-modified particles were able to sustain catalysis of H_2-driven NADH generation in the presence of 1-2 % O_2 in 98-99 % H_2, the effect of these mixtures on the activity of HbpA were therefore investigated.

7.3.1 Adsorption of substrate and product onto BP particles

Experiments were designed to quantify the amount of adsorption of substrate (biphenyl-2-ol) and product (2,3-dihydroxybiphenyl) onto carbon particles and investigate use of acetonitrile for extraction, Figure 7-6. Stock solutions (1 M) of substrate and product were prepared in DMSO to aid solubility before diluting in water to 1 mM. To aliquots of these solutions (1 mL) BP particles were added to give final loadings of 0.02, 0.2 and 2 mg mL^{-1}. Each sample was prepared in triplicate. After 2 hours the mixtures were sedimented by centrifugation and a portion of the supernatant removed (200 µL) and diluted (to 1 mL) for HPLC analysis. Acetonitrile (200 µL) was added to the remaining experiments, the solutions mixed, left for 2 hours, and an aliquot of the supernatant (250 µL) diluted for analysed using HPLC. The area of the substrate and product peaks were recorded and compared to known standards. The results are plotted in Figure 7-6.

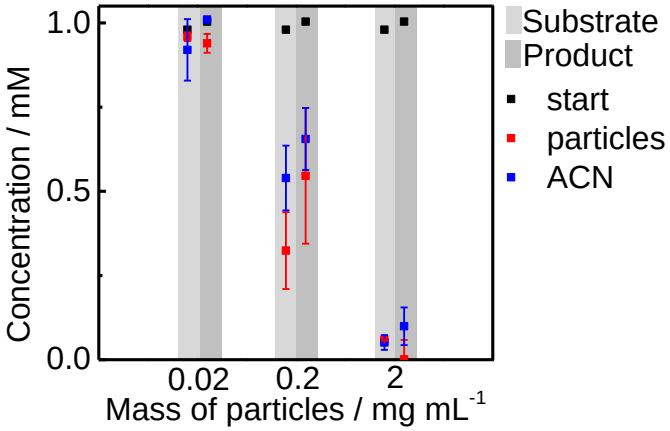

Figure 7-6: Adsorption of substrate (light grey) and product (dark grey) onto BP particles. Aliquots of BP particles were added to solutions containing substrate or product and analysed after 2 hours before (red). The effect of mixing the particle suspensions with acetonitrile was also analysed (blue). The initial samples were also analysed (black). The samples were analysed using HPLC, protocol detailed in Appendix E.

The results in Figure 7-6 demonstrate the adsorption of substrate and product onto BP particles over the course of 2 hours. After exposure to particles (0.2 mg mL^{-1}), approximately half of both the substrate and product were adsorbed with nearly all adsorbed at higher particle loading (2 mg mL^{-1}). A slight increase in the amount of substrate and product detected was

seen after addition of acetonitrile. This data suggests that if particles loadings less than 0.2 mg mL^{-1} are used, the ratio of substrate and product detected using HPLC should be representative of the extent of reaction, although the measured concentrations are likely to be an underestimate.

7.3.2 Activity of HbpA in low O_2 mixtures

**This experiment was performed by Ms Chloe Tomlinson under my supervision.*

Experiments analysing the rate of consumption of NADH by HbpA in the presence of biphenyl-2-ol at a range of O_2 partial pressures were carried out. For each experiment a solution containing biphenyl-2-ol (0.2 mM) and NADH (0.02 mM) in buffer (Tris-HCl, pH 8) was saturated with a chosen gas mixture. An aliquot of HbpA was injected and the sample analysed using UV-vis kinetics at 340 nm to observe NADH consumption activity. The gas mixture was not continuously bubbled as only an initial activity was recorded, therefore the concentration of O_2 in solution would not be significantly changed on the required timescale.

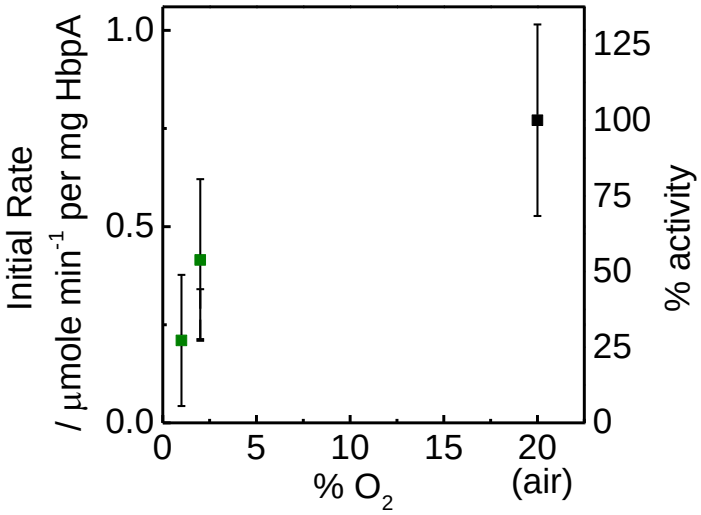

Figure 7-7: The activity of HbpA in different gas mixtures. Solutions containing NADH (0.02 mM) and substrate (0.02 mM) were prepared and saturated with either air (black) or a mixture of O_2 in H_2 (green). An aliquot of HbpA was then injected and the rate of NADH consumption recorded. Experiments performed in Tris-HCl, pH 8 at 25 ^oC, gas mixtures prepared using mass flow controllers.

The results in Figure 7-7 show that HbpA maintains a significant portion of activity at low O_2 partial pressures. Approximately half the activity was retained at 2 % O_2 in H_2 and 25 % at

1 % O_2. This result demonstrates that 1-2 % O_2 in H_2 is an appropriate gas atmosphere for HbpA catalysis and thus the enzyme is suitable for use in the enzyme-modified particle system.

7.4 H_2-driven NADH supply to HbpA

**This experiment was performed by Ms Chloe Tomlinson under my supervision.*

The enzyme-modified particles were investigated for NADH supply to HbpA. An aliquot of BP particles modified with Hyd-1 and NAD^+-reductase (Hox~~HY~~FU, 16 µg), were injected into a H_2-saturated solution containing NAD^+ (0.5 mM) to give a particle loading of 0.2 mg mL^{-1}. The experiment was performed in a sealed UV-vis cuvette (with bubbling of H_2 for the first 120 minutes). UV-vis spectra were recorded every 1-2 minutes, baseline corrected using the previously described methods, and the absorbance at 340 nm plotted as a function time (Figure 7-8). After 22 minutes, an aliquot of substrate (biphenyl-2-ol) was injected to give a concentration of 0.5 mM. An aliquot of air saturated HbpA (20 µL, 74 µg) was injected at 27 minutes. Further injections of air (100 µL) were made as indicated.

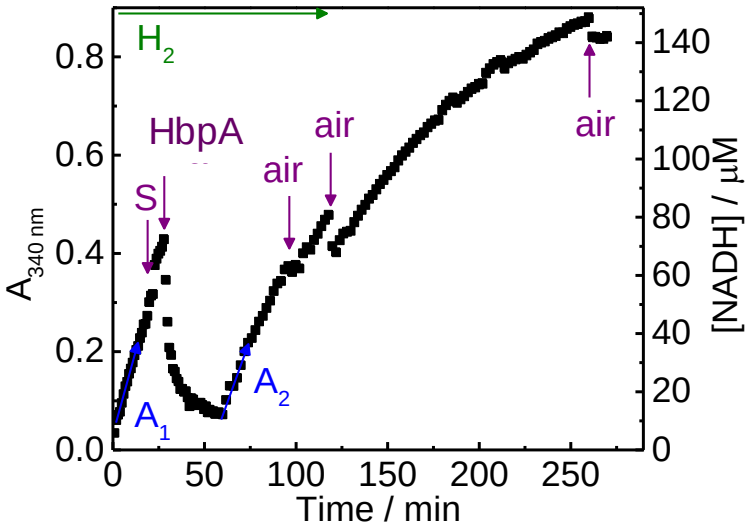

Figure 7-8: UV-vis spectroscopy was used to understand H_2-driven NADH supply to FMO. A plot of absorbance at 340 nm and therefore concentration of NADH as a function of time after addition of particles modified with hydrogenase (Hyd-1) and NAD^+-reductase (Hox~~HY~~FU) to H_2-saturated buffer containing NAD^+ (0.5 mM). Substrate (S), air-saturated FMO (20 µL) and air (100 µL) were injected as indicated by the arrows.

The results in Figure 7-8 show an increase in NADH concentration over the first 25 minutes demonstrating H_2-driven NADH generation with an activity of 0.14 µmole min^{-1} per mg NAD^+-reductase (A1). There was no observable change to the activity of the particles after injection of substrate (S). This is as expected since there should be no interaction between the substrate and the cofactor in the absence of HbpA and O_2. After injection of air-saturated HbpA the absorbance at 340 nm, and therefore the concentration of NADH, started to decrease. This is consistent with the HbpA using O_2 and NADH to oxidise the substrate. At *ca* 60 minutes, the concentration of NADH began to increase again at a rate of 0.095 µmole min^{-1} per mg NAD^+-reductase (A2), suggesting that either the substrate or the O_2 had been used up or that the enzyme had reached its equilibrium point. Subsequent injections of O_2 did not significantly affect the activity of the particles suggesting that no further conversion occurred.

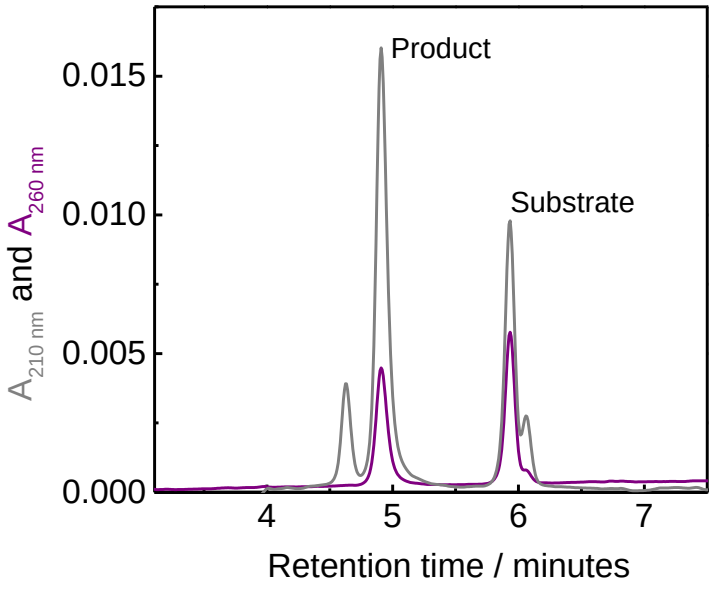

Figure 7-9: Analysis of the final reaction after the experiment in Figure 7-8. An HPLC chromatogram confirming generation of product (4.8 minutes) from substrate (5.9 minutes). The absorbance at 260 nm (purple) and 210 nm (grey) are shown.

An aliquot of the final mixture was analysed by HPLC. Acetonitrile was added to the particle suspension (0.2 mg mL^{-1} particles) to facilitate extraction of adsorbed substrate and product. The particles were then removed by centrifugation and the supernatant passed through a

30 kDa cut-off filter to remove excess enzyme (since the HbpA was used in solution). Integration of the substrate and product peaks and comparison to ratio standards suggests 33 % conversion; this is consistent with the UV-vis results which suggested consumption of *ca* 0.2 mM NADH.

The significant extent of substrate to product conversion calculated from the chromatogram confirms that the enzyme-modified particles provide a suitable approach to driving NADH-dependent monooxygenases.

7.5 Summary

This Chapter has demonstrated the operation of H_2-driven catalytic beads in the presence of O_2 by using an O_2-tolerant hydrogenase for H_2 oxidation catalysis. Although the overpotential requirement of the O_2-tolerant hydrogenase decreases the overall thermodynamic driving force for H_2-driven NAD^+ reduction, substantial activity for NADH generation was observed. The catalytic beads were further shown to supply NADH to a monooxygenase, HbpA, for the selective oxidation of biphenyl-2-ol to 2, 3-dihydroxybiphenyl. At least 30 % conversion to the oxidised product was seen; this result is competitive with existing approaches to using HbpA.[294–296]

As with use of the particles for hydrogenation reactions, these methods are appropriate for supply of NADH to other O_2-dependent enzymes including cytochrome P450s which are able to catalyse the oxidation of many substrate classes, including gaseous alkanes which may have applications in generation of convenient fuels for example ethanol and methanol.[114,115]

Chapter 8 Electrochemical devices for cofactor-dependent oxidation reactions

**Work in this Chapter includes experiments performed by part II students under my supervision (Ms J. Bradley, Mr T. Lyle and Mr B. Bluestone). A book chapter reviewing 'Bioelectrocatalysis for Direct Alcohol Fuel Cells' has been published. H. A. Reeve and K. A. Vincent, in Catalysts for Alcohol-Fuelled Direct Oxidation Fuel Cells, eds. Z.-X. Liang and T. s. Zhao, RSC, 2012, pp. 206–226.*

In the preceeding Chapters, cofactor regeneration systems have been developed and employed to simplify the use of cofactor-dependent enzymes for selective ketone reduction (Chapter 6) or O atom insertion (Chapter 7) reactions. However, there are other biotechnologies which would benefit from more efficient cofactor recycling, for example extracting energy from molecules such as sugars or waste products using enzyme catalysed fuel cells or using the substrate selectivity of many cofactor-dependent enzymes in self-powered biosensors. The electro-enzymatic cofactor regeneration system enables 'wiring' of any cofactor-dependent enzyme to an electrode; in this Chapter the possibility of using this approach in

electrochemical devices is explored.

8.1 Introduction

Electrochemical devices like fuel cells and electrochemical sensors rely on coupling two half reactions. In applications where selectivity is crucial – towards either substrate (biosensors) or product (fuel cells providing both electricity and desirable products) – enzymes could be considered as ideal catalysts. However, a significant limitation lies in the difficulty of wiring such enzymes to the electrode preventing electron transfer from occring.[11] Although there have been reports of an ethanol dehydrogenase from *Comanomas testosterone* and a cellobiose dehydrogenase from *Phanerochaete chrysosporium* undergoing direct electron transfer with an electrode during catalytic turnover,[297–299] more flexible systems allowing a range of molecules to be used as an energy source for a fuel cell, or target for a biosensor are desirable. Here, the NAD^+-reductase is assessed as a method for linking an NAD-depedent enzyme to an electrode. The reactions of interest tends to be an oxidation (of sugars or waste products), requiring stoichiometric NAD^+; the NAD^+-reductase will therefore be used to either sense NADH or regenerate the oxidised cofactor, NAD^+ by NADH oxidation.

Biosensors that have electrodes for the oxidation of NADH have been extensively investigated.[300] Due to the large overpotential requirement at standard electrodes (Section 1.4.2) and the relatively low thermodynamic potential for the NAD^+/NADH couple, electrodes for NAD^+ reduction would have to operate at impractical potentials (more negative that -1 V *vs* SHE) where undesired redox processes may interfere with the sensor system and are rarely reported in the literaure.[301] Similarly to electrochemical methods for NAD^+ reduction, mediators that can transfer 2 electrons and a proton are beneficial for NADH oxidation. In a biosensor the mediator should remain in close proximity to the electrode and preferably be immobilised. A range of redox dyes including meldola blue on a Sol-gel derived carbon composite electrode and methyl green in a carbon paste have been

trialled.[302,303] Similarly, enzyme-catalysed fuel cells obtain energy from molecules by coupling 'fuel' oxidation to O_2 reduction and thus require NADH oxidation to occur at the anode.

It has been previously demonstrated that the NAD^+-reductase enzymes from both *R. e* and *Rh. o* are bidirectional and therefore able to catalyse the oxidation of NADH using an electrode as an electron sink. The results in Chapter 4 suggested that the NAD^+-reductase from *Rh. o* may be more appropriate for operation in this direction due to a slightly lower catalytic bias towards NAD^+ reduction. The electro-enzymatic system developed in this work is a highly adaptable approach and may allow catalysis by any NAD^+-dependent enzyme to be either monitored or driven electrochemically.

8.1.1 Electrochemical devices set-up

An operational fuel cell or self-powered biosensor only requires two electrodes, an anode and a cathode. The two half reactions, chosen due to the appropriate spacing of their thermodynamic potentials, are catalysed at these electrodes. The potential is not externally applied and therefore no reference electrode is needed. In essence, the set-up operates in the same way as the H_2-driven particle system except that the oxidising an reducing enzyme moieties are separated onto two electrodes and the flow of electrons between them is either monitored or collected. The activity of the set-up (recorded as power or current) depends on the difference in the thermodynamic potentials of the half reactions, the potential at which the reactions are seen electrochemically, the activity of the two catalysts and the ratio of catalyst loading. In this Chapter, the anode was a carbon electrode modified with NAD^+-reductase catalysing NADH oxidation. During these developmental experiments the cathode used was a Pt wire for catalysis of O_2 reduction. Other cathode systems could be used including a laccase enzyme for O_2 reduction[14,304] or a hydrogenase for H^+ reduction. Although these options are not investigated here they are considered in the discussion sections.

For initial experiments a glass vial was used as an 'electrochemical device'. The cell was assembled using a carbon paper anode and a Pt cathode. The electrolyte (buffer) was air saturated to ensure a plentiful supply of O_2. The electrodes were connected to an analogue variable resistor (Time Electronics Decade Resistance Model 8000) and a digital voltmeter (Keithley 195A, internal resistance *ca* 1 GΩ). This allowed the potential to be recorded as a function of resistance. Using Equations [8-1] and [8-2], the current and power were calculated.

$$V = IR \qquad [8\text{-}1]$$

$$P = IR^2 \qquad [8\text{-}2]$$

Plots of either current *vs* potential difference or current *vs* power were constructed and compared for three different systems by changing the resistance between the anode and cathode, Figure 8-1.

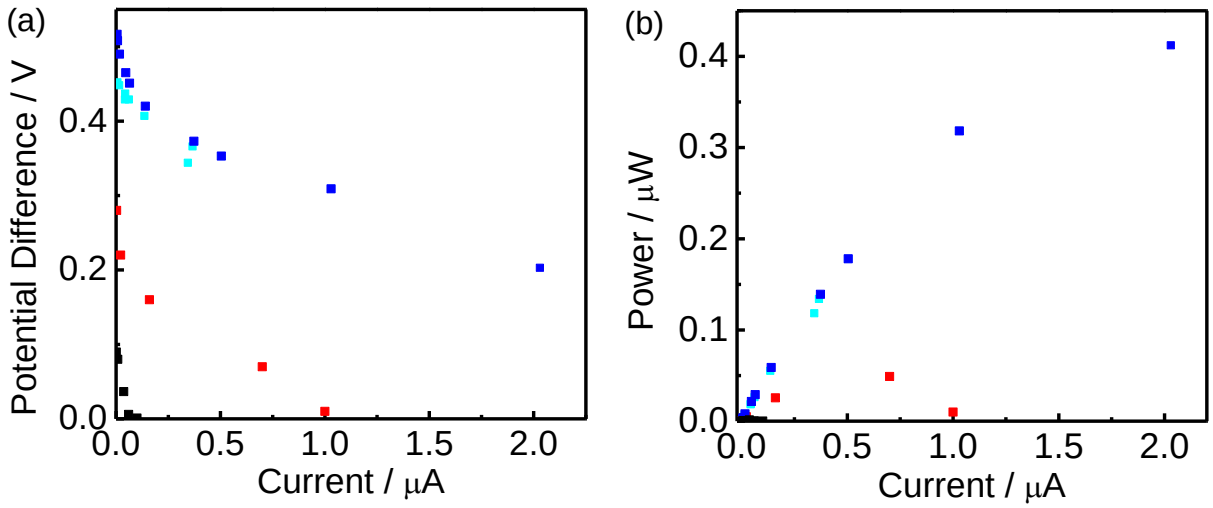

Figure 8-1: Comparison of different biosensor set-ups. (a) A plot of potential difference versus current. (b) A plot of power against current. The blue plots were conducted in the presence of NADH (1 mM) and NAD^+-reductase (*R. e* Hox~~HY~~FU, 5 µL) immobilised on carbon paper, dark and blue points correspond to decreasing and then increasing the resitance, respectively. The red plots were conducted in the presence of NADH (10 mM) and no NAD^+-reductase. The black plots were conducted with no NADH or NAD^+-reductase. All experiments were conducted in Tris-HCl buffer (pH 8, 50 mM) at 25 ºC.

First, a 'blank' cell (black) was tested in which the anode was a piece of carbon paper and no NAD^+-reductase or NADH was present. In the second, the same carbon paper electrode was

used, but NADH was added into solution at high concentration (10 mM, red). In the third the carbon paper electrode was modified with NAD^+-reductase (*R. e* Hox~~HY~~FU, 5 µg) and NADH was present in the electrolyte at a moderate concentration (1 mM, blue).

The results in Figure 8-1 compare the three anode systems connected to a Pt cathode at a range of resistances from 100 MΩ to10 KΩ in regular intervals. At the start of the each experiment the resistance was at its maximum (100 MΩ) and at this point the maximum potential difference was recorded and the calculated current was *ca* 0 µA. As the resistance was decreased in a step-wise manner the potential difference dropped gradually and the current calculated increased accordingly, Figure 8-1(a). Due to the large 'electrochemcially silent' window of unmodified carbon electrodes in aqueous buffer, no redox processes were occurring with significant activity. For this reason no significant voltage was observed in the absence of NADH at any resistance and the current was almost negligible across the resistance range used (black). On addition of NADH into solution, NADH oxidation at the unmodified carbon electrode was possible (> +0.2 V *vs* SHE, Section 3.1.2) and an open circuit potential of *ca* 0.28 V was observed at high resistance. As the resistance was decreased, the potential difference decreased and a significant current was calculated. The experiment was repeated with an NAD^+-reductase-modified carbon paper electrode; a higher open circuit potential was recorded and a much higher current calculated. These results demonstrate that the NAD^+-reductase enabled NADH oxidation at a less positive potential and with higher activity at any given resistance.

The data was also used to plot power as a function of current, Figure 8-1(b), for each anode. The unmodified carbon paper and NAD^+-reductase modified anode gave maximum power output of 0.05 and 0.4 µW, respectively. Negligible power was observed in the absence of NADH (black).

For the unmodified carbon anodes, the resistance was decreased until the cell potential

approached 0 V. However, as can be seen in Figure 8-1(a) the cell potential for the NAD^+-reductase-modified anode did not reach 0 V over the resistance range used. Care was taken to prevent exposure of the enzyme film to potentials likely to denature the enzyme. At 10 kΩ, the cell potential had reached approximately the same value as that for the unmodified carbon electrode suggesting that any further decrease in resistance may lead to NADH oxidation at the carbon electrode complicating the results, and any further increase in potential was likely to denature the enzyme therefore lower resistances were not used. To determine whether the enzyme was still active the resistance was increased step-wise to the starting value. The cell potentials (light blue) overlay the original values providing evidence that all of the enzyme has remained active over the course of this experiment. The corresponding power calculated for these points are also included in Figure 8-1(b).

Overall, the plots in Figure 8-1 follow the conventional shapes for a fuel cell.[305,306] A significant increase in potential difference and power was observed for the enzyme-modified electrode in comparison to the unmodified carbon electrode; however a higher OCP was expected. It is likely that there was significant O_2 reduction occurring at the carbon electrode contributing to these results. This result provides evidence that the NAD^+-reductase can be used in electrochemical devices either to detect NADH (biosensor) or recycle NAD^+ (fuel cell).

8.2 Towards a glycerol oxidation fuel cell

There are many organic molecules that could be used as energy carriers in enzyme catalysed fuel cells. The most obvious are sugars: Sony have developed an enzyme based bio-battery in which a cocktail of mediators and enzymes trapped at an electrode enable electrons to be extracted from glucose.[307] Tasca *et al.* have demonstrated a cellobiose dehydrogenase with substrate promiscuity incorporated into an Osmium redox polymer that displays a oxidation of lactose, glucose, cellobiose, maltose, mannose,galactose and xylose.[308] However, there are

concerns over using sugar molecules as a fuel source since they can also be used as food.

Enzymes may not compete with existing metal catalyst technologies for high power generation however they may allow complex molecules or fuel mixtures to be used in more 'niche' applications. Glycerol is a very versatile organic compound when pure and has a wide range of uses. It is the back bone of fats and fatty acids and produced in large quantities as a by-product during the esterification in biodiesel production,[309] Scheme 8-1. Ways to efficiently convert this large, cheap, but impure glycerol stock into value-added compounds are desirable. There are many valuable oxidation products of glycerol, in particular dihydroxyacetone (DHA); using traditional methods, selectivity and over oxidation are a problem. Using an enzyme catalysed fuel cell it could be possible to both generate electricity and an added-value product using a crude waste product as a fuel.

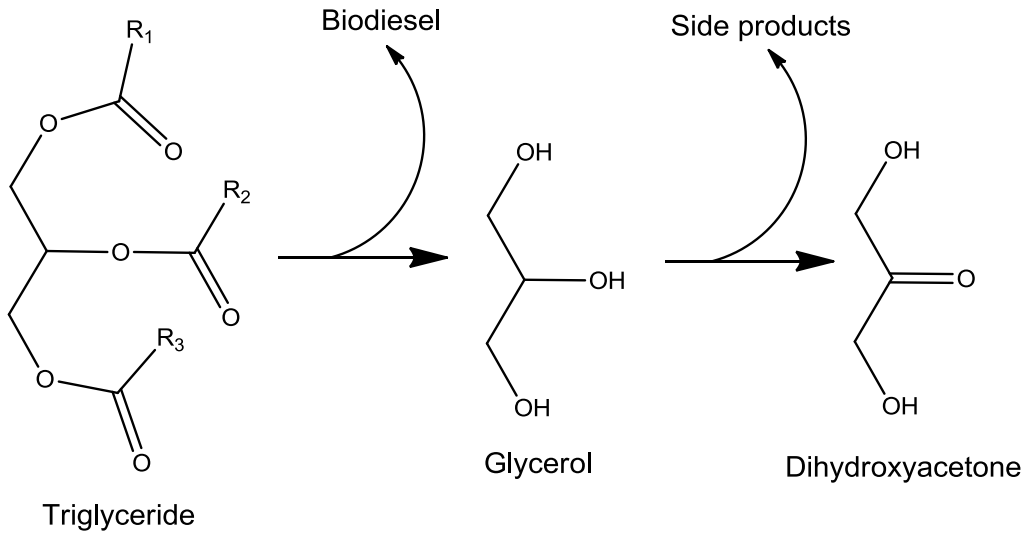

Scheme 8-1: Production of a value-added product from glycerol, a waste product of biodiesel production.

Glycerol dehydrogenases are a class of cofactor-dependent enzymes which are able to selectively oxidise glycerol using $NAD(P)^+$ as an oxidising equivalent. A number of these enzymes have been isolated and shown to have different selectivity for either the primary or secondary alcohol.[310,311] This Section therefore aims to use an NAD^+-reductase and a glycerol dehydrogenase to extract electrons from glycerol.

8.2.1 Limitations to using glycerol dehydrogenase

Many cofactor-dependent oxidation reactions have unfavourable equilibrium constants. This can be a significant limitation to using such enzymes for selective oxidations in chemical synthesis but is also a problem in their application in fuel cells.

$$Glycerol + NAD^+ \rightleftharpoons DHA + NADH + H^+ \quad [8\text{-}1]$$

$$k = \frac{[DHA][NADH][H^+]}{[Glycerol][NAD^+]} \approx 10^{-12} \quad [8\text{-}2]$$

Using Equation [8-1] an equilibrium constant, *k* (Equation [8-2]) can be derived. Liepens *et al*. have estimated this for a glycerol dehydrogenase from *Aspergillus niger* to be 3.1-4.6 x 10^{-12} M.[312] Thus a high pH and continuous product removal alongside efficient cofactor recycling are essential for high conversion. Here developments towards using an enzyme modified electrode for NADH oxidation to supply glycerol oxidation are investigated.

8.2.2 Electrochemical response from glycerol injections

In Section 6.3.2 the NAD^+-reductase and a LDH were co-immobilised on an electrode and the interaction between the two enzymes was monitored electrochemically. On addition of substrate, cofactor was cycled between the two enzymes and a change in catalytic current observed. Here, the NAD^+-reductase and the glycerol dehydrogenase were co-immobilised on a PGE RDE and analysed in the same way to determine if the enzymes cycled cofactor between them.

Initially a control experiment was performed to investigate the effect of glycerol on NAD^+-reductase activity. An electrode modified with only NAD^+-reductase was poised at 0 V *vs* SHE in the presence of NADH (1 mM) and the current monitored following injections of glycerol to give a cell concentration of 2.5, 5, 7.5 and 10 mM (as indicated by red arrows, Figure 8-2(a)). A clear catalytic current was observed due to NADH oxidation. There was no observable change to the magnitude of this current in the presence of glycerol. This

demonstrated that glycerol did not inhibit or denature the NAD^+-reductase under the conditions used.

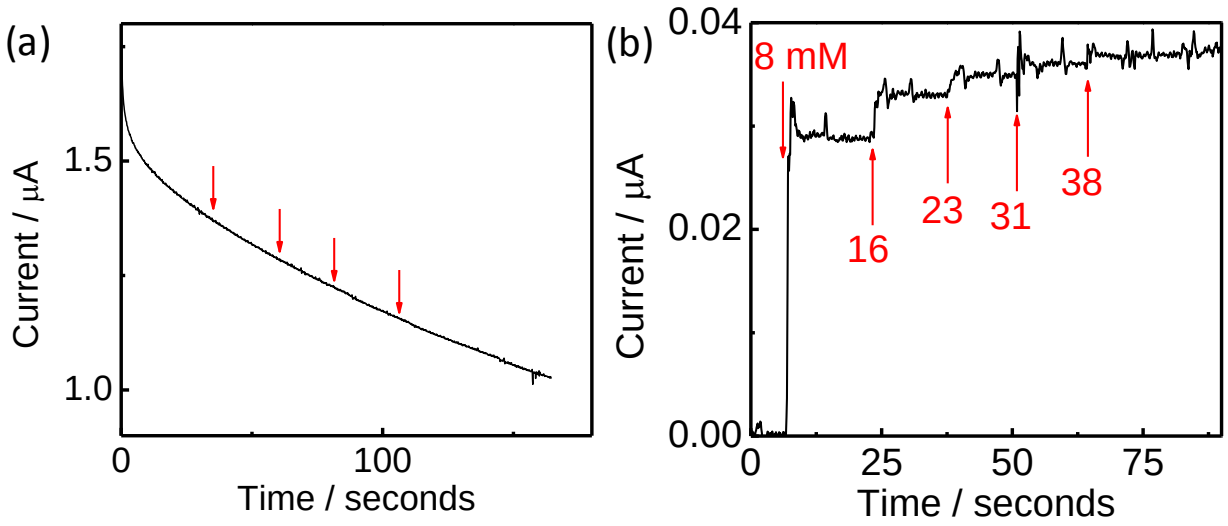

Figure 8-2: Chronoamperometry to test the effect of glycerol injections on a NAD^+-reductase-modified electrode. (a) Current response of an NAD^+-reductase (HoxFU) modified electrode poised at 0 V in the presence of NADH (1 mM). Aliquots of Glycerol (2.5, 5, 7.5, 10 mM) were injected over time to see the effect on the activity of the NAD^+-reductase. (b) Response of an electrode modified with NAD^+-reductase and GlyDH in the presence of NAD^+ (1 mM). Aliquots of glycerol were injected over time as indicated. Electrode rotation rate of 1000 rpm was used, experiment performed in CHES buffer, pH 9.

For the experiment in Figure 8-2(b), the electrode was modified with NAD^+-reductase and glycerol dehydrogenase and poised at an NADH oxidising potential (0 V *vs* SHE). At the start, the cell contained only NAD^+ (1 mM) and therefore no catalytic current was observed. The current was then recorded following injections of glycerol to give an overall cell concentration of 8, 16, 23, 31 and 38 mM (as indicated by red the arrows). The chronoamperometric trace in Figure 8-2 (b) shows that following injections of glycerol a positive current was recorded. This must be due to NADH oxidation by the NAD^+-reductase and therefore a build-up of NADH at the electrode. This scan was performed at 1000 rpm to aid fast mixing of the glycerol and to prevent mass transport limitations. This result is in good agreement with the experiments in Section 6.3.2 and demonstrates that the enzyme-modified electrode can extract electrons from glycerol by cycling the cofactor.

To develop a fuel cell, high surface area electrodes with high enzyme loading would be

required. Here, carbon paper modified with NAD^+-reductase and glycerol dehydrogenase were used following the protocols developed in Chapters 3 and 6. Briefly, the carbon paper was modified with NAD^+-reductase (HoxFU, 100 µg) and glycerol dehydrogenase (10 µg). The carbon paper electrode was then placed into an electrochemical cell containing NADH (1 mM) and poised at an NADH oxidising potential (0 V *vs* SHE). Initially a large NADH oxidation current was observed, indicating a high NAD^+-reductase loading on the carbon paper electrode.

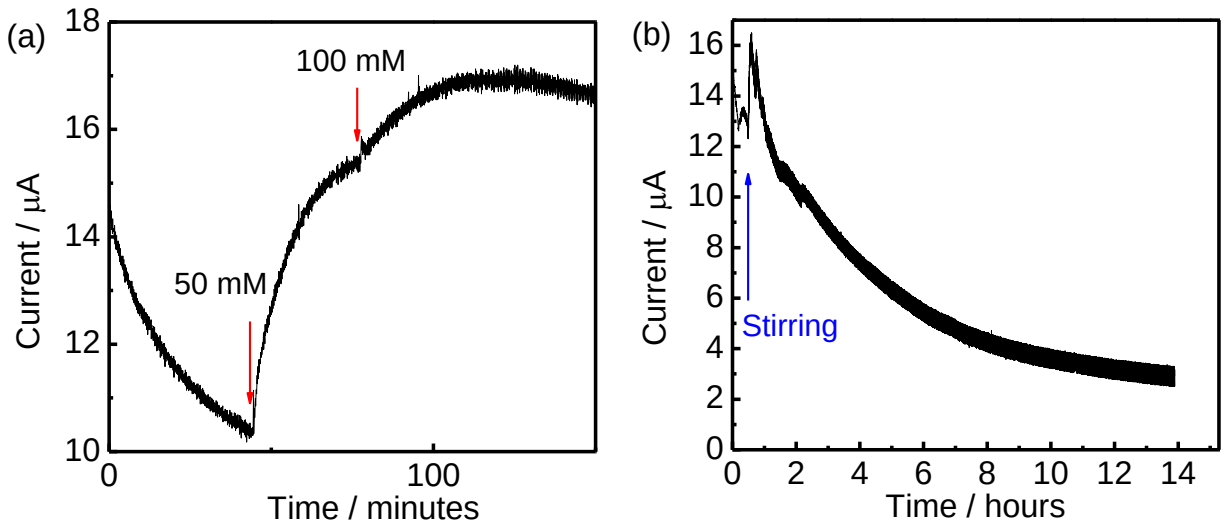

Figure 8-3: Carbon paper electrode modified with a mixture of NAD^+-reductase and glycerol dehydrogenase. (a) Electrode poised at -0.1 V in the presence of NADH (1 mM) in CHES buffer, pH 9. Aliquots of glycerol injected to give a cell concentration of 50 and 100 mM as indicated. (b) This electrode set-up was then left at -0.1 V with the solution stirring for 14 hours. This experiment was performed by Mr Thomas Lyle, Part II student, under my supervision.

The chronoamperometric trace in Figure 8-3(a) shows that a large increase in the magnitude of NADH oxidation current was achieved on addition of glycerol at high concentrations (up to 100 mM). During this experiment, the solution was not stirred, and for this reason the current takes *ca* 30 seconds to reach its maximum value following each injection of glycerol. The effect of stirring is seen in Figure 8-3(b) indicated by the blue arrow. An immediate increase in catalytic current was observed, suggesting that the current was limited by mass transport of glycerol therefore preventing maximum NADH generation by the glycerol dehydrogenase.

The current dropped steadily over the following 12 hours. By integration of the current over the time course of this experiment, 3.2 µmoles of electrons passed through the system. Assuming 100 % current efficiency this corresponds to 1.6 µmoles of NADH and therefore glycerol (= *ca* 0.53 mM) were used. Since the initial concentration of glycerol was high (100 mM), this provides evidence that the loss of activity over time was due to the instability of the enzyme film and not due to loss of glycerol from the system. An estimate of the half-life of the NAD^+-reductase in this system was made assuming that no other competing effects contributed to the loss of current over time. The time taken for the catalytic current to drop by half after the value at 1 hour in Figure 8-3 (b) was 3.9 hours. This is much higher than that determined for the NAD^+-reductase on a PGE electrode for NAD^+ reduction (Section 3.3.1) and corroborates with the theory that the NAD^+-reductase is more unstable at lower potentials. Overall, this result indicates that an electrode modified with the NAD^+-reductase and a NAD^+-dependent enzyme can be used to extract electrons from organic molecules.

8.2.3 Can glycerol dehydrogenase use crude biodiesel waste?

The above experiments used dilutions of pure glycerol. A very powerful niche application of this work could be a low-power fuel cell that generates electricity, an added-value product DHA (and H_2 if coupled to H^+ reduction using a hydrogenase) using impure, waste glycerol. A sample of waste glycerol was obtained, diluted (1:100 with water) and titrated to pH 10 using KOH. Aliquots of NAD^+ (0.2 mM) and glycerol dehydrogenase (0.7 mg) were added, and the sample was monitored using UV-vis spectroscopy to determine if any NADH was produced.

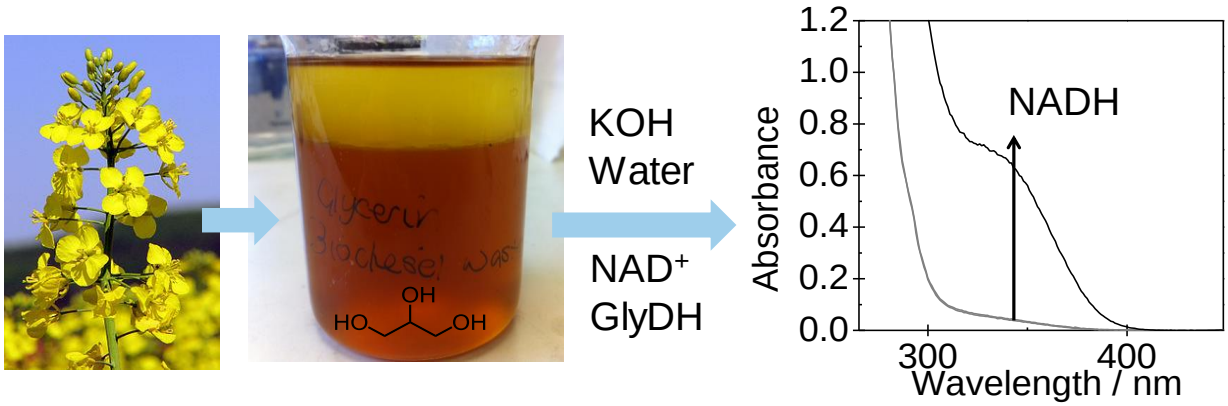

Figure 8-4: Glycerol dehydrogenase was able to generate NADH from NAD^+ in the presence of crude glycerol. UV-vis spectra were recorded before and after addition of glycerol dehydrogenase to a dilution of crude glycerol (1:100 in water) in the presence of NAD^+ (0.2 mM).

The result in Figure 8-4 demonstrates that was possible for the glycerol dehydrogenase to convert NAD^+ to NADH in the presence of unrefined biodiesel waste.

8.3 Development of a biosensor

Using the same approaches as for the glycerol fuel cell the enzyme-modified electrodes could also be used for a self-powered biosensor. Here, the power generated is not important but the selectivity towards a particular substrate is. If successful, any cofactor-dependent enzyme (or a number in series) could be 'linked' to an electrode array *via* the NAD^+-reductase and used to sense a huge library of targets.

Significant amounts of food are discarded since it is not easy to tell if they are spoiled. This is especially a problem with meat. Many of the bacteria that cause illness generate volatile alcohol products. One strategy to detect when food has become spoiled could be inclusion of a selective alcohol sensor in the packaging; alcohol oxidation inside the packaging could be coupled to O_2 reduction outside the packaging. There are also many medical situations that would benefit from 'tailor made' diagnostics of a range of molecules on small samples. For these applications, a high power density is not necessary, however a long linear phase that can quantify generation of VOCs is. Ethanol was used as a test substrate for this work with an

alcohol dehydrogenase from yeast (*y*ADH) as the cofactor-dependent enzyme.

A carbon paper electrode was modified with NAD^+-reductase (*Rh. o*, HoxFU) and *y*ADH. This was put into solution containing NAD^+ (5 mM). The resistance of the cell was held constant at 1 MΩ and injections of ethanol made. The potential difference after each injection was recorded and used to calculate the power generated. The results in Figure 8-5 demonstrate the dependence of the power recorded on the concentration of ethanol.

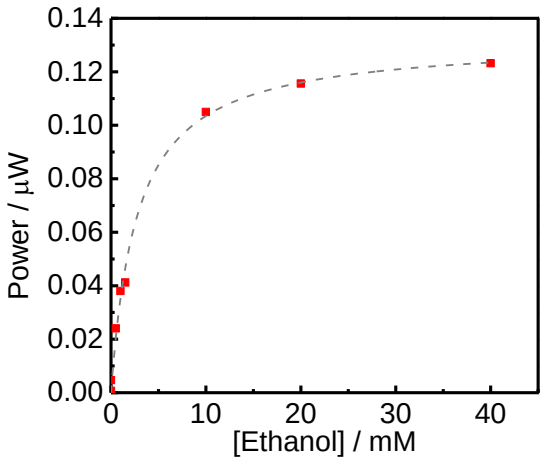

Figure 8-5: Demonstration of an ethanol biosensor. A carbon paper electrode modified with NAD^+-reductase (*Rh. o* HoxFU) and yeast ADH was connected to a Pt wire *via* a resistor (1 MΩ). The electrolyte contained NAD^+ (2.5 mM). The power was calculated following injections of ethanol. Experiments were performed in Tris-HCl buffer (50 mM, pH 8) at 25 ^{0}C.

The results in Figure 8-5 demonstrate that the power increases with increasing ethanol concentration and therefore that ethanol is being 'sensed'. There is a reasonably significant linear phase suggesting that quantitative analysis of the concentration of ethanol injected could be determined in this way. It would be possible to instead link this electrode set up to an LED system that would light up on addition of a target.

8.4 Summary

This Chapter has highlighted some proof-of-concept results for cofactor-dependent electrochemical devices in a fuel cell and a self-powered biosensor set-up. The current densities achieved for a glycerol fuel cell anode were low and although it would be possible to increase these (using the electrodes developed in Chapter 3 and 6), such an approach would

be most beneficial in a niche application where energy generation was a side-product of the selective oxidation reaction. This was investigated for the oxidation of crude glycerol to DHA but by linking to other cofactor dependent enzymes, could be adapted for oxidation of a wide range of sugars and waste products.

In the sensor application, an increase in power was observed on injection of ethanol. This was a promising result and provides evidence that a whole range of targets could be sensed in for a number of applications (medical, food safety and more).

This Chapter also demonstrates that the electro-enzymatic approach is suitable for recycling the oxidised cofactor NAD^+; this may have applications in chemical synthesis, particularly for the partial oxidation of terminal alcohols to generate an aldehyde. Here the selectivity of enzymes to prevent over-oxidation of primary alcohols to the carboxylic acid and for regio-selective alcohol oxidation in polyols is highly advantageous.

Chapter 9 Conclusion

The work presented in this Thesis has demonstrated two novel approaches to recycling the reduced cofactor, NADH using either an electrode or H_2 as the reducing equivalent. Both methods have a range of benefits in comparison to the existing enzymatic approaches, most significantly the very high atom efficiency and reusability of the immobilised enzymes. These factors are likely to simplify product isolation by decreasing the costs associated with product purification and catalyst removal and recovery. Furthermore, the ability to readily reuse the enzymes over multiple cycles decreases the catalyst-to-product costs. Electrochemical cofactor recycling has been extensively discussed in the literature, however there are very few examples of NAD^+ reduction occurring at an appreciable rate and at a moderate potential, and none which generate only enzyme-active NADH. In contrast, Chapter 3 described the development of an electro-enzymatic NADH generation system using an immobilised NAD^+-reductase which showed high current efficiency and selectivity. Other NAD^+-reductase constructs were discussed including a NAD^+-reductase variant suitable for $NADP^+$ reduction and use of a crude enzyme extract. These early stage investigations provide evidence that the

system can be easily adapted and industrially relevant enzyme preparations used. In Chapter 4 the soluble hydrogenase from *Rhodococcus opacus* was electrochemically characterised for the first time and shown to be suitable for use in the cofactor recycling system. Furthermore, this Chapter verifies that the electrochemical characterisation techniques developed in the Vincent Group are suitable for rapid determination of the applicability of NAD^+-reducing enzymes to the electro-enzymatic system using very small quantities of the protein samples.

In Chapter 5 the NAD^+-reductase was coupled to robust hydrogenase enzymes *via* electronically conducting carbon particles. These enzyme-modified particles were shown to catalyse H_2-driven NADH generation with high activity, up to 8 μmole min^{-1} per mg NAD^+-reductase, and high total turnover numbers, >100,000 NADH per NAD^+-reductase. Again, the system was demonstrated using a range of carbon materials, hydrogenase enzyme and NAD^+-reductase constructs.

In Chapter 6, these approaches were used to supply NADH to NADH-dependent enzymes for ketone to alcohol biotransformations. The electrochemical analysis provided evidence that co-immobilisation of the NAD^+-reductase and NADH-dependent enzyme in close proximity offer important advantages over using the NADH-dependent enzyme in solution. The cofactor was 'concentrated' at the electrode surface leading to a higher observed activity of the NAD^+-reductase and also means that a favourable NAD^+/NADH ratio can be maintained locally at the electrode without a need to convert NAD^+ from the bulk, 'unproductive', solution to NADH. When the whole H_2-driven systems were examined, high conversion and selectivity was observed. The results indicated that co-immobilisation increased the activity of the immobilised alcohol dehydrogenase in comparison to alcohol dehydrogenase in solution. Very low cofactor concentrations could be used, and cofactor turnover numbers of over 600 were achieved. By developing methods to increase the substrate concentration it should be possible to reach turnover nubers in the industrially relevant region of 10^3-10^5.

In Chapter 7, the modularity of the particle system was tested and the H_2-driven system was extended to operate in the presence of O_2. This was further used to supply NADH to a monooxygenase enzyme with very promising results for the oxidation of biphenyl-2-ol to 2, 3-dihydroxybiphenyl.

This Thesis has demonstrated and described the characterisation of new techniques for utilising cofactor-dependent enzymes for chemical synthesis. Although ketone to alcohol conversion has been the focus, the systems could be readily optimised to drive other classes of reaction including alkene reduction, imine reduction, ketone to amine conversion and other selective oxidations using O_2. The flexibility of the system could offer advantages in chemical synthesis where long development times are current needed to establish an appropriate biocatalytic pathway particularly when cofactor recycling is required.

Chapter 8 further extended the electro-enzymatic system to proof-of-concept electrochemical devices using the NAD^+-reductase to 'wire' cofactor-dependent enzymes to an electrode for use in adaptable fuel cells or biosensors. The approaches are not limited to the examples demonstrated but could be readily extended for a range of applications from biosensors to detect meat spoilage to fuel cells that convert waste products into value-added products.

The approaches developed in this Thesis simplify the use of cofactor dependent enzymes by allowing enzymes and enzyme cascades to be handled as heterogeneous catalysts and, if adopted by industry may increase implementation of biocatalytic routes.

Bibliography

1. P. Ramesh N, *Curr. Opin. Biotechnol.*, 2001, **12**, 587–604.

2. S. W. May and S. R. Padgette, *Nat Biotech*, 1983, **1**, 677–686.

3. D. Monti, G. Ottolina, G. Carrea, and S. Riva, *Chem. Rev.*, 2011, **111**, 4111–4140.

4. A. S. Bommarius, M. Schwarm, and K. Drauz, *J. Mol. Catal. B Enzym.*, 1998, **5**, 1–11.

5. F. Hollmann, I. W. C. E. Arends, and D. Holtmann, *Green Chem.*, 2011, **13**, 2285–2314.

6. B. M. Nestl, S. C. Hammer, B. A. Nebel, and B. Hauer, *Angew. Chem. Int. Ed. Engl.*, 2014, **53**, 3070–95.

7. A. Wells and H.-P. Meyer, *ChemCatChem*, 2014, **6**, 918–920.

8. D. W. Kimmel, G. LeBlanc, M. E. Meschievitz, and D. E. Cliffel, *Anal. Chem.*, 2012, **84**, 685–707.

9. C. R. Ispas, C. Georgeta, S. Andreescu, and G. Crivat, *Anal. Lett.*, 2012, **45**, 168–186.

10. G. S. Wilson and Y. Hu, *Chem. Rev.*, 2000, **100**, 2693–2704.

11. H. A. Reeve and K. A. Vincent, in *Catalysts for Alcohol-Fuelled Direct Oxidation Fuel Cells*, eds. Z.-X. Liang and T. s. Zhao, RSC, 2012, pp. 206–226.

12. D. Sokic-Lazic and S. D. Minteer, *Electrochem. Solid-State Lett.*, 2009, **12**, F26–F28.

13. R. Gillan, *Chem. Soc. Rev.*, 2007, **36**, C3–C3.

14. S. C. Barton, J. Gallaway, and P. Atanassov, *Chem. Rev.*, 2004, **104**, 4867–4886.

15. J. A. Cracknell, K. A. Vincent, and F. A. Armstrong, *Chem. Rev.*, 2008, **108**, 2439–2461.

16. M. Breuer, B. Hauer, A. Pletsch, and W. Siegel, 2011.

17. Q. Wu, C.-X. Chen, L.-L. Du, and X.-F. Lin, *Appl. Biochem. Biotechnol.*, 2010, **160**, 2026–35.

18. H. M. Moody, T. van der Does, and J. M. Van Der Laan, 2011.

19. A. A. Desai, *Angew. Chemie, Int. Ed. English*, 2011, **50**, 1974–1976.

20. R. Xue and J. M. Woodley, *Bioresour. Technol.*, 2012, **115**, 183–95.

21. D. J. Pollard and J. M. Woodley, *Trends Biotechnol.*, 2007, **25**, 66–73.

22. Industrial Biotechnology Innovation and Growth Team, *Maximising UK Opportunities from Industrial Biotechnology in a Low Carbon Economy*, 2009.

23. *http//www.codexis.com/screening_evolution, Nov 2013 http//www.codexis.com/code_evolver_code_xporter, Nov 2013*.

24. B. M. Nestl, B. A. Nebel, and B. Hauer, *Curr. Opin. Chem. Biol.*, 2011, **15**, 187–93.

25. M. J. Dougherty and F. H. Arnold, *Curr. Opin. Biotechnol.*, 2009, **20**, 486–91.

26. F. G. Mutti, J. Sattler, K. Tauber, and W. Kroutil, *ChemCatChem*, 2011, **3**, 109–111.

27. A. S. Bommarius, J. K. Blum, and M. J. Abrahamson, *Curr. Opin. Chem. Biol.*, 2011, **15**, 194–200.

28. C. K. Savile, J. M. Janey, E. C. Mundorff, J. C. Moore, S. Tam, W. R. Jarvis, J. C. Colbeck, A. Krebber, F. J. Fleitz, J. Brands, P. N. Devine, G. W. Huisman, and G. J. Hughes, *Science (80-.).*, 2010, **329**, 305–309.

29. *http://www.companiesandmarkets.com/News/Chemicals/95-of-pharmaceutical-drugs-to-be-chiral-by-2020/NI3449*, **May 2014**.

30. Y. Ni, D. Holtmann, and F. Hollmann, *ChemCatChem*, 2014, **6**, 930–943.

31. R. A. Sheldon, *Chem. Commun.*, 2008, 3352–3365.

32. G. W. Huisman, J. Liang, and A. Krebber, *Curr. Opin. Chem. Biol.*, 2010, **14**, 122–129.

33. J. Liang, E. Mundorff, R. Voladri, S. Jenne, L. Gilson, A. Conway, A. Krebber, J.

Wong, G. Huisman, S. Truesdell, and J. Lalonde, *Org. Process Res. Dev.*, 2010, **14**, 188–192.

34. J. Liang, J. Lalonde, B. Borup, V. Mitchell, E. Mundorff, N. Trinh, D. A. Kochrekar, R. N. Cherat, and G. G. Pai, *Org. Process Res. Dev.*, 2010, **14**, 193–198.

35. A. Mengel and O. Reiser, *Chem. Rev.*, 1999, **99**, 1191–1224.

36. L. Saudan, *Acc. Chem. Res.*, 2007, **40**, 1309–1319.

37. P. Maki-Arvel, J. Hajek, T. Salmi, and D. Murzin, *Appl. Catal. A*, 2005, **292**, 1–49.

38. J. Magano and J. R. Dunetz, *Org. Process Res. Dev.*, 2012, **16**, 1156–1184.

39. M. V. N. de Souza and T. R. A. Vasconcelos, 2006, **4**, 798–810.

40. T. J. Blacklock, T. K. Jones, D. J. Mathre, and L. C. Xavier, *Pat. number US 5189177 A*, 1993.

41. T. J. Blacklock, T. K. Jones, D. J. Mathre, and L. C. Xavier, *Pat. number EP 0453298 A2*, 1991.

42. B. McNerney, B. Whittlesey, D. B. Cordes, and C. Krempner, *Chem. - A Eur. J.*, 2014, n/a–n/a.

43. T. Ooi, T. Miura, and K. Maruoka, *Angew. Chemie Int. Ed.*, 1998, **37**, 2347–2349.

44. P. Nandi, A. Solovyov, A. Okrut, and A. Katz, *ACS Catal.*, 2014, **4**, 2492–2495.

45. B. T. Cho, *Chem. Soc. Rev.*, 2009, **38**, 443–52.

46. E. Corey and C. Helal, *Angew. CHEMIE-INTERNATIONAL Ed.*, 1998, **37**, 1987–2012.

47. E. J. Corey, R. K. Bakshi, and S. Shibata, *J. Am. Chem. Soc.*, 1987, **109**, 5551–5553.

48. E. J. Corey and J. O. Link, *J. Org. Chem.*, 1991, **56**, 442–444.

49. E. . Corey and C. J. Helal, *Tetrahedron Lett.*, 1996, **37**, 5675–5678.

50. G. S. Silverman and P. E. Rakita, *Handbook of Grignard Reagents*, CRC Press, 1996.

51. R. Noyori, *Nat. Chem.*, 2009, **1**, 5–6.

52. L. Zeng, F. Wu, Y.-Y. Li, Z.-R. Dong, and J.-X. Gao, *J. Organomet. Chem.*, 2014, **762**, 34–39.

53. R. Noyori, *<http//www.nobelprize.org/nobel_prizes/chemistry/laureates/2001/noyori-lecture.html>*, *Nobel Lect. Asymmetric Catal. Sci. Technol.*, 2001, Nobel Media AB 2014. Web. 15 July 2014.

54. R. Noyori, M. Kitamura, and T. Ohkuma, *Proc. Natl. Acad. Sci. U. S. A.*, 2004, **101**, 5356–62.

55. G. Beck, H. Jendralla, and K. Kesseler, *Synthesis (Stuttg).*, 1995, 1014–1018.

56. C. Chen, L. F. Frey, S. Shultz, D. J. Wallace, K. Marcantonio, J. F. Payack, E. Vazquez, S. A. Springfield, G. Zhou, P. Liu, G. R. Kieczykowski, A. M. Chen, B. D. Phenix, U. Singh, J. Strine, B. Izzo, and S. W. Krska, *Org. Process Res. Dev.*, 2007, **11**, 616–623.

57. M. Goto, T. Konishi, S. Kawaguchi, M. Yamada, T. Nagata, and M. Yamano, *Org. Process Res. Dev.*, 2011, **15**, 1178–1184.

58. D. S. Keegan, S. R. Hagen, and D. A. Johnson, *Tetrahedron: Asymmetry*, 1996, **7**, 3559–3564.

59. S. E. Clapham, A. Hadzovic, and R. H. Morris, *Coord. Chem. Rev.*, 2004, **248**, 2201–2237.

60. C. Wang, X. Wu, and J. Xiao, *Chem. Asian J.*, 2008, **3**, 1750–70.

61. S. I. Fujita, Y. Sano, B. M. Bhanage, and M. Arai, *J. Catal.*, 2004, **225**, 95–104.

62. A. Ghosh and R. Kumar, *Microporous Mesoporous Mater.*, 2005, **87**, 33–44.

63. F. Ammari, C. Milone, and R. Touroude, *J. Catal.*, 2005, **235**, 1–9.

64. J. K. A. Clarke, *Chem. Rev.*, 1975, **75**, 291–305.

65. P. Claus, *Top. Catal.*, 1998, **5**, 51–62.

66. M. Tamura, K. Tokonami, Y. Nakagawa, and K. Tomishige, *Chem. Commun.*, 2013, **49**, 7034–7036.

67. D. M. F. Sequeira and C. A. C. Santos, *J. Braz. Chem. Soc.*, 2009, **20**, 387–406.

68. H. Lund and O. Hammerich, Eds., *Organic Electrochemistry*, New York: Marcel Dekker, 4th edn., 2001.

69. R. Francke and R. D. Little, *Chem. Soc. Rev.*, 2014.

70. P. J. Elving and J. T. Leone, *J. Am. Chem. Soc.*, 1958, **80**, 1021–1029.

71. S. G. Mairanovskii, T. Y. Rubinskaya, V. P. Gul'tyai, and I. V. Proskurovskaya, *Bull. Acad. Sci. USSR Div. Chem. Sci.*, 1976, **25**, 2203–2205.

72. F. Teplý, *Collect. Czechoslov. Chem. Commun.*, 2011, **76**, 859–917.

73. L. J. Rono, H. G. Yayla, D. Y. Wang, M. F. Armstrong, and R. R. Knowles, *J. Am. Chem. Soc.*, 2013, **135**, 17735–8.

74. A. J. J. Straathof, S. Panke, and A. Schmid, *Curr. Opin. Biotechnol.*, 2002, **13**, 548–556.

75. S. Siedler, S. Bringer, and M. Bott, *Appl. Microbiol. Biotechnol.*, 2011, **92**, 929–37.

76. K. Goldberg, K. Schroer, S. Lütz, and A. Liese, *Appl. Microbiol. Biotechnol.*, 2007, **76**, 249–55.

77. P. A. Santacoloma and J. M. Woodley, in *Cascade Biocatalysis Integrating Stereoselective and Environmentally Friendly Reactions*, eds. S. Riva and W.-D. Fessner, Wiley, 2014, p. 350.

78. M. Kataoka, K. Yamamoto, H. Kawabata, M. Wada, K. Kita, H. Yanase, and S. Shimizu, *Appl. Microbiol. Biotechnol.*, 1999, **51**, 486–490.

79. B. A. Anderson, M. M. Hansen, A. R. Harkness, C. L. Henry, J. T. Vicenzi, and M. J. Zmijewski, *J. Am. Chem. Soc.*, 1995, **117**, 12358–12359.

80. M. M. Musa and R. S. Phillips, *Catal. Sci. Technol.*, 2011, **1**, 1311–1323.

81. A. Cuetos, A. Diaz-Rodriguez, and I. Lavandera, in *Synthetic Methods for Biologically Active Molecules: Exploring the Potential of Bioreductions*, ed. E. Brenna, Wiley-VCH, 2014, pp. 85–111.

82. S. C. Davis, J. H. Grate, D. R. Gray, J. M. Gruber, G. W. Huisman, S. K. Ma, L. M. Newman, R. Sheldon, and L. A. Wang, *Pat. number US 7807423 B2*, 2010.

83. E. Schmidt, O. Ghisalba, D. Gygax, and G. Sedelmeier, *J. Biotechnol.*, 1992, **24**, 315–327.

84. D. Dascier, S. Kambourakis, L. Hua, J. D. Rozzell, and J. D. Stewart, *Org. Process Res. Dev.*, 2014, **18**, 793–800.

85. K. Goldberg, K. Schroer, S. Lütz, A. Liese, and S. Luetz, *Appl. Microbiol. Biotechnol.*, 2007, **76**, 237–48.

86. A. Liese, T. Zelinski, M.-R. Kula, H. Kierkels, M. Karutz, U. Kragl, and C. Wandrey, *J. Mol. Catal. B Enzym.*, 1998, **4**, 91–99.

87. N. End and K.-U. Schoning, *Top. Curr. Chem.*, 2004, **242**, 273–317.

88. A.-M. Lupasteanu, A.-I. Galaction, and D. Cascaval, *Rom. Biotechnol. Lett.*, **12**, 3131–3138.

89. T. Jesionowski, J. Zdarta, and B. Krajewska, *Adsorption*, 2014, **20**, 801–821.

90. H. Zhao, *J. Chem. Technol. Biotechnol.*, 2010, **85**, 891–907.

91. R. C. Rodrigues, Á. Berenguer-Murcia, and R. Fernandez-Lafuente, *Adv. Synth. Catal.*, 2011, **353**, 2216–2238.

92. U. Hanefeld, L. Cao, and E. Magner, *Chem. Soc. Rev.*, 2013, **42**, 6211–2.

93. L. Cao, L. van Langen, and R. A. Sheldon, *Curr. Opin. Biotechnol.*, 2003, **14**, 387–394.

94. U. Hanefeld, L. Gardossi, and E. Magner, *Chem. Soc. Rev.*, 2009, **38**, 453–68.

95. R. A. Sheldon, *Adv. Synth. Catal.*, 2007, **349**, 1289–1307.

96. R. a Sheldon and S. van Pelt, *Chem. Soc. Rev.*, 2013, 6223–6235.

97. K. Holt-Tiffin, in *The Commercialisation and Application of Enzymes in Biotechnology*, 2014.

98. M. W. Fraaije and D. B. Janssen, in *Modern Biooxidation: Enzymes, Reactions and Applications*, eds. R. D. Schmid and V. Urlacher, Wiley-VCH, 2007, pp. 77–98.

99. R. A. Sheldon, in *The Activation of Dioxygen and Homogeneous Catalytic Oxidation*, eds. D. H. R. Barton, A. E. Martell, and D. T. Sawyer, Springer US, 1993, pp. 1773–1993.

100. I. Hermans, J. Peeters, and P. A. Jacobs, *Top. Catal.*, 2008, **50**, 124–132.

101. J. A. Labinger, *J. Mol. Catal. A Chem.*, 2004, **220**, 27–35.

102. T. Punniyamurthy, S. Velusamy, and J. Iqbal, *Chem. Rev.*, 2005, **105**, 2329–63.

103. L. Boisvert and K. I. Goldberg, *Acc. Chem. Res.*, 2012, **45**, 899–910.

104. W. J. H. van Berkel, N. M. Kamerbeek, and M. W. Fraaije, *J. Biotechnol.*, 2006, **124**, 670–89.

105. M. Held, A. Schmid, H. P. Kohler, W. Suske, B. Witholt, and M. G. Wubbolts, *Biotechnol. Bioeng.*, 1999, **62**, 641–8.

106. W. A. Suske, W. J. van Berkel, and H. P. Kohler, *J. Biol. Chem.*, 1999, **274**, 33355–65.

107. W. A. Suske, M. Held, A. Schmid, T. Fleischmann, M. G. Wubbolts, and H.-P. E. Kohler, *J. Biol. Chem.*, 1997, **272**, 24257–24265.

108. A. Meyer, M. Würsten, A. Schmid, H.-P. E. Kohler, and B. Witholt, *J. Biol. Chem.*, 2002, **277**, 34161–7.

109. A. Meyer, D. Tanner, A. Schmid, D. F. Sargent, H.-P. E. Kohler, and B. Witholt, *Acta Crystallogr. D. Biol. Crystallogr.*, 2003, **59**, 741–3.

110. A. Meyer, A. Schmid, M. Held, A. H. Westphal, M. Rothlisberger, H.-P. E. Kohler, W. J. H. van Berkel, and B. Witholt, *J. Biol. Chem.*, 2002, **277**, 5575–82.

111. A. Riebel, M. J. Fink, M. D. Mihovilovic, and M. W. Fraaije, *ChemCatChem*, 2013,

n/a–n/a.

112. S. G. Bell, X. Chen, F. Xu, Z. Rao, and L. L. Wong, *Biochem. Soc. Trans.*, 2003, **31**, 558–562.

113. C. F. Harford-Cross, A. B. Carmichael, F. K. Allan, P. A. England, D. A. Rouch, and L. L. Wong, *Protein Eng.*, 2000, **13**, 121–128.

114. C. J. C. Whitehouse, S. G. Bell, and L.-L. Wong, *Chem. Soc. Rev.*, 2012, **41**, 1218–60.

115. L.-L. Wong, *Curr. Opin. Chem. Biol.*, 1998, **2**, 263–268.

116. D. A. Grayson, Y. B. Tewari, M. P. Mayhew, V. L. Vilker, and R. N. Goldberg, *Arch. Biochem. Biophys.*, 1996, **332**, 239–247.

117. R. Bernhardt and V. B. Urlacher, *Appl. Microbiol. Biotechnol.*, 2014, **98**, 6185–203.

118. W. A. van der Donk and H. M. Zhao, *Curr. Opin. Biotechnol.*, 2003, **14**, 421–426.

119. W. F. Liu and P. Wang, *Biotechnol. Adv.*, 2007, **25**, 369–384.

120. V. Uppada, S. Bhaduri, and S. Noronha, *Curr. Sci.*, 2014, **106**, 946–957.

121. E. Brenna, Ed., *Synthetic Methods for Biologically Active Molecules: Exploring the Potential of Bioreductions*, Wiley-VCH, 1st edn., 2013.

122. Z. Shaked and G. M. Whitesides, *J. Am. Chem. Soc.*, 1980, **102**, 7104–7105.

123. H. Slusarczyk, S. Felber, M. R. Kula, and M. Pohl, *Eur. J. Biochem.*, 2000, **267**, 1280–1289.

124. W. Wu, D. Zhu, and L. Hua, *J. Mol. Catal. B-Enzymatic*, 2009, **61**, 157–161.

125. T. Kusumegi, *Pat. number WO 2011016102 A1*, 2013.

126. M.-R. Kula, M. Pohl, and H. Slusarczyk, *Pat. number CA 2253021 C*, 2007.

127. S. L. Goldberg, P. M. Cino, R. N. Patel, V. B. Nanduri, and R. M. Johnston, *Pat. number WO 2003054155 A2*, 2006.

128. H. Groeger and W. Hummel, *Pat. number WO 2004009825 A1*, 2005.

129. S. Kara, J. H. Schrittwieser, and F. Hollmann, in *Synthetic Methods for Biologically Active Molecules: Exploring the Potential of Bioreductions*, ed. E. Brenna, Wiley-VCH, pp. 209–238.

130. W. Kroutil, H. Mang, K. Edegger, and K. Faber, *Curr. Opin. Chem. Biol.*, 2004, **8**, 120–126.

131. G. de Gonzalo, I. Lavandera, K. Faber, and W. Kroutil, *Org. Lett.*, 2007, **9**, 2163–2166.

132. A. Weckbecker, H. Groeger, and W. Hummel, in *Biosystems Engineering I: Creating Superior Biocatalysts*, eds. C. Wittmann and W. R. Krull, 2010, vol. 120, pp. 195–242.

133. S. K. Ma, J. Gruber, C. Davis, L. Newman, D. Gray, A. Wang, J. Grate, G. W. Huisman, and R. a. Sheldon, *Green Chem.*, 2010, **12**, 81.

134. C. Ning, E. Su, Y. Tian, and D. Wei, *J. Biotechnol.*, 2014, **184**, 7–10.

135. I. Ali and S. Omanovic, *Int. J. Electrochem. Sci.*, 2013, **8**, 4283–4304.

136. R. DevauxBasseguy, A. Bergel, and M. Comtat, *Enzyme Microb. Technol.*, 1997, **20**, 248–258.

137. I. Ali, A. Gill, and S. Omanovic, *Chem. Eng. J.*, 2012, **188**, 173–180.

138. A. Damian, K. Maloo, and S. Omanovic, *Chem. Biochem. Eng. Q.*, 2007, **21**, 21–32.

139. I. Ali, T. Khan, and S. Omanovic, *J. Mol. Catal. A Chem.*, 2014, **387**, 86–91.

140. P. M. Allen and W. R. Bowen, *Trends Biotechnol.*, 1985, **3**, 145–149.

141. J. Gajdzik, J. Lenz, H. Natter, A. Walcarius, G. W. Kohring, F. Giffhorn, M. Göllü, A. S. Demir, and R. Hempelmann, *J. Electrochem. Soc.*, 2012, **159**, F10.

142. K. Vuorilehto, S. Lütz, and C. Wandrey, *Bioelectrochemistry*, 2004, **65**, 1–7.

143. A. A. Karyakin, Y. N. Ivanova, and E. E. Karyakina, *Electrochem. commun.*, 2003, **5**, 677–680.

144. V. Hoellrigl, K. Otto, and A. Schmid, *Adv. Synth. Catal.*, 2007, **349**, 1337–1340.

145. J. G. Zeikus and D. H. Park, *Pat. number US 20040241771 A1*, 2002.

146. H. Durliat, M. Comtat, and J.-L. Séris, *Pat. number US 5528867 A*, 1988.

147. J. Cantet, A. Bergel, and M. Comtat, *Bioelectrochemistry Bioenerg.*, 1992, **27**, 475–486.

148. J. Cantet, A. Bergel, M. Comtat, and J.-L. Séris, *J. Mol. Catal.*, 1992, **73**, 371–380.

149. J. Cantet, A. Bergel, and M. Comtat, *Enzyme Microb. Technol.*, 1996, **18**, 72–79.

150. A. Bergel, M. Comtat, and J.-L. Séris, *Pat. number EP0388267 A1*, 1989.

151. L. Lauterbach, Z. Idris, K. A. Vincent, and O. Lenz, *PLoS One*, 2011, **6**.

152. Y. Zu, R. J. Shannon, and J. Hirst, *J. Am. Chem. Soc.*, 2003, **125**, 6020–6021.

153. C. D. Barker, T. Reda, and J. Hirst, *Biochemistry*, 2007, **46**, 3454–3464.

154. L. Lauterbach, O. Lenz, and K. A. Vincent, *FEBS J.*, 2013, **280**, 3058–3068.

155. B. Payen, M. Segui, P. Monsan, K. Schneider, C. G. Friedrich, and H. G. Schlegel, *Biotechnol. Lett.*, 1983, **5**, 463–468.

156. J. Ratzka, L. Lauterbach, O. Lenz, and M. B. Ansorge-Schumacher, *J. Mol. Catal. B Enzym.*, 2012, **74**, 219–223.

157. J. Ratzka, L. Lauterbach, O. Lenz, and M. B. Ansorge-Schumacher, *Biocatal. Biotransformation*, 2011, **29**, 246–252.

158. R. Mertens, L. Greiner, E. C. . van den Ban, H. B. C. . Haaker, and A. Liese, *J. Mol. Catal. B Enzym.*, 2003, **24-25**, 39–52.

159. F. O. Bryant and M. W. W. Adams, *J. Biol. Chem.*, 1989, **264**, 5070–5079.

160. Y. Ni, P.-L. Hagedoorn, J.-H. Xu, I. W. C. E. Arends, and F. Hollmann, *Chem. Commun.*, 2012, **48**, 12056–12058.

161. Y. Maenaka, T. Suenobu, and S. Fukuzumi, *J. Am. Chem. Soc.*, 2012, **134**, 367–74.

162. R. T. Hembre, J. M. Penney, and P. S. Wagenknecht, *Pat. number WO2000053731 A2*, 2000.

163. S. Betanzos-Lara, Z. Liu, A. Habtemariam, A. M. Pizarro, B. Qamar, and P. J. Sadler, *Angew. Chem. Int. Ed. Engl.*, 2012, **51**, 3897–900.

164. C. E. Paul, I. W. C. E. Arends, and F. Hollmann, *ACS Catal.*, 2014, **4**, 788–797.

165. S. Yasui and A. Ohno, *Bioorg. Chem.*, 1986, **14**, 70–96.

166. K. E. Taylor and J. B. Jones, *J. Am. Chem. Soc.*, 1976, **98**, 5689–5694.

167. R. J. Knox, F. Friedlos, M. Jarman, L. C. Davies, P. Goddard, G. M. Anlezark, R. G. Melton, and R. F. Sherwood, *Biochem. Pharmacol.*, 1995, **49**, 1641–1647.

168. S. Kara, D. Spickermann, J. H. Schrittwieser, C. Leggewie, W. J. H. van Berkel, I. W. C. E. Arends, and F. Hollmann, *Green Chem.*, 2013, **15**, 330.

169. R. Cammack, M. Frey, and R. Robson, *Hydrogen As a Fuel: Learning From Nature*, Taylor and Francis, London, 2001.

170. P. M. Vignais, B. Billoud, and J. Meyer, *Fems Microbiol. Rev.*, 2001, **25**, 455–501.

171. M. T. M. Koper, *Fuel Cell Catal.*, 2009.

172. A. Volbeda, P. Amara, C. Darnault, J.-M. Mouesca, A. Parkin, M. M. Roessler, F. A. Armstrong, and J. C. Fontecilla-Camps, *Proc. Natl. Acad. Sci.*, 2012, **109**, 5305–5310.

173. P. M. Vignais and B. Billoud, *Chem. Rev.*, 2007, **107**, 4206–72.

174. K. A. Vincent, A. Parkin, and F. A. Armstrong, *Chem. Rev.*, 2007, **107**, 4366–4413.

175. F. A. Armstrong, N. A. Belsey, J. A. Cracknell, G. Goldet, A. Parkin, E. Reisner, K. A. Vincent, and A. F. Wait, *Chem. Soc. Rev.*, 2009, **38**, 36–51.

176. Y. Y. Higuchi and N. Yasuoka, *Structure*, 1997, **5**, 1671–1680.

177. Y. Montet, P. Amara, A. Volbeda, X. Vernede, E. C. Hatchikian, M. J. Field, M. Frey, and J. C. Fontecilla-Camps, *Nat. Struct. Biol.*, 1997, **4**, 523–526.

178. A. Volbeda, E. Garcin, C. Piras, A. L. de Lacey, V. M. Fernandez, E. C. Hatchikian, M. Frey, and J. C. Fontecilla-Camps, *J. Am. Chem. Soc.*, 1996, **118**, 12989–12996.

179. A. Volbeda, C. Darnault, A. Parkin, F. Sargent, F. A. Armstrong, and J. C. Fontecilla-Camps, *Structure*, 2013, **21**, 184–90.

180. P. A. Ash and K. A. Vincent, *Chem. Commun.*, 2012, **48**, 1400–9.

181. M. M. Roessler, R. M. Evans, R. A. Davies, J. Harmer, and F. A. Armstrong, *J. Am. Chem. Soc.*, 2013, **135**, 4159–4159.

182. T. Buhrke, O. Lenz, N. Krauss, and B. Friedrich, *J. Biol. Chem.*, 2005, **280**, 23791–6.

183. S. Dementin, F. Leroux, L. Cournac, A. L. de Lacey, A. Volbeda, C. Léger, B. Burlat, N. Martinez, S. Champ, L. Martin, O. Sanganas, M. Haumann, V. M. Fernández, B. Guigliarelli, J. C. Fontecilla-Camps, and M. Rousset, *J. Am. Chem. Soc.*, 2009, **131**, 10156–64.

184. T. Burgdorf, O. Lenz, T. Buhrke, E. van der Linden, A. K. Jones, S. P. J. Albracht, and B. Friedrich, *J. Mol. Microbiol. Biotechnol.*, 2005, **10**, 181–196.

185. T. Burgdorf, E. van der Linden, M. Bernhard, Q. Y. Yin, J. W. Back, A. F. Hartog, A. O. Muijsers, C. G. de Koster, S. P. J. Albracht, and B. Friedrich, *J. Bacteriol.*, 2005, **187**, 3122–3132.

186. M. Horch, L. Lauterbach, O. Lenz, P. Hildebrandt, and I. Zebger, *FEBS Lett.*, 2012, **586**, 545–56.

187. K. Schneider and H. G. Schlegel, *Biochim. Biophys. Acta*, 1976, **452**, 66–80.

188. N. Herr, J. Ratzka, L. Lauterbach, O. Lenz, and M. B. Ansorge-Schumacher, *J. Mol. Catal. B Enzym.*, 2013, **97**, 169–174.

189. T. Oda, K. Oda, H. Yamamoto, A. Matsuyama, M. Ishii, Y. Igarashi, and H. Nishihara, *Microb. Cell Fact.*, 2013, **12**, 2.

190. E. van der Linden, B. Faber, B. Bleijlevens, T. Burgdorf, M. Bernhard, B. Friedrich, and S. Albracht, *Eur. J. Biochem.*, 2004, **271**, 801–808.

191. P. W. Atkins, *Physical Chemsitry*, Oxford University Press, 1998.

192. C. F. Blanford, *Chem. Commun.*, 2013, **49**, 11130–2.

193. M. Eddowes and Hill, *J. Chem. Soc. Commun.*, 1977, 771–772.

194. F. A. Armstrong, *Photosynth. Res.*, 2009, **102**, 541–550.

195. K. A. Vincent and F. A. Armstrong, *Inorg. Chem.*, 2005, **44**, 798–809.

196. C. Leger, S. J. Elliott, K. R. Hoke, L. J. C. Jeuken, A. K. Jones, and F. A. Armstrong, *Biochemistry*, 2003, **42**, 8653–8662.

197. C. Leger and P. Bertrand, *Chem. Rev.*, 2008, **108**, 2379–2438.

198. L. J. C. Jeuken, *Nat. Prod. Rep.*, 2009, **26**, 1234–1240.

199. R. M. Evans and F. A. Armstrong, in *Metalloproteins Methods and Protocols*, eds. J. C. Fontecilla-Camps and Y. Nicolet, Humana Press, 2014.

200. J. Hirst and F. A. Armstrong, *Anal. Chem.*, 1998, **70**, 5062–5071.

201. D. T. Sawyer, A. Sobkowiak, and J. L. Roberts, *Electrochemical Methods: Fundamentals and Applications*, Wiley-Interscience New York, 2nd edn., 1995.

202. H. R. Pershad, J. L. C. Duff, H. A. Heering, E. C. Duin, S. P. J. Albracht, and F. A. Armstrong, *Biochemistry*, 1999, **38**, 8992–8999.

203. A. K. Jones, E. Sillery, S. P. J. Albracht, and F. A. Armstrong, *Chem. Commun.*, 2002, 866–867.

204. A. C. Fisher, *Electrode Dynamics*, Oxford University Press, 1996.

205. C. Leger, A. K. Jones, S. P. J. Albracht, and F. A. Armstrong, *J. Phys. Chem. B*, 2002, **106**, 13058–13063.

206. O. Rüdiger, C. Gutiérrez-Sánchez, D. Olea, I. A. C. Pereira, M. Vélez, V. M. Fernández, and A. L. De Lacey, *Electroanalysis*, 2010, **22**, 776–783.

207. A. J. Healy, H. A. Reeve, and K. A. Vincent, *Faraday Discuss.*, 2011, **148**, 345–357.

208. A. J. Healy, H. A. Reeve, A. Parkin, and K. A. Vincent, *Electrochim. Acta*, 2011, **56**, 10786–10790.

209. L. Xu and F. A. Armstrong, *Energy Environ. Sci.*, 2013, **6**, 2166.

210. S. . Morozov, E. . Karyakina, N. . Zorin, S. . Varfolomeyev, S. Cosnier, and A. . Karyakin, *Bioelectrochemistry*, 2002, **55**, 169–171.

211. S. Krishnan and F. A. Armstrong, *Chem. Sci.*, 2012, **3**, 1015.

212. J. Quinson, R. Hidalgo, P. A. Ash, F. Dillon, N. Groberta, and K. A. Vincent, *Faraday*

Discuss., 2014.

213. J. Zhang, Y. Zhang, and S. Feng, *Pat. number CN101787212-A*, 2010.

214. T. R. Ralph and M. P. Hogarth, *Platin. Met. Rev.*, 2002, **46**, 3–14.

215. D. Bevers, R. Rogers, and M. von Bradke, *J. Power Sources*, 1996, **63**, 193–201.

216. M. J. Watt-Smith, S. P. Rigby, T. R. Ralpha, and F. C. Walsh, *J. Power Sources*, 2008, **184**, 29–37.

217. Y. Kamitaka, S. Tsujimura, N. Setoyama, T. Kajino, and K. Kano, *Phys. Chem. Chem. Phys.*, 2007, **15**, 1793–1801.

218. A. Cornish-Bowden, *Fundamentals of enzyme kinetics*, Portland Press Ltd, 3rd edn., 2004.

219. J. M. Berg, J. L. Tymoczko, and L. Stryer, *Biochemistry*, W. H. Freeman and Company, New York, 6th edn., 2006.

220. A. Gopalan, D. Ragupathy, H.-T. Kim, K. M. Manesh, and K.-P. Lee, *Spectrochim. Acta. A. Mol. Biomol. Spectrosc.*, 2009, **74**, 678–84.

221. E. Hald, P. Lehmann, and J. Ziegenhorn, 1975, **21**, 884–887.

222. Z. Idris, *D.Phil Thesis, Univeristy of Oxford*, 2012.

223. L. Rover, J. C. B. Fernandes, G. de O. Neto, L. T. Kubota, E. Katekawa, and S. H. P. Serrano, *Anal. Biochem.*, 1998, **260**, 50–55.

224. A. J. Healy, P. A. Ash, O. Lenz, and K. A. Vincent, *Phys. Chem. Chem. Phys.*, 2013, **15**, 7055–7059.

225. W. Lubitz, H. Ogata, O. Rüdiger, and E. Reijerse, *Chem. Rev.*, 2014, **114**, 4081–148.

226. L. Lauterbach, J. Liu, M. Horch, P. Hummel, A. Schwarze, M. Haumann, K. A. Vincent, O. Lenz, and I. Zebger, *Eur. J. Inorg. Chem.*, 2011, **2011**, 1067–1079.

227. J. P. Klinman, *Crc Crit. Rev. Biochem.*, 1981, **10**, 39–78.

228. G. Pettersson, *Crc Crit. Rev. Biochem.*, 1987, **21**, 349–389.

229. M. M. Kreevoy, D. Ostovic, I. S. H. Lee, D. A. Binder, and G. W. King, *J. Am. Chem. Soc.*, 1988, **110**, 524–530.

230. C. A. Coleman, J. G. Rose, and C. J. Murray, *J. Am. Chem. Soc.*, 1992, **114**, 9755–9762.

231. J. Cheng and Y. Lu, *J. Phys. Org. Chem.*, 1997, **10**, 577–584.

232. K. M. Zaman, S. Yamamoto, N. Nishimura, J. Maruta, and S. Fukuzumi, *J. Am. Chem. Soc.*, 1994, **116**, 12099–12100.

233. J. Yuasa and S. Fukuzumi, *J. Am. Chem. Soc.*, 2006, **128**, 14281–14292.

234. S. Ramaswamy, H. Eklund, and B. V. Plapp, *Biochemistry*, 1994, **33**, 5230–5237.

235. S. Pilkington, M. Skehel, R. Gennis, and J. Walker, *Biochemistry*, 1991, **30**, 2166–2175.

236. C. Chothia and A. M. Lesk, *EMBO J.*, 1986, **5**, 823–826.

237. L. A. Sazanov and P. Hinchliffe, *Science,*, 2006, **311**, 1430–1436.

238. K. Schneider and H. Schlegel, *Biochem. Biophys. Res. Commun.*, 1978, **84**, 564–571.

239. S. Albracht, E. van der Linden, and B. Faber, *Biochim. Biophys. Acta-Bioenergetics*, 2003, **1557**, 41–49.

240. S. P. J. Albracht and R. Hedderich, *FEBS Lett.*, 2000, **485**, 1–6.

241. J. Wang, G. Yin, Y. Shao, S. Zhang, Z. Wang, and Y. Gao, *J. Power Sources*, 2007, **171**, 331–339.

242. A. J. Healy, *D.Phil Thesis, Univeristy of Oxford*, 2013.

243. P. N. Bartlett, *Bioelectrochemistry: fundamentals, experimental techniques and applications*, Wiley, 2008.

244. T. H. Lonsdale, *Part II Thesis, Univ. Oxford*, 2013.

245. A. Hansel and P. Lindblad, *Appl. Microbiol. Biotechnol.*, 1998, **50**, 153–160.

246. A. Porthun, M. Bernhard, and B. Friedrich, *Arch. Microbiol.*, 2002, **177**, 159–66.

247. K. Schneider, H. G. Schlegel, and K. Jochim, *Eur. J. Biochem.*, 1984, **138**, 533–541.

248. P. Gros, C. Zaborosch, H. G. Schlegel, and A. Bergel, *J. Electroanal. Chem.*, 1996, **405**, 189–195.

249. L. Lauterbach and O. Lenz, *J. Am. Chem. Soc.*, 2013, **135**, 17897–905.

250. C. Zaborosch, K. Schneider, H. G. Schlegel, and H. Kratzin, *Eur. J. Biochem.*, 1989, **181**, 175–180.

251. C. Zaborosch, M. Koster, and E. Bill, 1995, **8**, 149–162.

252. J. Bradley, *Part II Thesis, Univ. Oxford*, 2013.

253. J. Liu, *D.Phil Thesis, Univ. Oxford*, 2011.

254. A. K. Jones, S. E. Lamle, H. R. Pershad, K. A. Vincent, S. P. J. Albracht, and F. A. Armstrong, *J. Am. Chem. Soc.*, 2003, **125**, 8505–8514.

255. K. A. Vincent, X. Li, C. F. Blanford, N. A. Belsey, J. H. Weiner, and F. A. Armstrong, *Nat Chem Biol*, 2007, **3**, 761–762.

256. O. Lazarus, T. W. Woolerton, A. Parkin, M. J. Lukey, E. Reisner, J. Seravalli, E. Pierce, S. W. Ragsdale, F. Sargent, and F. A. Armstrong, *J. Am. Chem. Soc.*, 2009, **131**, 14154.

257. H. A. Reeve, L. Lauterbach, P. A. Ash, O. Lenz, and K. A. Vincent, *Chem. Commun.*, 2012, **48**, 1589–1591.

258. H. A. Reeve, *Part II Thesis, Univ. Oxford*, 2010.

259. A. A. . Karyakin, S. V. . Morozov, E. E. . Karyakina, N. A. . Zorin, V. V. . Perelygin, and S. Cosnier, *Biochem. Soc. Trans.*, 2005, **33**, 73–75.

260. T. Matsumoto, S. Eguchi, H. Nakai, T. Hibino, K.-S. Yoon, and S. Ogo, *Angew. Chem. Int. Ed. Engl.*, 2014, **53**, 8895–8.

261. W. Lubitz, E. Reijerse, and M. van Gastel, *Chem. Rev.*, 2007, **107**, 4331–65.

262. M. J. Corr and J. A. Murphy, *Chem. Soc. Rev.*, 2011, **40**, 2279–92.

263. P. M. E. Siegbahn, J. W. Tye, and M. B. Hall, *Chem. Rev.*, 2007, **107**, 4414–4435.

264. K. A. Vincent, N. A. Belsey, W. Lubitz, and and F. A. Armstrong, *J. Am. Chem. Soc.*, 2006, **128**, 7448–7449.

265. M. J. Lukey, A. Parkin, M. M. Roessler, B. J. Murphy, J. Harmer, T. Palmer, F. Sargent, and F. A. Armstrong, *J. Biol. Chem.*, 2010, **285**, 3928–38.

266. E.-D. Schulze and H. A. Mooney, *Biodiversity and ecosystem function*, Springe-Verlag, 1993.

267. C. Fichtner, C. Laurich, E. Bothe, and W. Lubitz, *Biochemistry*, 2006, **45**, 9706–9716.

268. P. Kellers, M. E. Pandelia, L. J. Currell, H. Gorner, and W. Lubitz, *Phys. Chem. Chem. Phys.*, 2009, **11**, 8680–8683.

269. D. Millo, M.-E. Pandelia, T. Utesch, N. Wisitruangsakul, M. A. Mroginski, W. Lubitz, P. Hildebrandt, and I. Zebger, *J Phys Chem B*, 2009, **113**, 15344–15351.

270. *http://www.strem.com/uploads/technical_notes/96-4012tech.pdf*, **May 2014**.

271. W. Feng and P. Ji, *Biotechnol. Adv.*, 2011, **29**, 889–95.

272. V. F. Selmi and C. G. Ciamician, 2013, **46**.

273. E. Van Hooijdonk, C. Bittencourt, R. Snyders, and J.-F. Colomer, *Beilstein J. Nanotechnol.*, 2013, **4**, 129–52.

274. W. Lubitz and W. Tumas, *Chem. Rev.*, 2007, **107**, 3900–3903.

275. M. Höhne and U. T. Bornscheuer, *ChemCatChem*, 2009, **1**, 42–51.

276. M. Rauter, J. Kasprzak, K. Becker, K. Baronian, R. Bode, G. Kunze, and H.-M. Vorbrodt, *J. Mol. Catal. B Enzym.*, 2014, **104**, 8–16.

277. J. A. Cracknell, K. A. Vincent, M. Ludwig, O. Lenz, B. Friedrich, and F. A. Armstrong, *J. Am. Chem. Soc.*, 2007, **130**, 424–425.

278. O. Lenz, M. Ludwig, T. Schubert, I. Burstel, S. Ganskow, T. Goris, A. Schwarze, and B. Friedrich, *Chemphyschem*, 2010, **11**, 1107–1119.

279. M. Ludwig, J. A. Cracknell, K. A. Vincent, F. A. Armstrong, and O. Lenz, *J. Biol. Chem.*, 2009, **284**, 465–477.

280. K. A. Vincent, J. A. Cracknell, O. Lenz, I. Zebger, B. Friedrich, and F. A. Armstrong, *Proc. Natl. Acad. Sci. U. S. A.*, 2005, **102**, 16951–16954.

281. K. A. Vincent, A. Parkin, O. Lenz, S. P. J. Albracht, J. C. Fontecilla-Camps, R. Cammack, B. Friedrich, and F. A. Armstrong, *J. Am. Chem. Soc.*, 2005, **127**, 18179–18189.

282. T. W. Woolerton and K. A. Vincent, *Electrochim. Acta*, 2009, **54**, 5011–5017.

283. K. A. Vincent, J. A. Cracknell, J. R. Clark, M. Ludwig, O. Lenz, B. Friedrich, and F. A. Armstrong, *Chem. Commun.*, 2006, 5033–5035.

284. B. J. Murphy, F. Sargent, and F. A. Armstrong, *Energy Environ. Sci.*, 2014, **7**, 1426.

285. M. J. Lukey, M. M. Roessler, A. Parkin, R. M. Evans, R. A. Davies, O. Lenz, B. Friedrich, F. Sargent, and F. A. Armstrong, *J. Am. Chem. Soc.*, 2011, **133**, 16881–92.

286. R. M. Evans, A. Parkin, M. M. Roessler, B. J. Murphy, H. Adamson, M. J. Lukey, F. Sargent, A. Volbeda, J. C. Fontecilla-Camps, and F. A. Armstrong, *J. Am. Chem. Soc.*, 2013, **135**, 2694–707.

287. J. Fritsch, P. Scheerer, S. Frielingsdorf, S. Kroschinsky, B. Friedrich, O. Lenz, and C. M. T. Spahn, *Nature*, 2011, **479**, 249–252.

288. T. Goris, A. F. Wait, M. Saggu, J. Fritsch, N. Heidary, M. Stein, I. Zebger, F. Lendzian, F. A. Armstrong, B. Friedrich, and O. Lenz, *Nat. Chem. Biol.*, 2011, **7**, 310–8.

289. K. Grubel and P. L. Holland, *Angew. Chem. Int. Ed. Engl.*, 2012, **51**, 3308–10.

290. S. V Hexter, F. Grey, T. Happe, V. Climent, and F. A. Armstrong, *Proc. Natl. Acad.*

Sci. U. S. A., 2012, **109**, 11516–21.

291. A. Parkin, L. Bowman, M. M. Roessler, R. A. Davies, T. Palmer, F. A. Armstrong, and F. Sargent, *FEBS Lett.*, 2012, **586**, 536–44.

292. M. Saggu, I. Zebger, M. Ludwig, O. Lenz, B. Friedrich, P. Hildebrandt, and F. Lendzian, *J. Biol. Chem.*, 2009, **284**, 16264–16276.

293. J. A. Cracknell, A. F. Wait, O. Lenz, B. Friedrich, and F. A. Armstrong, *Proc. Natl. Acad. Sci. U. S. A.*, 2009, **106**, 20681–20686.

294. F. Hollmann, A. Schmid, and E. Steckhan, *Angew. Chemie*, 2001, **40**, 169–171.

295. A. Schmid, I. Vereyken, M. Held, and B. Witholt, *J. Mol. Catal. B Enzym.*, 2001, **11**, 455–462.

296. J. Lutz, V. Mozhaev, Y. L. Khmelnitsky, B. Witholt, and A. Schmid, *J. Mol. Catal. B Enzym.*, 2002, **19-20**, 177–187.

297. A. Oubrie, H. J. Rozeboom, K. H. Kalk, E. G. Huizinga, and B. W. Dijkstra, *J. Biol. Chem.*, 2002, **227**, 3727.

298. B. M. Hallberg, T. Bergfors, K. Backbro, G. Pettersson, G. Henriksson, and C. Divne, *Struct. Fold. Des.*, 2000, **8**, 79.

299. B. M. Hallberg, G. Henriksson, G. Pettersson, and C. Divne, *J. Mol. Biol.*, 2002, **315**, 421.

300. P. N. Bartlett, *Bioelectrochemistry: fundamentals, experimental techniques and applications*, John Wiley & Sons Ltd, 2008.

301. L. Gorton and P. N. Bartlett, in *Biochemistry: Fundamentals, Experimental Techniques and Applications*, ed. P. N. Bartlett, Wiley, 1st edn., 2008, pp. 157–198.

302. S. Sampath and O. Lev, *J. Electroanal. Chem.*, 1998, **446**, 57–65.

303. H. Chen, A. Yu, J. Han, and Y. Mi, *Anal. Lett.*, 1995, **28**, 1579–1591.

304. C. F. Blanford, C. E. Foster, R. S. Heath, and F. A. Armstrong, *Faraday Discuss.*, 2009, **140**, 319–335.

305. J. Zhang, *PEM Fuel Cell Electrocatalysts and Catalyst Layers*, Springer, 2008.

306. S. Srinivasan, *Fuel Cells: From Fundamentals to Applications*, Springer Science & Business Media, 2006.

307. H. Sakai, T. Nakagawa, Y. Tokita, T. Hatazawa, T. Ikeda, S. Tsujimura, and K. Kano, *Energy Environ. Sci.*, 2009, **2**, 133–138.

308. F. Tasca, L. Gorton, W. Harreither, D. Haltrich, R. Ludwig, and G. Noll, *J. Phys.*

Chem. C, 2008, **112**, 13668.

309. M. A. Dasari, P.-P. Kiatsimkul, W. R. Sutterlin, and G. J. Suppes, *Appl. Catal. A*, 2005, **281**, 225.

310. S. N. Ruzheinikov, J. Burke, S. Sedelnikova, P. J. Baker, R. Taylor, P. A. Bullough, N. M. Muir, M. G. Gore, and D. W. Rice, *Structure*, 2001, **9**, 789–802.

311. A. W. Kormann, R. O. Hurst, and T. G. Flynn, *Biochim. Biophys. Acta - Enzymol.*, 1972, **258**, 40–55.

312. J. Liepins, S. Kuorelahti, M. Penttilä, and P. Richard, *FEBS J.*, 2006, **273**, 4229–35.

Appendices

A.UV-vis to determine the NAD^+/NADH ratio

Uv-vis spectroscopy can be used to determine the concentration ratio of NAD^+/NADH using the ratio of absorbance at 260 and 340 nm. Figure A1(A) shows UV-vis spectra of NAD^+ (red) and NADH (blue). Using spectra of different NAD^+/NADH ratios (with a constant total cofactor concentration) a plot of $[NAD^+]/[NADH]$ *vs* $A_{260\ nm}/A_{340\ nm}$ was constructed, Figure A1(B).

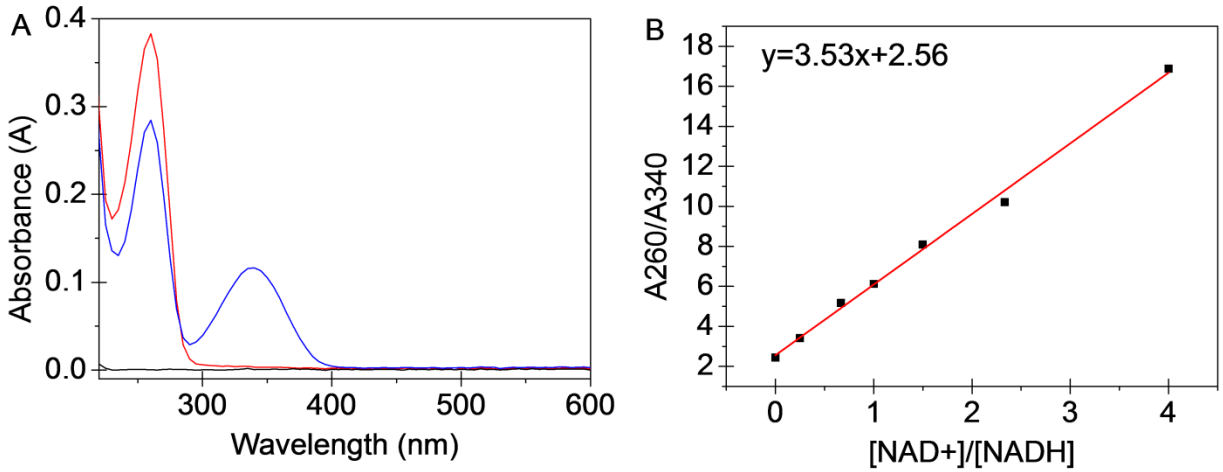

Figure A1: (a) Uv-vis spectra of NAD^+ (red) and NADH (blue). (b) A plot of $[NAD^+]/[NADH]$ *vs* $A_{260\ nm}/A_{340\ nm}$ can be used to determine the concentration ratio of an unknown sample.

The $A_{260\ nm}/A_{340\ nm}$ value for NADH is consistent with the literature values.[A1]

[A1] S. A. Margolis, B. F. Howell, and R. Schaffer, *Clin. Chem.*, 1976, **22**, 1322–9.

B.Cornish-Bowden Plots

Cornish-Bowden plots to determine the type of inhibition experienced by *Rh. o* HoxFU on addition of product (inhibitor) at a range of substrate concentrations.

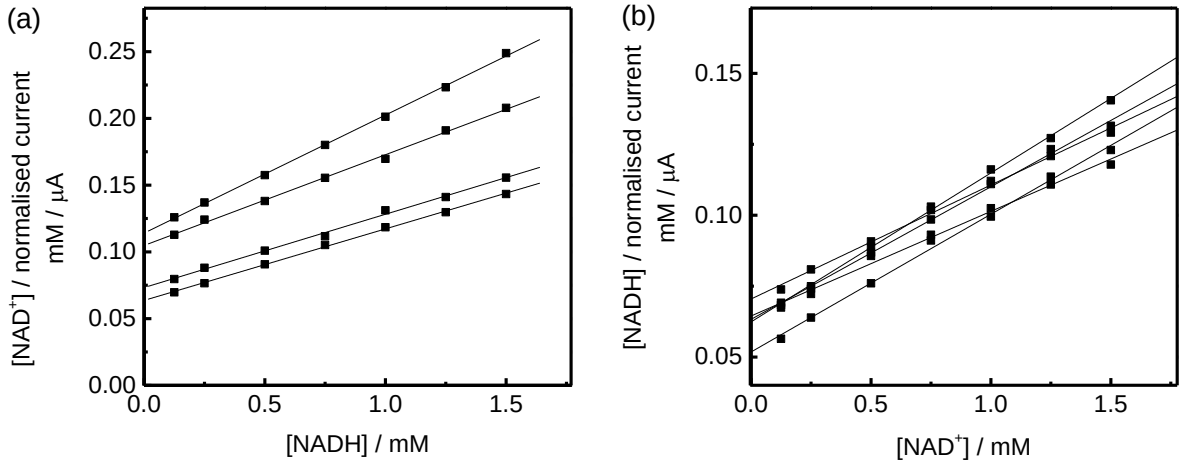

Figure B1: Cornish-Bowden plots for the data in Section **Figure 4-5**. Constructed by plotting [substrate] / normalised current *vs* [inhibitor].

The lines in panels (a) and (b) are approximately parallel. This suggests that product inhibition is likely to be competitive.

C. The peak positions for electronic states of Hyd-1

The peak positions for the CO and CN ligands in Hyd-1 in different electronic states were determined using the ATR cell by Dr Adam Healy. The table below is reproduced from his DPhil Thesis.[B1]

Table C1: Summary of ν(CO) and ν(CN) values (in cm-1) for different redox states of Hyd-1. The redox level relative to the most oxidised state has been extrapolated from IR and EPR spectroelectrochemical data of Hyd-1 and other [NiFe]-hydrogenases, and the state labels adapted from regular [NiFe]-hydrogenase nomenclature. nd = not determined.

redox level relative to oxidised (Ni-B) state	state label	ν(CO)	ν_a(CN)	ν_b(CN)
0	Ni-B	1943	2081	2099
-1	Ni-S	1929	2076	2085
-2	Ni-C	1951	*nd*	*nd*
-2	Ni-LII	1877	2051	2034
-2	Ni-LIII	1866	2045	2029
-3	Ni-RII	1922	2053	2070
-3	Ni-RIII	1914	2049	2066

[B1]A. J. Healy, *D.Phil Thesis, Univeristy of Oxford*, 2013.

D. HPLC traces from Section 5.4.4

The whole chromatograms from Figure 5-10 are shown here.

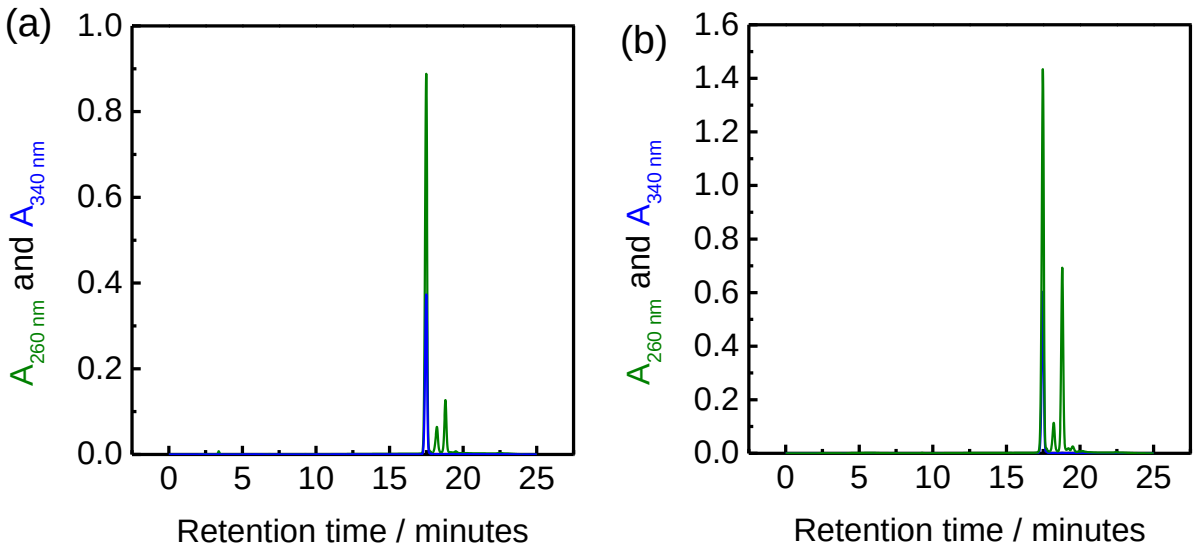

Figure D1: HPLC chromatograms from the experiments described in Section 5.4.4 using particles in the presence of NAD^+ at a concentration of (a) 0.5 mM and (b) 5 mM.

The only peaks observed are due to NADH, NAD^+ and the impurity found in as-bought NAD^+. This confirms that no UV-vis active forms of the cofactor are generated by the particle system.

E.HPLC protocols

HPLC was used to analyse NADH-dependent enzyme catalysed reactions in Chapters 6 and 7. Here the protocols are detailed and the standard curves displayed for acetophenone to phenylethanol, pyruvate to lactate and biphenyl-2-ol to 2, 3-dihydroxybiphenly conversion.

E1.Acetopheone to phenylethanol

Acetophenone and phenylethanol were separated using a Chromolith® Performance, 100-3 mm column (Merck). The mobile phase was a mixture of 80 % water and 20 % acetonitrile running at 1 mL min^{-1}, the column was maintained at a temperature of 40 ^{o}C, the absorbance at 210 nm were monitored for detection of acetophenone and phenylethanol. Absorbance at 260 nm was recorded and used to identify peaks due to the cofactors.

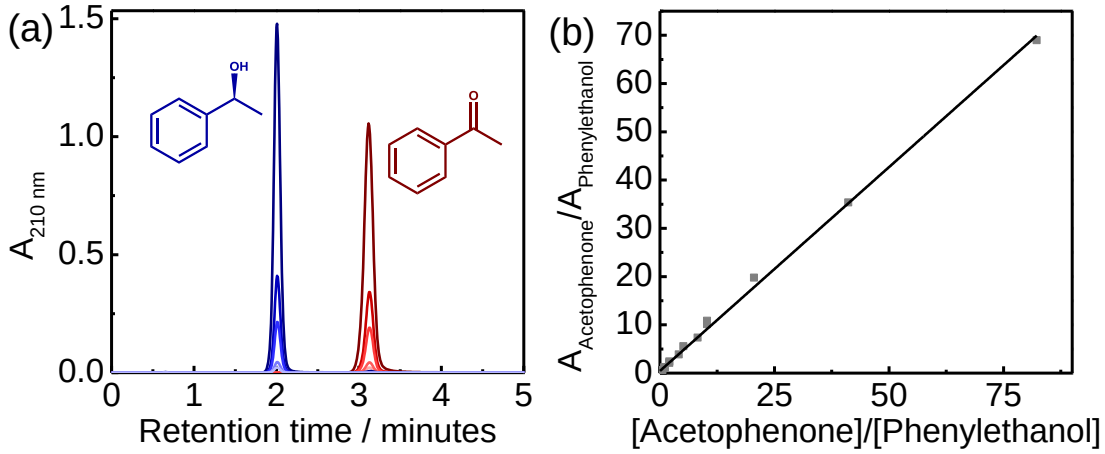

Figure E1: (a) HPLC trace showing the retention times for phenylethanol (1.87 min) and acetophenone (3.28 min). The samples were prepared in water and injected onto a monolithic column. The mobile phase was a mixture of water and acetonitrile (80:20). The column was maintained at a temperature of 40 ^{o}C and the flow rate was 1 mL/min. Acetophenone and phenylethanol samples of 20, 5, 2.5, 0.5, 0.25 nmoles (dark to light red and blue respectively) are shown. (b) A ratio of the peak areas vs concentration ratio is plotted and can be used to determine the ratio of acteophenone to phenylethanol in an unknown mixture. A linear fit of this data gave an R2 value of 0.998.

Samples of known concentration were injected, the retention time for acetophenone and phenylethanol were 1.9 and 3.2 minutes respectively. Linear fits of the peak area *vs* concentration gave R^2 values of 0.999 and 0.998 for acetophenone and phenylethanol

respectively (not shown). The area of the acetophenone and phenylethanol peaks was used to determine the concentration of an unknown sample.

A plot of [acetophenone]/[phenylethanol] *vs* $A_{acetophenone}/A_{phenylethanol}$ was constructed and gave a straight line, R^2=0.998. This was used to determine the extent of conversion of acetophenone to phenylethanol.

E2.Pyruvate to lactate

Pyruvate and lactate were separated using a C18-reverse phase column using a 0.1 % phosphoric acid mobile phase running at 0.45 mL min^{-1} with a column temperature of 50 ^{o}C. The retention time for lactate was 12.5 minutes. Separation of the cofactors (NAD^+ and NADH) and pyruvate was not possible using this method, therefore only the concentration of lactate was analysed quantitatively.

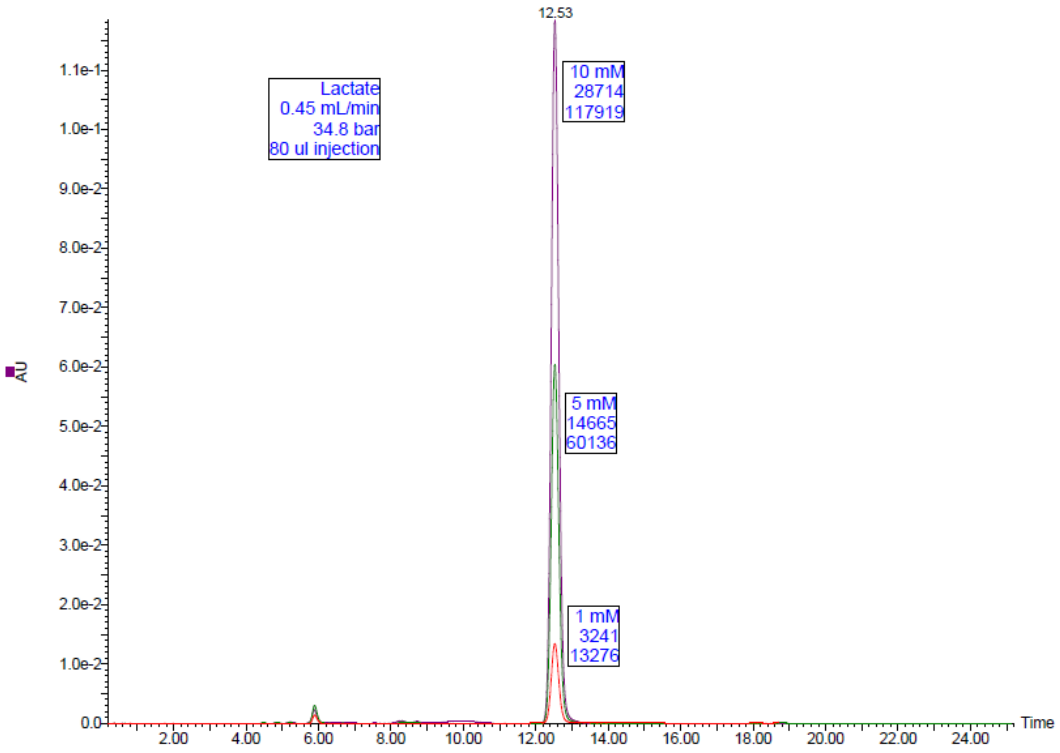

Figure E2: Lactate standards analysed by HPLC. Samples of lactate were prepared in waster and injected onto a C18-reverse phase column. The mobile phase (0.1 % phosphoric acid) was run at 1 mL min^{-1} and the column was maintained at 50 ^{o}C. Experiments performed at Harwell Research Complex.

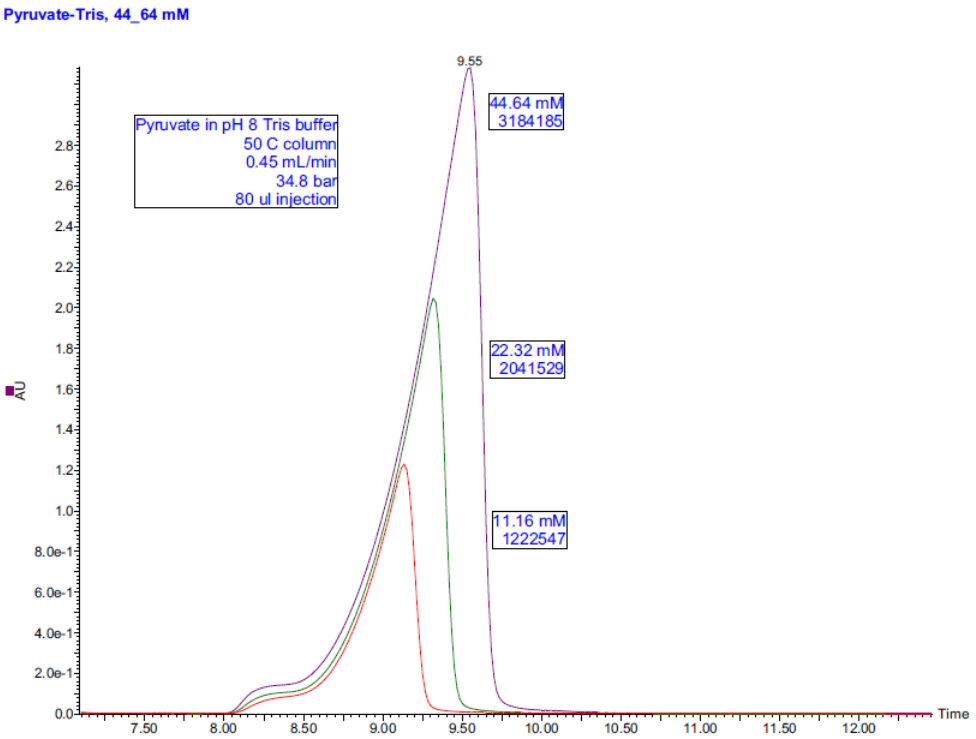

Figure E3: Pyruvate standards analysed using HPLC. Samples of pyruvate were prepared in Tris-HCl buffer and injected onto the C18-reverse phase column. The mobile phase (0.1 % phosphoric acid) was run at 1 mL min^{-1} and the column was maintained at 50 ^{o}C. Experiments performed at Harwell Research Complex.

E3.Biphenyl-2-ol to 2, 3-dihydroxybiphenyl

Biphenyl-2-ol and 2,3-dihydroxybiphenyl were separated using a Chromolith® Performance, 100-3 mm column (Merck). The column was held at 40 ^{o}C and initially equilibrated with 80 % water and 20 % acetonitrile. After injection of a sample, a gradient was applied such that the mobile phase was 25 % water : 75 % acetonitrile after 10 minutes. The initial 80 % water : 20 % acetonitrile mixtures was applied after 11 minutes and left to equilibrate for 5 minutes before another sample was run. Biphenyl-2-ol and 2,3-dihydroxybiphenyl were observed at 7.8 and 6.2 minutes, respectively. The cofactor and DMSO were observed at *ca* 0.5 min and therefore did not complicated analysis.

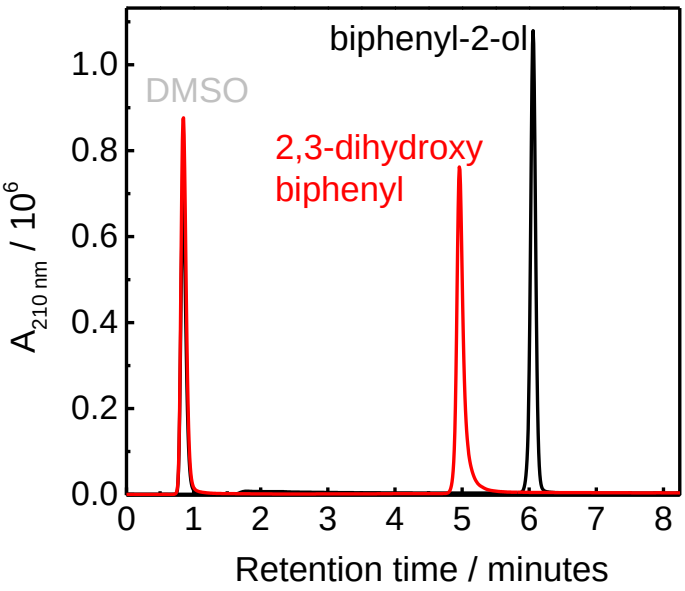

Figure E4: Standards of biphenyl-2-ol (black) and 2,3-dihydroxybiphenyl (red) prepared as stocks in DMSO and diluted in water. A sample of cofactor prepared in water is also shown (grey). Absorbance to 210 nm was recorded.

Standards were used to determine either the concentration of the substrate and product or the substrate/product concentration ratio. The absorbance at 210 nm was used.

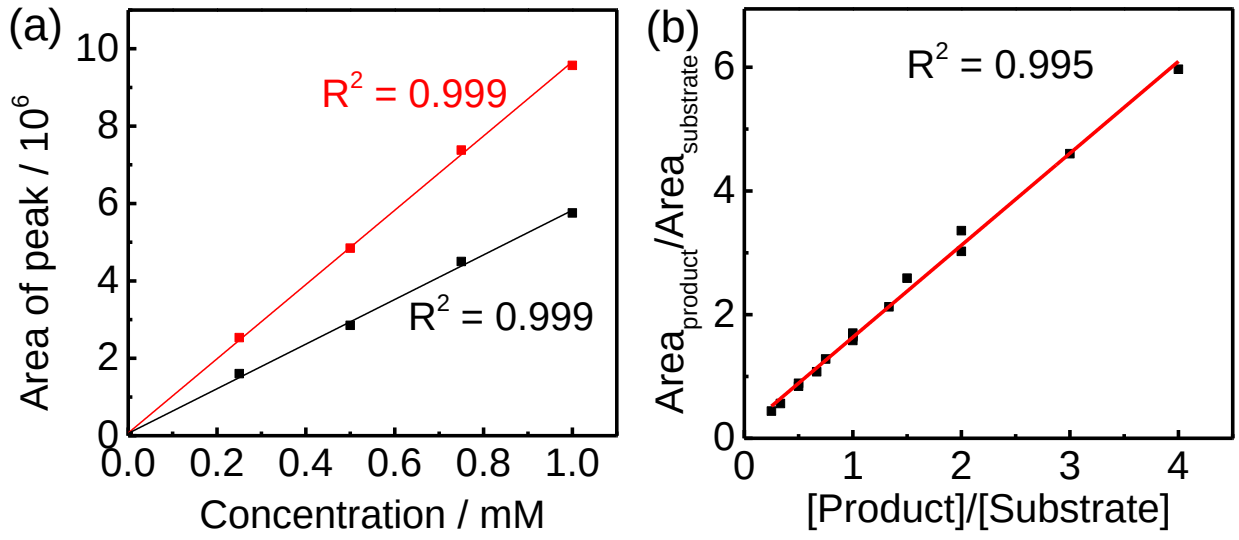

Figure E5: Standards of biphenyl-2-ol (black) and 2,3-dihydroxybiphenyl (red) were used to determine concentrations of unknown samples. A ratio of the area of substrate and product peaks was used to determine concentration ratios in samples of unknown overall concentration.

F. UV-vis calibration for ADH assays in Section 6.2

The extinction coefficient for NADH at 380 nm was determined. UV-vis scans were recorded at a range of NADH concentrations, panel (a). The absorbance at 380 nm was plotted as a function of NADH concentration. This gave a straight line with a gradient of 0.981 A mM^{-1}, panel (b) and therefore an extinction coefficient of 0.981 mM^{-1} cm^{-1}.

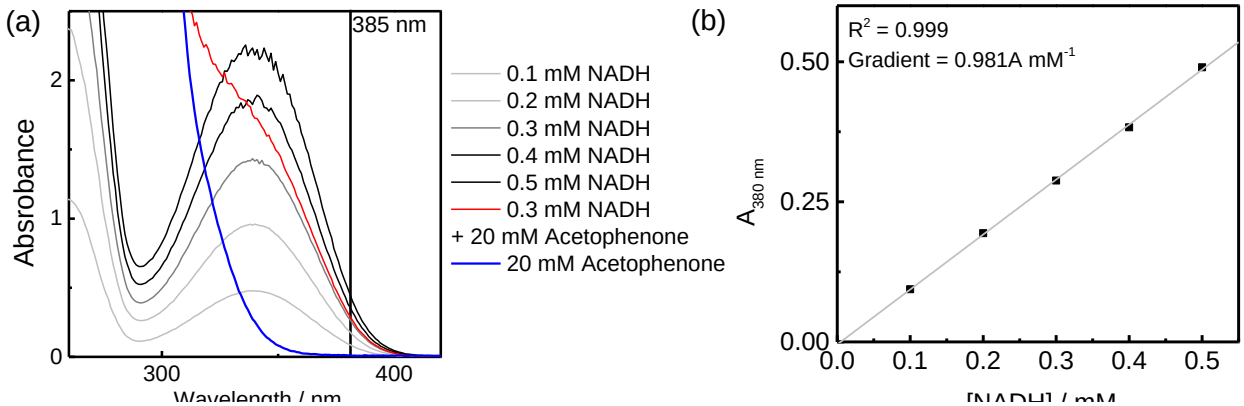

Figure F6: UV-vis spectroscopy was used to determine the extinction coefficient of NADH at 380 mM. (a) UV-vis spectra recorded with NADH concentrations between 0.1 and 0.5 mM (grey – black). Spectra of solutions containing either acetophenone (20 mM) or NADH and acetophenone (0.3 mM and 20 mM, respectively) are shown in blue and red, respectively, for comparison. (b) A plot of absorbance at 380 nm *vs* [NADH] was used to determine the extinction coefficient.

The UV-vis spectra in Figure F6(a) demonstrate that acetophenone leads to significant absorbance at 340 nm and thus compromises analysis of NADH consumption at this wavelength. For this reason, UV-vis kinetics at 385 nm was carried out.

G. HPLC data for Section 6.4.2

Typical HPLC data for particles modified with hydrogenase, NAD^+-reductase and ADH demonstrating the selectivity.

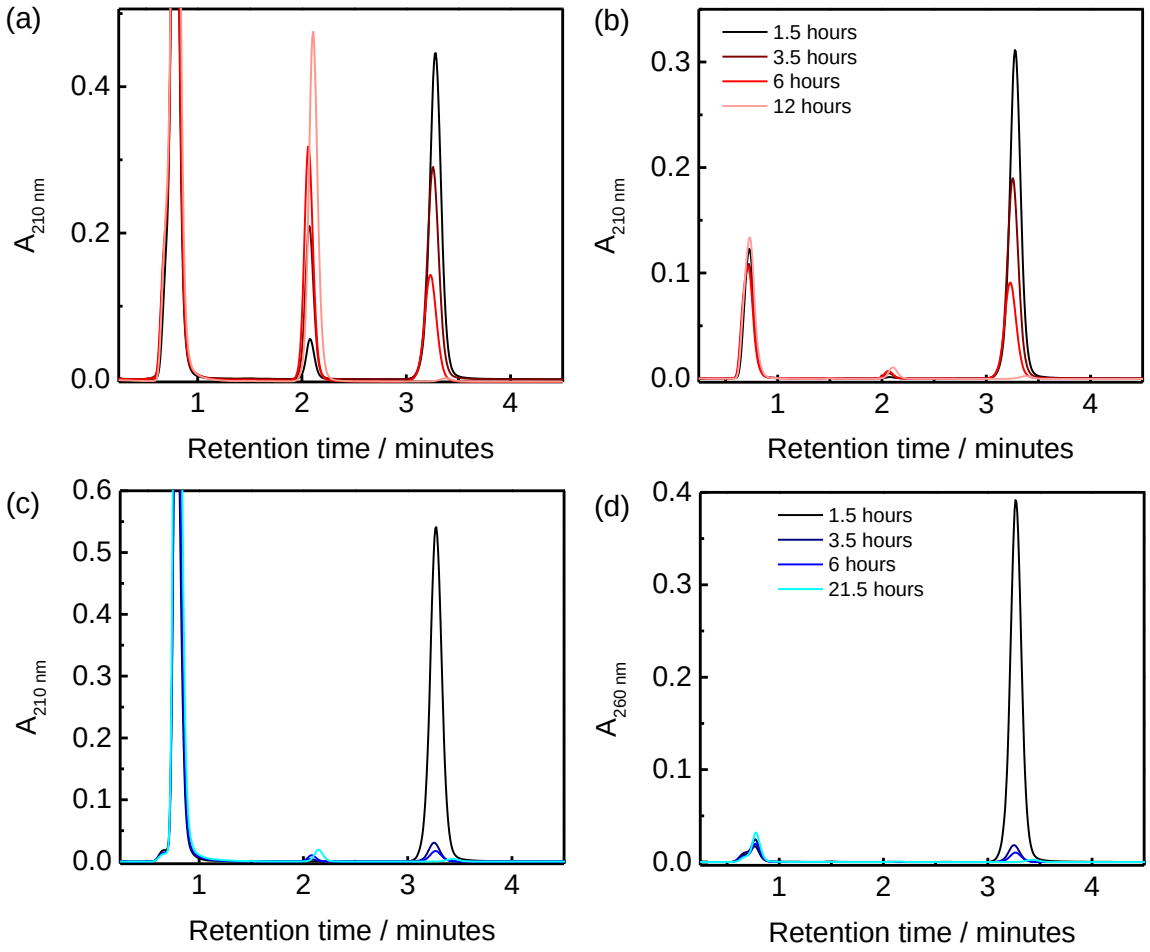

Figure G1: The HPLC traces showing absorbance at (a) 210 nm and (b) 260 nm for particles modified with hydrogenase, NAD^+-reductase and ADH in the presence of acetophenone and NAD^+ (10 mM and 1 mM, respectively). The HPLC traces at (c) 210 nm and (d) 260 nm when ADH was used in solution in the presence of acetophenone and NAD^+ (10 mM) and 0.01 mM, respectively). This corresponds to the data in Table 6-4 in Section 6.4.2.

The HPLC trace in Figure G1(a) shows the absorbance at 210 nm and correlates well to the standards for acetophenone (3.2 minutes) and phenylethanol (2 minutes) in Appendix E. The peak at 3.2 minutes decreased over time as the absorbance at 2 minutes increased demonstrating conversion of acetophenone to phenylethanol. The overall absorbance is fairly constant suggesting that there was not significant absorbance of the acetophenone and phenylethanol. The large peak at *ca* 0.5 minutes is DMSO. The absorbance at 260 nm is shown in panel (b). The peak at *ca* 0.75 minutes is due to the

cofactors (NAD^+ and NADH) and was reasonably constant over time.

The HPLC traces in (c) and (d) correspond to hydrogenase and NAD^+-reductase modified particle for NADH supply to ADH in solution. The absorbance for the cofactor is much less than in (b) consistent with the much lower cofactor concentration used. The absorbance of acetophenone onto the carbon particles is clear, the peak at 3.2 minutes almost completely disappears and there is only a small increase in the absorbance at 2 minutes. This complicated analysis of the extent of acetophenone conversion to phenylethanol therefore this data is not included in Table 6-4.

The HPLC are very clear from other peaks, this demonstrates that the H_2-driven particle systems are highly selective.

H. Data for Table 6-5

Experiments were performed to demonstrate the activity of enzyme-modified particles for H_2-driven NADH generation in the presence of different cofactor concentrations. The particles were monitored using the *in situ* approach and the concentration of NADH was calculated using the extinction coefficient at 340 nm.

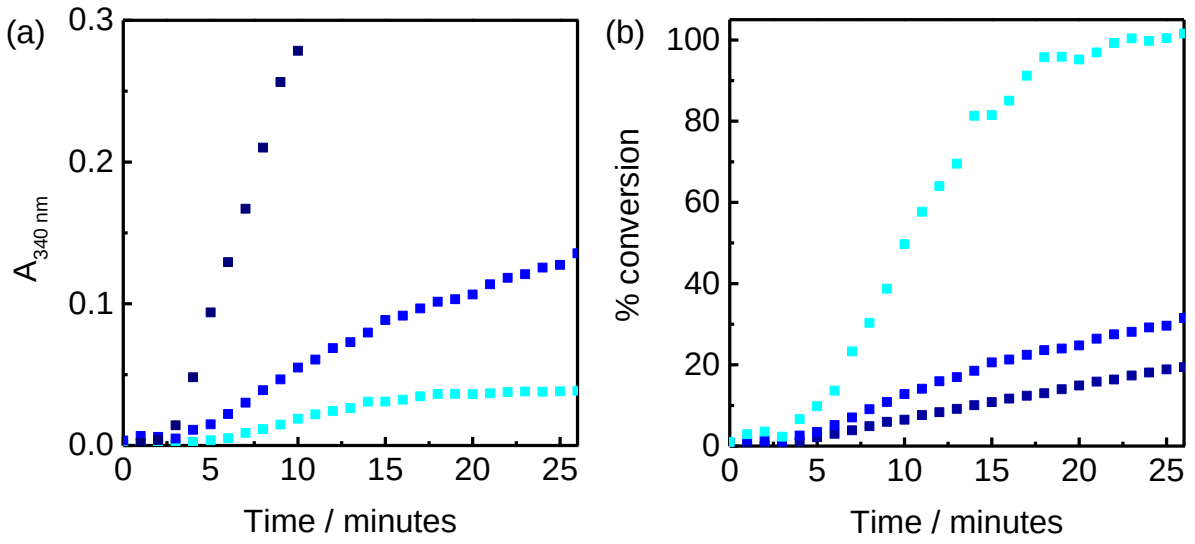

Figure H1: Particles modified with hydrogenase (Hyd-2) and NAD^+-reductase (Hox~~HY~~FU) were injected into H_2-saturated solutions containing 0.01, 0.1 and 1 mM NAD^+ corresponding to the light blue, blue and dark blue lines respectively. A plot of the absorbance at 340 nm (a) and the % conversion (b) are shown. The experiments were performed in Tris-HCl buffer,pH 8 at 30 ^oC in a UV-vis cuvette with stirring.

The results in Figure H1(a) show that the particles in the presence of 1 mM NAD^+ (dark blue) operated at a much faster rate than the particles in 0.1 mM (blue) or 0.01 mM (light blue) NAD^+. The results in Figure H1(b) show that the % conversion of NAD^+ to NADH is much faster at low cofactor concentration, near complete conversion occurred after *ca* 20 minutes. This high conversion of NAD^+ to NADH is likely to aid acetophenone to phenylethanol conversion when coupled to an ADH (for example in Table 6-4.

Science Innovation Plus, Final Report 2013-2013

As part of the Science Innovation Plus program I wrote a Technology, Markets and Organisational capabilities report (TMO) on the H_2-driven particle system for NADH-dependent chemical synthesis.